ISSN 1949-8470 (online)

World Journal of *Radiology*

World J Radiol 2016 February 28; 8(2): 117-225

Published by Baishideng Publishing Group Inc

WJR World Journal of Radiology

A peer-reviewed, online, open-access journal of Radiology

Editorial Board

2014-2017

The *World Journal of Radiology* Editorial Board consists of 365 members, representing a team of worldwide experts in radiology. They are from 36 countries, including Afghanistan (1), Argentina (2), Australia (5), Austria (7), Belgium (2), Brazil (8), Canada (6), Chile (1), China (43), Croatia (1), Denmark (4), Egypt (6), France (5), Germany (22), Greece (10), India (12), Iran (6), Ireland (2), Israel (3), Italy (47), Japan (13), Netherlands (1), New Zealand (1), Pakistan (1), Poland (2), Portugal (1), Serbia (1), Singapore (3), Slovakia (1), South Korea (18), Spain (4), Sweden (2), Switzerland (4), Thailand (1), Turkey (26), United Kingdom (11), and United States (82).

Yue-Qi Zhu, *Shanghai*

Croatia

Goran Kusec, Osijek

Denmark

Poul E Andersen, *Odense*
Lars J Petersen, *Aalborg*
Thomas Z Ramsoy, *Frederiksberg*
Morten Ziebell, *Copenhagen*

Egypt

Mohamed F Bazeed, *Mansoura*
Mohamed Abou El-Ghar, *Mansoura*
Reem HA Mohamed, *Cairo*
Mohamed R Nouh, *Alexandria*
Ahmed AKA Razek, *Mansoura*
Ashraf A Zytoon, *Shebin El-Koom*

France

Sabine F Bensamoun, *Compiègne*
Romaric Loffroy, *Dijon*
Stephanie Nougaret, *Montpellier*
Hassane Oudadesse, *Rennes*
Vincent Vinh-Hung, *Fort-de-France*

Germany

Henryk Barthel, *Leipzig*
Peter Bannas, *Hamburg*
Martin Beeres, *Frankfurt*
Ilja F Ciernik, *Dessau*
A Dimitrakopoulou-Strauss, *Heidelberg*
Peter A Fasching, *Erlanegn*
Andreas G Schreyer, *Regensburg*
Philipp Heusch, *Duesseldorf*
Sonja M Kirchhoff, *Munich*
Sebastian Ley, *Munich*
Adel Maataoui, *Frankfurt am Main*
Stephan M Meckel, *Freiburg*
Hans W Muller, *Duesseldorf*
Kay Raum, *Berlin*
Dirk Rades, *Luebeck*
Marc-Ulrich Regier, *Hamburg*
Alexey Surov, *Halle*
Martin Walter, *Magdeburg*
Axel Wetter, *Essen*
Christoph Zilkens, *Düsseldorf*

Greece

Panagiotis Antoniou, *Thessaloniki*
Nikos Efthimiou, *Athens*
Dimitris Karnabatidis, *Patras*
George Latsios, *Athens*
Stylianos Megremis, *Iraklion*
Alexander D Rapidis, *Athens*
Kiki Theodorou, *Larissa*
Ioannis A Tsalafoutas, *Athens*
Evanthia E Tripoliti, *Ioannina*
Athina C Tsili, *Ioannina*

India

Ritesh Agarwal, *Chandigarh*
Chandan J Das, *New Delhi*
Prathamesh V Joshi, *Mumbai*
Naveen Kalra, *Chandigarh*
Chandrasekharan Kesavadas, *Trivandrum*
Jyoti Kumar, *New Delhi*
Atin Kumar, *New Delhi*
Kaushala P Mishra, *Allahabad*
Daya N Sharma, *New Delhi*
Binit Sureka, *New Delhi*
Sanjay Sharma, *New Delhi*
Raja R Yadav, *Allahabad*

Iran

Majid Assadi, *Bushehr*
SeyedReza Najafizadeh, *Tehran*
Mohammad Ali Oghabian, *Tehran*
Amir Reza Radmard, *Tehran*
Ramin Sadeghi, *Mashhad*
Hadi Rokni Yazdi, *Tehran*

Ireland

Tadhg Gleeson, *Wexford*
Frederik JAI Vernimmen, *Cork*

Israel

Dafna Ben Bashat, *Tel Aviv*
Amit Gefen, *Tel Aviv*
Tamar Sella, *Jerusalem*

Italy

Adriano Alippi, *Rome*
Dante Amelio, *Trento*
Michele Anzidei, *Rome*
Filippo F Angileri, *Messinas*
Stefano Arcangeli, *Rome*
Roberto Azzoni, *San Donato milanese*
Tommaso V Bartolotta, *Palermo*
Tommaso Bartalena, *Imola*
Livia Bernardin, *San Bonifacio*
Federico Boschi, *Verona*
Sergio Casciaro, *Lecce*
Emanuele Casciani, *Rome*
Musa M Can, *Napoli*
Alberto Cuocolo, *Napoli*
Michele Ferrara, *Coppito*
Mauro Feola, *Fossano*
Giampiero Francica, *Castel Volturno*
Luigi De Gennaro, *Rome*
Giulio Giovannetti, *Pisa*
Francesca Iacobellis, *Napoli*
Formato Invernizzi, *Monza Brianza*
Francesco Lassandro, *Naples*
Lorenzo Livi, *Florence*
Pier P Mainenti, *Napoli*
Laura Marzetti, *Chieti*
Giuseppe Malinverni, *Crescentino*
Enrica Milanesi, *Turin*
Giovanni Morana, *Treviso*
Lorenzo Monti, *Milan*
Silvia D Morbelli, *Genoa*
Barbara Palumbo, *Perugia*
Cecilia Parazzini, *Milan*
Stefano Pergolizzi, *Messina*
Antonio Pinto, *Naples*
Camillo Porcaro, *Rome*
Carlo C Quattrocchi, *Rome*
Alberto Rebonato, *Perugia*
Giuseppe Rizzo, *Rome*
Roberto De Rosa, *Naples*
Domenico Rubello, *Rovigo*
Andrea Salvati, *Bari*
Sergio Sartori, *Ferrara*
Luca M Sconfienza, *Milano*
Giovanni Storto, *Rionero*
Nicola Sverzellati, *Parma*
Alberto S Tagliafico, *Genova*
Nicola Troisi, *Florence*

Japan

Yasuhiko Hori, *Chiba*
Hidetoshi Ikeda, *Koriyama*
Masahito Kawabori, *Sapporo*
Tamotsu Kamishima, *Sapporo*
Hiro Kiyosue, *Yufu*
Yasunori Minami, *Osaka-sayama*
Yasuhiro Morimoto, *Kitakyushu*
Satoru Murata, *Tokyo*
Shigeki Nagamachi, *Miyazaki*
Hiroshi Onishi, *Yamanashi*
Morio Sato, *Wakayama Shi*
Yoshito Tsushima, *Maebashi*
Masahiro Yanagawa, *Suita*

Netherlands

Willem Jan van Rooij, *Tilburg*

New Zealand

W Howell Round, *Hamilton*

Pakistan

Wazir Muhammad, *Abbottabad*

Poland

Maciej S Baglaj, *Wroclaw*

Piotr Czauderna, *Gdansk*

Portugal

Joao Manuel RS Tavares, *Porto*

Serbia

Olivera Ciraj-Bjelac, *Belgrade*

Singapore

Gopinathan Anil, *Singapore*
Terence KB Teo, *Singapore*
Cher Heng Tan, *Singapore*

Slovakia

Stefan Sivak, *Martin*

South Korea

Ki Seok Choo, *Busan*
Seung Hong Choi, *Seoul*
Dae-Seob Choi, *Jinju*
Hong-Seok Jang, *Seoul*
Yong Jeong, *Daejeon*
Chan Kyo Kim, *Seoul*
Se Hyung Kim, *Seoul*
Joong-Seok Kim, *Seoul*
Sang Eun Kim, *Seongnam*
Sung Joon Kwon, *Seoul*
Jeong Min Lee, *Seoul*
In Sook Lee, *Busan*
Noh Park, *Goyang*
Chang Min Park, *Seoul*
Sung Bin Park, *Seoul*
Deuk Jae Sung, *Seoul*
Choongsoo Shin, *Seoul*
Kwon-Ha Yoon, *Iksan*

Spain

Miguel A De Gregorio, *Zaragoza*
Antonio Luna, *Jaén*
Enrique Marco de Lucas, *Santander*
Fernando Ruiz Santiago, *Granada*

Sweden

Dmitry Grishenkov, *Stockholm*
Tie-Qiang Li, *Stockholm*

Switzerland

Nicolau Beckmann, *Basel*
Christian Boy, *Bern*
Giorgio Treglia, *Bellinzona*

Stephan Ulmer, *Kiel*

Thailand

Sirianong Namwongprom, *Chiang Mai*

Turkey

Kubilay Aydin, *Istanbul*
Ramazan Akdemir, *Sakarya*
Serhat Avcu, *Ankara*
Ayse Aralasmak, *Istanbul*
Oktay Algin, *Ankara*
Nevbahar Akcar, *Meselik*
Bilal Battal, *Ankara*
Zulkif Bozgeyik, *Elazig*
Nazan Ciledag, Aakara
Fuldem Y Donmez, *Ankara*
Gulgun Engin, *Istanbul*
Ahmet Y Goktay, *Izmir*
Oguzhan G Gumustas, *Bursa*
Kaan Gunduz, *Ankara*
Pelin Ozcan Kara, *Mersin*
Kivanc Kamburoglu, *Ankara*
Ozgur Kilickesmez, *Istanbul*
Furuzan Numan, *Istanbul*
Cem Onal, *Adana*
Ozgur Oztekin, *Izmir*
Seda Ozbek (Boruban), *Konya*
Selda Sarikaya, *Zonguldak*
Figen Taser, *Kutahya*
Baran Tokar, *Eskisehir*
Ender Uysal, *Istanbul*
Ensar Yekeler, *Istanbul*

United Kingdom

Indran Davagnanam, *London*
M DC Valdés Hernández, *Edinburgh*
Alan Jackson, *Manchester*
Suneil Jain, *Belfast*
Long R Jiao, *London*
Miltiadis Krokidis, *Cambridge*
Pradesh Kumar, *Liverpool*
Peter D Kuzmich, *Derby*
Georgios Plataniotis, *Brighton*
Vanessa Sluming, *Liverpool*

United States

Garima Agrawal, *Saint Louis*
James R Brasic, *Baltimore*
Rajendra D Badgaiyan, *Buffalo*
Ulas Bagci, *Bethesda*
Anat Biegon, *Stony Brook*
Ramon Casanova, *Winston Salem*
Wenli Cai, *Boston*
Zheng Chang, *Durham*
Corey J Chakarun, *Long Beach*
Kai Chen, *Los Angeles*
Hyun-Soon Chong, *Chicago*
Marco Cura, *Dallas*
Ravi R Desai, *Bensalem*
Delia DeBuc, *Miami*
Carlo N De Cecco, *Charleston*
Timm-Michael L Dickfeld, *Baltimore*
Subba R Digumarthy, *Boston*
Huy M Do, *Stanford*
Todd A Faasse, *Grand Rapids*
Salomao Faintuch, *Boston*
Girish M Fatterpekar, *New York*
Dhakshinamoorthy Ganeshan, *Houston*
Robert J Griffin, *Little Rock*
Andrew J Gunn, *Boston*
Sandeep S Hedgire, *Boston*
Timothy J Hoffman, *Columbia*
Mai-Lan Ho, *San Francisco*
Juebin Huang, *Jackson*
Abid Irshad, *Charleston*
Matilde Inglese, *New York*
El-Sayed H Ibrahim, *Jacksonville*
Paul R Julsrud, *Rochester*
Pamela T Johnson, *Baltimore*
Ming-Hung Kao, *Tempe*
Sunil Krishnan, *Houston*
Richard A Komoroski, *Cincinnati*
Sandi A Kwee, *Honolulu*
King Kim, *Ft. Lauderdale*
Guozheng Liu, *Worcester*
Yiyan Liu, *Newark*
Venkatesh Mani, *New York*
Lian-Sheng Ma, *Pleasanton*
Rachna Madan, *Boston*
Zeyad A Metwalli, *Houston*
Yilong Ma, *Manhasset*
Hui Mao, *Atlanta*
Feroze B Mohamed, *Philadelphia*
Gul Moonis, *Boston*
John L Nosher, *New Brunswick*
Rahmi Oklu, *Boston*
Aytekin Oto, *Chicago*
Bishnuhari Paudyal, *Philadelphia*
Rajul Pandya, *Youngstown*
Chong-Xian Pan, *Sacramento*
Jay J Pillai, *Baltimore*
Neal Prakash, *Duarte*
Reza Rahbar, *Boston*
Ali S Raja, *Boston*
Gustavo J Rodriguez, *El Paso*
David J Sahn, *Portlsand*
Steven Schild, *Scottsdale*
Ali R Sepahdari, *Los Angeles*
Li Shen, *Indianapolis*
JP Sheehan, *Charlottesville*
Atul B Shinagare, *Boston*
Sarabjeet Singh, *Boston*
Charles J Smith, *Columbia*
Kenji Suzuki, *Chicago*
Monvadi Srichai-Parsia, *Washington*
Sree H Tirumani, *Boston*
Hebert A Vargas, *New York*
Sachit Verma, *Philadelphia*
Yoichi Watanabe, *Minneapolis*
Li Wang, *Chapel Hill*
Carol C Wu, *Boston*
Shoujun Xu, *Houston*
Min Yao, *Cleveland*
Xiaofeng Yang, *Atlanta*
Qingbao Yu, *Albuquerque*
Aifeng Zhang, *Chicago*
Chao Zhou, *Bethlehem*
Hongming Zhuang, *Philadelphia*

WJR World Journal of Radiology

Contents

Monthly Volume 8 Number 2 February 28, 2016

SYSTEMATIC REVIEWS

World Journal of Radiology
Volume 8 Number 2 February 28, 2016

Contents

NAME OF JOURNAL
World Journal of Radiology

ISSN
ISSN 1949-8470 (online)

LAUNCH DATE
January 31, 2009

FREQUENCY
Monthly

EDITORIAL OFFICE
Jin-Lei Wang, Director
Xiu-Xia Song, Vice Director
World Journal of Radiology
Room 903, Building D, Ocean International Center,
No. 62 Dongsihuan Zhonglu, Chaoyang District,
Beijing 100025, China
Telephone: +86-10-59080039
Fax: +86-10-85381893
E-mail: editorialoffice@wjgnet.com
Help Desk: http://www.wjgnet.com/esps/helpdesk.aspx
http://www.wjgnet.com

PUBLISHER
Baishideng Publishing Group Inc
8226 Regency Drive,
Pleasanton, CA 94588, USA
Telephone: +1-925-223-8242
Fax: +1-925-223-8243
E-mail: bpgoffice@wjgnet.com
Help Desk: http://www.wjgnet.com/esps/helpdesk.aspx
http://www.wjgnet.com

PUBLICATION DATE
February 28, 2016

INSTRUCTIONS TO AUTHORS
Full instructions are available online at http://www.wjgnet.com/bpg/g_info_20160116143427.htm

ONLINE SUBMISSION
http://www.wjgnet.com/esps/

World Journal of Radiology

Submit a Manuscript: http://www.wjgnet.com/esps/
Help Desk: http://www.wjgnet.com/esps/helpdesk.aspx
DOI: 10.4329/wjr.v8.i2.117

World J Radiol 2016 February 28; 8(2): 117-123
ISSN 1949-8470 (online)

FRONTIER

Brainstem tegmental lesions in neonates with hypoxic-ischemic encephalopathy: Magnetic resonance diagnosis and clinical outcome

Carlo Cosimo Quattrocchi, Giuseppe Fariello, Daniela Longo

Carlo Cosimo Quattrocchi, Department of Medicine and Surgery, Università Campus Bio-Medico di Roma, 00128 Rome, Italy

Giuseppe Fariello, Fatebenefratelli S. Pietro Hospital, 00128 Rome, Italy

Daniela Longo, Unit of Neuroradiology, Bambino Gesù Children's Research Hospital IRCCS, 00128 Rome, Italy

Author contributions: Quattrocchi CC conceived and designed the study and wrote the manuscript; Fariello G critically revised the manuscript for important intellectual content; Longo D supervised the study, collected diagnostic images and references and critically revised the manuscript for important intellectual content.

Conflict-of-interest statement: The authors declare no conflict of interest.

Correspondence to: Carlo Cosimo Quattrocchi, MD, PhD, Department of Medicine and Surgery, Università Campus Bio-Medico di Roma, via Alvaro del Portillo, 00128 Rome, Italy. c.quattrocchi@unicampus.it
Telephone: +39-062-25411708

Received: August 31, 2015
Peer-review started: September 1, 2015
First decision: September 29, 2015
Revised: October 11, 2015
Accepted: December 9, 2015
Article in press: December 11, 2015
Published online: February 28, 2016

Abstract

Lesions of the brainstem have been reported in the clinical scenarios of hypoxic-ischemic encephalopathy (HIE), although the prevalence of these lesions is probably underestimated. Neuropathologic studies have demonstrated brainstem involvement in severely asphyxiated infants as an indicator of poor outcome. Among survivors to HIE, the most frequent clinical complaints that may be predicted by brainstem lesions include feeding problems, speech, language and communication problems and visual impairments. Clinical series, including vascular and metabolic etiologies, have found selective involvement of the brainstem with the demonstration of symmetric bilateral columnar lesions of the tegmentum. The role of brainstem lesions in HIE is currently a matter of debate, especially when tegmental lesions are present in the absence of supratentorial lesions. Differential diagnosis of tegmental lesions in neonates and infants include congenital metabolic syndromes and drug-related processes. Brainstem injury with the presence of supratentorial lesions is a predictor of poor outcome and high rates of mortality and morbidity. Further investigation will be conducted to identify specific sites of the brainstem that are vulnerable to hypoxic-ischemic and toxic-metabolic insults.

Key words: Magnetic resonance; Asphyxia; Hypoxic-ischemic encephalopathy; Tegmentum; Neonates; Brainstem

Core tip: Brainstem tegmental lesions in neonates with hypoxico-ischemic encephalopathy: Magnetic resonance diagnosis and clinical outcome.

lesions in neonates with hypoxic-ischemic encephalopathy: Magnetic resonance diagnosis and clinical outcome. *World J Radiol* 2016; 8(2): 117-123 Available from: URL: http://www.wjgnet.com/1949-8470/full/v8/i2/117.htm DOI: http://dx.doi.org/10.4329/wjr.v8.i2.117

HYPOXIC-ISCHEMIC ENCEPHALOPATHY IN NEONATES

Neonatal hypoxic-ischemic encephalopathy (HIE) is a pathological pattern secondary to perinatal events that reduce blood flow in the brain of neonates[1]. Most cases of encephalopathy in neonates born at term are related to HIE that occurs *in utero* or during the delivery from different intrapartum conditions[2]. Despite strategies of therapeutic hypothermia such as the whole body cooling have been adopted as a standard treatment for HIE and data from the TOBY (Total Body Hypothermia for Neonatal Encephalopathy) trial have demonstrated its efficacy in improving neurologic outcomes at 18 mo and at 6-7 years of age[3,4], HIE is still an important cause of early mortality or morbidity and adverse neurodevelopmental outcome in children[1].

In pre-term or very low birthweight neonates, periventricular leukomalacia is observed in at least 50% of the cases[2]. In infants born at 32 gestation weeks and above, neonatal and perinatal strokes are expected in about 1 in 4000 live births[5] and encephalopathy is expected in up to 2 per 1000 term live births[6].

Brain magnetic resonance (MR) is able to discriminate normal from pathological patterns in the neonatal brain[7]. Three typical MR imaging patterns have been recognized in neonates with HIE: (1) "watershed", involving the cerebral cortex and subcortical white matter especially in the posterior lobes, following a mild to moderate hypotension or a partial hypoxia with prolonged duration; (2) "basal ganglia-thalamus", following an acute short-duration severe hypoxic or profound hypotensive event; and (3) "total brain injury", involving supra- and infra-tentorial areas following a prolonged and severe hypoxic or hypotensive event[8]. While peripheral and basal ganglia-thalamus patterns involve supra-tentorial structures exclusively, the total brain injury shows diffuse supra-tentorial involvement that may be associated with damage of the dorsal brainstem and/or the entire cerebral cortex[8,9].

Involvement of the brainstem in HIE and MR diagnosis

Lesions of the brainstem have been reported at MR imaging in the clinical scenarios of HIE[10-15], although the prevalence of these lesions is probably underestimated due to the small size of the brainstem, to the need of dedicated MR protocols under sedation in neonates and, probably, to the "satisfaction of search" effect when diffuse supra-tentorial lesions are present in the condition of total brain injury[16,17].

Neuropathologic studies have demonstrated brainstem involvement in severely asphyxiated infants as an indicator of poor outcome[18-20]. Leech *et al*[20] reported brainstem injury in 93% of asphyxiated infants, especially after prolonged insults. Several gray matter nuclei were involved including the substantia nigra, inferior colliculi, inferior olives, the nuclei of cranial nerves Ⅲ, Ⅳ and Ⅵ, the superior olive, the vestibular nuclei, and the nuclei of the solitary tract, gracile tracts, cuneate tracts and reticular formation[20]. A neuropathologic study in autoptic cases of patients with various developmental disorders including HIE and congenital metabolic errors highlighted the involvement of the central tegmental tract (CTT)[21]. CTT is located between the medio-central tegmentum of the pons and dorsomedial part of the medulla oblongata and has been reported to be included in the dentato-rubro-olivary system, also called Guillain–Mollaret triangle, whose lesions are associated with the inferior olivary nucleus hypertrophic degeneration[22].

The physiopathological mechanisms underlying HIE-related brainstem alterations are currently unknown and debated. From a topographical point of view, selective vulnerability of the tegmentum, territorial vascularization, haemodynamic compensatory mechanisms under hypoxia, metabolic and biochemical mechanisms have been advocated. In fact: (1) the tegmentum of the brainstem represents the watershed area of the vertebro-basilar vascularization between the terminal territories of the paramedian and circumferential branches[15,23] (Figure 1); (2) the dorsal brainstem has higher metabolic demands than the ventral one and could be selectively damaged under hypoxic-ischemic conditions[24]; and (3) experimental studies in mammals have shown that blood flow of the brainstem increases after acute hypoxia[25], as opposed to a blood flow reduction in the cerebrum, suggesting a relative protection of the brainstem fetal circulation. In summary, neuropathologic studies in humans and experimental studies lead to consider the brainstem a less vulnerable site to HIE, with the tegmentum being considered at risk only in the context of severe total brain injury[26].

More recent clinical series[14,15,27-29] have reported on neonates with less severe birth asphyxia than previous neuropathology reports and found selective involvement of the brainstem with the demonstration of symmetric columnar bilateral lesions of the brainstem tegmentum, even in the absence of supratentorial lesions in some cases. In neonates with isolated injury of the brainstem tegmentum, MR imaging shows faint hyperintense signal on T2 weighted images that is associated with the clinical pattern of the so-called "dorsal brainstem syndrome". Bilateral and symmetric lesions of the tegmentum are found that involve the dorsal para-central portions on axial planes and the medulla oblongata and caudal pons cranio-caudally, with sparing of the rostral pons and midbrain (Figure 2). As it has been speculated, these brainstem sites are supplied by branches of the vertebro-basilar artery with less flow compensation from the anterior circulation, as compared with the midbrain; also fetal risk factors may

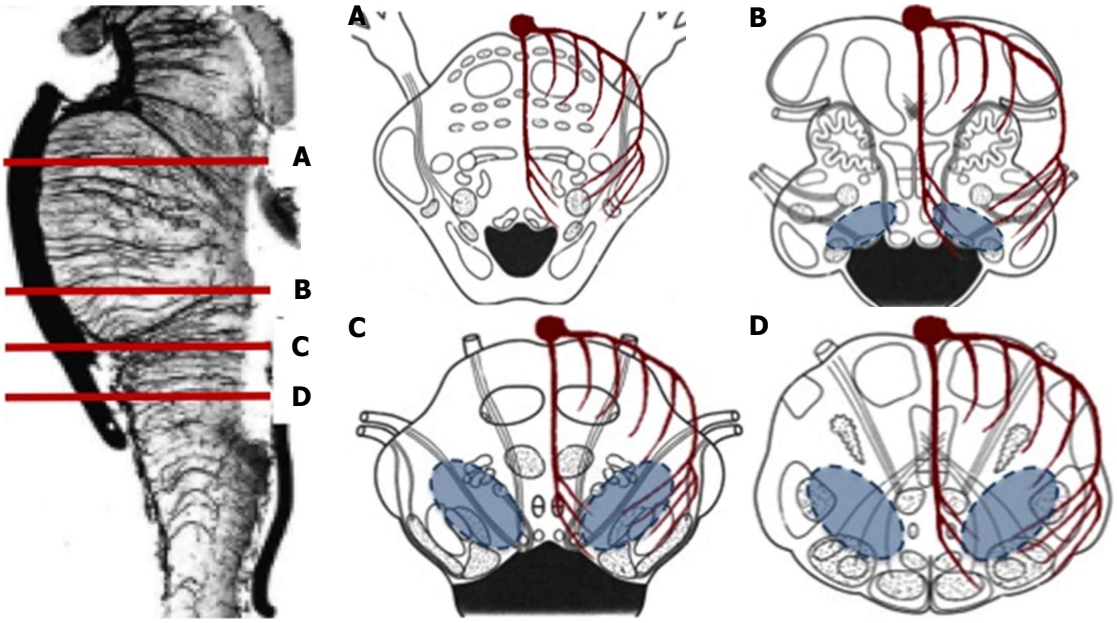

Figure 1 Schematic diagram of the brainstem vasculature. A: Rostral pons; B: Caudal pons; C: Rostral medulla oblongata; D: Caudal medulla oblongata. Basilar artery, the terminal paramedian, short circumferential and long circumferential arteries are depicted. Blue shaded areas represent the tegmental watershed areas that are most frequently affected in neonates and infants with dorsal brainstem syndrome and a history of hypoxic-ischemic encephalopathy.

exist and confer vulnerability to the brainstem, even after not prolonged periods of hypoxia/hypotension[24], such as polyhydramnios or oligoidramnios[15,29]. Moreover, unknown genetic susceptibility could be taken into consideration.

Differential diagnosis for this MR pattern includes the columnar-shaped bilateral and symmetric T2 hyperintense signal of the central tegmental tracts that have been reported in various developmental disorders[21,30-32], metabolic diseases including non-ketotic hyperglycinemia[33], mitochondrial diseases[34], perinatal asphyxia[27], during vigabatrin treatment, and even in control children younger than 25 mo of age[35], with a prevalence of about 5% in children ranging between 1 and 6 years of age[36]. A physiological maturation process that may be influenced by different genetic, metabolic or toxic factors has been proposed to explain its presence in both control and diseased children[35]. These lesions usually show net margins on T2 weighted images, involve the dorsal para-central portions on axial planes and the pons and midbrain in a preferential manner (Figure 3).

In summary, the discrepancy between neuropathology reports, experimental studies in animals and clinical observations has generated a debate on the role of brainstem lesions in HIE. In fact, the severity of hypoxic-ischemic injury is an important issue to consider when interpreting results from autopsy studies and comparing them to clinical studies that are conducted on neonates who survived to HIE; also, the pathologic conditions and related events that lead to HIE in neonates are complex and very difficult to replicate in the experimental design of animal studies. Nevertheless, neonates with HIE and isolated brainstem lesions (in the absence of detectable supratentorial injury) suggest that a "brainstem watershed pattern" of brain HIE-related injury might exist, although rare in prevalence[15].

Clinico-radiological correlation and outcome

Tegmental lesions of the brainstem involve several structures that are crucial for vital functions: The tegmentum of the medulla oblongata includes the XII nerve nucleus, dorsal nucleus of the X cranial nerve, nucleus ambiguus, gracile nucleus of Goll, cuneate nucleus of Burdach, spinal nucleus of the trigeminal nerve, reticular formation, solitary tract and the pre-Botzinger complex, crucial for the stereotyped sequence of feeding and respiration[37]; the tegmentum of the pons includes the VII and VI cranial nerve nucleus, spinal nucleus, main sensory nucleus and mesencephalic nucleus of the V cranial nerve and reticular formation; the tegmentum of the midbrain includes the central nucleus of the inferior colliculus, the III and IV cranial nerve nucleus, the mesencephalic nucleus of the V cranial nerve, locus coeruleus, and reticular formation.

In the clinical scenario of total asphyxia the involvement of the brainstem in neonates has been associated with oculomotor disturbances, bilateral facial nerve palsy, ventilatory disturbances, and impaired sucking and swallowing[8,15]. These patients also show hypotonia, spastic tetraplegia, seizures, and psychomotor delay in different combinations and carry a high risk of postnatal mortality[15]. Association studies do not demonstrate causality, especially in the case of respiratory and swallowing alterations that are finely modulated by the functional and structural connectivity between the brainstem, suprabulbar cortex and basal ganglia. Nevertheless, the central pattern generators of these functions are located in the brainstem[37] and their damage needs to be considered in neonates and infants with HIE.

A preferential involvement of the brainstem with

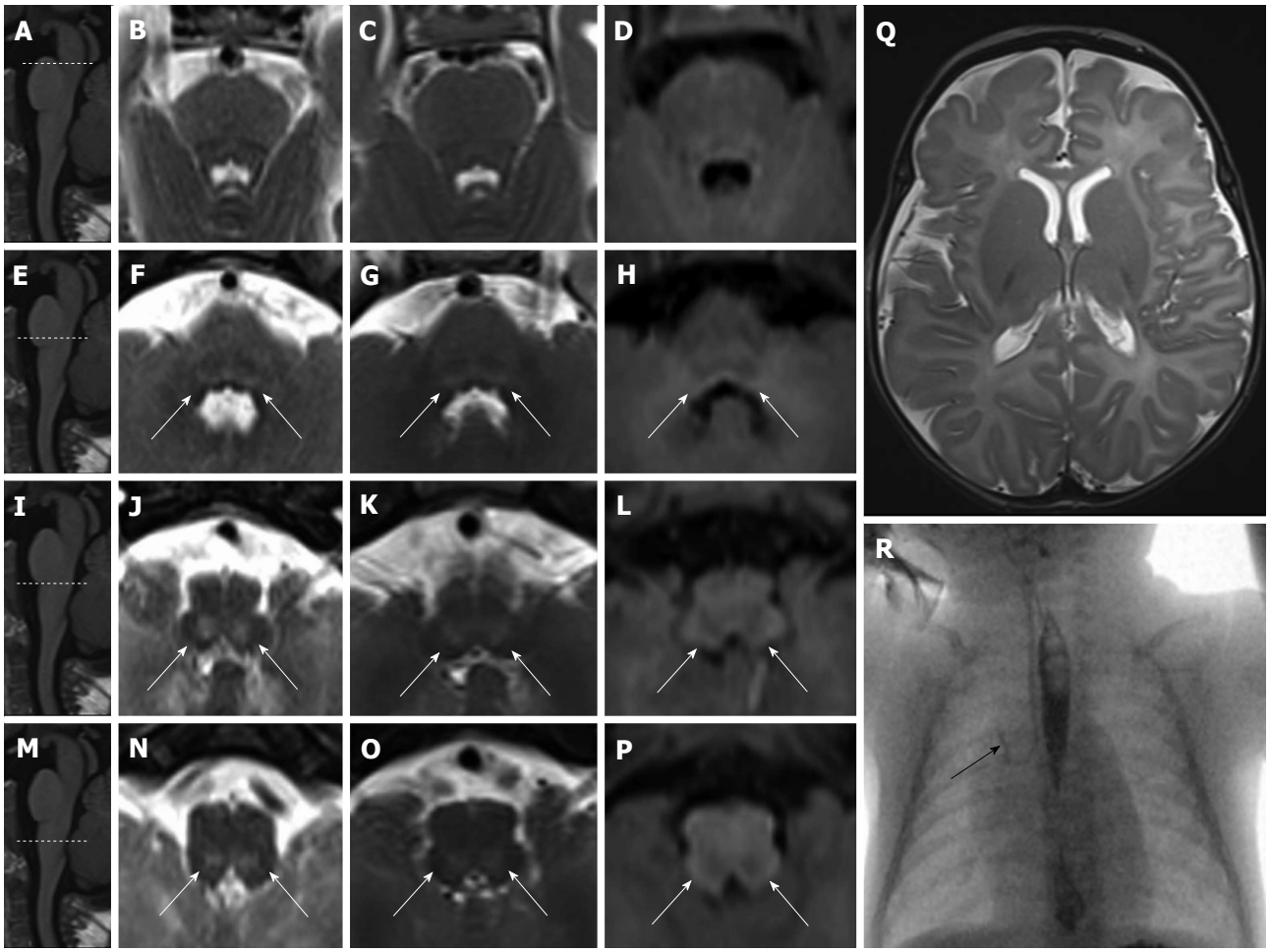

Figure 2 Brainstem tegmental lesions and oral motor dysfunction. An infant with perinatal asphyxia due to knotting of umbilical cord around the neck is shown. Apgar score at five minutes after birth. Eighteen days after birth (panels B, F, J and N), MR images show faint T2 hyperintense (white arrows in F, J, and N) bilateral and symmetric tegmental lesions of the caudal pons and medulla oblongata. Forty days after birth (panels C, D, G, H, K, L, O and P), MR images confirm T2 hyperintense (white arrows in G, K, and O) and T1 hypointense (white arrows in H, L, and P) bilateral and symmetric tegmental lesions of the caudal pons and medulla oblongata. No signal alterations are detected at the level of the cranial pons (B-D) and at supratentorial level (Q). At 1 mo, an upper GI tract X-ray showed iodinated contrast (Iopamidol, IOPAMIRO 300) inhalation (black arrow in panel R points to the right bronchus). Gastrostomy was performed. At the age of 2 years, psychomotor delay and dysphagia are present. Sagittal views of the brainstem (panels A, E, I and M) are used for reference of axial images. MR: Magnetic resonance.

specific involvement of the facial and abducens nuclei has been known as Möbius syndrome. A spectrum of symptoms caused by lesions located rostral and caudal to these nuclei may be associated with other oculomotor nerve nuclei and with dysphagia-gastroesophageal reflux complex[15,29]. Heterogeneity of clinical presentation, outcome[38] and genetic loci involved in Möbius syndrome[39,40] led to propose a syndromic spectrum that may also include the rarely reported cases of neonates with a history of HIE or perinatal sentinel events of HIE[41], who present tegmental lesions without supratentorial involvement at MR imaging[15,29]. A recent systematic review conducted on the literature published between 1980 and 2011 has shown that there is currently limited evidence on the relationship of early sucking and swallowing problems in neonatal brain injury with patterns of neonatal brain injury[42]. Early sucking and swallowing problems were reported to be present in 35% to 48% of infants with different types of neonatal brain injury. However, data from the few available relevant studies were shown to be heterogeneous in terms of the research design, levels of evidence (levels Ⅱ, Ⅲ and Ⅳ), infant populations described, and assessment measures used[42].

When lesions in the brainstem are diagnosed with basal ganglia-thalamus and/or cortex lesions, the outcome is often dismal and brainstem injury is the most powerful predictor of death[43,44] in children with HIE, with up to 50% of children dying in the neonatal period or during infancy[45]. Among survivors to HIE, the most frequent clinical complaints that may be predicted by brainstem lesions include feeding problems, speech, language and communication problems and visual impairments. Prediction of these symptoms is crucial to appropriately plan the short and long term care of an infant who has suffered with HIE and counsel the parents for a better neurocognitive development and outcome[44].

Feeding problems can range from some difficulties with swallowing solids or liquids to being unable to

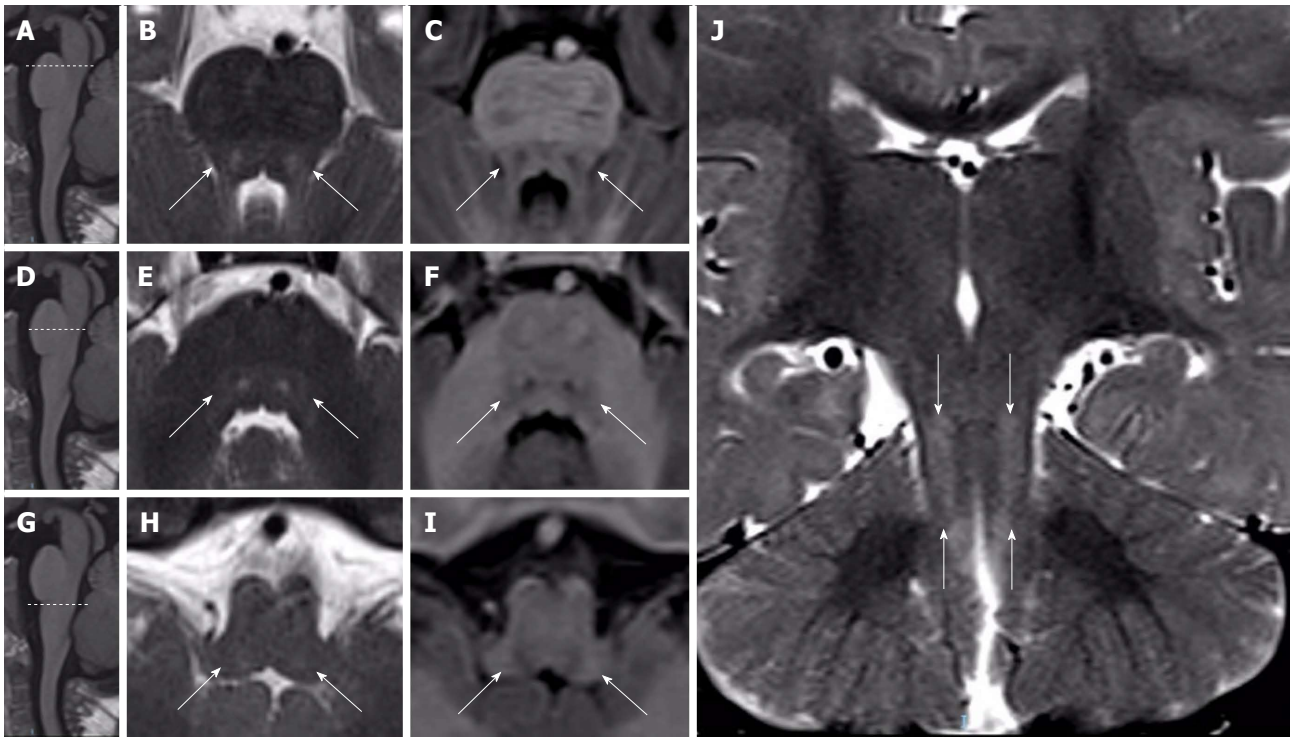

Figure 3 Brainstem tegmental lesions of the central tegmental tracts. A 1-year-old infant shows generalized hypotonia, macrocephaly and psycho-motor developmental delay, without a history of hypoxic-ischemic encephalopathy or adverse perinatal events. A genetic syndrome is suspected and is currently not known. MR images show isolated T2 hyperintense (white arrows in B, E, and H) and T1 hypointense (white arrows in C, F, and I) bilateral and symmetric tegmental lesions of the pons and caudal midbrain. Faint T2 hyperintense signal is observed at the rostral medulla oblongata. Columnar shape of alterations is demonstrated in coronal T2 weighted images (J). No signal alterations are detected at the supratentorial level (J). Sagittal views of the brainstem (A, D, and G) are used for reference of axial images. MR: Magnetic resonance.

feed orally with the need for long-term gavage feeding. When gavage feeding is necessary, almost all neonates show involvement of the brainstem[15,45]. Logistic regression analyses have shown that only the severity of basal ganglia-thalamus and mesencephalic injury are independently associated with feeding impairment and that only the severity of basal ganglia-thalamus injury and pontine involvement are independently associated with gastrostomy insertion[45].

These data show that assessment of the brainstem on neonatal MRI may provide important prognostic information about the severity of feeding impairments in survivors to neonatal HIE.

Despite their impact on children quality of life and prevention of malnutrition and other complications, gavage feeding and gastrostomy are procedures that are not easily accepted by parents. Thus, early identification of infants likely to need these procedures, allows early implementation of strategies in the care of children and their families[45].

Future perspectives

The current knowledge on the so-called "dorsal brainstem syndrome" is limited, mainly due to the relative low frequency of isolated brainstem involvement in neonates with HIE, which remains an exceptional event. However, timing of scans, high quality neonatal MRI and radiologist awareness are necessary pre-requisites to identify brainstem lesions. Also the wide range of differential diagnoses for T2 hyperintense tegmental lesions requires careful analysis of images and often second opinion for a correct interpretation. Prospective multicenter studies should be designed to conduct analyses on larger and homogeneous populations of neonates and infants. Such studies will help to identify vulnerable children carrying susceptibility genes, to find mechanisms of early vulnerability of the brainstem to hypoxic-ischemic damage and to predict motor and/or neurocognitive outcomes.

REFERENCES

1 **Douglas-Escobar M**, Weiss MD. Hypoxic-ischemic encephalopathy: a review for the clinician. *JAMA Pediatr* 2015; **169**: 397-403 [PMID: 25685948]

2 **Volpe JJ**. Brain injury in premature infants: a complex amalgam of destructive and developmental disturbances. *Lancet Neurol* 2009; **8**: 110-124 [PMID: 19081519 DOI: 10.1016/S1474-4422(08)70294-1]

3 **Jacobs SE**, Berg M, Hunt R, Tarnow-Mordi WO, Inder TE, Davis PG. Cooling for newborns with hypoxic ischaemic encephalopathy. *Cochrane Database Syst Rev* 2013; **1**: CD003311 [PMID: 23440789 DOI: 10.1002/14651858.CD003311]

4 **Azzopardi D**, Strohm B, Marlow N, Brocklehurst P, Deierl A, Eddama O, Goodwin J, Halliday HL, Juszczak E, Kapellou O, Levene M, Linsell L, Omar O, Thoresen M, Tusor N, Whitelaw A, Edwards AD. Effects of hypothermia for perinatal asphyxia on childhood outcomes. *N Engl J Med* 2014; **371**: 140-149 [PMID: 25006720 DOI: 10.1056/NEJMoa1315788]

5 **Estan J**, Hope P. Unilateral neonatal cerebral infarction in full

term infants. *Arch Dis Child Fetal Neonatal Ed* 1997; **76**: F88-F93 [PMID: 9135286]
6 **Pierrat V**, Haouari N, Liska A, Thomas D, Subtil D, Truffert P. Prevalence, causes, and outcome at 2 years of age of newborn encephalopathy: population based study. *Arch Dis Child Fetal Neonatal Ed* 2005; **90**: F257-F261 [PMID: 15846019]
7 **Counsell SJ**, Tranter SL, Rutherford MA. Magnetic resonance imaging of brain injury in the high-risk term infant. *Semin Perinatol* 2010; **34**: 67-78 [PMID: 20109974 DOI: 10.1053/j.semperi.2009.10.007]
8 **Ghei SK**, Zan E, Nathan JE, Choudhri A, Tekes A, Huisman TA, Izbudak I. MR imaging of hypoxic-ischemic injury in term neonates: pearls and pitfalls. *Radiographics* 2014; **34**: 1047-1061 [PMID: 25019441 DOI: 10.1148/rg.344130080]
9 **Quattrocchi CC**, Longo D, Delfino LN, Errante Y, Aiello C, Fariello G, Bernardi B. MR differential diagnosis of acute deep grey matter pathology in paediatric patients. *Pediatr Radiol* 2013; **43**: 743-761 [PMID: 23196927 DOI: 10.1007/s00247-012-2491-2]
10 **Voit T**, Lemburg P, Neuen E, Lumenta C, Stork W. Damage of thalamus and basal ganglia in asphyxiated full-term neonates. *Neuropediatrics* 1987; **18**: 176-181 [PMID: 3317104]
11 **Pasternak JF**, Predey TA, Mikhael MA. Neonatal asphyxia: vulnerability of basal ganglia, thalamus, and brainstem. *Pediatr Neurol* 1991; **7**: 147-149 [PMID: 2059257]
12 **Barkovich AJ**. MR and CT evaluation of profound neonatal and infantile asphyxia. *AJNR Am J Neuroradiol* 1992; **13**: 959-972; discussion 973-975 [PMID: 1590198]
13 **Barkovich AJ**, Westmark K, Partridge C, Sola A, Ferriero DM. Perinatal asphyxia: MR findings in the first 10 days. *AJNR Am J Neuroradiol* 1995; **16**: 427-438 [PMID: 7793360]
14 **Sugama S**, Eto Y. Brainstem lesions in children with perinatal brain injury. *Pediatr Neurol* 2003; **28**: 212-215 [PMID: 12770675]
15 **Quattrocchi CC**, Longo D, Delfino LN, Cilio MR, Piersigilli F, Capua MD, Seganti G, Danhaive O, Fariello G. Dorsal brain stem syndrome: MR imaging location of brain stem tegmental lesions in neonates with oral motor dysfunction. *AJNR Am J Neuroradiol* 2010; **31**: 1438-1442 [PMID: 20395394 DOI: 10.3174/ajnr.A2103]
16 **Alderliesten T**, Nikkels PG, Benders MJ, de Vries LS, Groenendaal F. Antemortem cranial MRI compared with postmortem histopathologic examination of the brain in term infants with neonatal encephalopathy following perinatal asphyxia. *Arch Dis Child Fetal Neonatal Ed* 2013; **98**: F304-F309 [PMID: 23172767 DOI: 10.1136/archdischild-2012-301768]
17 **Berbaum KS**, Franken EA, Dorfman DD, Rooholamini SA, Kathol MH, Barloon TJ, Behlke FM, Sato Y, Lu CH, el-Khoury GY. Satisfaction of search in diagnostic radiology. *Invest Radiol* 1990; **25**: 133-140 [PMID: 2312249]
18 **Gilles FH**. Hypotensive brain stem necrosis. Selective symmetrical necrosis of tegmental neuronal aggregates following cardiac arrest. *Arch Pathol* 1969; **88**: 32-41 [PMID: 5793687]
19 **Schneider H**, Ballowitz L, Schachinger H, Hanefeld F, Dröszus JU. Anoxic encephalopathy with predominant involvement of basal ganglia, brain stem and spinal cord in the perinatal period. Report on seven newborns. *Acta Neuropathol* 1975; **32**: 287-298 [PMID: 1180007]
20 **Leech RW**, Alvord EC. Anoxic-ischemic encephalopathy in the human neonatal period. The significance of brain stem involvement. *Arch Neurol* 1977; **34**: 109-113 [PMID: 836361]
21 **Shioda M**, Hayashi M, Takanashi J, Osawa M. Lesions in the central tegmental tract in autopsy cases of developmental brain disorders. *Brain Dev* 2011; **33**: 541-547 [PMID: 20970935 DOI: 10.1016/j.braindev.2010.09.010]
22 **Goyal M**, Versnick E, Tuite P, Cyr JS, Kucharczyk W, Montanera W, Willinsky R, Mikulis D. Hypertrophic olivary degeneration: metaanalysis of the temporal evolution of MR findings. *AJNR Am J Neuroradiol* 2000; **21**: 1073-1077 [PMID: 10871017]
23 **Sarnat HB**. Watershed infarcts in the fetal and neonatal brainstem. An aetiology of central hypoventilation, dysphagia, Möibius syndrome and micrognathia. *Eur J Paediatr Neurol* 2004; **8**: 71-87 [PMID: 15253055]
24 **Leong S**, Ashwell KW. Is there a zone of vascular vulnerability in the fetal brain stem? *Neurotoxicol Teratol* 1997; **19**: 265-275 [PMID: 9253005]
25 **Jensen A**, Garnier Y, Berger R. Dynamics of fetal circulatory responses to hypoxia and asphyxia. *Eur J Obstet Gynecol Reprod Biol* 1999; **84**: 155-172 [PMID: 10428339]
26 **Myers RE**. Two patterns of perinatal brain damage and their conditions of occurrence. *Am J Obstet Gynecol* 1972; **112**: 246-276 [PMID: 4621486]
27 **Sugama S**, Ariga M, Hoashi E, Eto Y. Brainstem cranial-nerve lesions in an infant with hypoxic cerebral injury. *Pediatr Neurol* 2003; **29**: 256-259 [PMID: 14629914]
28 **Saito Y**, Kawashima Y, Kondo A, Chikumaru Y, Matsui A, Nagata I, Ohno K. Dysphagia-gastroesophageal reflux complex: complications due to dysfunction of solitary tract nucleus-mediated vago-vagal reflex. *Neuropediatrics* 2006; **37**: 115-120 [PMID: 16967360]
29 **Hiyane M**, Saito Y, Saito T, Komaki H, Nakagawa E, Sugai K, Sasaki M, Sato N, Yamamoto T, Imai Y. A case of bulbar type cerebral palsy: representative symptoms of dorsal brainstem syndrome. *Brain Dev* 2012; **34**: 787-791 [PMID: 22306266 DOI: 10.1016/j.braindev.2012.01.003]
30 **van der Knaap MS**, Barth PG, Gabreëls FJ, Franzoni E, Begeer JH, Stroink H, Rotteveel JJ, Valk J. A new leukoencephalopathy with vanishing white matter. *Neurology* 1997; **48**: 845-855 [PMID: 9109866]
31 **Tada H**, Takanashi J, Barkovich AJ, Yamamoto S, Kohno Y. Reversible white matter lesion in methionine adenosyltransferase I/III deficiency. *AJNR Am J Neuroradiol* 2004; **25**: 1843-1845 [PMID: 15569761]
32 **Takanashi J**, Kanazawa M, Kohno Y. Central tegmental tract involvement in an infant with 6-pyruvoyltetrahydropterin synthetase deficiency. *AJNR Am J Neuroradiol* 2006; **27**: 584-585 [PMID: 16551996]
33 **Khong PL**, Lam BC, Chung BH, Wong KY, Ooi GC. Diffusion-weighted MR imaging in neonatal nonketotic hyperglycinemia. *AJNR Am J Neuroradiol* 2003; **24**: 1181-1183 [PMID: 12812951]
34 **Sakai Y**, Kira R, Torisu H, Ihara K, Yoshiura T, Hara T. Persistent diffusion abnormalities in the brain stem of three children with mitochondrial diseases. *AJNR Am J Neuroradiol* 2006; **27**: 1924-1926 [PMID: 17032867]
35 **Aguilera-Albesa S**, Poretti A, Honnef D, Aktas M, Yoldi-Petri ME, Huisman TA, Häusler M. T2 hyperintense signal of the central tegmental tracts in children: disease or normal maturational process? *Neuroradiology* 2012; **54**: 863-871 [PMID: 22271318 DOI: 10.1007/s00234-012-1006-z]
36 **Yoshida S**, Hayakawa K, Yamamoto A, Aida N, Okano S, Matsushita H, Kanda T, Yamori Y, Yoshida N, Hirota H. Symmetrical central tegmental tract (CTT) hyperintense lesions on magnetic resonance imaging in children. *Eur Radiol* 2009; **19**: 462-469 [PMID: 18795297 DOI: 10.1007/s00330-008-1167-7]
37 **Jean A**. Brain stem control of swallowing: neuronal network and cellular mechanisms. *Physiol Rev* 2001; **81**: 929-969 [PMID: 11274347]
38 **Matsui K**, Kataoka A, Yamamoto A, Tanoue K, Kurosawa K, Shibasaki J, Ohyama M, Aida N. Clinical characteristics and outcomes of Möbius syndrome in a children's hospital. *Pediatr Neurol* 2014; **51**: 781-789 [PMID: 25306435 DOI: 10.1016/j.pediatrneurol.2014.08.011]
39 **MacKinnon S**, Oystreck DT, Andrews C, Chan WM, Hunter DG, Engle EC. Diagnostic distinctions and genetic analysis of patients diagnosed with moebius syndrome. *Ophthalmology* 2014; **121**: 1461-1468 [PMID: 24612975 DOI: 10.1016/j.ophtha.2014.01.006]
40 **Tomas-Roca L**, Tsaalbi-Shtylik A, Jansen JG, Singh MK, Epstein JA, Altunoglu U, Verzijl H, Soria L, van Beusekom E, Roscioli T, Iqbal Z, Gilissen C, Hoischen A, de Brouwer AP, Erasmus C, Schubert D, Brunner H, Pérez Aytés A, Marin F, Aroca P, Kayserili H, Carta A, de Wind N, Padberg GW, van Bokhoven H. De novo mutations in PLXND1 and REV3L cause Möbius syndrome. *Nat Commun* 2015; **6**: 7199 [PMID: 26068067 DOI: 10.1038/

ncomms8199]
41 **Martinez-Biarge M**, Madero R, González A, Quero J, García-Alix A. Perinatal morbidity and risk of hypoxic-ischemic encephalopathy associated with intrapartum sentinel events. *Am J Obstet Gynecol* 2012; **206**: 148.e1-148.e7 [PMID: 22079054 DOI: 10.1016/j.ajog.2011.09.031]
42 **Slattery J**, Morgan A, Douglas J. Early sucking and swallowing problems as predictors of neurodevelopmental outcome in children with neonatal brain injury: a systematic review. *Dev Med Child Neurol* 2012; **54**: 796-806 [PMID: 22607330 DOI: 10.1111/j.1469-8749.2012.04318.x]
43 **Martinez-Biarge M**, Diez-Sebastian J, Kapellou O, Gindner D, Allsop JM, Rutherford MA, Cowan FM. Predicting motor outcome and death in term hypoxic-ischemic encephalopathy. *Neurology* 2011; **76**: 2055-2061 [PMID: 21670434 DOI: 10.1212/WNL.0b013e31821f442d]
44 **Logitharajah P**, Rutherford MA, Cowan FM. Hypoxic-ischemic encephalopathy in preterm infants: antecedent factors, brain imaging, and outcome. *Pediatr Res* 2009; **66**: 222-229 [PMID: 19390490 DOI: 10.1203/PDR.0b013e3181a9ef34]
45 **Martinez-Biarge M**, Diez-Sebastian J, Wusthoff CJ, Lawrence S, Aloysius A, Rutherford MA, Cowan FM. Feeding and communication impairments in infants with central grey matter lesions following perinatal hypoxic-ischaemic injury. *Eur J Paediatr Neurol* 2012; **16**: 688-696 [PMID: 22658307 DOI: 10.1016/j.ejpn.2012.05.001]

P- Reviewer: Gao BL, Nouh MR, Razek AA, Storto G
S- Editor: Qiu S **L- Editor**: Wang TQ **E- Editor**: Liu SQ

World Journal of Radiology

Submit a Manuscript: http://www.wjgnet.com/esps/
Help Desk: http://www.wjgnet.com/esps/helpdesk.aspx
DOI: 10.4329/wjr.v8.i2.124

World J Radiol 2016 February 28; 8(2): 124-131
ISSN 1949-8470 (online)

TOPIC HIGHLIGHT

2016 Inflammatory Bowel Disease: Global view

Role of imaging in the evaluation of inflammatory bowel disease: How much is too much?

Kelly Haas, Erika Rubesova, Dorsey Bass

Kelly Haas, Dorsey Bass, Department of Gastroenterology, Hepatology, and Nutrition, Lucile Packard Children's Hospital Stanford, Palo Alto, CA 94304, United States

Erika Rubesova, Department of Radiology, Lucile Packard Children's Hospital Stanford, Palo Alto, CA 94304, United States

Author contributions: Haas K performed the literature review and wrote the manuscript with oversight, mentorship, and contribution to the manuscript by Rubesova E and Bass D.

Conflict-of-interest statement: The authors have no conflict of interest to report.

Correspondence to: Dr. Kelly Haas, Department of Gastroenterology, Hepatology, and Nutrition, Lucile Packard Children's Hospital Stanford, 750 Welch Road, Suite 116, Palo Alto, CA 94304, United States. kbhaas@stanford.edu
Telephone: +1-650-7235070
Fax: +1-650-4985608

Received: April 29, 2015
Peer-review started: May 8, 2015
First decision: September 8, 2015
Revised: November 24, 2015
Accepted: January 5, 2016
Article in press: January 7, 2016
Published online: February 28, 2016

Abstract

Inflammatory bowel disease (IBD) is a lifelong condition with waxing and waning disease course that requires reassessment of disease status as well as screening for complications throughout a patient's lifetime. Laboratory testing, endoscopic assessment, and fecal biomarkers are often used in the initial diagnosis and ongoing monitoring of a patient with IBD. Imaging plays an integral role in the diagnosis and evaluation of IBD. Different imaging modalities can be used over the course of a patient's lifetime, from the initial screening and diagnosis of IBD, to determining the extent of intestinal involvement, monitoring for disease activity, and evaluating for complications of uncontrolled IBD. The various imaging modalities available to the provider each have a unique set of risks and benefits when considering cost, radiation exposure, need for anesthesia, and image quality. In this article we review the imaging techniques available for the evaluation of IBD including fluoroscopic small bowel follow-through, computed tomography enterography, magnetic resonance enterography, and transabdominal ultrasound with particular focus on the judicious use of imaging and the risks and benefits of each option. We also review the risks of ionizing radiation, strategies to reduce exposure to ionizing radiation, and current imaging guidelines among pediatric and adult patient with IBD.

Key words: Inflammatory bowel disease; Ultrasound; Fluoroscopy; Magnetic resonance imaging; Computed tomography

Core tip: Imaging plays a key role in the diagnosis and lifelong evaluation of a patient with inflammatory bowel disease (IBD). Several imaging modalities are available, each with a unique set of risks and benefits when considering cost, anesthesia risk in the pediatric population, ionizing radiation, image quality, and availability. In this article, we review the imaging techniques

available for evaluation of IBD, with particular focus on judicious use of ionizing radiation. We also review current imaging guidelines among pediatric and adult patients with IBD.

Haas K, Rubesova E, Bass D. Role of imaging in the evaluation of inflammatory bowel disease: How much is too much? *World J Radiol* 2016; 8(2): 124-131 Available from: URL: http://www.wjgnet.com/1949-8470/full/v8/i2/124.htm DOI: http://dx.doi.org/10.4329/wjr.v8.i2.124

INTRODUCTION

Inflammatory bowel disease (IBD), including Crohn's disease (CD) and ulcerative colitis (UC), is a relapsing and remitting lifelong illness often diagnosed in childhood or early adulthood that is increasing in prevalence. Over 3 million people have inflammatory bowel disease worldwide[1,2]. The prevalence is thought to be as high as 249 per 100000 in North America and 505 per 100000 in Europe[3]. There is a global rise in the incidence of pediatric onset inflammatory bowel disease; approximately 25% of patients with IBD are diagnosed in childhood or adolescence[4,5]. Though the exact etiology of IBD remains unclear, it is thought to be a combination of immune dysregulation, environmental factors, and dysbiosis in a genetically predisposed host.

The diagnosis of IBD involves a detailed history and physical exam, laboratory testing, imaging, and endoscopic evaluation. Serum blood tests, fecal biomarkers, and imaging are important noninvasive tools to distinguish IBD from non-inflammatory conditions with similar clinical presentations. Imaging can be especially helpful in the screening and evaluation of possible IBD to rule out other abdominal pathology. Low cost, limited radiation, and feasibility are particularly important during the screening and evaluation of patients with possible IBD. Previously used imaging techniques such as enteroclysis and nuclear medicine studies (positron emission topography scan or tagged white blood cell scan) have fallen out of favor due to newer cross sectional imaging techniques such as magnetic resonance imaging (MRI) without the risk of ionizing radiation. It can be challenging to identify an imaging modality with sufficient sensitivity while limiting cost and radiation to the patient.

Imaging also plays a pivotal role in monitoring disease activity, determining extent of small bowel involvement, and identifying complications such as abscesses or bowel obstruction. The additional information imaging provides beyond endoscopic assessment may alter therapeutic decisions and impact future disease course. In this review, we will discuss the increasingly important role imaging plays as a noninvasive measure of disease activity in the long term management of IBD patients. We will summarize the different imaging modalities available with an emphasis on the risks and benefits as well as the sensitivity in detecting IBD activity. Lastly, we will review the hazards of ionizing radiation and discuss how this may impact the optimal timing and type of imaging in the best interest of the patient.

TYPES OF IMAGING

Fluoroscopic small bowel follow-through

Small bowel imaging with fluoroscopic barium small bowel follow-through (SBFT) was at one time considered the gold standard in evaluating pediatric IBD and is still used in the initial diagnosis of IBD despite the increasing availability of magnetic resonance enterography (MRE) and computed tomography enterography (CTE). This fluoroscopic study involves drinking barium contrast with serial X-ray images as the contrast progresses through the small intestine to the cecum. SBFT can provide an assessment of the small intestinal luminal anatomy by evaluating for strictures or wall thickening but generally does not provide information on colonic inflammation (Figure 1). SBFT has many benefits including relatively low cost, wide availability, and the ability to complete the study without sedation in the pediatric population. The downsides of SBFT include radiation exposure, length of study, operator dependent quality of images, and lack of extraintestinalevaluation (Table 1). The effective dose of radiation for SBFT in a pediatric patient is estimated to be 1.8-2.2 millisieverts (mSv)[6] with an average effective dose of 5 mSv in the adult population[7], though the actual radiation exposure can increase based on number of films obtained and radiologist technique.

Based on several retrospective studies among pediatric patients with IBD, the sensitivity of SBFT in detecting terminal ileum inflammation using histology as a gold standard is 45%-76% with specificity of 67%-96%[8-10]. A prospective study among adults with newly diagnosed IBD similarly showed the sensitivity and specificity of SBFT detecting terminal ileum inflammation was 67%-72% and 100% respectively[11]. This study found that there was not a statistically significant difference in the sensitivity in detecting terminal ileitis between SBFT, CTE and MRE, but CTE and MRE had significantly greater sensitivity for detection of extraintestinal complications[11]. Overall, SBFT is an imaging technique that has a role in identifying small bowel inflammation given its low cost and ease of performing the study. However, it has been falling out of favor given risks of radiation and improved sensitivity in detecting extraintestinal complications with newer cross sectional imaging techniques.

CTE

CTE was first described in 1997 as a modification of standard abdominal computed tomography (CT) to better evaluate the small bowel in CD[12]. Patients typically drink 1-2 Lofa neutral or low-density oral contrast mixture and receive intravenous (*IV*) contrast during the study to optimize luminal distention and assessment of the bowel wall[13]. Diagnostic criteria for IBD disease

Table 1 Summary of risks and benefits of imaging studies for evaluation of inflammatory bowel disease

Imaging study	Utility	Approximate radiation	Length of study	Pediatric sedation	Relative cost	Contrast	Sensitivity diagnosing IBD	Specificity diagnosing IBD
SBFT	Baseline diagnosis	Pediatric 2 mSv Adult 5 mSv	Total: 1-3 h Scan time: 1 h	None	$	Oral < 1 L	45%-76%[8-10]	67%-100%[8-10]
CTE	Baseline diagnosis, follow-up, contraindication to MRE	Pediatric 3-16 mSv Adult 5-20 mSv	Total: 1 h Scan time: Several minutes	None	$$	Oral 1-2 L, intravenous	84%[23]	95%[23]
MRE	Baseline diagnosis, follow-up, complications of IBD	None	Total: 1-2 h Scan time 1-2 h	Often depending on hospital protocol	$$$	Oral 1-2 L, intravenous	93%[23]	93%[23]
Ultrasound	Screening if low suspicion for IBD, monitoring of disease activity	None	Total: 30-60 min Scan time: 30 min	None	$	Oral < 1 L	90%[23]	96%[23]

SBFT: Small bowel follow through; CTE: Computed tomography enterography; MRE: Magnetic resonance enterography; mSv: Millisieverts; IBD: Inflammatory bowel disease.

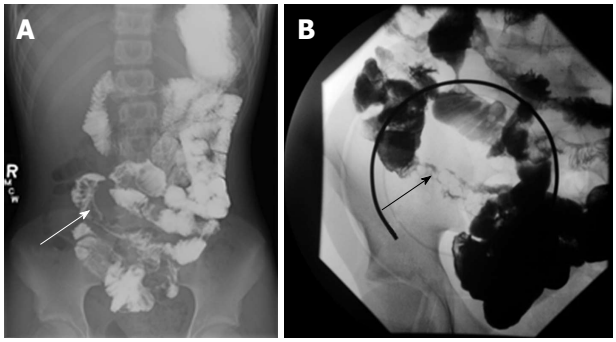

Figure 1 Small bowel follow-through examination in two patients with Crohn's disease. A and B demonstrate mucosal irregularity and luminal narrowing of the terminal ileum (arrows).

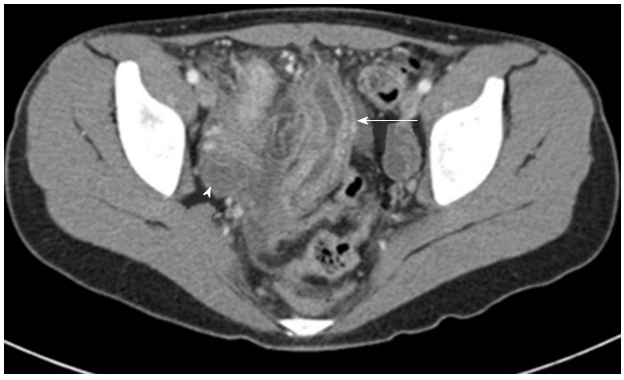

Figure 2 Axial computed tomography image of the pelvis in an adolescent boy with Crohn's disease. It demonstrates bowel wall thickening of the distal small bowel and enhancement of the mucosa (arrow). There is surrounding free fluid (arrowhead).

activity using CTE include bowel wall thickening, bowel hyperemia, submucosal fat deposition, and lymphadenopathy[14,15] (Figure 2). This cross-sectional imaging technique can evaluate for complications of IBD including bowel obstruction, fistula, perforation, or abscess[14,15]. The advantages of CTE include rapid scan time, cross-sectional imaging for evaluation of extraintestinal complications, relatively lower cost compared to MRE, and ability to perform the study without sedation in children (Table 1).

The main disadvantage to CTE is exposure to ionizing radiation, though the need to ingest a large volume of contrast and cost may also be prohibitive. The estimated effective dose of radiation is approximately 10 mSv for standard abdominal CT and 10-20 mSv for CTE in the adult population[7,16]. In the pediatric population, estimated effective doses as low as 2.9-4 mSv have been reported for abdominal CT using multiple detector computed tomography[6] and varied 64-320 detector CT scanners[17]. Newer adaptive iterative dose reduction techniques have been described that greatly reduce the radiation exposure among pediatric patients undergoing CTE from 16.7 milligray (mGy) to 6.1 mGy, with minimal reduction in diagnostic sensitivity and specificity[18]. Similarly, newly proposed CTE imaging techniques using low-dose radiation and noise reduction techniques among adults can reduce effective dose radiation exposure by 53%-60% from 15-20 mSv to 5-7 mSv[19]. Ultimately, effective doses of radiation from abdominal CT and CTE are dependent on protocols at individual institutions and can vary greatly, but promising new techniques may be able to reduce the radiation exposure to levels equivalent to SBFT.

CTE was previously recommended as the imaging study of choice in initial diagnosis and suspected complications of CD among adults and children[20], but it has fallen out of favor as MRE has become more widely available with faster scanning protocols for pediatrics[20-22]. According to a recent meta-analysis,sensitivity and specificity of CTE in diagnosing IBD is 84% and 95% respectively[23], with growing evidence that CTE is more sensitive than SBFT in diagnosing IBD among adults and children[11,24-26]. CTE is useful both in the initial diagnosis of IBD as well as monitoring disease activity and screening for complications over the course of a patient's lifetime. CTE findings including unsuspected penetrating

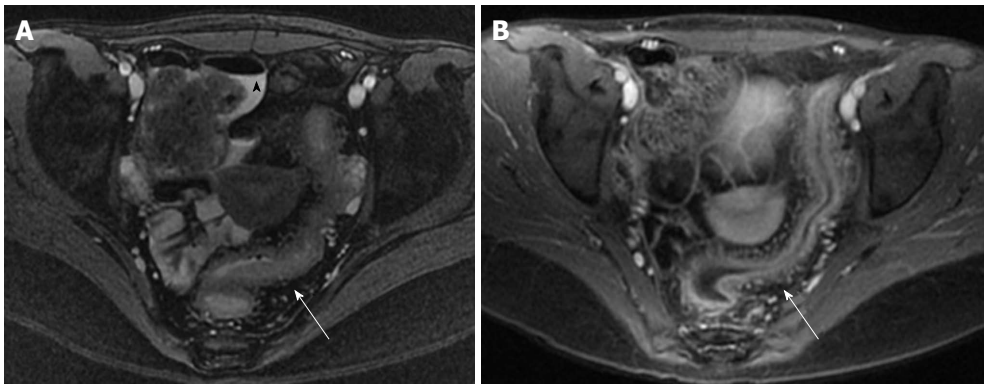

Figure 3 Magnetic resonance enterography study of the pelvis in an adolescent patient with active Crohn's disease. T2 weighted image (A) demonstrating free fluid (arrowhead) and bowel wall thickening (arrow); T1 weighted image (B) with contrast demonstrating enhancement of the bowel and increased mesenteric vascularity (arrow).

disease, fistula, abscess, or stricture have been shown to alter medical management plans in 61% of patients and lead to interventional procedures in 18% of patients with known or suspected CD[27]. CTE remains an instrumental study in diagnosing IBD, monitoring disease activity, and identifying complications; though the risk of ionizing radiation often limits its use to emergency situations when MRE is not feasible.

MRE

MRE has become an increasingly important cross sectional imaging modality in the initial diagnosis of IBD as well as disease activity monitoring. Patients typically drink 1-2 L of a hyper osmolar oral contrast material to distend the bowel lumen, which can be difficult for younger patients and is often not well tolerated. Intravenous gadolinium contrast and spasmolytic medications such as glucagon are often administered during the study[28,29]. The imaging procedure generally takes 1-2 h to complete, and patients must comply with instructions to hold their breath intermittently. Historically, young children undergo anesthesia for this procedure, but newer protocols to reduce scan time, limit oral contrast, and enlist child life team support have made MRE without anesthesia more feasible[30-32]. Signs of active IBD using MRE include bowel wall thickening, increased T2 bowel wall signal, bowel wall hyperemia, and creeping fat[29,33] (Figure 3). The major benefit of MRE is the absence of ionizing radiation.Other advantages include the ability to evaluate extraintestinal manifestations of disease activity and to obtain a dynamic assessment of the bowel with real time imaging sequences. The potential disadvantages of MRE are lack of availability at certain centers, longer scan time with possible need for sedation in younger children, and higher cost than other imaging techniques (Table 1).

MRE is now recommended as the imaging modality of choice for the diagnosis of IBD among children, monitoring disease activity among children and adults, and evaluation of perianal disease among children and adults[20-22]. A meta-analysis of prospective studies shows MRE has a sensitivity of 93% and specificity of 93% in diagnosing IBD[23]. MRE is the preferred study for evaluation of perianal disease and possible fistulas[34,35]. There is not a statistically significant difference between CTE and MRE in diagnostic accuracy for detecting active inflammation in IBD[36]. However, MRE is superior to CTE for differentiating bowel fibrosis from active inflammation (sensitivity 57% and 42%, specificity 82% and 68% respectively)[36]. The addition of diffusion weighted imaging on MRE has been shown to aid in identifying colonic inflammation and improve diagnostic confidence among children with IBD without the need for *IV* contrast[37,38]. Newer techniques such as automated motility mapping analysis can improve the identification of inflammatory lesions among patients with IBD[39]. MRE has also been shown to detect endoscopic remission with 83% accuracy and aphthous ulcer healing with 90% accuracy in a prospective multicenter study[40]. The ability of MRE to confirm the absence of disease rather than to identify inflammation or complications of IBD is novel. Future studies are needed to determine if this imaging modality will play a larger role in noninvasive routine CD monitoring.

Ultrasound

Transabdominal ultrasound is a well-established imaging technique for the evaluation of IBD among children and adolescents; though primarily used in Europe, it is gaining popularity in North America. More recently, intraluminal contrast enhanced ultrasound (SICUS) has been used with improved bowel visualization. It involves drinking a relatively small volume (200-500 mL) of non-absorbable contrast solution approximately 30 min prior to abdominal ultrasound, and the scan time generally takes less than an hour. Conventional ultrasound is typically performed first using a 3.5-5 MHz probe to evaluate for extraintestinal abnormalities; then a high frequency 7.5-17 Hz probe is used to evaluate bowel wall thickness as well as Doppler assessment of blood flow to the intestine[41]. Sonographic evidence of active IBD include bowel wall thickening greater than 3 mm and bowel wall hyperemia[41] (Figure 4). Abdominal ultrasound can also assess for extraintestinal

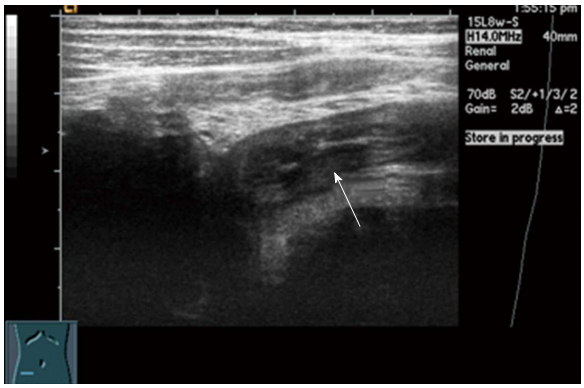

Figure 4 Transabdominal ultrasound in a 12-year-old boy with Crohn's disease. It demonstrates bowel wall thickening of the terminal ileum.

complications such as abscess, lymphadenopathy, or other complications of active IBD such as stricture or fistula. Bowel ultrasound has many advantages including low cost, lack of ionizing radiation, dynamic real-time bowel assessment, and no need for sedation in the pediatric population (Table 1). The potential disadvantage of bowel ultrasound is the need for a skilled operator to provide optimal sensitivity and imaging, which may not be available in all centers.

Ultrasound has been shown to have similar sensitivity and specificity in identifying IBD compared to MRE and CTE[23]. Though most studies use bowel wall thickening greater than 3 mm as a marker of active inflammation, studies have also demonstrated that bowel hyperemia as measured by Doppler blood flow is associated with active bowel inflammation[41,42]. A meta-analysis showed abdominal ultrasound had a sensitivity of 89.7% and a specificity of 95.6% for diagnosing IBD[23]. One group demonstrated 57% sensitivity in detecting undiagnosed CD among adults[43] and 76% sensitivity among undiagnosed children[44] with transabdominal ultrasound. Addition of enteral contrastdemonstrated improved sensitivity to as high as 94% among adults and 100% among children. Further studies are needed to confirm these findings. SICUS has excellent accuracy in diagnosing complications of CD such as stricture, abscess, and fistula compared to surgical findings[45]. Abdominal ultrasound findings have also been shown to correlate with endoscopic severity in moderate to severe UC[46]. Though still an experimental technique, some studies have shown that *IV* microbubble contrast can also be used to better detect vascular density and predict IBD disease activity[47].

Ultrasound is cost-effective, highly accurate in detecting bowel inflammation, and does not involve ionizing radiation or sedation. It is particularly beneficial in the pediatric population and in monitoring disease activity over time given these attributes. The routine use of bowel ultrasound has not been adopted in North America though it is widely used in Europe. There is concern that the diagnostic accuracy is operator dependent, and this may impact the utility in more widespread use.

IONIZING RADIATION

One of the strongest arguments for the prudent use of certain imaging techniques such as SBFT and CTE is the long term risks of ionizing radiation. Much of what we understand about the risks of ionizing radiation comes from studies among atomic bomb survivors.Studies have demonstrated a linear no-threshold relationship between radiation exposure dose and risk of solid tumors; the risk is greatest among those exposed during childhood[48]. Some epidemiological data suggests that cumulative radiation exposure as low as 50 mSv may increase risk of certain solid tumors[49]. A recent study demonstrated multiple CT scans in childhood with cumulative radiation exposure of 50 mSv tripled the relative risk of leukemia and brain cancer[50]. Retrospective data among the pediatric IBD population suggests the average cumulative effective dose (CED) over an extended period of time was 20.5 mSv among children with CD and 11.7 mSv with UC[51]. Retrospective data among adults with IBD estimates CED was 20.1 mSv for patients with CD and 15.1 mSv with UC[52]. Approximately 5.8% of children and 7.1%-13% of adults with IBD had an estimated CED > 50 mSv[51-53]. Children and adults with CD, history of prior surgery, and prednisone use are more likely to have increased radiation exposure[51,52]. Adults with IBD are also at risk for increased radiation exposure within the first year after diagnosis[52].

Strategies for reducing ionizing radiation exposure include limiting unnecessary imaging studies and choosing an imaging modality without ionizing radiation when possible. The use of CT has increased particularly in the emergency department (ED) in the past 10 years[54]. Despite the increasing use of abdominal CT among adults with CD in the ED from 47% of encounters to 78% of encounters over an 8-year period, there was no significant difference in the detection of complications of IBD including perforation, obstruction, or abscess[55]. Alternative imaging techniques without the risk of ionizing radiation such as ultrasound and MRI are preferred in patients who are clinically stable to undergo such evaluation. Imaging forms without ionizing radiation are particularly beneficial among the pediatric population who are at greater risk of the harmful effects of ionizing radiation and have a lifetime of periodic imaging for possible complications of IBD or assessment of disease activity ahead of them.

IMAGING GUIDELINES

There are many clinical scenarios from initial presentation and diagnosis to assessment for disease complications years after diagnosis where imaging is necessary to evaluate a patient with IBD. When considering the potential risks of imaging-including ionizing radiation, cost, and potential need for sedation in the pediatric population-it is prudent to consider the minimum imaging all patients with IBD require. Pediatric and adult guidelines in the United States and Europe recommend

small bowel imaging for any patient with newly diagnosed CD or newly diagnosed UC with atypical endoscopic appearance of colonic inflammation[21,22,56]. It has been proposed that ultrasound or MRE are the preferred imaging modalities in pediatric patients with suspected IBD; MRE or CTE are recommended for complete assessment of the small bowel in newly diagnosed pediatric patients with IBD; and MRE is the modality of choice for assessment of complications of IBD[56]. Adult and pediatric European guidelines recommend MRE as the imaging modality of choice for assessment of the small bowel in newly diagnosed CD or atypical UC as well as for monitoring therapeutic response and screening for complications of IBD[21,22]. There are no evidence-based guidelines currently that describe the minimum necessary frequency of abdominal imaging in IBD.Studies have shown MRE to be accurate in detecting mucosal healing and therapeutic response[40], but it remains unclear what the optimal interval for repeat imaging may be and how to implement in clinical practice.

CONCLUSION

Imaging plays a pivotal role in the diagnosis and ongoing evaluation of IBD activity over the course of a patient's life. Noninvasive imaging techniques without ionizing radiation such as ultrasound and MRE are likely to become increasingly important in monitoring for disease activity. This may be particularly true for the growing pediatric IBD population given concerns for potential risks of repeated anesthesia and invasive procedures to assess for disease activity during childhood. No imaging modality is perfect, but each option has a potential role in the evaluation of IBD. It is the clinician's responsibility to weigh the risks and benefits in each unique clinical scenario while considering patient stability, availability, and what information is needed. We advocate for the judicious use of imaging studies that require ionizing radiation, and to consider an alternative method of evaluation when possible.

REFERENCES

1 **Ananthakrishnan AN**. Epidemiology and risk factors for IBD. *Nat Rev Gastroenterol Hepatol* 2015; **12**: 205-217 [PMID: 25732745 DOI: 10.1038/nrgastro.2015.34]

2 **Cosnes J**, Gower-Rousseau C, Seksik P, Cortot A. Epidemiology and natural history of inflammatory bowel diseases. *Gastroenterology* 2011; **140**: 1785-1794 [PMID: 21530745 DOI: 10.1053/j.gastro.2011.01.055]

3 **Molodecky NA**, Soon IS, Rabi DM, Ghali WA, Ferris M, Chernoff G, Benchimol EI, Panaccione R, Ghosh S, Barkema HW, Kaplan GG. Increasing incidence and prevalence of the inflammatory bowel diseases with time, based on systematic review. *Gastroenterology* 2012; **142**: 46-54.e42; quiz e30 [PMID: 22001864 DOI: 10.1053/j.gastro.2011.10.001]

4 **Benchimol EI**, Fortinsky KJ, Gozdyra P, Van den Heuvel M, Van Limbergen J, Griffiths AM. Epidemiology of pediatric inflammatory bowel disease: a systematic review of international trends. *Inflamm Bowel Dis* 2011; **17**: 423-439 [PMID: 20564651 DOI: 10.1002/ibd.21349]

5 **Abraham BP**, Mehta S, El-Serag HB. Natural history of pediatric-onset inflammatory bowel disease: a systematic review. *J Clin Gastroenterol* 2012; **46**: 581-589 [PMID: 22772738 DOI: 10.1097/MCG.0b013e318247c32f]

6 **Gaca AM**, Jaffe TA, Delaney S, Yoshizumi T, Toncheva G, Nguyen G, Frush DP. Radiation doses from small-bowel follow-through and abdomen/pelvis MDCT in pediatric Crohn disease. *Pediatr Radiol* 2008; **38**: 285-291 [PMID: 18183380 DOI: 10.1007/s00247-007-0702-z]

7 **Mettler FA**, Huda W, Yoshizumi TT, Mahesh M. Effective doses in radiology and diagnostic nuclear medicine: a catalog. *Radiology* 2008; **248**: 254-263 [PMID: 18566177 DOI: 10.1148/radiol.2481071451]

8 **Batres LA**, Maller ES, Ruchelli E, Mahboubi S, Baldassano RN. Terminal ileum intubation in pediatric colonoscopy and diagnostic value of conventional small bowel contrast radiography in pediatric inflammatory bowel disease. *J Pediatr Gastroenterol Nutr* 2002; **35**: 320-323 [PMID: 12352520 DOI: 10.1097/00005176-200209000-00015]

9 **Giles E**, Barclay AR, Chippington S, Wilson DC. Systematic review: MRI enterography for assessment of small bowel involvement in paediatric Crohn's disease. *Aliment Pharmacol Ther* 2013; **37**: 1121-1131 [PMID: 23638954 DOI: 10.1111/apt.12323]

10 **Stenerson M**, Vittinghoff E, Heyman MB, Kim GE, Gupta N. Role of small bowel follow-through in diagnosing inflammation of the terminal ileum in pediatric patients. *J Pediatr Gastroenterol Nutr* 2010; **51**: 433-436 [PMID: 20562720 DOI: 10.1097/MPG.0b013e3181d67ea7]

11 **Lee SS**, Kim AY, Yang SK, Chung JW, Kim SY, Park SH, Ha HK. Crohn disease of the small bowel: comparison of CT enterography, MR enterography, and small-bowel follow-through as diagnostic techniques. *Radiology* 2009; **251**: 751-761 [PMID: 19276325 DOI: 10.1148/radiol.2513081184]

12 **Raptopoulos V**, Schwartz RK, McNicholas MM, Movson J, Pearlman J, Joffe N. Multiplanar helical CT enterography in patients with Crohn's disease. *AJR Am J Roentgenol* 1997; **169**: 1545-1550 [PMID: 9393162 DOI: 10.2214/ajr.169.6.9393162]

13 **Ilangovan R**, Burling D, George A, Gupta A, Marshall M, Taylor SA. CT enterography: review of technique and practical tips. *Br J Radiol* 2012; **85**: 876-886 [PMID: 22553291 DOI: 10.1259/bjr/27973476]

14 **Gore RM**, Balthazar EJ, Ghahremani GG, Miller FH. CT features of ulcerative colitis and Crohn's disease. *AJR Am J Roentgenol* 1996; **167**: 3-15 [PMID: 8659415 DOI: 10.2214/ajr.167.1.8659415]

15 **Duigenan S**, Gee MS. Imaging of pediatric patients with inflammatory bowel disease. *AJR Am J Roentgenol* 2012; **199**: 907-915 [PMID: 22997386 DOI: 10.2214/AJR.11.7966]

16 **Swanson G**, Behara R, Braun R, Keshavarzian A. Diagnostic medical radiation in inflammatory bowel disease: how to limit risk and maximize benefit. *Inflamm Bowel Dis* 2013; **19**: 2501-2508 [PMID: 23792551 DOI: 10.1097/MIB.0b013e31828dc6b6]

17 **Johnston JH**, Podberesky DJ, Yoshizumi TT, Angel E, Toncheva G, Larson DB, Egelhoff JC, Anderson-Evans C, Nguyen GB, Barelli A, Alsip C, Salisbury SR, Frush DP. Comparison of radiation dose estimates, image noise, and scan duration in pediatric body imaging for volumetric and helical modes on 320-detector CT and helical mode on 64-detector CT. *Pediatr Radiol* 2013; **43**: 1117-1127 [PMID: 23636537 DOI: 10.1007/s00247-013-2690-5]

18 **Wallihan DB**, Podberesky DJ, Sullivan J, Denson LA, Zhang B, Salisbury SR, Towbin AJ. Diagnostic Performance and Dose Comparison of Filtered Back Projection and Adaptive Iterative Dose Reduction Three-dimensional CT Enterography in Children and Young Adults. *Radiology* 2015; **276**: 233-242 [PMID: 25654668 DOI: 10.1148/radiol.14140468]

19 **Del Gaizo AJ**, Fletcher JG, Yu L, Paden RG, Spencer GC, Leng S, Silva AM, Fidler JL, Silva AC, Hara AK. Reducing radiation dose in CT enterography. *Radiographics* 2013; **33**: 1109-1124 [PMID: 23842974 DOI: 10.1148/rg.334125074]

20 **Huprich JE**, Rosen MP, Fidler JL, Gay SB, Grant TH, Greene FL, Lalani T, Miller FH, Rockey DC, Sudakoff GS, Gunderman R, Coley BD. ACR Appropriateness Criteria on Crohn's disease. *J Am Coll Radiol* 2010; **7**: 94-102 [PMID: 20142082 DOI: 10.1016/j.jacr.2009.10.009]

21 **Levine A**, Koletzko S, Turner D, Escher JC, Cucchiara S, de Ridder L, Kolho KL, Veres G, Russell RK, Paerregaard A, Buderus S, Greer ML, Dias JA, Veereman-Wauters G, Lionetti P, Sladek M, Martin de Carpi J, Staiano A, Ruemmele FM, Wilson DC; European Society of Pediatric Gastroenterology, Hepatology, and Nutrition. ESPGHAN revised porto criteria for the diagnosis of inflammatory bowel disease in children and adolescents. *J Pediatr Gastroenterol Nutr* 2014; **58**: 795-806 [PMID: 24231644]

22 **Panes J**, Bouhnik Y, Reinisch W, Stoker J, Taylor SA, Baumgart DC, Danese S, Halligan S, Marincek B, Matos C, Peyrin-Biroulet L, Rimola J, Rogler G, van Assche G, Ardizzone S, Ba-Ssalamah A, Bali MA, Bellini D, Biancone L, Castiglione F, Ehehalt R, Grassi R, Kucharzik T, Maccioni F, Maconi G, Magro F, Martín-Comín J, Morana G, Pendsé D, Sebastian S, Signore A, Tolan D, Tielbeek JA, Weishaupt D, Wiarda B, Laghi A. Imaging techniques for assessment of inflammatory bowel disease: joint ECCO and ESGAR evidence-based consensus guidelines. *J Crohns Colitis* 2013; **7**: 556-585 [PMID: 23583097 DOI: 10.1016/j.crohns.2013.02.020]

23 **Horsthuis K**, Bipat S, Bennink RJ, Stoker J. Inflammatory bowel disease diagnosed with US, MR, scintigraphy, and CT: meta-analysis of prospective studies. *Radiology* 2008; **247**: 64-79 [PMID: 18372465 DOI: 10.1148/radiol.2471070611]

24 **Hara AK**, Leighton JA, Heigh RI, Sharma VK, Silva AC, De Petris G, Hentz JG, Fleischer DE. Crohn disease of the small bowel: preliminary comparison among CT enterography, capsule endoscopy, small-bowel follow-through, and ileoscopy. *Radiology* 2006; **238**: 128-134 [PMID: 16373764 DOI: 10.1148/radiol.2381050296]

25 **Wold PB**, Fletcher JG, Johnson CD, Sandborn WJ. Assessment of small bowel Crohn disease: noninvasive peroral CT enterography compared with other imaging methods and endoscopy--feasibility study. *Radiology* 2003; **229**: 275-281 [PMID: 12944602 DOI: 10.1148/radiol.2291020877]

26 **Jamieson DH**, Shipman PJ, Israel DM, Jacobson K. Comparison of multidetector CT and barium studies of the small bowel: inflammatory bowel disease in children. *AJR Am J Roentgenol* 2003; **180**: 1211-1216 [PMID: 12704025 DOI: 10.2214/ajr.180.5.1801211]

27 **Booya F**, Akram S, Fletcher JG, Huprich JE, Johnson CD, Fidler JL, Barlow JM, Solem CA, Sandborn WJ, Loftus EV. CT enterography and fistulizing Crohn's disease: clinical benefit and radiographic findings. *Abdom Imaging* 2009; **34**: 467-475 [PMID: 18551336 DOI: 10.1007/s00261-008-9419-1]

28 **Mollard BJ**, Smith EA, Dillman JR. Pediatric MR enterography: technique and approach to interpretation-how we do it. *Radiology* 2015; **274**: 29-43 [PMID: 25531478 DOI: 10.1148/radiol.14122449]

29 **Anupindi SA**, Terreblanche O, Courtier J. Magnetic resonance enterography: inflammatory bowel disease and beyond. *Magn Reson Imaging Clin N Am* 2013; **21**: 731-750 [PMID: 24183523 DOI: 10.1016/j.mric.2013.05.002]

30 **Courtier J**, Cardenas A, Tan C, Towne M, Rhee SJ, Heyman M, MacKenzie JD. Non-Anesthesia MR Enterography in Very Young Children-Feasibility, Technique and Performance. *J Pediatr Gastroenterol Nutr* 2015; Epub ahead of print [PMID: 25564800 DOI: 10.1097/MPG.0000000000000712]

31 **McGee K**. The role of a child life specialist in a pediatric radiology department. *Pediatr Radiol* 2003; **33**: 467-474 [PMID: 12819835]

32 **MacKenzie JD**, Vasanawala SS. Advances in pediatric MR imaging. *Magn Reson Imaging Clin N Am* 2008; **16**: 385-402, v [PMID: 18585595 DOI: 10.1016/j.mric.2008.04.008]

33 **Mentzel HJ**, Reinsch S, Kurzai M, Stenzel M. Magnetic resonance imaging in children and adolescents with chronic inflammatory bowel disease. *World J Gastroenterol* 2014; **20**: 1180-1191 [PMID: 24574794 DOI: 10.3748/wjg.v20.i5.1180]

34 **Towbin AJ**, Sullivan J, Denson LA, Wallihan DB, Podberesky DJ. CT and MR enterography in children and adolescents with inflammatory bowel disease. *Radiographics* 2013; **33**: 1843-1860 [PMID: 24224581 DOI: 10.1148/rg.337105140]

35 **Koelbel G**, Schmiedl U, Majer MC, Weber P, Jenss H, Kueper K, Hess CF. Diagnosis of fistulae and sinus tracts in patients with Crohn disease: value of MR imaging. *AJR Am J Roentgenol* 1989; **152**: 999-1003 [PMID: 2705359 DOI: 10.2214/ajr.152.5.999]

36 **Quencer KB**, Nimkin K, Mino-Kenudson M, Gee MS. Detecting active inflammation and fibrosis in pediatric Crohn's disease: prospective evaluation of MR-E and CT-E. *Abdom Imaging* 2013; **38**: 705-713 [PMID: 23361877 DOI: 10.1007/s00261-013-9981-z]

37 **Kinner S**, Blex S, Maderwald S, Forsting M, Gerken G, Lauenstein TC. Addition of diffusion-weighted imaging can improve diagnostic confidence in bowel MRI. *Clin Radiol* 2014; **69**: 372-377 [PMID: 24360512 DOI: 10.1016/j.crad.2013.09.022]

38 **Sirin S**, Kathemann S, Schweiger B, Hahnemann ML, Forsting M, Lauenstein TC, Kinner S. Magnetic resonance colonography including diffusion-weighted imaging in children and adolescents with inflammatory bowel disease: do we really need intravenous contrast? *Invest Radiol* 2015; **50**: 32-39 [PMID: 25215934 DOI: 10.1097/RLI.0000000000000092]

39 **Hahnemann ML**, Nensa F, Kinner S, Maderwald S, Umutlu L, Gerken G, Lauenstein TC. Improved detection of inflammatory bowel disease by additional automated motility analysis in magnetic resonance imaging. *Invest Radiol* 2015; **50**: 67-72 [PMID: 25260093 DOI: 10.1097/RLI.0000000000000097]

40 **Ordás I**, Rimola J, Rodríguez S, Paredes JM, Martínez-Pérez MJ, Blanc E, Arévalo JA, Aduna M, Andreu M, Radosevic A, Ramírez-Morros AM, Pinó S, Gallego M, Jauregui-Amezaga A, Ricart E, Panés J. Accuracy of magnetic resonance enterography in assessing response to therapy and mucosal healing in patients with Crohn's disease. *Gastroenterology* 2014; **146**: 374-82.e1 [PMID: 24177375 DOI: 10.1053/j.gastro.2013.10.055]

41 **Strobel D**, Goertz RS, Bernatik T. Diagnostics in inflammatory bowel disease: ultrasound. *World J Gastroenterol* 2011; **17**: 3192-3197 [PMID: 21912467 DOI: 10.3748/wjg.v17.i27.3192]

42 **Drews BH**, Barth TF, Hänle MM, Akinli AS, Mason RA, Muche R, Thiel R, Pauls S, Klaus J, von Boyen G, Kratzer W. Comparison of sonographically measured bowel wall vascularity, histology, and disease activity in Crohn's disease. *Eur Radiol* 2009; **19**: 1379-1386 [PMID: 19184036 DOI: 10.1007/s00330-008-1290-5]

43 **Pallotta N**, Tomei E, Viscido A, Calabrese E, Marcheggiano A, Caprilli R, Corazziari E. Small intestine contrast ultrasonography: an alternative to radiology in the assessment of small bowel disease. *Inflamm Bowel Dis* 2005; **11**: 146-153 [PMID: 15677908 DOI: 10.1097/00054725-200502000-00008]

44 **Pallotta N**, Civitelli F, Di Nardo G, Vincoli G, Aloi M, Viola F, Capocaccia P, Corazziari E, Cucchiara S. Small intestine contrast ultrasonography in pediatric Crohn's disease. *J Pediatr* 2013; **163**: 778-784.e1 [PMID: 23623514 DOI: 10.1016/j.jpeds.2013.03.056]

45 **Pallotta N**, Vincoli G, Montesani C, Chirletti P, Pronio A, Caronna R, Ciccantelli B, Romeo E, Marcheggiano A, Corazziari E. Small intestine contrast ultrasonography (SICUS) for the detection of small bowel complications in crohn's disease: a prospective comparative study versus intraoperative findings. *Inflamm Bowel Dis* 2012; **18**: 74-84 [PMID: 21438095 DOI: 10.1002/ibd.21678]

46 **Parente F**, Molteni M, Marino B, Colli A, Ardizzone S, Greco S, Sampietro G, Foschi D, Gallus S. Are colonoscopy and bowel ultrasound useful for assessing response to short-term therapy and predicting disease outcome of moderate-to-severe forms of ulcerative colitis?: a prospective study. *Am J Gastroenterol* 2010; **105**: 1150-1157 [PMID: 19997096 DOI: 10.1038/ajg.2009.672]

47 **Romanini L**, Passamonti M, Navarria M, Lanzarotto F, Villanacci V, Grazioli L, Calliada F, Maroldi R. Quantitative analysis of contrast-enhanced ultrasonography of the bowel wall can predict disease activity in inflammatory bowel disease. *Eur J Radiol* 2014; **83**: 1317-1323 [PMID: 24908589 DOI: 10.1016/j.ejrad.2014.05.012]

48 **Preston DL**, Shimizu Y, Pierce DA, Suyama A, Mabuchi K. Studies of mortality of atomic bomb survivors. Report 13: Solid cancer and noncancer disease mortality: 1950-1997. *Radiat Res* 2003; **160**: 381-407 [PMID: 12968934 DOI: 10.1667/rr3049]

49 **Brenner DJ**, Doll R, Goodhead DT, Hall EJ, Land CE, Little JB, Lubin JH, Preston DL, Preston RJ, Puskin JS, Ron E, Sachs RK, Samet JM, Setlow RB, Zaider M. Cancer risks attributable to low

doses of ionizing radiation: assessing what we really know. *Proc Natl AcadSci USA* 2003; **100**: 13761-13766 [PMID: 14610281 DOI: 10.1073/pnas.2235592100]

50 **Pearce MS**, Salotti JA, Little MP, McHugh K, Lee C, Kim KP, Howe NL, Ronckers CM, Rajaraman P, Sir Craft AW, Parker L, Berrington de González A. Radiation exposure from CT scans in childhood and subsequent risk of leukaemia and brain tumours: a retrospective cohort study. *Lancet* 2012; **380**: 499-505 [PMID: 22681860 DOI: 10.1016/S0140-6736(12)60815-0]

51 **Fuchs Y**, Markowitz J, Weinstein T, Kohn N, Choi-Rosen J, Levine J. Pediatric inflammatory bowel disease and imaging-related radiation: are we increasing the likelihood of malignancy? *J Pediatr Gastroenterol Nutr* 2011; **52**: 280-285 [PMID: 21297507]

52 **Levi Z**, Fraser E, Krongrad R, Hazazi R, benjaminov O, meyerovitch J, Tal OB, Choen A, Niv Y, Fraser G. Factors associated with radiation exposure in patients with inflammatory bowel disease. *Aliment Pharmacol Ther* 2009; **30**: 1128-1136 [PMID: 19899197 DOI: 10.1111/j.1365-2036.2009.04140.x]

53 **Hou JK**, Malaty HM, Thirumurthi S. Radiation exposure from diagnostic imaging studies among patients with inflammatory bowel disease in a safety-net health-care system. *Dig Dis Sci* 2014; **59**: 546-553 [PMID: 24026402 DOI: 10.1007/s10620-013-2852-1]

54 **Kocher KE**, Meurer WJ, Fazel R, Scott PA, Krumholz HM, Nallamothu BK. National trends in use of computed tomography in the emergency department. *Ann Emerg Med* 2011; **58**: 452-62.e3 [PMID: 21835499 DOI: 10.1016/j.annemergmed.2011.05.020]

55 **Kerner C**, Carey K, Mills AM, Yang W, Synnestvedt MB, Hilton S, Weiner MG, Lewis JD. Use of abdominopelvic computed tomography in emergency departments and rates of urgent diagnoses in Crohn's disease. *Clin Gastroenterol Hepatol* 2012; **10**: 52-57 [PMID: 21946122 DOI: 10.1016/j.cgh.2011.09.005]

56 **Anupindi SA**, Grossman AB, Nimkin K, Mamula P, Gee MS. Imaging in the evaluation of the young patient with inflammatory bowel disease: what the gastroenterologist needs to know. *J Pediatr Gastroenterol Nutr* 2014; **59**: 429-439 [PMID: 24979661 DOI: 10.1097/MPG.0000000000000475]

P- Reviewer: Sipahi AM **S- Editor**: Gong ZM
L- Editor: A **E- Editor**: Liu SQ

World Journal of Radiology

Submit a Manuscript: http://www.wjgnet.com/esps/
Help Desk: http://www.wjgnet.com/esps/helpdesk.aspx
DOI: 10.4329/wjr.v8.i2.132

World J Radiol 2016 February 28; 8(2): 132-141
ISSN 1949-8470 (online)

REVIEW

Multi-modality imaging review of congenital abnormalities of kidney and upper urinary tract

Subramaniyan Ramanathan, Devendra Kumar, Maneesh Khanna, Mahmoud Al Heidous, Adnan Sheikh, Vivek Virmani, Yegu Palaniappan

Subramaniyan Ramanathan, Devendra Kumar, Maneesh Khanna, Mahmoud Al Heidous, Department of Clinical Imaging, Al-Wakra Hospital, Hamad Medical Corporation, Doha, Qatar

Adnan Sheikh, Department of Medical Imaging, the Ottawa Hospital, Ottawa, K1Y 4E9, Canada

Vivek Virmani, Department of Radiology, Dr. Everett Chalmers Hospital, Fredericton, NB E3B 5N5, Canada

Yegu Palaniappan, Shree Meenakshi Multi Specialty Hospital, Pudukottai 622001, India

Author contributions: All authors equally contributed to this paper with conception and design of the study, literature review and analysis, drafting and critical revision and editing, and final approval of the final version.

Conflict-of-interest statement: No potential conflicts of interest.

Correspondence to: Dr. Subramaniyan Ramanathan, MD, DNB, Consultant, Department of Clinical Imaging, Al-Wakra Hospital, Hamad Medical Corporation, PO Box 82228, Doha, Qatar. rm_subbu2000@yahoo.com
Telephone: +974-50117935
Fax: +974-40114509

Received: August 26, 2015
Peer-review started: August 30, 2015
First decision: September 28, 2015
Revised: October 21, 2015
Accepted: December 18, 2015
Article in press: December 20, 2015

Published online: February 28, 2016

Abstract

Congenital abnormalities of the kidney and urinary tract (CAKUT) include a wide range of abnormalities ranging from asymptomatic ectopic kidneys to life threatening renal agenesis (bilateral). Many of them are detected in the antenatal or immediate postnatal with a significant proportion identified in the adult population with varying degree of severity. CAKUT can be classified on embryological basis in to abnormalities in the renal parenchymal development, aberrant embryonic migration and abnormalities of the collecting system. Renal parenchymal abnormalities include multi cystic dysplastic kidneys, renal hypoplasia, number (agenesis or supernumerary), shape and cystic renal diseases. Aberrant embryonic migration encompasses abnormal location and fusion anomalies. Collecting system abnormalities include duplex kidneys and Pelvi ureteric junction obstruction. Ultrasonography (US) is typically the first imaging performed as it is easily available, non-invasive and radiation free used both antenatally and postnatally. Computed tomography (CT) and magnetic resonance imaging (MRI) are useful to confirm the ultrasound detected abnormality, detection of complex malformations, demonstration of collecting system and vascular anatomy and more importantly for early detection of complications like renal calculi, infection and malignancies. As CAKUT are one of the leading causes of end stage renal disease, it is important for the radiologists to be familiar with the varying imaging appearances of CAKUT on US, CT and MRI, thereby helping in prompt diagnosis and optimal management.

Key words: Congenital abnormalities; Kidney; Urinary tract; Multi cystic dysplastic kidneys; Pelvi ureteric junction obstruction; Computed tomography urography;

Congenital abnormalities of the kidney and urinary tract; End stage renal disease; Horse shoe kidneys

Core tip: Congenital abnormalities of the kidney and urinary tract (CAKUT) are one of the leading causes of end stage renal disease. They can be classified on embryological basis in to three major categories: (1) abnormalities in the renal parenchymal development; (2) aberrant embryonic migration; and (3) abnormalities of the collecting system. Ultrasonography, computed tomography and magnetic resonance imaging are the primary imaging modalities used in the detection of various CAKUT. Clinical features vary widely depending on the type, severity and laterality of renal anomaly. Timely diagnosis is crucial in selected anomalies to minimize renal damage, prevent or delay the onset of end stage renal disease (ESRD), and provide supportive care to avoid complications of ESRD.

Ramanathan S, Kumar D, Khanna M, Al Heidous M, Sheikh A, Virmani V, Palaniappan Y. Multi-modality imaging review of congenital abnormalities of kidney and upper urinary tract. *World J Radiol* 2016; 8(2): 132-141 Available from: URL: http://www.wjgnet.com/1949-8470/full/v8/i2/132.htm DOI: http://dx.doi.org/10.4329/wjr.v8.i2.132

INTRODUCTION

Congenital abnormalities of the kidney and urinary tract occur in 3-6 per 1000 live births and is the leading cause of end-stage renal disease (ESRD) in children and also cause subsequent renal problems in adulthood like stone formation, infection, hypertension, and renal failure[1]. The North American Pediatric Renal Trials and Collaborative Studies report indicated that 30% to 50% of cases of ESRD are related to congenital anomalies of the kidney and the urinary tract[2]. Therefore, it is crucial to have early diagnosis and management, whether medical or surgical, to minimize renal damage and to avoid or delay end-stage renal damage. Imaging helps in the early diagnosis, follow-up, surgical planning, detection of complications and associated renal and extra renal malformations. This review summarizes the various congenital anomalies of kidneys and upper urinary tract, their embryological basis, clinical presentation, imaging features and complications.

RELEVANT EMBRYOLOGY

The kidneys develop from three structures which succeed each other: The pronephros and the mesonephric and metanephric ducts. Pronephros is the most immature form of kidney and develops from intermediate mesoderm towards the end of 3rd week of gestation. It is non-functional in human beings and regresses by 4th week leaving no adult lineage and replaced by mesonephros which later forms the portion of the male and female genital tracts. The kidneys develop during the 4th week of gestation by the union of the ureteric bud with the metanephric mass of intermediate mesoderm at the level of the first or second sacral segment. The kidneys initially lie close to each other with the hila directed anteriorly in the pelvis. During 4th to 8th weeks of gestation both kidneys gradually ascend to the lumbar region moving further apart from each other and rotate medially almost 90 degrees with the hila now facing anteromedially[3,4].

CLASSIFICATION

Congenital anomalies of the kidneys can be classified on embryological basis in to abnormalities in the renal parenchymal development, aberrant embryonic migration and abnormalities of the collecting system[5]. Renal parenchymal abnormalities include multi cystic dysplastic kidneys (MCDK), renal hypoplasia, number (agenesis or supernumary), shape and cystic renal diseases. Aberrant embryonic migration encompasses abnormal location and fusion anomalies. Collecting system abnormalities include duplex kidneys and Pelvi ureteric junction obstruction (PUJO). We have included only upper urinary system anomalies in this review.

CLINICAL PRESENTATION AND IMAGING APPROACH

Clinical features vary widely depending on the type, severity and laterality of renal anomaly. Many of them like hypoplasia, ectopic kidneys, and anomalies in shape can be asymptomatic and detected incidentally in adults. Others like renal agenesis, MCDK, bilateral PUJO and cystic renal diseases can present early either antenatally with oligohydramnios or later with urinary tract infection, hypertension, proteinuria, renal impairment, abdominal mass, hematuria or stones[6].

Antenatal screening ultrasonography (US) allows demonstration of fetal kidneys and urinary bladder from early second trimester and enables to detect a number of major congenital anomalies of the urinary system. The ultrasound examination of the normal urinary tract consists of the assessment of the presence, location and size of both kidneys and the evaluation of their structure and echogenicity. Evaluation of fetal bladder, external genitalia and the amount of amniotic fluid compliments the examination. Abnormalities detected in antenatal US include hydronephrosis, hydroureter, thickened bladder, cystic kidney, small or dysplastic kidney and absent kidney. Antenatal detection of renal abnormalities warrants postnatal physical examination and postnatal renal ultrasound soon after birth and again at 4-6 wk of age[5,7].

Cross sectional imaging include computed tomo-

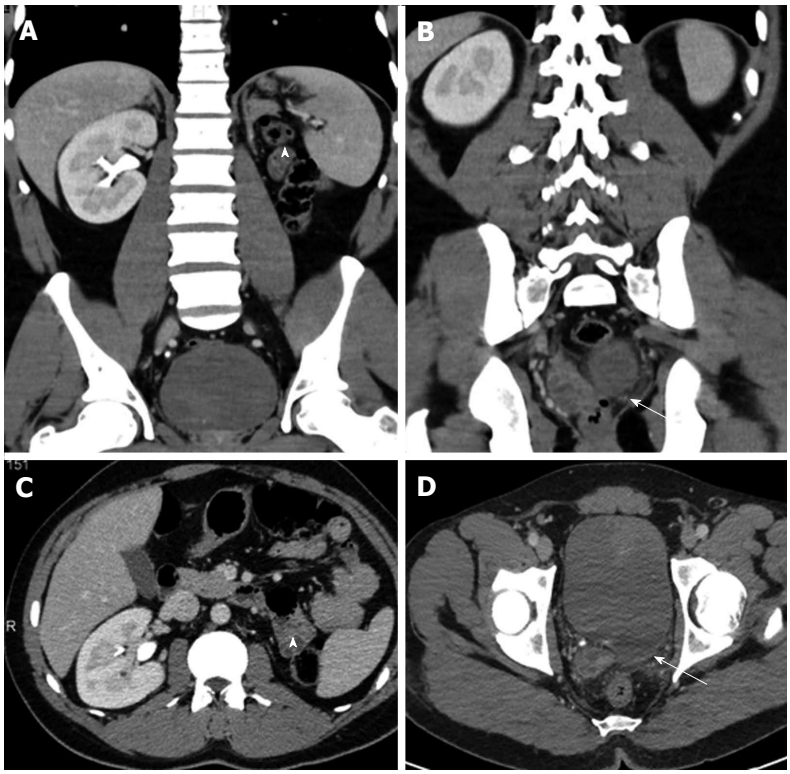

Figure 1 A 35-year-old man with left renal agenesis. Coronal (A and B) and axial (C and D) contrast enhanced CT shows absent left kidney (arrowhead) and absent left seminal vesicle (arrow). CT: Computed tomography.

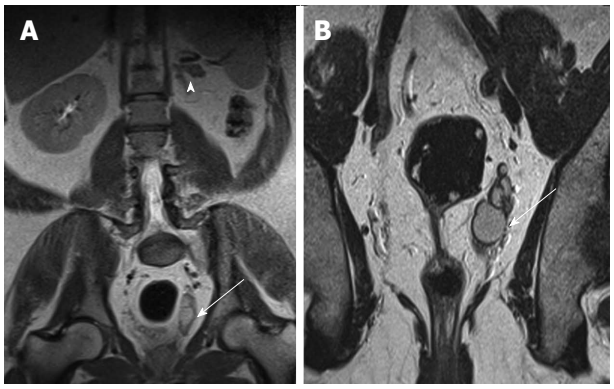

Figure 2 A 40-year-old man with left renal agenesis. Coronal T2W magnetic resonance imaging abdomen (A) and pelvis (B) shows absent left kidney (arrowhead) and left seminal vesicle cyst (arrow).

graphy (CT) and magnetic resonance imaging (MRI) help in resolving the complex anatomy, ectopic kidneys not detected on US, duplex collecting system, preoperative evaluation in PUJO and to look for complications like pyelonephritis, renal stones, and malignancies. Non contrast CT can detect renal stones and nephrocalcinosis. CT urography is useful in duplex system, their complex course, distal opening and associated other genitourinary malformations. MRI has the advantages of lack of ionizing radiation, better soft tissue contrast and detection of collecting system abnormalities even without contrast[8]. Disadvantage is requirement of sedation in small children, cost and availability[3,9,10].

RENAL PARENCHYMAL MALFORMATION

Anomalies in number

Renal agenesis: Complete absence of one or both kidneys indicates renal agenesis. It thought to result from a lack of induction of the metanephric blastema by the ureteral bud. Bilateral agenesis is incompatible with life and is associated with pulmonary hypoplasia and limb defects. Unilateral renal agenesis is not uncommon, seen in 1/1300 pregnancies[11]. It is often asymptomatic and compensatory hypertrophy in other kidney may cause glomerulosclerosis in adults. Unilateral renal agenesis is often incidentally detected in adults in US or CT performed for other reasons. Associated abnormalities can be seen like ipsilateral seminal vesicle cyst, ipsilateral absence of seminal vesicle or mullerian abnormalities[12,13] (Figures 1 and 2).

Supernumary kidneys: A supernumerary kidney is an uncommon urogenital anomaly with less than 100 cases reported in the literature. In this one or more accessory kidneys are seen often on the left and caudal to the native kidney. Mostly the accessory kidney is smaller in size with reduced function. It can be detected on US, CT, MRI and Nuclear Medicine studies like dimercaptosuccinic acid (DMSA) and diethylene triamine pentaacetic acid (DTPA) scans. US is useful in the morphological characterisation while the rest aid in functional assessment. Supernumary kidneys commonly have associated various urogenital and non

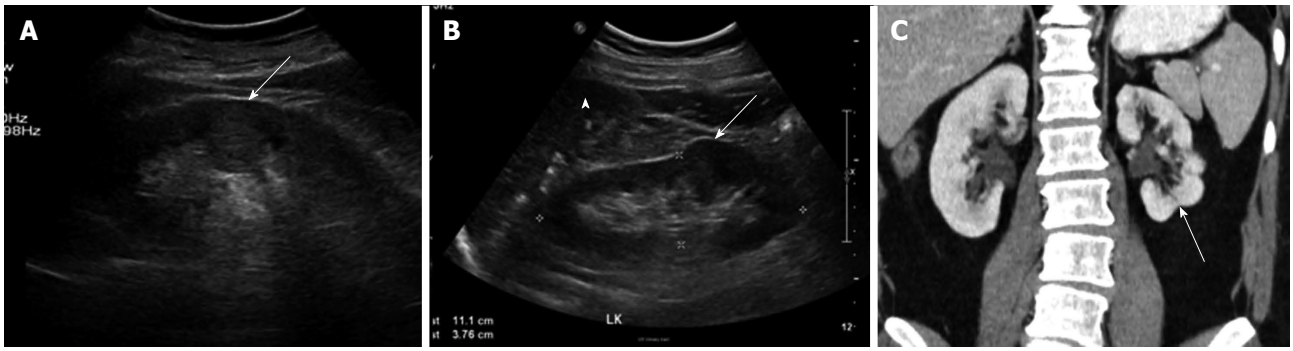

Figure 3 Persistent fetal lobulations. A: USG shows pseudomass from hypertrophied column of Bertin (arrow); B: USG shows Dromedary hump (arrow) from splenic impression (arrowhead); C: Coronal CT shows small LK with persistent fetal lobulations (arrow) inbetween the pyramids. CT: Computed tomography; USG: Ultrasonogram; LK: Left kidney.

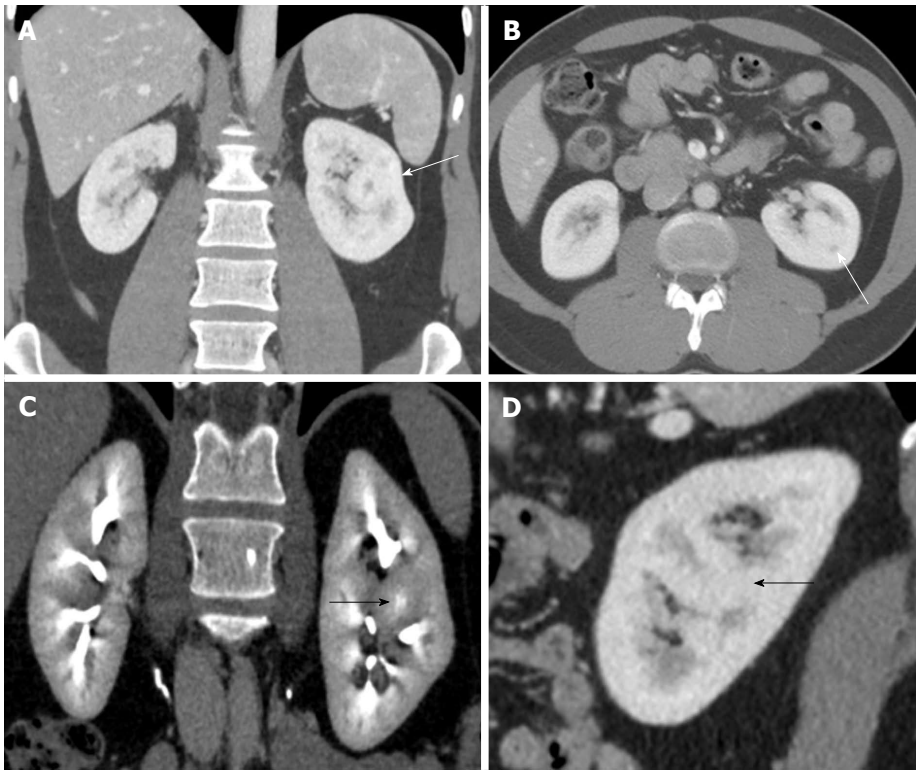

Figure 4 A 50-year-old woman with suspicious solid mass in left kidney on ultrasonogram. Coronal (A and C), axial (B) and sagittal (D) computed tomography showing hypertrophied column of Bertin in interpolar region of LK (arrows) showing density and enhancement pattern similar to adjacent normal renal cortex. LK: Left kidney.

urogenital anomalies[14,15].

Anomalies in shape

Persistent fetal lobulations: Persistent fetal lobulations is a normal variant seen in adult kidneys due to incomplete fusion of the developing renal lobules and could be mistaken for renal scarring. However it is seen as smooth indentation of the renal outline in-between the pyramids on ultrasonogram (USG), CT OR MRI as compared to renal scarring where indentation is not smooth, asymmetrical and it overlies the renal pyramids[16] (Figure 3).

Hypertrophied column of bertini: It is the extension of renal cortical tissue which separates the pyramids towards the central parenchyma. It is important as it can be mistaken for a renal mass on US. It is usually located in the mid portion of the left kidney. Key to correct identification is the fact that it is in continuity with, and have signature of normal renal parenchyma regardless of the type of imaging modality, CT or MRI[17,18] (Figures 3-5).

Dromedary hump: Normal variant of renal contour appearing as focal contour bulge, caused by the splenic impression onto the superolateral left kidney. It can mimic a renal mass and the key to diagnosis is it is identical to renal parenchyma in density/signal intensity

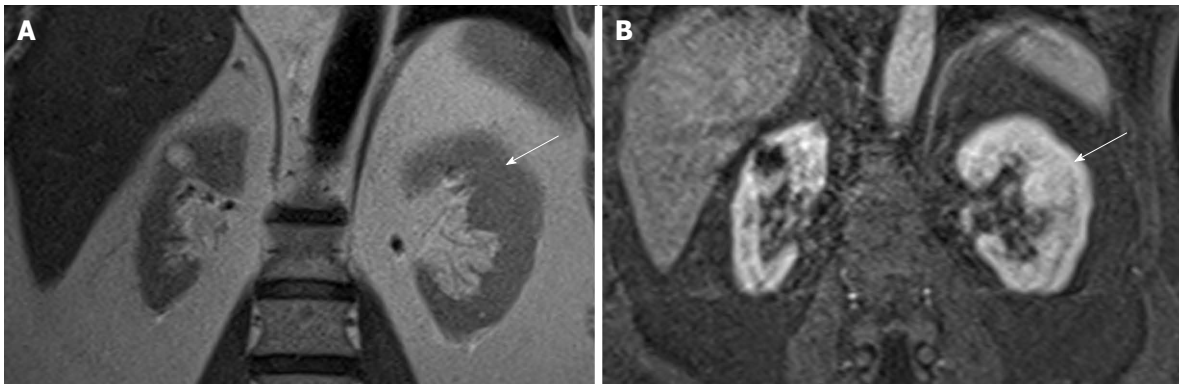

Figure 5 A 60-year-old man with suspicious mass in the left kidney on ultrasonogram. Coronal T2W (A) and contrast enhanced T1W magnetic resonance imaging (B) shows hypertrophied column of Bertin in interpolar region of LK (arrows). LK: Left kidney.

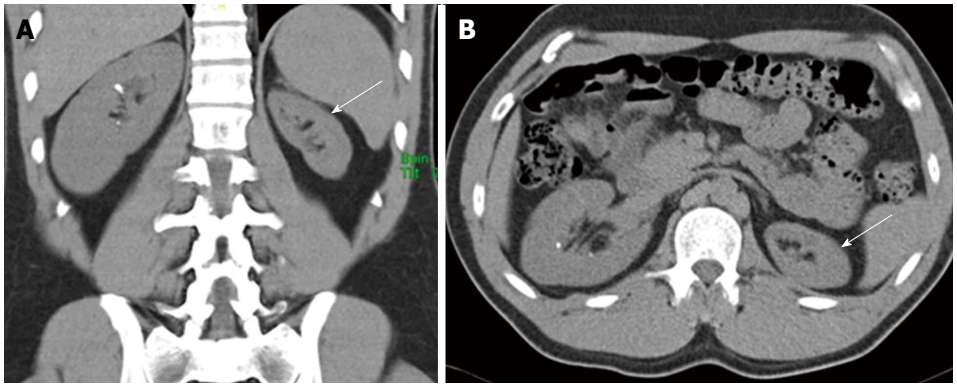

Figure 6 A 35-year-old man presented with right flank pain and incidental left renal hypoplasia. Coronal (A) and axial (B) non-contrast computed tomography shows uniformly small left kidney with no scarring (arrow). Compensatory hypertrophy of right kidney seen with tiny calculi.

on both precontrast and contrast sequences. Another clue is calyces underlying the hump extend further laterally into the hump than the other calyces[16] (Figure 3).

Renal hilar lip: A renal hilar lip is an infolding of the cortex at the level of the renal sinus giving a pseudo mass appearance. Again cortical signature and careful evaluation of contiguous images on CT or MRI help in resolving the confusion[19].

Junctional parenchymal defect: It is a normal variant seen as a triangular echogenic area due to the extension of sinus fat into the cortex. It results from embryonic fusion of renunculi. It can be distinguished from small angiomyolipoma (AML) or scar by its continuity with renal sinus fat and its typical location in interpolar region[16,17].

Renal hypoplasia

Renal hypoplasia refers to congenital small kidney with lesser number of calices and papilla (< 6) due to incomplete renal development. It is often unilateral and can have normal or mildly reduced function. It can be global or segmental. Global hypoplasia needs to be differentiated from atrophic kidneys due to pyelonephritis or chronic vascular diseases in adults. Atrophic kidneys from pyelonephritis usually show irregular outline from scarring with focal dilatation/clubbing of calices in contrast to smooth outline and non-dilated calices in global hypoplasia. Small smooth kidney from chronic vascular diseases are difficult to differentiate from hypoplasia[4]. Segmental renal hypoplasia also known as Ask-Upmark kidney is a cause of secondary hypertension in young adults. Imaging reveals small nonfunctioning kidney or focal hypoplasia of upper or lower pole and final diagnosis is made on characteristic histological features[4,5,20] (Figures 6 and 7).

Renal dysplasia

MCDK is a developmental disorder of the kidney, in which the normal renal parenchyma is replaced by multiple, non-communicating cysts of varying size with poorly identified echogenic parenchyma and atretic upper ureters. The incidence is about 1/4300 pregnancies[21]. USG (antenatal or postnatal) is diagnostic and should be differentiated from hydronephrosis which have communicating cysts[7]. Polycystic kidney disease presenting in adults shows multiple non communicating cysts similar to MCDK. However adult age of onset, bilateralism, enlarged kidney, intervening normal renal parenchyma and positive family history are helpful in differentiating

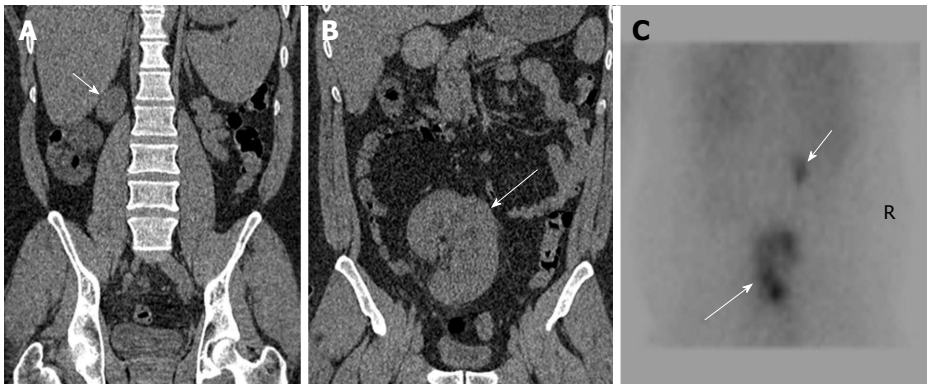

Figure 7 A 45-year-old man presenting with recurrent lower abdominal pain. Coronal non-contrast computed tomography (A and B) shows hypoplastic right kidney (short arrow) and ectopic left kidney (long arrow). Nuclear scan (C) show small poorly functioning right kidney (short arrow) and ectopic left kidney (long arrow).

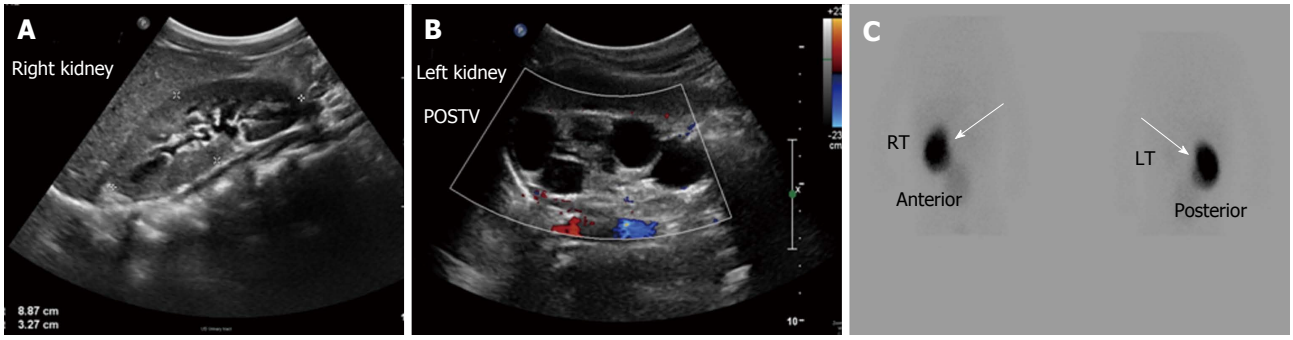

Figure 8 A 15-year-old girl with non-specific abdominal pain. USG (A and B) shows normal right kidney and multiple non communicating cysts replacing left kidney. Nuclear scan (C) non functioning left kidney (arrows). USG: Ultrasonogram.

from MCDK[22]. DMSA can be performed to establish non functioning kidney (Figure 8). In 25%-40% the contralateral kidney will also be abnormal, reflux being the most frequently associated anomaly and should be investigated with a voiding cysto urethrogram. The natural course *in utero* is variable and the final result is a non-functional kidney[23]. Bilateral multicystic kidney disease occurs in about 10%-20% of cases and is a lethal condition.

ABNORMAL MIGRATION

Congenital renal anomalies in the position and in the renal fusion are the result of impaired cephalic migration from the pelvis to the flank of the ureteric bud and metanephric blastema. This process of ascent begins in 5th week and ends at 9th week of gestation. It includes both ectopic location of kidneys and abnormal fusion of whole or part of the kidneys.

Ectopic kidneys

Renal ectopia is a congenital renal anomaly characterized by abnormal location of kidneys outside the flank region (L1-L3 vertebral levels). It can be simple ectopia where ectopic kidney is located on the same as its ureter or crossed ectopia when it is located on the opposite from its ureteric orifice. Both can be unilateral or bilateral. Simple renal ectopia is seen in 1:3000 and bilateral in 10% of cases[24]. The location, in order of frequency, may be pelvic, iliac, abdominal or chest. Ectopic kidney is usually smaller with varying degree of malrotation. The ureter has a length according to the location of the kidney and blood supply is from iliac or infrarenal abdominal aorta with typically multiple arteries. USG is diagnostic in most of the cases and cross sectional imaging or nuclear medicine studies are needed when USG visualized is suboptimal due to bowel gas, small kidneys or intrathoracic location[25]. Crossed renal ectopia is seen in 1:7000 and often incidentally detected. It can be fused in 85% where the ectopic kidney fuses with the orthotopic kidneys[9,26]. Commonest fusion pattern is fusion of lower pole of orthotopic kidney to the upper pole of crossed ectopic kidney. Other described patterns include sigmoid, L shaped, discoid and cake kidneys. USG shows absent kidney on one side and careful evaluation often reveals it on the opposite lumbar or iliac region. Often there is associated other genitourinary malformations and ectopic kidneys are complicated by stones, infection or hypertension from multiple anomalous arteries[3]. CT urography is helpful in confirming the diagnosis and demonstration of collecting system, arterial supply and complications. Ectopic kidneys need to be differentiated from renal transplants, nephroptosis, surgical repositioning of kidneys and

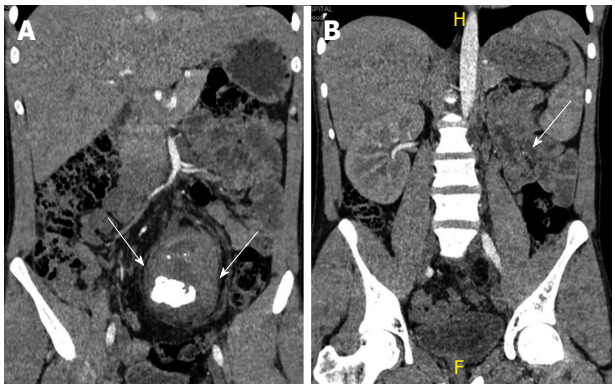

Figure 9 A 40-year-old man with long standing recurrent lower abdominal pain. Coronal non-contrast computed tomography (A and B) shows ectopic left kidney in the pelvis with stag horn calculus causing hydronephrosis (arrows).

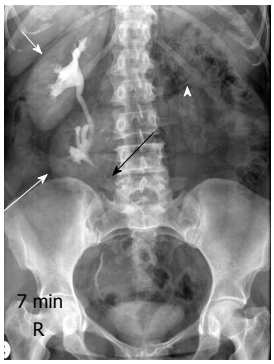

Figure 10 A 30-year-old man with crossed ectopia without fusion. Intravenous urography shows crossed ectopia of left kidney (long arrow) below the normal right kidney (short arrow). Note ureter of ectopic left kidney crossing to left side (black arrow) and empty left renal fossa (arrowhead).

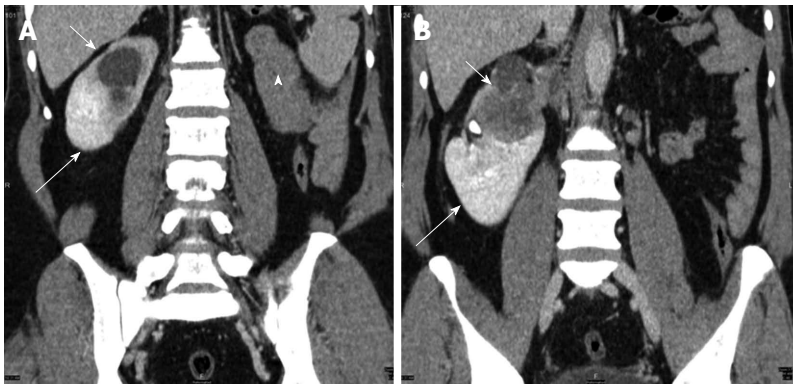

Figure 11 A 42-year-old man with crossed fused ectopia on the right side. Coronal contrast enhanced computed tomography (A and B) shows empty left renal fossa (arrowhead) with crossed fused ectopic left kidney (long arrow) fused with the right kidney (short arrow) which shows infiltrating transitional cell carcinoma.

nephrectomy (Figures 9-11).

Horse shoe kidney

Horseshoe kidney is the most common congenital anomaly seen in 1 in 500 adults[27]. It is formed by fusion across the midline of two distinct functioning kidneys, one on each side of the midline. They are connected by an isthmus of functioning renal parenchyma or fibrous tissue. In the vast majority of cases the fusion is between the lower poles (90%). In the remainder the superior or both the superior or inferior poles are fused. It is due to normal ascent of kidneys impaired by inferior mesenteric artery which hooks over the isthmus resulting in a lower abdominal location and abnormal rotation, especially at the lower poles (Figure 12). The pelvis and ureters are anterior, ventrally crossing the isthmus[3]. Horse shoe kidney is prone to numerous complications due to its location and poor drainage like hydronephrosis, secondary to pelviureteric junction obstruction, renal calculus, infection, increased incidence of malignancy (Wilms tumour, transitional cell carcinoma, carcinoid and possibly renal cell carcinoma)[28] and increased susceptibility to trauma. On USG, clue to diagnosis is poor visualization of bilateral lower pole which should alert the sonographer to look for abnormal tissue anterior to aorta representing the isthmus. Lack of awareness could lead to overlooking the diagnosis with underestimation of renal length or mistaking the preaortic tissue for mass or lymphnode[17,29,30]. CT and MRI help in delineating the details of collecting system and arterial anatomy, differentiating functioning isthmus from fibrous tissue and for early detection of complications (Figures 13 and 14).

ABNORMAL COLLECTING SYSTEM

Duplex collecting system

A duplex collecting system is one of the most common congenital renal tract abnormalities, characterised by an incomplete fusion of upper and lower pole moieties resulting in a variety of complete or incomplete duplications of the collecting system. Duplication occurs when two separate ureteric buds arise from a single Wolffian duct[31]. Based on the degree of fusion, it can present as bifid renal pelvis, partial ureteric duplication (Y-shaped ureter), incomplete ureteric duplication with ureters joining near or in bladder wall (V-shaped ureter) and complete ureteric duplication with separate ureteric orifices[32,33]. This is often asymptomatic and incidentally detected. USG has limited role in detecting duplication when no hydronephrosis. CTU and MRU are the modality of choice and help in demonstrating

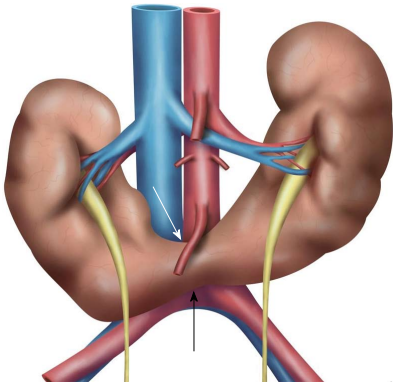

Figure 12 Schematic diagram showing the horse shoe kidneys due to the arrested migration of isthmus as the inferior mesenteric artery (white arrow) hooks over the isthmus (black arrow).

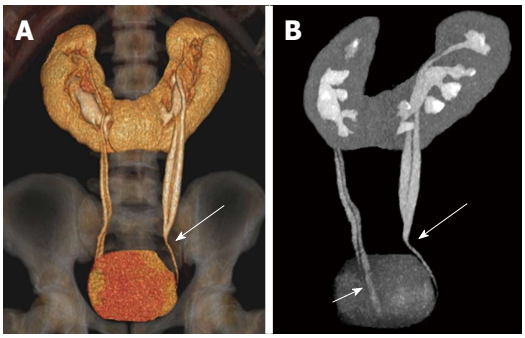

Figure 13 A 32-year-old woman with combined horse shoe kidney and duplex ureters. Coronal volume rendered image (A) and Maximum intensity projection image (B) images show horse-shoe kidney with bilateral duplex ureters joining at the midureter level (long arrow) on left side and close to bladder (short arrow) on the right side.

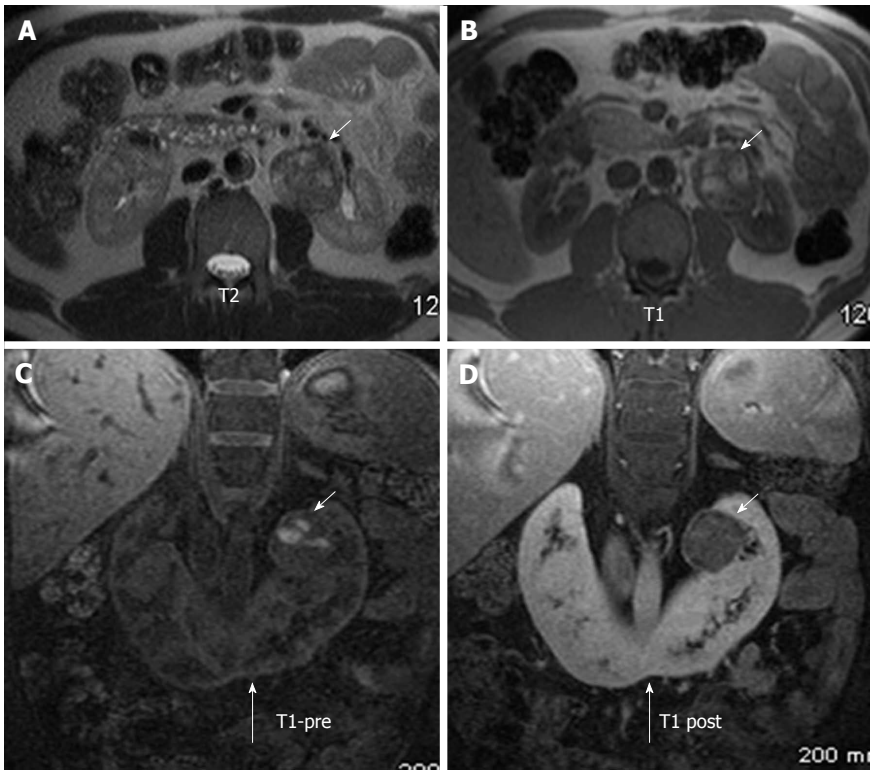

Figure 14 A 43-year-old man on follow up for horse shoe kidney. Axial T2W (A) and T1W (B) MRI show horse shoe kidney (long arrow) with heterogenous mass in the left renal moiety showing T1 hyperintensity suggestive of blood products. Coronal T1 precontrast (C) and post contrast (D) MRI shows mild enhancement in the renal mass (short arrows). Histopathology came out as renal carcinoid. MRI: Magnetic resonance imaging.

the detailed anatomy of the collecting system, level of fusion and status of ureteric orifices[29,34]. Double ureters follow Weigert-Meyer rule (Upper moiety ureter inserts ectopically inferior and medial to the lower pole moiety ureter). Upper moiety often ends in an ureterocele with obstruction and lower pole moiety shows reflux. Because of this upper pole moiety shows hydronephrosis causing mass effect on the lower pole which is seen as drooping lily sign on intravenous urogram[35-37]. Drooping lily sign is a classic urographic sign which refers to the inferolateral displacement of the opacified lower pole moiety due to an obstructed (and unopacified) upper pole moiety[36]. Upper pole moiety ureter can insert into the prostatic urethra in males or vaginal vault in females (Figures 15 and 16).

PUJO

Congenital PUJO is one of the commonest causes of antenatal hydronephrosis reported in 1 per 500 live births[38]. Etiology is debatable and include inadequate canalization during 10-12 wk of gestation, extrinsic obstructions secondary to bands, kinks, and aberrant vessels[39]. Patients can be asymptomatic or present with recurrent urinary tract infections, stone formation or palpable flank mass. Classically intermittent pain after drinking large volumes of fluid or fluids with a diuretic

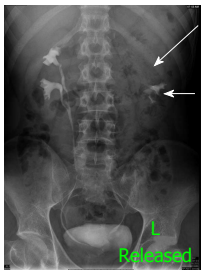

Figure 15 A 25-year-old man with bilateral duplex kidneys and "drooping lily" sign on the left side. One hour delayed radiograph after computed tomography urogram shows bilateral duplex system with hydronephrotic left upper moiety (long arrow) displacing the lower moiety (short arrow).

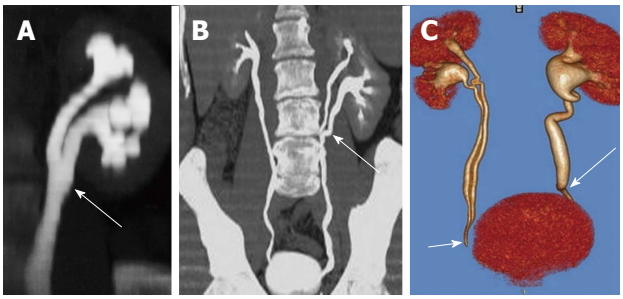

Figure 16 Different forms of duplex kidneys based on the level of fusion. A: Bifid renal pelvis; B: Y shaped ureter; C: V shaped ureter (short arrow). Also seen left lower ureteric stricture (long arrow).

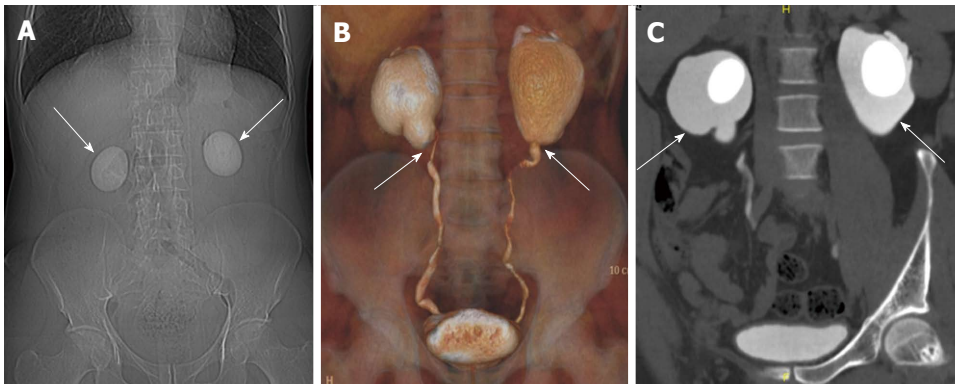

Figure 17 A 24-year-old man with bilateral flank pain. A: Computed tomography scannogram shows bilateral large round renal calculi; B: Coronal Volume rendered image shows narrowing at bilateral Pelvi-ureteric junction; C: Coronal maximum intensity projection image shows bilateral ballooning of pelvis (arrows) with large round renal pelvic calculi.

effect is described, due to the reduced outflow from the renal pelvis into the ureter (Dietl's crisis). Antenatal and postnatal USG are diagnostic and show disproportionately dilated renal pelvis with mild dilatation of calices and non dilated ureters[40]. DTPA is performed to assess the degree of obstruction and split renal function. CT is helpful in demonstrating the crossing vessels before surgical planning[41] (Figure 17). Depending on the degree of obstruction and residual function, surgery is often performed in the form of pyeloplasty or stenting.

CONCLUSION

Congenital anomalies of the kidneys and upper urinary tract encompass a wide spectrum of conditions varying from asymptomatic ectopic kidneys to life threatening renal agenesis (bilateral). US is typically the first imaging performed as it is easily available, non-invasive and radiation free used both antenatally and postnatally. CT and MRI are useful to confirm the ultrasound detected abnormality, detection of complex malformations, demonstration of collecting system and vascular anatomy and more importantly for early detection of complications like renal calculi, infection and malignancies. It is essential for the radiologists to be familiar with the imaging features of wide spectrum of renal anomalies and their complications which will help in timely diagnosis and appropriate management.

REFERENCES

1 **Yosypiv IV**. Congenital anomalies of the kidney and urinary tract: A genetic disorder? *Int J Nephrol* 2012; **2012**: 20 [DOI: 10.1155/2012/909083]
2 **Seikaly MG**, Ho PL, Emmett L, Fine RN, Tejani A. Chronic renal insufficiency in children: the 2001 Annual Report of the NAPRTCS. *Pediatr Nephrol* 2003; **18**: 796-804 [PMID: 12811650 DOI: 10.1007/s00467-003-1158-5]
3 **Glodny B**, Petersen J, Hofmann KJ, Schenk C, Herwig R, Trieb T, Koppelstaetter C, Steingruber I, Rehder P. Kidney fusion anomalies revisited: clinical and radiological analysis of 209 cases of crossed fused ectopia and horseshoe kidney. *BJU Int* 2009; **103**: 224-235 [PMID: 18710445 DOI: 10.1111/j.1464-410X.2008.07912.x]
4 **Toka HR**, Toka O, Hariri A, Nguyen HT. Congenital anomalies of kidney and urinary tract. *Semin Nephrol* 2010; **30**: 374-386 [PMID: 20807610 DOI: 10.1016/j.semnephrol.2010.06.004]
5 **Daneman A**, Alton DJ. Radiographic manifestations of renal anomalies. *Radiol Clin North Am* 1991; **29**: 351-363 [PMID: 1998056]
6 **Soliman NA**, Ali RI, Ghobrial EE, Habib EI, Ziada AM. Pattern of clinical presentation of congenital anomalies of the kidney and urinary tract among infants and children. *Nephrology* (Carlton) 2015; **20**: 413-418 [PMID: 25645028 DOI: 10.1111/nep.12414]
7 **Dias T**, Sairam S, Kumarasiri S. Ultrasound diagnosis of fetal renal abnormalities. *Best Pract Res Clin Obstet Gynaecol* 2014; **28**: 403-415 [PMID: 24524801 DOI: 10.1016/j.bpobgyn.2014.01.009]
8 **Leyendecker JR**, Barnes CE, Zagoria RJ. MR urography: techniques and clinical applications. *Radiographics* 2008; **28**: 23-46; discussion 46-47 [PMID: 18203929 DOI: 10.1148/rg.281075077]
9 **Türkvatan A**, Olçer T, Cumhur T. Multidetector CT urography of renal fusion anomalies. *Diagn Interv Radiol* 2009; **15**: 127-134 [PMID: 19517383]

10 **Nikken JJ**, Krestin GP. MRI of the kidney-state of the art. *Eur Radiol* 2007; **17**: 2780-2793 [PMID: 17646992 DOI: 10.1007/s00330-007-0701-3]
11 **Cascio S**, Paran S, Puri P. Associated urological anomalies in children with unilateral renal agenesis. *J Urol* 1999; **162**: 1081-1083 [DOI: 10.1016/S0022-5347(01)68074-1]
12 **Livingston L**, Larsen CR. Seminal vesicle cyst with ipsilateral renal agenesis. *AJR Am J Roentgenol* 2000; **175**: 177-180 [PMID: 10882270 DOI: 10.2214/ajr.175.1.1750177]
13 **Mishra A**. Renal agenesis: report of an interesting case. *Br J Radiol* 2007; **80**: e167-e169 [PMID: 17762048 DOI: 10.1259/bjr/79912069]
14 **Conrad GR**, Loes DJ, Franken EA. General case of the day. Ectopic supernumerary kidney. *Radiographics* 1987; **7**: 815-817 [PMID: 3448656 DOI: 10.1148/radiographics.7.4.3448656]
15 **Oto A**, Kerimoğlu U, Eskiçorapçi S, Hazirolan T, Tekgül S. Bilateral supernumerary kidney: imaging findings. *JBR-BTR* 2002; **85**: 300-303 [PMID: 12553660]
16 **Bhatt S**, MacLennan G, Dogra V. Renal pseudotumors. *AJR Am J Roentgenol* 2007; **188**: 1380-1387 [PMID: 17449786 DOI: 10.2214/AJR.06.0920]
17 **Zeman RK**, Cronan JJ, Rosenfield AT, Choyke PL, Paushter DM, Clark LR, Jaffe MH, Schiebler ML. Computed tomography of renal masses: pitfalls and anatomic variants. *Radiographics* 1986; **6**: 351-372 [PMID: 3685502 DOI: 10.1148/radiographics.6.3.3685502]
18 **Lafortune M**, Constantin A, Breton G, Vallee C. Sonography of the hypertrophied column of Bertin. *AJR Am J Roentgenol* 1986; **146**: 53-56 [PMID: 3510045 DOI: 10.2214/ajr.146.1.53]
19 **Kolbenstvedt A**, Lien HH. Isolated renal hilar lip on computed tomography. *Radiology* 1982; **143**: 150 [PMID: 7063720 DOI: 10.1148/radiology.143.1.7063720]
20 **Ask-upmark E**. One-sided kidney affections and arterial hypertension. *Acta Med Scand* 1963; **173**: 141-146 [PMID: 13965219 DOI: 10.1111/j.0954-6820.1963.tb16515.x]
21 **Schreuder MF**, Westland R, van Wijk JA. Unilateral multicystic dysplastic kidney: a meta-analysis of observational studies on the incidence, associated urinary tract malformations and the contralateral kidney. *Nephrol Dial Transplant* 2009; **24**: 1810-1818 [PMID: 19171687 DOI: 10.1093/ndt/gfn777]
22 **Akoh JA**. Current management of autosomal dominant polycystic kidney disease. *World J Nephrol* 2015; **4**: 468-479 [PMID: 26380198 DOI: 10.5527/wjn.v4.i4.468]
23 **Winyard P**, Chitty LS. Dysplastic kidneys. *Semin Fetal Neonatal Med* 2008; **13**: 142-151 [PMID: 18065301 DOI: 10.1016/j.siny.2007.10.009]
24 **Barakat AJ**, Drougas JG. Occurrence of congenital abnormalities of kidney and urinary tract in 13,775 autopsies. *Urology* 1991; **38**: 347-350 [DOI: 10.1016/0090-4295(91)80150-6]
25 **Kakitsubata Y**, Kakitsubata S, Watanabe K, Natsuda Y, Miyanaga I. Pelvic kidney associated with other congenital anomalies: US and CT manifestations. *Radiat Med* 1993; **11**: 107-109 [PMID: 8372238]
26 **Boyan N**, Kubat H, Uzum A. Crossed renal ectopia with fusion: report of two patients. *Clin Anat* 2007; **20**: 699-702 [PMID: 17309069 DOI: 10.1002/ca.20464]
27 **O'Brien J**, Buckley O, Doody O, Ward E, Persaud T, Torreggiani W. Imaging of horseshoe kidneys and their complications. *J Med Imaging Radiat Oncol* 2008; **52**: 216-226 [PMID: 18477115 DOI: 10.1111/j.1440-1673.2008.01950.x]
28 **Fazio L**, Razvi H, Chin JL. Malignancy in horseshoe kidneys: review and discussion of surgical implications. *Can J Urol* 2003; **10**: 1899-1904 [PMID: 12892577]
29 **Eze AR**, White JV, Pathak AS, Grabowski MW. "Pancake kidney": a renal anomaly complicating aortic reconstruction. *Ann Vasc Surg* 1998; **12**: 278-281 [PMID: 9588516 DOI: 10.1007/s100169900153]
30 **Dyer RB**, Chen MY, Zagoria RJ. Classic signs in uroradiology. *Radiographics* 2004; **24** Suppl 1: S247-S280 [PMID: 15486245 DOI: 10.1148/rg.24si045509]
31 **Inamoto K**, Tanaka S, Takemura K, Ikoma F. Duplication of the renal pelvis and ureter: associated anomalies and pathological conditions. *Radiat Med* 1983; **1**: 55-64 [PMID: 6679897]
32 **Share JC**, Lebowitz RL. The unsuspected double collecting system on imaging studies and at cystoscopy. *AJR Am J Roentgenol* 1990; **155**: 561-564 [PMID: 2117358 DOI: 10.2214/ajr.155.3.2117358]
33 **Fernbach SK**, Feinstein KA, Spencer K, Lindstrom CA. Ureteral duplication and its complications. *Radiographics* 1997; **17**: 109-127 [PMID: 9017803 DOI: 10.1148/radiographics.17.1.9017803]
34 **Adeb M**, Darge K, Dillman JR, Carr M, Epelman M. Magnetic resonance urography in evaluation of duplicated renal collecting systems. *Magn Reson Imaging Clin N Am* 2013; **21**: 717-730 [PMID: 24183522 DOI: 10.1016/j.mric.2013.04.002]
35 **Fernbach SK**, Zawin JK, Lebowitz RL. Complete duplication of the ureter with ureteropelvic junction obstruction of the lower pole of the kidney: imaging findings. *AJR Am J Roentgenol* 1995; **164**: 701-704 [PMID: 7863898 DOI: 10.2214/ajr.164.3.7863898]
36 **Callahan MJ**. The drooping lily sign. *Radiology* 2001; **219**: 226-228 [PMID: 11274561 DOI: 10.1148/radiology.219.1.r01ap01226]
37 **Zissin R**, Apter S, Yaffe D, Kots E, Gayer G, Nissenkorn I, Hertz M. Renal duplication with associated complications in adults: CT findings in 26 cases. *Clin Radiol* 2001; **56**: 58-63 [PMID: 11162699 DOI: 10.1053/crad.2000.0639]
38 **Liang CC**, Cheng PJ, Lin CJ, Chen HW, Chao AS, Chang SD. Outcome of prenatally diagnosed fetal hydronephrosis. *J Reprod Med* 2002; **47**: 27-32 [PMID: 11838306]
39 **Ismaili K**, Piepsz A. The antenatally detected pelvi-ureteric junction stenosis: advances in renography and strategy of management. *Pediatr Radiol* 2013; **43**: 428-435 [PMID: 23525768 DOI: 10.1007/s00247-012-2505-0]
40 **Kleiner B**, Callen PW, Filly RA. Sonographic analysis of the fetus with ureteropelvic junction obstruction. *AJR Am J Roentgenol* 1987; **148**: 359-363 [PMID: 3541550 DOI: 10.2214/ajr.148.2.359]
41 **Quillin SP**, Brink JA, Heiken JP, Siegel CL, McClennan BL, Clayman RV. Helical (spiral) CT angiography for identification of crossing vessels at the ureteropelvic junction. *AJR Am J Roentgenol* 1996; **166**: 1125-1130 [PMID: 8615256 DOI: 10.2214/ajr.166.5.8615256]

P- Reviewer: Cerwenka HR, Lassandro F **S- Editor**: Song XX
L- Editor: A **E- Editor**: Liu SQ

World Journal of Radiology

Submit a Manuscript: http://www.wjgnet.com/esps/
Help Desk: http://www.wjgnet.com/esps/helpdesk.aspx
DOI: 10.4329/wjr.v8.i2.142

World J Radiol 2016 February 28; 8(2): 142-147
ISSN 1949-8470 (online)

Importance of establishing radiation protection culture in Radiology Department

Agapi Ploussi, Efstathios P Efstathopoulos

Agapi Ploussi, Efstathios P Efstathopoulos, 2nd Department of Radiology, Medical School, National and Kapodistrian University of Athens, 12462 Athens, Greece

Author contributions: All authors equally contributed to the design of the manuscript and the literature review.

Conflict-of-interest statement: None declared.

Correspondence to: Efstathios P Efstathopoulos, PhD, 2nd Department of Radiology, Medical School, National and Kapodistrian University of Athens, 1 Rimini St, 12462 Athens, Greece. stathise@med.uoa.gr
Telephone: +30-210-5831818
Fax: +30-210-5831831

Received: August 28, 2015
Peer-review started: August 31, 2015
First decision: September 8, 2015
Revised: October 16, 2015
Accepted: December 16, 2015
Article in press: December 18, 2015
Published online: February 28, 2016

Abstract

The increased use of ionization radiation for diagnostic and therapeutic purposes, the rapid advances in computed tomography as well as the high radiation doses delivered by interventional procedures have raised serious safety and health concerns for both patients and medical staff and have necessitated the establishment of a radiation protection culture (RPC) in every Radiology Department. RPC is a newly introduced concept. The term culture describes the combination of attitudes, beliefs, practices and rules among the professionals, staff and patients regarding to radiation protection. Most of the time, the challenge is to improve rather than to build a RPC. The establishment of a RPC requires continuing education of the staff and professional, effective communication among stakeholders of all levels and implementation of quality assurance programs. The RPC creation is being driven from the highest level. Leadership, professionals and associate societies are recognized to play a vital role in the embedding and promotion of RPC in a Medical Unit. The establishment of a RPC enables the reduction of the radiation dose, enhances radiation risk awareness, minimizes unsafe practices, and improves the quality of a radiation protection program. The purpose of this review paper is to describe the role and highlight the importance of establishing a strong RPC in Radiology Departments with an emphasis on promoting RPC in the Interventional Radiology environment.

Key words: Radiation protection culture; Radiation safety; Radiology Department; Interventional radiology

Core tip: Radiation protection culture (RPC) is a combination of knowledge, beliefs and practices related to radiation safety. The establishment of a RPC in a Radiology Department demands substantial knowledge of radiation risks, safety rules and active participation of all stakeholders. Professionals have the key role in the creation of a RPC. A strong RPC provides more effective diagnosis and treatment, improves patient and staff safety and reduces radiation exposure. The objective of our study is to highlight the role of RPC in a Radiology Department with an emphasis on promoting RPC in the Interventional Radiology environment.

Ploussi A, Efstathopoulos EP. Importance of establishing radiation protection culture in Radiology Department. *World J Radiol* 2016; 8(2): 142-147 Available from: URL: http://www.wjgnet.com/1949-8470/full/v8/i2/142.htm DOI: http://dx.doi.org/10.4329/wjr.v8.i2.142

INTRODUCTION

Culture is one of the most complicated and obscure concepts. Among the many definitions one may find in the literature, the most attractive one for the purpose of this text is that culture is "…the total range of activities and ideas of a group of people with shared traditions, which are transmitted and reinforced by members of the group…"[1]. The term culture is not only associated with a high level of art, civilization and religion but also strongly affects business, communication, marketing and safety.

During the recent years the concept of safety culture has been gaining ground in organizations mainly due to the rapid advancement of technology and the concern about employees' health and safety. Safety culture reflects attitudes, values, norms and practices that professional and employees share concerning risk and safety. Safety culture is often used in conjunction with terms like "nuclear safety culture", "patient safety culture", "health safety culture", "occupational safety culture", "organization safety culture" and "environment safety culture".

Regarding the safe use of ionizing radiation in the medical field and nuclear industry, International Radiation Protection Association (IRPA) first established the concept of radiation protection culture (RPC) in 2008 following the proposal of the French Society for Radiation Protection. The proposal was favourably greeted by the participating Associate Societies, the World Health Organisation (WHO) and the European ALARA Network. At the first Workshop of IRPA on RPC in 2009, professionals proposed a number of definitions for RPC and prepared the action plan for the development of a strong RPC. Two years later, after a series of meetings, the Association published the final draft on Guiding Principles for Establishing a RPC and very recently, in June 2014, the draft was issued in its final form and published in the website of IRPA[2].

Hence, the RPC is a newly introduced concept for professionals, staff and patients. The goal of this paper is to provide the role of RPC with an emphasis on promoting RPC in the Interventional Radiology environment.

A DEFINITION FOR RPC

A thorough understanding of the term RPC is the first step towards developing a strong RPC in a Radiology Department. According to IRPA, RPC is defined as "The combination of knowledge, values, behaviours and experience of radiation protection in all its aspects for patients, workers, population and environment, and in all exposure situations, combining scientific and social dimensions"[2]. In other words, RPC is the assembly of attitudes, strategies and practices among staff and leaders that should be emphasized in radiation protection safety. As it is obvious, RPC is a part of safety culture oriented on the effects and risks of ionization radiation.

Each Radiology Department has guidelines and practical rules for the safe use of ionizing radiation even if not all members of the department are aware of that. Does this actual mean that every Radiology Department has a RPC program? On this question, opinions diverge. Some support that RPC exists in every Radiology Department; however this culture can be positive or negative, strong or weak. Others recognize that culture is a combination of attitudes and regulations and claim that RPC is either present or absent within a Radiology Department. In authors' opinion, RPC exists in most Radiology Departments. The challenge is to improve rather than to build a RPC. Most often, it proves to be more difficult to improve an existing culture rather than to create a new one as workers and all stakeholders must unlearn the old behaviors and practices before they adopt the new ones.

The objectives of RPC are to provide a safe working environment, promote knowledge of radiation risks, minimize unsafe practices, control radiation risks, share responsibility among workers and improve the quality of an already existing radiation protection program. All the aforementioned objectives are achieved through the active participation and interaction of all the workers inside the department.

WHY THE ESTABLISHMENT OF RPC IS IMPORTANT IN A RADIOLOGY DEPARTMENT

The increasing use of ionization radiation for diagnostic and therapeutic purposes especially in higher dose procedures such as computed tomography (CT) and interventional radiology have raised serious safety and health concerns for both patients and medical staff.

During the last 15-year period the number of CT examinations has almost tripled and now contribute to more than 60% of the total collective dose from X-ray examinations[3,4]. A typical head CT scan, which is the most frequent CT examination in adults and children, delivers an effective dose of about 4 mSv whereas the effective doses for abdomen and coronary angiography CT examinations can reach 25 and 32 mSv, respectively (Figure 1)[5,6].

The concern for the increased use of CT exams is more pronounced for pediatric patients. A recent survey revealed that the frequency of CT examinations has doubled in children under 5 years old while it has tripled in older children the last 20 years[7]. Pediatric patients are more sensitive to radiation-induced risks

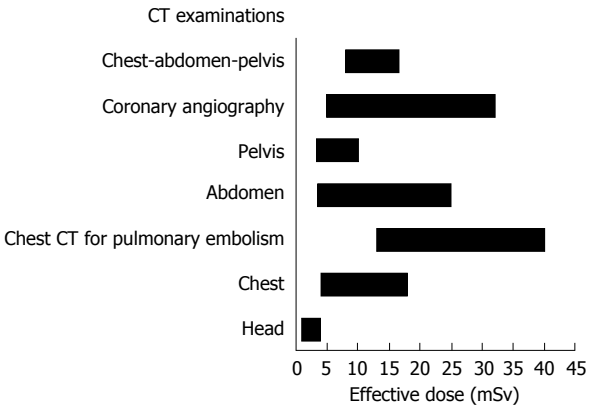

Figure 1 Effective dose from various computed tomography examinations[5,6]. CT: Computed tomography.

compared to adults due to their longer post-exposure life expectancy and their rapidly dividing cells. Two recent epidemiological studies on large pediatric populations demonstrated positive association between radiation exposures received from CT scans and cancer incidence[8,9]. It is worth mentioning that even today there is lack of optimized, size-based protocols for pediatric procedures in clinical routine and therefore children may be over-exposed to radiation.

Concerning the field of interventional radiology (IR), the new advances in fluoroscopy imaging equipment as well as the development of new interventional tools and devices (balloon, catheters, stents) led to a significant increase of 78% in interventional (non-CT) procedures the period between 1998-2008[3].

Radiation protection and safety is an extremely important issue for IR medical staff. IR procedures are usually complex, demands high fluoroscopy times, high dose rates and a large number of cine acquisitions. Therefore, they deliver high radiation doses both to patients and medical staff. Figure 2 presents the effective dose from various IR examinations for patients and medical staff[5,10,11]. IR procedures deliver effective dose to the patients ranging from 5 to 160 mSv[5] and contribute about 8% to collective dose[3] even though they consist of a small percentage in the total number of X-ray examinations performed in a given population. Variations in the value of occupational doses for the same type of procedure are largely due variations in the X-ray equipment, the technique, the training of health professionals on radiation protection issues, the optimization of protocols as well as to the availability and use of protection tools.

There are several reports in the literature concerning radiation-induced deterministic effects on both patients and medical staff during IR procedures[12,13]. The most common deterministic effects in patients are erythema, skin necrosis, hair loss and permanent epilation as well as cataract formation in occupational settings. Most of the time, the deterministic injuries arise from the poor knowledge on radiation protection rules, the lack of quality assurance programs, the performance of wrong practices and the improper or no use of radiation protection tools.

WAYS OF ESTABLISHMENT A RPC

The key role for the implementation of RPC in a Radiology Department is initially the development of a strategic plan where every decision and process takes into account radiation safety of staff and patients. Then this strategic plan must be turned into an action plan in order to create the conditions for the incorporation of radiation safety in the routine work of the department. But how we can achieve the establishment of a RPC program in Radiology Departments and how easy is it to apply a "culture" on a daily basis?

The most important factor contributing to the creation of a RPC is the continuous education and training of the staff and professionals with the attendance of courses, workshops, seminars and electronic-learning programs in a normal periodical basis. Theoretical education and practical training in radiation protection aim to ensure that healthcare professionals will obtain a strong foundation in radiation protection and a basic knowledge of the technology of each modality. Education is an essential aspect for the optimization of clinical protocols and the reduction of radiation exposure. Physicians, radiographers, nurses and other medical staff need to have a substantial knowledge of radiation protection regulations and a comprehensive understanding of the factors that affect patient and occupational dose in order to minimize the harmful effects of ionizing radiation. Medical staff should be adequately trained in order to keep the dose as low as reasonably achievable (ALARA principle), be familiar with radiation quantity units, pay special attention to radiation protection of pregnant and pediatric patients and proper use of the radiation protection equipment.

Literature review revealed that there is poor education in radiation protection of medical staff. A study from Salerno *et al*[14] on the evaluation of radiation risks knowledge in pediatric fellows and resident demonstrated that only 35% of medical staff have sufficient knowledge for radiation risk from common radiological examinations. Furthermore, it is impressive to be noted that a multicenter study conducted by Vano *et al*[15] in pediatric interventional cardiology departments in Latin America revealed that only 64% of the physicians used their personnel dosimeter and only 36% were aware of the doses received. European Commission[16] and more recently the International Commission of Radiation Protection[17] published guidelines highlighting the need for education and training of medical staff on radiation protection. It is important to understand that education does not only offer new knowledge but also facilitates the development of new skills and attitudes.

The active stakeholder engagement of all levels including health authorities, researchers, medical staff and patients is the second milestone for the establishment of a RPC. In a Radiology Department, multi-disciplinary

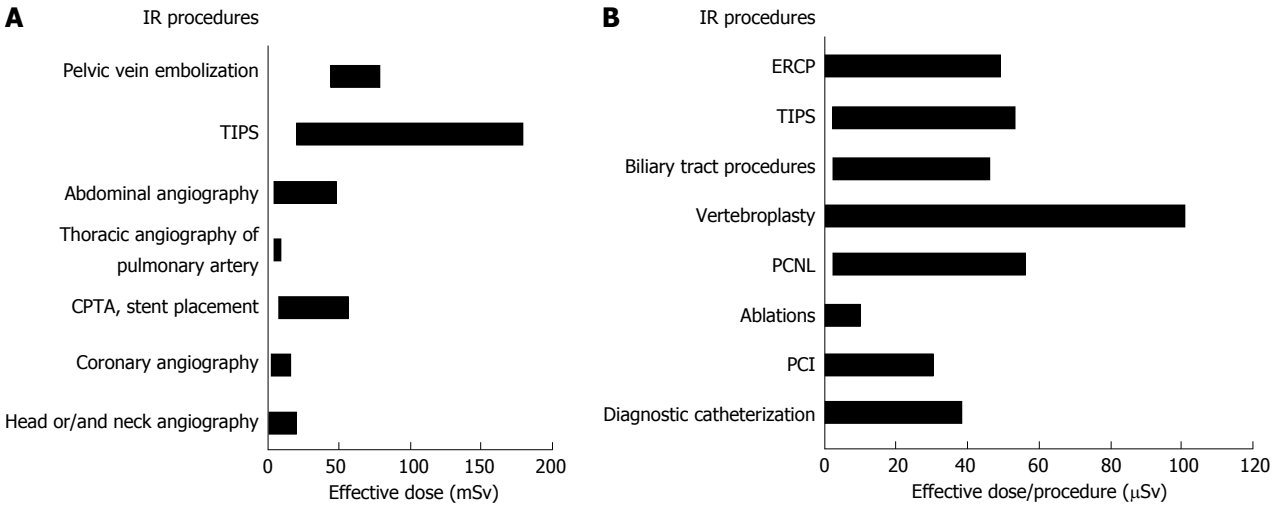

Figure 2 Effective doses from various interventional radiology procedures. A: Patients[5]; B: Occupational[10,11]. TIPS: Transjugular intrahepatic portosystemic shunt; CPTA: Carotid percutaneous transluminal angioplasty; ERCP: Endoscopic retrograde cholangiopancreatography; PCNL: Percutaneous nephrolithotomy; PCI: Percutaneous coronary intervention; IR: Interventional radiology.

collaboration is needed. Radiologists, medical physicists, radiographers, nurses and other specialists must collaborate closely one to each other, in order to ensure patient safety and best clinical outcome. RPC is strongly dependent on the behavior of all stakeholders. The effective communication among workers leads to the creation of a supportive and motivating work environment where everyone has a clear role. A positive workplace is characterized by trust and respect among stakeholders and allows the exchange of experience and knowledge. A strong leadership increases the radiation risk awareness and allows the performance of safer practices, which prompts minimizing errors.

Quality assurance (QA) program is another essential step in the implementation of RPC. According to WHO, the QA program in diagnostic radiology is defined as "an organized effort by the staff operating a facility to ensure that the diagnostic images produced are of sufficiently high quality so that they consistently provide adequate diagnostic information at the lowest possible cost and with the least possible exposure of the patient to radiation"[18]. The objectives of a QA program is to improve patient care and comfort, ensure accurate diagnosis and proper function of the equipment, produce high quality images following the ALARA principle, ensure patient and staff safety and minimize cost. A QA program should include the following major elements[19,20]: (1) Responsibility: There should be an assignment of the responsibility with specific duties for the performance of QA procedures. Both managers and employee are responsible for the implementation and improvement of QA programs in clinical routine; (2) Equipment specifications: Accurate specifications must be provided for each modality according to the facilities needs; (3) Standards for image quality: Standards, criteria and limits for diagnostic acceptable images should be documented and accessible; (4) Monitoring and maintenance: Monitoring, testing and maintenance of radiology equipment should be established and performed on a regular basis; (5) Evaluation: There must be regularly recurring evaluation of the adequacy and effectiveness of the X-ray equipment performance and the QA program itself; (6) Records: Every department should keep records about the equipment, quality control tests, dosimetry data, maintenance and repair of the modalities. The records must be easily accessible to the staff; (7) Manual: The manual must include list of duties and responsibilities of the staff as well as a list of the tests to be performed; (8) Education: QA specialists shall have continuing education and training in order to be qualified and up-to-date; (9) Committee: Each department should establish a committee composed of radiologists, medical physicists and radiographers with the top priority being the QA and the radiation safety; and (10) Review: Ongoing review of the QA program is important in order to assess the effectiveness of the QA procedures.

THE ROLE OF PROFESSIONALS AND STAFF

The implementation of a RPC should be driven from the highest level. Managers, medical professionals and workers should be directly involved and have a key role in the execution of RPC in every department. Radiation protection experts enhance safety culture, provide leadership, develop relationships with the administration and the employees and are responsible for the staff training and the creation of guidelines and recommendations under the guidance of radiation protection associates (*e.g.*, IRPA). Managers should be able to change unsafe practices and behavioral hazards, recognize safe practices and report accidents in order to prevent recurrence. Furthermore, the healthcare staff should implement the guidelines and the recommendations, ensure the proper practice of exami-

nations, improve patient health care and build trust between patients and staff.

THE IMPACT OF RPC

The direct impact of the implementation of RPC is the substantial reduction of radiation dose on both patients and staff. Fetterly *et al*[21] showed a significant reduction of about 40% on cumulative skin dose of patients in an invasive cardiovascular laboratory after the establishment of a safety culture. The ways in which the safety culture was achieved included a number of practical and technical changes such as reporting of high air-kerma procedures, training for fellows on radiation exposure safety issues, maximum distance between the X-ray source and patient, increased use of X-ray beam spectral filters and reduced fluoroscopy frame rates. A strong RPC enables more efficient diagnosis and treatment and helps minimize harmful effects. The foundation of a RPC program has an important effect on the operation of the Radiology Department: It improves the efficiency and service quality, reduces cost and incorrect practices and promotes a good reputation.

CONCLUSION

RPC is a combination of attitudes, priorities, policies and practices concerning radiation safety. The foundation of a RPC program is a dynamic process that needs continuous evaluation and systematic improvement with the use of quantitative and qualitative tools in order to examine how well the RPC is being implemented and to check whether the program is achieving the desired goals. RPC should be an integral part of clinical routine and demands deep knowledge of radiation risks, safety rules and active participation of all stakeholders. Insufficient knowledge and lack of collaboration are the most significant barriers in the implementation of RPC. For the successful establishment of a strong RPC program, authorities, professionals, employee and patients must fully comprehend the role and the impact of RPC in a Radiology Department and fill the gap between theory and practice.

REFERENCES

1 **Hanks P**. Collins Dictionary of the England Language. 1st ed. Glasgow: William Collins Sons and Co, 2004: 407
2 IRPA Guiding Principles for Establishing a Radiation Protection Culture. Available from: URL: http://www.irpa.net/members/IRPA-Guiding%20Principles%20on%20RP%20Culture%20-2014%20.pdf
3 **Hart D**, Wall, BF, Hillier MC, Shrimpton PC. Frequency and collective dose for medical and dental X-ray examinations in the UK, 2008. Chilton: Health Protection Agency, 2010: HPA-CRCE-012
4 **Smith-Bindman R**, Miglioretti DL, Johnson E, Lee C, Feigelson HS, Flynn M, Greenlee RT, Kruger RL, Hornbrook MC, Roblin D, Solberg LI, Vanneman N, Weinmann S, Williams AE. Use of diagnostic imaging studies and associated radiation exposure for patients enrolled in large integrated health care systems, 1996-2010. *JAMA* 2012; **307**: 2400-2409 [PMID: 22692172 DOI: 10.1001/jama.2012.5960]
5 **Mettler FA**, Huda W, Yoshizumi TT, Mahesh M. Effective doses in radiology and diagnostic nuclear medicine: a catalog. *Radiology* 2008; **248**: 254-263 [PMID: 18566177 DOI: 10.1148/radiol.2481071451]
6 **Dougeni E**, Faulkner K, Panayiotakis G. A review of patient dose and optimisation methods in adult and paediatric CT scanning. *Eur J Radiol* 2012; **81**: e665-e683 [PMID: 21684099 DOI: 10.1016/j.ejrad.2011.05.025]
7 **Miglioretti DL**, Johnson E, Williams A, Greenlee RT, Weinmann S, Solberg LI, Feigelson HS, Roblin D, Flynn MJ, Vanneman N, Smith-Bindman R. The use of computed tomography in pediatrics and the associated radiation exposure and estimated cancer risk. *JAMA Pediatr* 2013; **167**: 700-707 [PMID: 23754213 DOI: 10.1001/jamapediatrics.2013.311]
8 **Pearce MS**, Salotti JA, Little MP, McHugh K, Lee C, Kim KP, Howe NL, Ronckers CM, Rajaraman P, Sir Craft AW, Parker L, Berrington de González A. Radiation exposure from CT scans in childhood and subsequent risk of leukaemia and brain tumours: a retrospective cohort study. *Lancet* 2012; **380**: 499-505 [PMID: 22681860 DOI: 10.1016/S0140-6736(12)60815-0]
9 **Mathews JD**, Forsythe AV, Brady Z, Butler MW, Goergen SK, Byrnes GB, Giles GG, Wallace AB, Anderson PR, Guiver TA, McGale P, Cain TM, Dowty JG, Bickerstaffe AC, Darby SC. Cancer risk in 680,000 people exposed to computed tomography scans in childhood or adolescence: data linkage study of 11 million Australians. *BMJ* 2013; **346**: f2360 [PMID: 23694687 DOI: 10.1136/bmj.f2360]
10 **Kim KP**, Miller DL, Balter S, Kleinerman RA, Linet MS, Kwon D, Simon SL. Occupational radiation doses to operators performing cardiac catheterization procedures. *Health Phys* 2008; **94**: 211-227 [PMID: 18301095 DOI: 10.1097/01.HP.0000290614.76386.35]
11 **Kim KP**, Miller DL, Berrington de Gonzalez A, Balter S, Kleinerman RA, Ostroumova E, Simon SL, Linet MS. Occupational radiation doses to operators performing fluoroscopically-guided procedures. *Health Phys* 2012; **103**: 80-99 [PMID: 22647920 DOI: 10.1097/HP.0b013e31824dae76]
12 **Balter S**, Hopewell JW, Miller DL, Wagner LK, Zelefsky MJ. Fluoroscopically guided interventional procedures: a review of radiation effects on patients' skin and hair. *Radiology* 2010; **254**: 326-341 [PMID: 20093507 DOI: 10.1148/radiol.2542082312]
13 **Sun Z**, AbAziz A, Yusof AK. Radiation-induced noncancer risks in interventional cardiology: optimisation of procedures and staff and patient dose reduction. *Biomed Res Int* 2013; **2013**: 976962 [PMID: 24027768 DOI: 10.1155/2013/976962]
14 **Salerno S**, Marchese P, Magistrelli A, Tomà P, Matranga D, Midiri M, Ugazio AG, Corsello G. Radiation risks knowledge in resident and fellow in paediatrics: a questionnaire survey. *Ital J Pediatr* 2015; **41**: 21 [PMID: 25881170 DOI: 10.1186/s13052-015-0130-x]
15 **Vano E**, Ubeda C, Miranda P, Leyton F, Durán A, Nader A. Radiation protection in pediatric interventional cardiology: An IAEA PILOT program in Latin America. *Health Phys* 2011; **101**: 233-237 [PMID: 21799339 DOI: 10.1097/HP.0b013e3182135fd1]
16 **European Commission**. Guidelines on Radiation Protection Education and Training of Medical Professionals in the European Union (RP 175). Luxembourg: Publications Office of the European Union, 2014
17 **Vañó E**, Rosenstein M, Liniecki J, Rehani MM, Martin CJ, Vetter RJ. ICRP Publication 113. Education and training in radiological protection for diagnostic and interventional procedures. *Ann ICRP* 2009; **39**: 7-68 [PMID: 21788173 DOI: 10.1016/j.icrp.2011.01.002]
18 **World Health Organization**. Quality Assurance in Diagnostic Radiology. Geneva: Macmillan Procrom, 1982
19 **Inkoom S**, Schandorf C, Emi-Reynolds G, Fletcher JJ. Quality Assurance and Quality Control of Equipment in Diagnostic Radiology Practice - The Ghanaian Experience. Available from: URL: http://cdn.intechopen.com/pdfs-wm/23741.pdf
20 Code of Federal regulations - Title 21 - Food and Drugs, Part

800-1299, revised as of April 2015. Available from: URL: http://www.ecfr.gov/cgi-bin/text-idx?SID=3ee286332416f26a91d9e6d78-6a604ab&mc=true&tpl=/ecfrbrowse/Title21/21tab_02.tpl

21 **Fetterly KA**, Mathew V, Lennon R, Bell MR, Holmes DR, Rihal CS. Radiation dose reduction in the invasive cardiovascular laboratory: implementing a culture and philosophy of radiation safety. *JACC Cardiovasc Interv* 2012; **5**: 866-873 [PMID: 22917459 DOI: 10.1016/j.jcin.2012.05.003]

P- Reviewer: Chow J, Faasse T, Landrigan-Ossar M
S- Editor: Kong JX **L- Editor**: A **E- Editor**: Liu SQ

World Journal of Radiology

Submit a Manuscript: http://www.wjgnet.com/esps/
Help Desk: http://www.wjgnet.com/esps/helpdesk.aspx
DOI: 10.4329/wjr.v8.i2.148

World J Radiol 2016 February 28; 8(2): 148-158
ISSN 1949-8470 (online)

MINIREVIEWS

Advances in determining abdominal aortic aneurysm size and growth

Nikolaos Kontopodis, Stella Lioudaki, Dimitrios Pantidis, George Papadopoulos, Efstratios Georgakarakos, Christos V Ioannou

Nikolaos Kontopodis, Stella Lioudaki, Dimitrios Pantidis, George Papadopoulos, Christos V Ioannou, Department of Cardiothoracic and Vascular Surgery, University of Crete Medical School, 71100 Heraklion, Greece

Efstratios Georgakarakos, Department of Vascular Surgery, Democritus University of Thrace, University Hospital of Alexandroupolis, 68100 Alexandroupolis, Greece

Author contributions: Kontopodis N conceived the subject and wrote the article; Lioudaki S collected data and critically revised paper; Pantidis D collected data and summarized evidence in Tables; Papadopoulos G collected data and designed images; Georgakarakos E and Ioannou CV had the overall responsibility, revised manuscript and gave final approval for submission.

Conflict-of-interest statement: Authors declare no conflict of interest for this article.

Correspondence to: Christos V Ioannou, MD, PhD, Assistant Professor, Head of Vascular Surgery, Department of Cardiothoracic and Vascular Surgery, University of Crete Medical School, PO Box 1352, 71110 Heraklion, Greece. ioannou@med.uoc.gr
Telephone: +30-281-3402379
Fax: +30-281-0375365

Received: June 6, 2015
Peer-review started: June 7, 2015
First decision: August 16, 2015
Revised: September 6, 2015
Accepted: December 17, 2015
Article in press: December 18, 2015
Published online: February 28, 2016

Abstract

Abdominal aortic aneurysm is a common pathology in the aging population of the developed world which carries a significant mortality in excess of 80% in case of rupture. Aneurysmal disease probably represents the only surgical condition in which size is such a critical determinant of the need for intervention and therefore the ability to accurately and reproducibly record aneurysm size and growth over time is of outmost importance. In the same time that imaging techniques may be limited by intra- and inter-observer variability and there may be inconsistencies due to different modalities [ultrasound, computed tomography (CT)], rapid technologic advancement have taken aortic imaging to the next level. Digital imaging, multi-detector scanners, thin slice CT and most- importantly the ability to perform 3-dimensional reconstruction and image post-processing have currently become widely available rendering most of the imaging modalities used in the past out of date. The aim of the current article is to report on various imaging methods and current state of the art techniques used to record aneurysm size and growth. Moreover we aim to emphasize on the future research directions and report on techniques which probably will be widely used and incorporated in clinical practice in the near future.

Key words: Abdominal aortic aneurysm; Size; Growth; Maximum diameter; Volume; Ultrasound; Computed tomography

Core tip: Abdominal aortic aneurysms probably represent the only surgical condition in which size is such a critical determinant of the need for intervention. Recent advances in imaging techniques have raised new possibilities in medical imaging regarding aneurysmal disease making size recordings more accurate and

reproducible than ever. This review article summarizes available techniques, reports state of the art imaging modalities and discusses future perspectives regarding aortic aneurysms' imaging and decision making.

Kontopodis N, Lioudaki S, Pantidis D, Papadopoulos G, Georgakarakos E, Ioannou CV. Advances in determining abdominal aortic aneurysm size and growth. *World J Radiol* 2016; 8(2): 148-158 Available from: URL: http://www.wjgnet.com/1949-8470/full/v8/i2/148.htm DOI: http://dx.doi.org/10.4329/wjr.v8.i2.148

INTRODUCTION

Abdominal aortic aneurysm (AAA) is a focal, balloon-like dilation of the aorta exceeding 50% of its normal diameter which is a common health problem in western societies. Aneurysmal disease is growing in prevalence in the elderly population, with approximately 150000 new cases being diagnosed every year[1,2]. The most feared complication of this condition is rupture which is often reported as an intra-abdominal catastrophe since it is accompanied by an overall mortality rate in excess of 80% in the same time that it is ranked as the 13th most common cause of death in the United States[3].

Diagnostic and therapeutic protocols regarding AAAs, aim to prevent this disastrous scenario and elective AAA repair with either surgical or endovascular means is being employed for this purpose. Nevertheless and despite the technological progress and accumulated experience which have led to significant improvement of surgical outcomes, current repair techniques are not without complications, while most AAA patients are elderly with several co-morbidities[4,5]. Accordingly, the randomized control trials comparing surgical and endovascular techniques for AAA repair report a peri-procedural mortality rate of 0.6% to 6.2% for the former and a 0.6%-2.1% for the latter techniques. Therefore clinicians often have to balance between surgical risk on one hand and risk of rupture on the other in order to set the indication for AAA elective repair[6-9].

Currently aneurysm size and growth rate are being used as the only indices to determine the need for intervention *vs* surveillance of AAAs since there is firm scientific evidence that increased size and rapid growth indicate a high rupture risk[10,11]. In fact AAAs represent the only surgical condition in which size is such a critical determinant of the need to intervene. Although, there are certain limitations in the prognostic value of these variables and there is an ongoing search for additional risk markers to be found (*i.e.*, biomechanical parameters, morphometric characteristics, blood biomarkers, *etc.*) current guidelines for AAA management consider aneurysm size, as it is defined by its maximum diameter (Dmax) as well as aneurysm growth rate (GR) as the only variables in which therapeutic decisions are based[10-12]. Therefore cut-off points have been set by the European Society for Vascular Surgery (SVS) and the SVS (Dmax $\geqslant$ 55 mm, GR $\geqslant$ 10 mm/year) that are generally thought appropriate for intervention to be recommended[10,11]. Unfortunately landmark studies comparing open surgery *vs* observation alone took place in the early 90 s, thus before the advents of thin-slice computed tomography (CT), digital imaging and the three-dimensional (3D) reconstruction of AAA surface become widely available. Therefore they have used either ultrasonography (US) (UKSAT trial) or axial CT measurements (ADAM trial)[13,14]. On the other hand the most recent randomized trials comparing endovascular aneurysm repair (EVAR) with surveillance, have used orthogonal maximum diameter measurements to determine aneurysm size (PIVOTAL, CAESAR)[15,16]. Currently, reporting standards for endovascular aneurysm repair from the SVS recommend that AAA size is most accurately measured using orthogonal measurements, perpendicular to the centerline of flow after 3D reconstruction of the 2D CT images[17].

Moreover in contemporary clinical practice, EVAR becomes increasingly popular among physicians, having overcome open surgery and currently 80% of all AAA elective repairs are being performed by endovascular means[18]. This is due to its less invasive nature, reduced peri-operative morbidity and mortality, decreased length of hospitalization, need for blood products, intensive care unit stay, *etc*[6-9]. Nevertheless this modality is hampered by the continuous need for surveillance at specific time intervals to assess the successful exclusion of the aneurysm sac from systemic circulation and pressurization. Increase in aneurysm size post-procedurally, usually indicates the need for re-interventions to avoid risk of late aneurysm rupture[10,11]. Therefore AAA size and expansion rate except being essential variables to set the indication for elective repair, are also important determinants of the successful exclusion of AAAs post-EVAR. Except Dmax, aneurysm volume has been suggested to accurately display changes in aneurysm size after EVAR.

Therefore in the same time that reproducible and accurate methods to record AAA size are needed, there may be inconsistencies due to different imaging modalities (*i.e.*, US, CT) but also different modes of measurements (*i.e.*, axial *vs* orthogonal CT measurements, Dmax *vs* Volume measurements, *etc.*). Subsequently the aim of this review is to report on different imaging techniques and assess their comparability and their value to accurately display aneurysm size and growth and assist therapeutic management of these patients.

ULTRASOUND MEASUREMENTS

Ultrasound was the initial imaging modality used to record aneurysm size, still being the preferred technique for AAAs screening and surveillance[19]. It has the advantage of wide availability, low cost, and freedom from radiation exposure while it has been reported to

have a high sensitivity for the detection of AAAs[20-22]. On the other hand US imaging is hampered by the fact that ultrasound waves are disrupted by air and therefore it may not be an ideal imaging technique for organs obscured by the bowel while in large patients, imaging may be ambiguous. In the same time there may be a high operator dependency.

According to Jaakkola *et al*[23], the inter-observer difference in US was < 2 mm in 65% of the anteroposterior and 61% of the transverse measurements and > 5 mm in 11% of the anteroposterior and 14% in the transverse measurements in 102 observer-pairs for all aortas. This difference was significantly larger with reference to AAAs compared to normal aortas. Specifically, for the latter group 78% of differences were < 2 mm and 4% were > 5 mm whereas corresponding values for AAAs were 53% and 16% respectively. Interestingly, in 5% of cases differences exceeded 10 mm. These authors used the term clinically acceptable difference, which was defined as 5 mm and found 84% of measurements to be below this threshold with regard to the anteroposterior AAA diameter.

Singh *et al*[24] subsequently confirmed abovementioned findings, indicating that both the intra- and interobserver variability were less than 4 mm for all sonographers in measurements of maximal infrarenal aortic diameter for both anteroposterior and transverse Dmax recordings. Specifically they found that 96% and 97% of measurements presented a difference < 4 mm and 88% and 93% of these measurements differed < 3 mm. Nevertheless this report is limited by the fact that almost all examinations regarded normal aortas whereas only one AAA was included.

Ellis *et al*[25] investigated repeatability, observer bias and instrument bias of ultrasound and found that the repeatability of maximum aortic diameter measurement by US was better for anterorposterior than transverse diameter, with coefficients of repeatability 3.0-7.5 mm and 10-15 mm respectively. According to their results, at best a single, experienced observer, using the same instrument may provide aortic diameters using US accurate to within 5 mm, but more commonly such aortic diameter is only accurate to within 8 mm.

Hartshorne *et al*[26] in a more recent study reported that the reproducibility coefficients for differences between different operators were 3 mm for inner to inner wall and 4.2 mm for outer to outer wall indicating that in the same time that there was an expected difference in AAA diameter between the two methods of 0.27 mm, inner to inner wall method was measurably more reproducible.

A recent systematic review studying the reproducibility of ultrasound measurement of the abdominal aortic diameter included 9 studies and found that 6/9 reported intraobserver repeatability coefficients for anteroposterior aortic diameter measurements of 1.6-4.4 mm, which were below the 5 mm level generally regarded as acceptable. In the same time, 5/9 studies had interobserver reproducibility below the level of 5 mm but 4/9 reported poor reproducibility ranging from (-2 to 5.2) to (-10.5 to 10.4), which may introduce significant inaccuracies on management of AAA patients. These authors concluded that since various studies use different methodologies with no standardized measurement techniques, a standard training and formal quality assurance of ultrasound measurements are important components of an effective AAA screening program[27].

Overall, among asymptomatic patients, ultrasound detects the presence of an abdominal aortic aneurysm accurately, reproducibly, and at low cost. There is evidence in the literature to support the use of anteroposterior rather than transverse diameter measurement since the latter has worse repeatability[25]. Both the external and the internal diameter may be measured bearing in mind that that evidence from the UKSAT study was based on external aortic diameter[13]. In the same time the MASS trial, the largest aneurysm screening trial, recorded internal aortic diameter which may be more reproducibly recorded but generally is approximately 3 mm smaller than external diameter, while other screening trials have reported data based on external aortic diameter[19,28-30]. Accordingly, ultrasound is the preferred imaging modality for screening, but may be inadequate to accurately record aneurysm size and growth which are important determinants of rupture risk[11].

2D Dmax CT MEASUREMENTS

As early as in 1995, Lederle *et al*[31] published a report based on the population of the ADAM trial which included 806 subjects with an AAA indicating that the interobserver difference between local and central CT measurements of AAA diameter was 2 mm or less in 65% of pairs, but in 17% it was at least 5 mm. For intraobserver pairs of central CT re-measurements, 90% differed by 2 mm or less, 70% were within 1 mm, and only one differed by 5 mm, which is suggestive of the superior CT reproducibility and reliability compare to US measurements. Moreover out of 258 ultrasound-measured and central CT pairs, the difference was 2 mm or less in 44% and at least 5 mm in 33%. Finally ultrasound measurements were smaller than central CT measurements by an average of 2.7 mm. These results were produced with the use of older technologies meaning, previous generation CT scanners, use of 10 mm slice thickness without intravenous contrast and measuring maximum external diameter in any direction.

In another report published in 2002 which generally used similar CT parameters as those abovementioned, the authors compared US to CT measurements in aneurysmal aortas and found that the limits of agreement between methods was 8.7 ± 7.3 mm for anteroposterior measurements and 10.2 ± 11.0 mm for transverse measurements. Therefore it could be expected that 95% of differences would be less than 8.0 mm in anteroposterior measurements and less than 10.6 mm

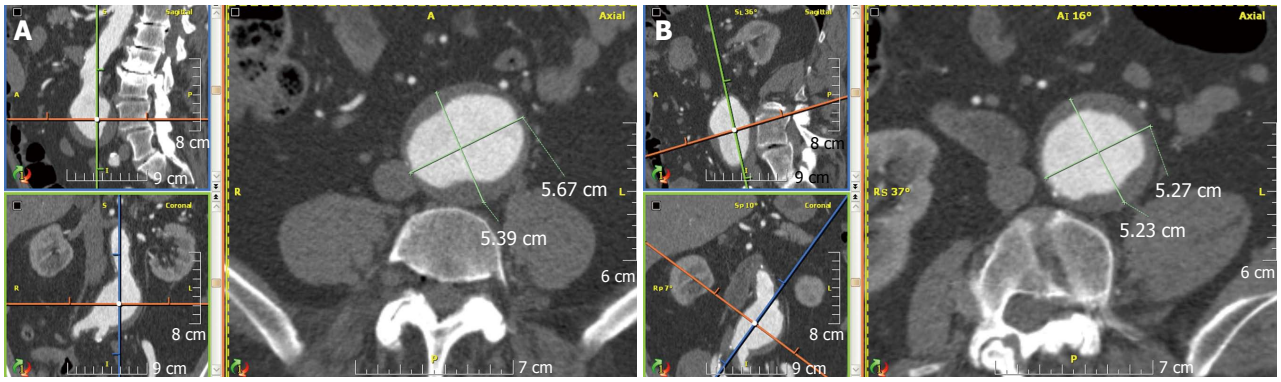

Figure 1 An abdominal aortic aneurysm after three dimensional reconstruction. In panel A the axis are not perpendicular to the vessel lumen while in panel B they are. An overestimation of the maximum diameter has been observed using axial versus orthogonal measurements.

in transverse measurements. A clinically acceptable difference (< 5 mm) was found in 76% and 67% for anteroposterior and transverse measurements respectively and therefore 1 out of 4 patients scanned, would have a difference greater 5 mm between US and CT measurements[32].

Sprouse *et al*[33] studied a total of 334 AAA patients and found a significantly larger Dmax when this was evaluated with CT than with ultrasound (56.9 mm *vs* 47.4 mm, $P < 0.001$). Moreover Dmax measured with CT was greater than that measured with US in 95% of cases. The correlation coefficient between these recordings indicated a strong correlation of 0.705, but interestingly, the difference between the two methods was less than 10 mm in only 51%. Limits of agreement exceeded the limits of clinical acceptability and therefore these authors postulated that assessment of AAA diameter with CT and US is not equivalent and that maximal AAA diameter at CT is significantly and consistently larger than maximal diameter at US.

Singh *et al*[34] confirmed these results and indicated that US slightly underestimated the diameter in normal aortas and tended to overestimate the diameter in aneurysmal aortas compared to CT measurements. In 555 US-CT pairs, the absolute differences were < 2 mm in 62%, 60% and 77% in anteroposterior, transverse and maximum diameter in any plane, respectively. The corresponding figures for an absolute difference of 5 mm or more were 14%, 18% and 8%, respectively while variability increased with increasing diameter.

Overall, it may be suggested that CT is more reproducible than ultrasound, in the same time that standard axial CT imaging generally results in larger diameter recordings which likely reflects the fact that aortic cross-section obtained by axial imaging does not account for vessel tortuosity or may be elliptical and therefore could overestimate AAA size. In the same time that the advantages of portability and decreased expense have made ultrasound the preferred diagnostic technique for aneurysm screening and surveillance CT is the primary modality for operative planning, given its capacity to determine the extent and morphology of the aneurysm[11].

3D Dmax CT MEASUREMENTS

The advents of thin-slice CT, digital imaging and more importantly technological advances that have made 3D-reconstruction of AAA surface feasible, have recently allowed for more accurate measurements of AAA size parameters. Many vascular centers currently use modern imaging and analytic technology that allows precise computer-based measurement as well as automatic centerline determination. Therefore and in order to avoid overestimation of the AAA maximum diameter on axial CT slices due to vessel tortuosity and elliptical cross-sections, reporting standards of the SVS recommend that diameter should be measured in an orthogonal plane, meaning perpendicular to the vessel centerline of flow[17]. Figure 1 presents an AAA after 3D reconstruction, using commercially available software and displaying differences between orthogonal and axial diameter measurements.

Sprouse *et al*[35] compared between US, axial CT and orthogonal CT measurements of AAA maximum diameter as obtained after 3D reconstruction. They suggested that mean axial Dmax was significantly larger than that measured by US or in an orthogonal plane. The difference between US and orthogonal CT measurements was insignificant. Moreover these authors indicated that when aortic angulation was < 25°, axial CT, US and orthogonal CT Dmax were similar while, when aortic angulation was > 25°, axial CT Dmax was significantly larger. The limits of agreement between axial CT measurements and those obtained by US or orthogonal CT were poor and exceeded clinical acceptability (5 mm). On the contrary the variation between US and orthogonal CT recordings was minimal with an acceptable limits of agreement.

Similarly, Manning *et al*[36] compared between ultrasound, axial and orthogonal maximum diameter measurements in order to record discrepancies between various methods. They indicated that the mean of each series of readings on CT was significantly larger than the mean US measurement, and that CT measurements also differed significantly from each other. The axial CT diameter was larger than the orthogonal by a mean

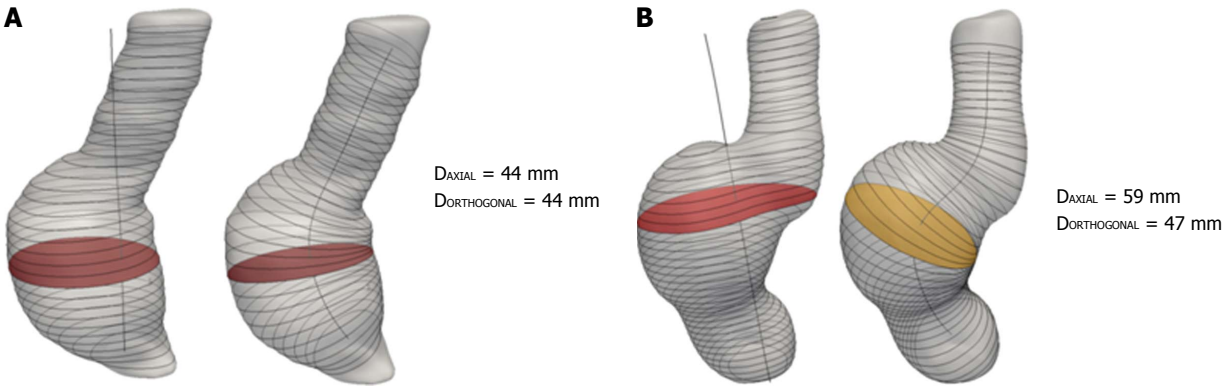

Figure 2 Two abdominal aortic aneurysms are presented after three dimensional reconstruction of the computed tomography images. In the left panels cross sections are perpendicular to the y-axis of the CT scanner coordinator system (axial), while in the right panels cross-section are perpendicular to the centerline of flow (orthogonal). Large discrepancies between methods may be encountered in case of high regional asymmetry as in case B. CT: Computed tomography.

of 2.4 ± 5 mm. The US diameter was smaller than CT axial by 9.6 ± 8.0 mm and CT orthogonal diameter by 7.3 ± 7.0 mm, while AAA size did not significantly affect these differences. Seventy-eight percent of 120 pairs of intraobserver CT measurements and 65% of interobserver CT measurements differed by < 2 mm. Therefore, CT-based measurements of aneurysm size tended to be larger than the US measurement and axial are consistently larger than orthogonal diameters.

Others have compared between US and CT measurements and found a larger AAA maximum diameter of 2.1 mm with the latter modality, in the same time that limits of agreement were -5.5 to 9.6 mm, exceeding clinical acceptability. Mean difference was higher in subjects with a maximum diameter between 50-55 mm as assessed by ultrasound compared to those presenting with larger AAAs above 55 mm (3.9 mm *vs* 1 mm). Remarkably, 70% of those patients with a US recording between 50 and 55 mm had CT scans revealing diameters greater than 55 mm. Therefore these authors conclude that significant differences between imaging modalities do exist and recommend AAAs measuring > 50 mm on US, to undergo earlier CT imaging[37].

Our study group specifically examined discrepancies between axial and orthogonal CT measurements in sixty CT scans and showed that there is a consistent overestimation of AAAs maximum diameter when measured on an axial plane. Although the mean difference between measurements was low there was a wide range among cases that can change therapeutic decisions in a significant 20% of cases. Asymmetry of the axial sections can easily be determined from 2D CT slices by introducing Shape Index which is defined as: Section minor axis/section major axis. In case of high regional asymmetry (shape index $\leqslant$ 0.8) an overestimation of maximum diameter by > 5 mm might be expected. In this instance orthogonal measurements should be pursued to determine actual aneurysm size. For shape index > 0.8, axial measurements alone are usually adequate. Figure 2 presents axial and orthogonal diameter measurements for two AAAs, one of which would display large discrepancy due to high regional asymmetry. Moreover we were the first to examine discrepancies in growth rate determination using various CT measurements. There were insignificant differences in growth rates when determined using orthogonal or axial measurements in both examinations (median growth rate: 2.3 and 3.3 mm/year respectively $P = 0.2$) in the same time that there were remarkable differences when orthogonal measurements were used at initial and axial measurements at follow-up examination or vice versa (median growth rate: 4.9 and 0.9 mm/year respectively $P < 0.001$). Therefore growth rates of AAAs should be calculated using the same method of measurements in both CTs otherwise there can be significant discrepancies[38].

Overall it can be concluded that the advents of thin-slice CT, digital imaging and readily available software to perform 3D-reconstruction, have rendered previously described measuring methods out-of-date. However, one should bear in mind that current thresholds to determine the need for intervention are based on older studies, using less sophisticated techniques. Therefore if someone considers the UKSAT trial, surgical repair would be indicated for aneurysms > 55 mm of maximal US anteroposterior diameter[13]. According to the study by Manning *et al*[36], the currently recommended CT measurement technique, shows consistent bias toward a larger diameter value than US measured diameter, with a mean difference of 7 mm which means that, what would be a 56 mm aneurysm by current standards is actually a 49 mm aneurysm using UKSAT method which would lead to the surveillance rather than surgical correction of this aneurysm. The current SVS reporting standards recommend that diameter should be recorded perpendicular to the line of blood flow in order to display actual aneurysm size[17]. Nevertheless, diameters measured in this way, actually have not previously been used in the trials that have determined appropriate thresholds for surgical AAA repair. Overall, a summary of studies comparing different techniques to record AAA

Table 1 Summary of studies comparing between various Dmax measurements

Ref.	Journal, yr	Variables	Main results	Highlights
Lederle *et al*[31]	*J Vasc Surg*, 1995	US, CTaxial	US smaller than CTaxial an average of 0.27 cm	Difference < 0.2 cm in 44% and > 0.5 cm in 33% of patients
Jaakkola *et al*[23]	*Eur J Vasc Endovasc Surg*, 1996	US, CTaxial	Mean AAA anteroposterior CTaxial-US difference was 2.6 ± 3.9 mm. Mean transverse difference was 0.8 ± 4.4	Interobserver differences < 5 mm in 84% of the US and 91% of the CTaxial recordings
Wanhainen *et al*[32]	*Eur J Vasc Endovasc Surg*, 2002	US, CTaxial	In AAAs the mean diameter did not differ significantly	95% of differences between US and CTaxial are expected to be < 8.0 mm in anteroposterior and < 10.6 mm in transverse measurements
Sprouse *et al*[33]	*J Vasc Surg*, 2003	US, CTaxial	CTaxial (5.69 ± 0.89 cm) significantly larger than US (4.74 ± 0.91 cm)	Strong correlation between CTmax and US (r = 0.705), but difference < 1.0 cm in only 51% of cases
Singh *et al*[34]	*Eur J Vasc Endovasc Surg*, 2004	US, CTaxial	Total: US smaller by -0.11 mm, aortas < 30 mm: US smaller by -0.64 mm, aortas 30-39 mm: CT smaller by 0.67 mm, aortas > 40 mm: CT smaller 1.09 mm	Differences > 5 mm are expected in 8% of patients. Variability increases with increasing diameter
Sprouse *et al*[35]	*Eur J Vasc Endovasc Surg*, 2004	US, CTaxial CTorth	Mean CTaxial (58.0 mm) significantly larger than USmax (53.9 mm) or CTorth (54.7 mm). Insignificant difference between US and Dorth	When aortic angulation was < 25°, Daxial (55.3 mm), US (54.3 mm), and Dorth (54.1 mm) were similar. When aortic angulation was > 25°, Daxial (60.1 mm) was significantly larger than US (53.8 mm) and Dorth (55.0 mm)
Manning *et al*[36]	*J Vasc Surg*, 2009	US, CTaxial, CTorth	US smaller than CTaxial by 9.6 mm and CTorth by 7.3 mm	Of all CT recordings, diameter perpendicular to the maximal ellipse on axial sections most closely approximates the findings of US and therefore this most closely approximates criteria used in the UKSAT
Foo *et al*[37]	*Eur J Vasc Endovasc Surg*, 2011	US, CTorth	US underestimated AAA size compared to CTorth by a mean difference of 0.21 (± 0.39) cm	Limits of agreement were -0.55 to 0.96 cm, exceeding clinical acceptability. 70% of patients with US < 5.5 cm presented CTorth > 5.5 cm
Kontopodis *et al*[38]	*Eur J Radiol*, 2013	CTaxial, CTorth	CTaxial greater than CT orth by 2 mm (range: 0-12.3 mm)	20% of the CTs presented Daxial above and Dorth below 5.5 cm which is threshold for repair. Growth rates should be determined with either axial or orthogonal technique not interchanging between methods

AAA: Abdominal aortic aneurysm; CT: Computed tomography; CTorth: Orthogonal maximum diameter measured from CT images; CTaxial: Axial maximum diameter measured from CT images; US: Ultrasonography.

Dmax are presented in Table 1.

3D VOLUMETRIC INDICES

Currently, commercially available software allow image post-processing and accurate as well as rapid volume recording of aneurysmal sac[39]. Subsequently this latter variable has been tested against the traditional index of Dmax regarding its accuracy in determining aneurysm size and its sensitivity to capture aneurysm growth over time.

Parr *et al*[40] in a study including 57 patients indicated that the reproducibility of measurements regarding both aortic volume and diameter was excellent with an average coefficient of variation < 4%. When they classified size changes according to the 95% limits of agreement for each outcome (aortic expansion: When volume or diameter changes exceeded the appropriate limit of agreement and stasis: When volume or diameter changes were below the appropriate limit of agreement) they found that a significant 42% of patients who had increased aortic volume did not display corresponding axial or orthogonal diameter changes. Therefore despite the fact that total aortic volume and maximum diameter can both be measured reproducibly, volume changes are not always reflected by similar changes in diameter.

Similarly, Kauffmann *et al*[41] investigated the ability of a semi-automated segmentation combined with 3D-3D registration between baseline and follow-up examinations to enable fast volumetric follow-up by operators with minimal training in untreated AAA patients to evaluate the software's ability to detect growth. They were able to show an excellent interobserver agreement with a repeatability coefficient < 3 mm for Dmax, < 7% for relative Dmax growth, < 6 mL for volume and < 6% for relative volume growth. Remarkably, using absolute growth, 22/28 patients had volumetric increase above the 95% limits of agreement whereas 18/28 patients had diameter increase above the 95% limits of agreement. Thus, 4/28 (14.3%) of patients had discordance between volumetric and diameter changes during follow-up. These authors conclude that AAA volume was a more sensitive mean to detect AAA growth than Dmax. It should be mentioned that the average time to segment the AAA was < 4 min which shows the ease of this method.

Kritpracha *et al*[42] studied 68 patients post-EVAR in order to detect size changes and compared between diameter and volume measurements. They used a cutoff value of 5 mm for diameter and 10% for volume change to define significant size change. The volume recordings identified AAA size change in 81% of studies (15% increase and 66% decrease) whereas orthogonal

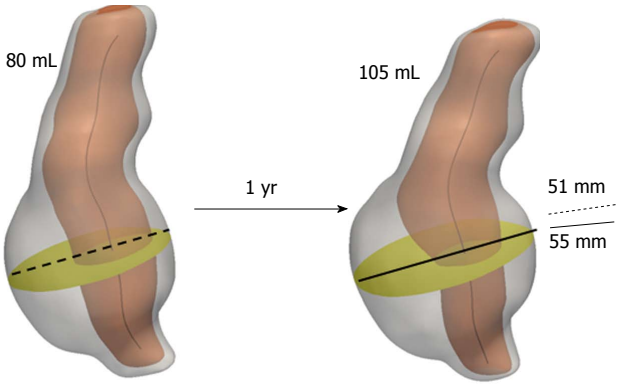

Figure 3 A case of an abdominal aortic aneurysm. An increase of 4 mm/year (may not be considered significant according to current standards taking into account increases > 5 mm), is accompanied by an increase or 20 mL representing 25% of its initial volume which is significant. Volume growth is not always represented in Dmax increase.

Dmax showed AAA size change less frequently (57% of studies, 4% increase and 53% decrease). Volume was stable in 19% of studies, while Dmax showed a greater number of stable AAAs (43%). Among the 20 studies with increased volume, Dmax increased in only 5 (25%).

van Keulen *et al*[43] in a study examining patients having undergone EVAR, indicated that transverse diameter measurements would have missed 63% and orthogonal measurements would have missed 50% of the volume increases, in patients with type Ⅱ endoleaks. Therefore in the presence of type Ⅱ endoleaks (in which there is still no consensus about reintervention), volumetry may provide a useful parameter to discriminate between type Ⅱ endoleaks that either do or do not need reintervention.

In a recent study from our institution we aimed to examine if 3D volumetric measurements during assessment of AAA expansion, associate with the need for surgical repair, and compare to the traditionally used maximum diameter measurements. Firstly, we found that 25/34 AAAs presented volumetric growth rates above the respective upper 95% level of agreement while the same applied to 19/34 AAAs with respect to diameter measurements. This means that 6/34 (18%) of AAAs, according to volume measurements presented a growth beyond inter-observer variability while they did not display significant change regarding diameter measurements. Moreover there was a strong correlation between volume and diameter growth rates which was statistically significant (Spearman's rho 0.6, P = 0.002). The most remarkable result of this report is the increased contingency between high growth rate as determined by AAA volume and need for intervention, which was not confirmed for diameter measurements. Specifically, with regard to Dmax growth rates 10 of the 15 AAAs that underwent intervention were in the high growth rate and 5 in the low growth rate group (P = 0.17). Taking into account AAA volume 12 of the 15 AAAs having undergone surgical correction were in the high and only 3 in the low growth rate group (P = 0.005). Significant association with need for surgical repair could only be established for AAA volumes but not for maximum diameter. Subsequently, an AAA that presented a rapid volume increase presented a 10-fold risk to reach appropriate thresholds for surgical repair compared to an AAA presenting a slow volume increase. The risk was only 3-fold when accounting for Dmax growth. Sensitivity and specificity to predict need for surgical intervention were superior for volume measurements (Sensitivity 80% *vs* 66%, Specificity 74% *vs* 63%)[44]. Figure 3 displays an AAA which despite presenting a small Dmax increase, had a rapid volumetric growth.

Overall it can be postulated that according to published literature volumetric indices may be superior compared to Dmax for both untreated AAA surveillance but also to determine size changes post-EVAR[41,45,46]. This may be due to the fact that since AAA volumes are much larger than corresponding diameters, absolute changes over time may be bigger and allow for an increased sensitivity in measurements. In a simplified model of AAA expansion a growth of 1 mm in diameter would equal an increase of 10 mL for an AAA of 60 mm length[40]. Furthermore, in the same time that diameter measurements only record AAA size at one site, not taking into account changes at other sites, volume measurements also reflect the gradual changes of aneurysm morphology such as lengthening and therefore may be more appropriate in order to record changes in AAA size than maximum diameter[40,44]. Findings of studies comparing Dmax *vs* Volume measurements are presented in Table 2.

REGIONAL GROWTH MEASUREMENTS

Since aneurysm rupture is in fact a material failure of the aneurysmal tissue to withhold stress due to systemic pressurization which is a localized phenomenon, spatial distribution of mechanical properties of the aneurysmal wall has been suggested to be of critical importance for AAAs natural history[47]. Indeed, aneurysm rupture or non-rupture is determined on a pinpoint comparison of wall strength and stress for every point of the aneurysm surface, which would ultimately lead to rupture whenever the forces exerted on the wall, exceed strength of it. Raghavan *et al*[48] explored the regional distribution of wall thickness and failure properties in human AAAs indicating that thickness varied regionally and between different AAAs from as low as 0.23 mm at a rupture site to 4.26 mm at a calcified site. Wall thickness was slightly lower in the posterior and right regions, while the failure tension of specimen strips varied regionally and between AAAs from as low as 5.5 N/cm close to a blister site in the ruptured AAA to 42.3 N/cm at the undilated neck of an unruptured AAA. Similarly, a wide variation of failure stress was recorded ranging from 33.6 to 235.1 N/cm^2 in the same time that there was no perceptible pattern in failure properties along the circumference.

Subsequently the use of universal size variables

Table 2 Summary of studies comparing between orthogonal diameter computed tomography and volume measurements

Ref.	Journal, yr	Population	Definition of size-change	Main results
Wever *et al*[45]	*Eur J Vasc Endovasc Surg*, 2000	Post-EVAR	LOAs	37%, discordance Dmax and volume measurements. A decrease in aneurysm size was missed using Dmax in 14% of cases and an increase in 19% of cases
Prinssen *et al*[46]	*Eur J Vasc Endovasc Surg*, 2003	Post-EVAR	NA	Volume data resulted in more "good/wait" while Diameter data resulted in more "not good/further diagnostics"-decisions
Kritpracha *et al*[42]	*JEVT*, 2004	Post-EVAR	10% for volume, 5 mm for diameter	Volume changed in 81% of studies (15% increase and 66% decrease). Dmax changed 57% (4% increase and 53% decrease). Among 20 studies with increased volume, Dmax increased in only 5
van Keulen *et al*[43]	*J Endovasc Ther*, 2009	Post-EVAR	5% for volume, 5 mm for diameter	Volumetry detected aneurysm growth in 24% and shrinkage in 54% of patients, which was reflected by Dmax in 10.6% and 28% respectively
Parr *et al*[40]	*Eur J Radiol*, 2011	Small AAAs	LOAs	42% of patients who had increased aortic volume did not display corresponding diameter changes
Kauffmann *et al*[41]	*Eur J Radiol*, 2012	Small AAAs	LOAs	4/28 (14.3%) patients presented volume increase which was not reflected in Dmax
Kontopodis *et al*[44]	*Eur J Radiol*, 2014	Small AAAs	LOAs	18% of patients who had increased aortic volume did not display corresponding diameter changes. AAAs presenting rapid volume increase had a 10-fold risk to be operated, while the risk was 3-fold for rapid Dmax increase

LOAs: Limits of agreement; AAA: Ab dominal aortic aneurysm; EVAR: Endovascular aneurysm repair; NA: Not available.

as maximum diameter and volume, in order to record aneurysm expansion is inherently hampered by the lack of information about regional distribution of growth rate. Our study group has previously developed a methodology to record regional growth and applied this to a rapidly growing AAA. For this purpose the centerlines of the aneurysmal wall as well as lumen surfaces were created and used to extract perpendicular cross sections every 1 mm. To determine the aneurysm's pattern of expansion, cross-sectional area change from initial to follow-up examination was plotted against the distance from aortic bifurcation which was considered as the reference point for registration of initial and final CT angiograms. ILT thickness and eccentricity of ILT deposition were also recorded along the aneurysm for both AAA models. Maximum AAA and ILT cross-sectional areas were observed at the same distance from aortic bifurcation that was 4 cm for both AAA models as presented in Figure 4[49,50].

In the same context, Martufi *et al*[51] monitored diameter development over the entire aneurysm to record sites of the fastest diameter growth. They suggested that development of an AAA's maximum diameter or its volume over time can assess the mean diameter growth but not the maximum diameter growth. Interestingly, the annual diameter growth measured at the site of maximum expansion was 16%, almost four times larger than the mean diameter expansion of 4.4%. According to this study the site of maximum diameter growth did not coincide with the position of the maximum baseline. Moreover the overall aneurysm sac length increased from 84 to 89 mm during the follow-up, which relates to a median annual longitudinal growth of 3.5% in the same time that the neck length shortened, on average, by 6.2% per year. Therefore these authors postulate that neither maximum diameter nor volume measurements, are able to record the fastest diameter growth of the aneurysm sac and consequently, expansion-related wall weakening might be inappropriately reflected by this type of surveillance data. In contrast, localized spots of fast diameter growth can be detected through multiple centerline based diameter measurements over the entire aneurysm sac.

CONCLUSION

Currently, significant technological advancements regarding abdominal imaging have made AAA size and growth recordings more accurate and reproducible than ever. According to evidence reported in the literature which has also been implemented in current guidelines, ultrasound may be used as the primary imaging modality for aneurysm screening and follow up and a policy of ultrasonographic surveillance is advised for small asymptomatic AAAs. In order to accurately capture aneurysm size and determine need but also method (*i.e.,* open surgery or EVAR) for AAA repair, CT imaging is appropriate additional to US, if an AAA is approaching a size requiring intervention, or if rapid growth is suspected. Moreover, standards for reporting on EVAR highlight the significance of orthogonal diameter measurements indicating that preferably, maximum diameter should be measured perpendicular to the centerline of flow with 3D-reconstruction of CT images. The potential role of volumetric indices is also underlined since taking into account that variations in size occur in three dimensions, relatively small diameter shifts that may be difficult to accurately measure with conventional imaging techniques, may be correlated with a significant change in aneurysm volume. Finally regional growth recordings are based in a sound biomechanical ground and therefore may represent the emerging method to

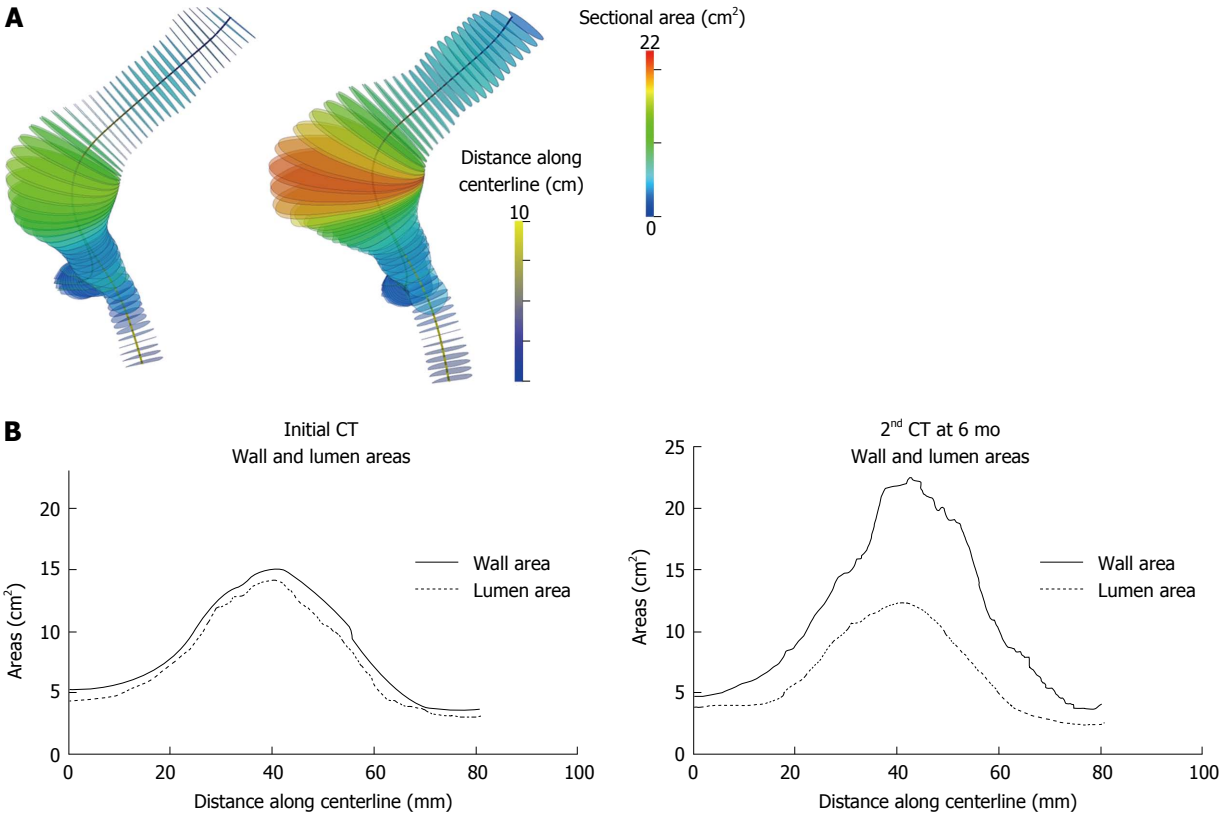

Figure 4 Cross-sections perpendicular to the centerline with regard to sectional areas for initial and follow-up abdominal aortic aneurysm-models. Maximum sectional areas present values of 22.5 cm^2 and 15 cm^2 respectively. Color scale on the centerlines depicts distance along the centerline with 8 cm representing aortic bifurcation. Sections areas are displayed against distance along the centerline indicating that maximum values are obtained in the same distance from aortic bifurcation (approximately 4 cm). Figure originally published at Kontopodis *et al*[50].

capture aneurysm size and growth which will become increasingly used in the future.

REFERENCES

1 **Ouriel K**, Green RM, Donayre C, Shortell CK, Elliott J, DeWeese JA. An evaluation of new methods of expressing aortic aneurysm size: relationship to rupture. *J Vasc Surg* 1992; **15**: 12-18; discussion 19-20 [PMID: 1728670 DOI: 10.1016/0741-5214(92)70008-9]

2 **Bengtsson H**, Sonesson B, Bergqvist D. Incidence and prevalence of abdominal aortic aneurysms, estimated by necropsy studies and population screening by ultrasound. *Ann N Y Acad Sci* 1996; **800**: 1-24 [PMID: 8958978 DOI: 10.1111/j.1749-6632.1996.tb33294.x]

3 **Patel MI**, Hardman DT, Fisher CM, Appleberg M. Current views on the pathogenesis of abdominal aortic aneurysms. *J Am Coll Surg* 1995; **181**: 371-382 [PMID: 7551334]

4 **Lederle FA**, Johnson GR, Wilson SE. Abdominal aortic aneurysm in women. *J Vasc Surg* 2001; **34**: 122-126 [PMID: 11436084 DOI: 10.1067/mva.2001.115275]

5 **Lederle FA**, Johnson GR, Wilson SE, Chute EP, Hye RJ, Makaroun MS, Barone GW, Bandyk D, Moneta GL, Makhoul RG. The aneurysm detection and management study screening program: validation cohort and final results. Aneurysm Detection and Management Veterans Affairs Cooperative Study Investigators. *Arch Intern Med* 2000; **160**: 1425-1430 [PMID: 10826454 DOI: 10.1001/archinte.160.10.1425]

6 **Lederle FA**, Freischlag JA, Kyriakides TC, Matsumura JS, Padberg FT, Kohler TR, Kougias P, Jean-Claude JM, Cikrit DF, Swanson KM; OVER Veterans Affairs Cooperative Study Group. Long-term comparison of endovascular and open repair of abdominal aortic aneurysm. *N Engl J Med* 2012; **367**: 1988-1997 [PMID: 23171095 DOI: 10.1056/NEJMoa1207481]

7 **De Bruin JL**, Baas AF, Buth J, Prinssen M, Verhoeven EL, Cuypers PW, van Sambeek MR, Balm R, Grobbee DE, Blankensteijn JD; DREAM Study Group. Long-term outcome of open or endovascular repair of abdominal aortic aneurysm. *N Engl J Med* 2010; **362**: 1881-1889 [PMID: 20484396 DOI: 10.1056/NEJMoa0909499]

8 **United Kingdom EVAR Trial Investigators**, Greenhalgh RM, Brown LC, Powell JT, Thompson SG, Epstein D, Sculpher MJ. Endovascular versus open repair of abdominal aortic aneurysm. *N Engl J Med* 2010; **362**: 1863-1871 [PMID: 20382983 DOI: 10.1056/NEJMoa0909305]

9 **Becquemin JP**, Pillet JC, Lescalie F, Sapoval M, Goueffic Y, Lermusiaux P, Steinmetz E, Marzelle J; ACE trialists. A randomized controlled trial of endovascular aneurysm repair versus open surgery for abdominal aortic aneurysms in low- to moderate-risk patients. *J Vasc Surg* 2011; **53**: 1167-1173.e1 [PMID: 21276681 DOI: 10.1016/j.jvs.2010.10.124]

10 **Moll FL**, Powell JT, Fraedrich G, Verzini F, Haulon S, Waltham M, van Herwaarden JA, Holt PJ, van Keulen JW, Rantner B, Schlösser FJ, Setacci F, Ricco JB; European Society for Vascular Surgery. Management of abdominal aortic aneurysms clinical practice guidelines of the European society for vascular surgery. *Eur J Vasc Endovasc Surg* 2011; **41** Suppl 1: S1-S58 [PMID: 21215940 DOI: 10.1016/j.ejvs.2010.09.011]

11 **Chaikof EL**, Brewster DC, Dalman RL, Makaroun MS, Illig KA, Sicard GA, Timaran CH, Upchurch GR Jr, Veith FJ; Society for Vascular Surgery. The care of patients with an abdominal aortic aneurysm: the Society for Vascular Surgery practice guidelines. *J Vasc Surg* 2009; **50**: S2-49 [PMID: 19786250 DOI: 10.1016/j.jvs.2009.07.002]

12 **Kontopodis N**, Metaxa E, Papaharilaou Y, Tavlas E, Tsetis D, Ioannou C. Advancements in identifying biomechanical determinants for abdominal aortic aneurysm rupture. *Vascular* 2015; **23**: 65-77 [PMID: 24757027 DOI: 10.1177/1708538114532

084]
13 **The UK Small Aneurysm Trial Participants**. Mortality results for randomised controlled trial of early elective surgery or ultrasonographic surveillance for small abdominal aortic aneurysms. The UK Small Aneurysm Trial Participants. *Lancet* 1998; **352**: 1649-1655 [PMID: 9853436 DOI: 10.1016/S0140-6736(98)10137-X]
14 **Lederle FA**, Wilson SE, Johnson GR, Reinke DB, Littooy FN, Acher CW, Ballard DJ, Messina LM, Gordon IL, Chute EP, Krupski WC, Busuttil SJ, Barone GW, Sparks S, Graham LM, Rapp JH, Makaroun MS, Moneta GL, Cambria RA, Makhoul RG, Eton D, Ansel HJ, Freischlag JA, Bandyk D. Immediate repair compared with surveillance of small abdominal aortic aneurysms. *N Engl J Med* 2002; **346**: 1437-1444 [PMID: 12000813 DOI: 10.1056/NEJMoa012573]
15 **Cao P**; CAESAR Trial Collaborators. Comparison of surveillance vs Aortic Endografting for Small Aneurysm Repair (CAESAR) trial: study design and progress. *Eur J Vasc Endovasc Surg* 2005; **30**: 245-251 [PMID: 16130206 DOI: 10.1016/j.ejvs.2005.05.043]
16 **Ouriel K**. The PIVOTAL study: a randomized comparison of endovascular repair versus surveillance in patients with smaller abdominal aortic aneurysms. *J Vasc Surg* 2009; **49**: 266-269 [PMID: 19174266 DOI: 10.1016/j.jvs.2008.11.048]
17 **Chaikof EL**, Blankensteijn JD, Harris PL, White GH, Zarins CK, Bernhard VM, Matsumura JS, May J, Veith FJ, Fillinger MF, Rutherford RB, Kent KC; Ad Hoc Committee for Standardized Reporting Practices in Vascular Surgery of The Society for Vascular Surgery/American Association for Vascular Surgery. Reporting standards for endovascular aortic aneurysm repair. *J Vasc Surg* 2002; **35**: 1048-1060 [PMID: 12021727 DOI: 10.1067/mva.2002.123763]
18 **Sachs T**, Schermerhorn M, Pomposelli F, Cotterill P, O'Malley J, Landon B. Resident and fellow experiences after the introduction of endovascular aneurysm repair for abdominal aortic aneurysm. *J Vasc Surg* 2011; **54**: 881-888 [PMID: 21620615 DOI: 10.1016/j.jvs.2011.03.008]
19 **Ashton HA**, Buxton MJ, Day NE, Kim LG, Marteau TM, Scott RA, Thompson SG, Walker NM; Multicentre Aneurysm Screening Study Group. The Multicentre Aneurysm Screening Study (MASS) into the effect of abdominal aortic aneurysm screening on mortality in men: a randomised controlled trial. *Lancet* 2002; **360**: 1531-1539 [PMID: 12443589 DOI: 10.1016/S0140-6736(02)11522-4]
20 **Quill DS**, Colgan MP, Sumner DS. Ultrasonic screening for the detection of abdominal aortic aneurysms. *Surg Clin North Am* 1989; **69**: 713-720 [PMID: 2501880]
21 **Graeve AH**, Carpenter CM, Wicks JD, Edwards WS. Discordance in the sizing of abdominal aortic aneurysm and its significance. *Am J Surg* 1982; **144**: 627-634 [PMID: 7149120 DOI: 10.1016/0002-9610(82)90539-6]
22 **Wilmink AB**, Forshaw M, Quick CR, Hubbard CS, Day NE. Accuracy of serial screening for abdominal aortic aneurysms by ultrasound. *J Med Screen* 2002; **9**: 125-127 [PMID: 12370324 DOI: 10.1136/jms.9.3.125]
23 **Jaakkola P**, Hippeläinen M, Farin P, Rytkönen H, Kainulainen S, Partanen K. Interobserver variability in measuring the dimensions of the abdominal aorta: comparison of ultrasound and computed tomography. *Eur J Vasc Endovasc Surg* 1996; **12**: 230-237 [PMID: 8760988 DOI: 10.1016/S1078-5884(96)80112-2]
24 **Singh K**, Jacobsen BK, Solberg S, Bønaa KH, Kumar S, Bajic R, Arnesen E. Intra- and interobserver variability in the measurements of abdominal aortic and common iliac artery diameter with computed tomography. The Tromsø study. *Eur J Vasc Endovasc Surg* 2003; **25**: 399-407 [PMID: 12713777 DOI: 10.1053/ejvs.2002.1856]
25 **Ellis M**, Powell JT, Greenhalgh RM. Limitations of ultrasonography in surveillance of small abdominal aortic aneurysms. *Br J Surg* 1991; **78**: 614-616 [PMID: 2059819 DOI: 10.1002/bjs.1800780529]
26 **Hartshorne TC**, McCollum CN, Earnshaw JJ, Morris J, Nasim A. Ultrasound measurement of aortic diameter in a national screening programme. *Eur J Vasc Endovasc Surg* 2011; **42**: 195-199 [PMID: 21439859 DOI: 10.1016/j.ejvs.2011.02.030]
27 **Beales L**, Wolstenhulme S, Evans JA, West R, Scott DJ. Reproducibility of ultrasound measurement of the abdominal aorta. *Br J Surg* 2011; **98**: 1517-1525 [PMID: 21861264 DOI: 10.1002/bjs.7628]
28 **Scott RA**, Wilson NM, Ashton HA, Kay DN. Influence of screening on the incidence of ruptured abdominal aortic aneurysm: 5-year results of a randomized controlled study. *Br J Surg* 1995; **82**: 1066-1070 [PMID: 7648155 DOI: 10.1002/bjs.1800820821]
29 **Lindholt JS**, Juul S, Fasting H, Henneberg EW. Screening for abdominal aortic aneurysms: single centre randomised controlled trial. *BMJ* 2005; **330**: 750 [PMID: 15757960 DOI: 10.1136/bmj.38369.620162.82]
30 **Norman PE**, Jamrozik K, Lawrence-Brown MM, Le MT, Spencer CA, Tuohy RJ, Parsons RW, Dickinson JA. Population based randomised controlled trial on impact of screening on mortality from abdominal aortic aneurysm. *BMJ* 2004; **329**: 1259 [PMID: 15545293 DOI: 10.1136/bmj.38272.478438.55]
31 **Lederle FA**, Wilson SE, Johnson GR, Reinke DB, Littooy FN, Acher CW, Messina LM, Ballard DJ, Ansel HJ. Variability in measurement of abdominal aortic aneurysms. Abdominal Aortic Aneurysm Detection and Management Veterans Administration Cooperative Study Group. *J Vasc Surg* 1995; **21**: 945-952 [PMID: 7776474 DOI: 10.1016/S0741-5214(95)70222-9]
32 **Wanhainen A**, Bergqvist D, Björck M. Measuring the abdominal aorta with ultrasonography and computed tomography - difference and variability. *Eur J Vasc Endovasc Surg* 2002; **24**: 428-434 [PMID: 12435343 DOI: 10.1053/ejvs.2002.1748]
33 **Sprouse LR**, Meier GH, Lesar CJ, Demasi RJ, Sood J, Parent FN, Marcinzyck MJ, Gayle RG. Comparison of abdominal aortic aneurysm diameter measurements obtained with ultrasound and computed tomography: Is there a difference? *J Vasc Surg* 2003; **38**: 466-471; discussion 471-472 [PMID: 12947257 DOI: 10.1016/S0741-5214(03)00367-7]
34 **Singh K**, Jacobsen BK, Solberg S, Kumar S, Arnesen E. The difference between ultrasound and computed tomography (CT) measurements of aortic diameter increases with aortic diameter: analysis of axial images of abdominal aortic and common iliac artery diameter in normal and aneurysmal aortas. The Tromsø Study, 1994-1995. *Eur J Vasc Endovasc Surg* 2004; **28**: 158-167 [PMID: 15234697 DOI: 10.1016/j.ejvs.2004.03.018]
35 **Sprouse LR**, Meier GH, Parent FN, DeMasi RJ, Glickman MH, Barber GA. Is ultrasound more accurate than axial computed tomography for determination of maximal abdominal aortic aneurysm diameter? *Eur J Vasc Endovasc Surg* 2004; **28**: 28-35 [PMID: 15177228 DOI: 10.1016/j.ejvs.2004.03.022]
36 **Manning BJ**, Kristmundsson T, Sonesson B, Resch T. Abdominal aortic aneurysm diameter: a comparison of ultrasound measurements with those from standard and three-dimensional computed tomography reconstruction. *J Vasc Surg* 2009; **50**: 263-268 [PMID: 19631858 DOI: 10.1016/j.jvs.2009.02.243]
37 **Foo FJ**, Hammond CJ, Goldstone AR, Abuhamdiah M, Rashid ST, West RM, Nicholson AA, Scott DJ. Agreement between computed tomography and ultrasound on abdominal aortic aneurysms and implications on clinical decisions. *Eur J Vasc Endovasc Surg* 2011; **42**: 608-614 [PMID: 21852165 DOI: 10.1016/j.ejvs.2011.07.003]
38 **Kontopodis N**, Metaxa E, Gionis M, Papaharilaou Y, Ioannou CV. Discrepancies in determination of abdominal aortic aneurysms maximum diameter and growth rate, using axial and orhtogonal computed tomography measurements. *Eur J Radiol* 2013; **82**: 1398-1403 [PMID: 23727377 DOI: 10.1016/j.ejrad.2013.04.031]
39 **Yushkevich PA**, Piven J, Hazlett HC, Smith RG, Ho S, Gee JC, Gerig G. User-guided 3D active contour segmentation of anatomical structures: significantly improved efficiency and reliability. *Neuroimage* 2006; **31**: 1116-1128 [PMID: 16545965 DOI: 10.1016/j.neuroimage.2006.01.015]
40 **Parr A**, Jayaratne C, Buttner P, Golledge J. Comparison of volume and diameter measurement in assessing small abdominal aortic aneurysm expansion examined using computed tomographic angiography. *Eur J Radiol* 2011; **79**: 42-47 [PMID: 20061105 DOI: 10.1016/j.ejrad.2009.12.018]
41 **Kauffmann C**, Tang A, Therasse E, Giroux MF, Elkouri S,

Melanson P, Melanson B, Oliva VL, Soulez G. Measurements and detection of abdominal aortic aneurysm growth: Accuracy and reproducibility of a segmentation software. *Eur J Radiol* 2012; **81**: 1688-1694 [PMID: 21601403 DOI: 10.1016/j.ejrad.2011.04.044]

42 **Kritpracha B**, Beebe HG, Comerota AJ. Aortic diameter is an insensitive measurement of early aneurysm expansion after endografting. *J Endovasc Ther* 2004; **11**: 184-190 [PMID: 15056034 DOI: 10.1583/03-976.1]

43 **van Keulen JW**, van Prehn J, Prokop M, Moll FL, van Herwaarden JA. Potential value of aneurysm sac volume measurements in addition to diameter measurements after endovascular aneurysm repair. *J Endovasc Ther* 2009; **16**: 506-513 [PMID: 19702341 DOI: 10.1583/09-2690.1]

44 **Kontopodis N**, Metaxa E, Papaharilaou Y, Georgakarakos E, Tsetis D, Ioannou CV. Value of volume measurements in evaluating abdominal aortic aneurysms growth rate and need for surgical treatment. *Eur J Radiol* 2014; **83**: 1051-1056 [PMID: 24768189 DOI: 10.1016/j.ejrad.2014.03.018]

45 **Wever JJ**, Blankensteijn JD, Th M Mali WP, Eikelboom BC. Maximal aneurysm diameter follow-up is inadequate after endovascular abdominal aortic aneurysm repair. *Eur J Vasc Endovasc Surg* 2000; **20**: 177-182 [PMID: 10942691 DOI: 10.1053/ejvs.1999.1051]

46 **Prinssen M**, Verhoeven EL, Verhagen HJ, Blankensteijn JD. Decision-making in follow-up after endovascular aneurysm repair based on diameter and volume measurements: a blinded comparison. *Eur J Vasc Endovasc Surg* 2003; **26**: 184-187 [PMID: 12917836 DOI: 10.1053/ejvs.2002.1892]

47 **Vorp DA**. Biomechanics of abdominal aortic aneurysm. *J Biomech* 2007; **40**: 1887-1902 [PMID: 17254589 DOI: 10.1016/j.jbiomech.2006.09.003]

48 **Raghavan ML**, Kratzberg J, Castro de Tolosa EM, Hanaoka MM, Walker P, da Silva ES. Regional distribution of wall thickness and failure properties of human abdominal aortic aneurysm. *J Biomech* 2006; **39**: 3010-3016 [PMID: 16337949 DOI: 10.1016/j.jbiomech.2005.10.021]

49 **Kontopodis N**, Lipsa L, Metaxa E, Georgakarakos E Papaharilaou Y, Tsetis D, Ioannou CV. Thrombus morphology may be an indicator for aneurysm expansion. *J Cardiovasc Surg* (Torino) 2014; **55**: 301-302 [PMID: 24172600]

50 **Kontopodis N**, Metaxa E, Papaharilaou Y, Georgakarakos E, Tsetis D, Ioannou CV. Changes in geometric configuration and biomechanical parameters of a rapidly growing abdominal aortic aneurysm may provide insight in aneurysms natural history and rupture risk. *Theor Biol Med Model* 2013; **10**: 67 [PMID: 24304476 DOI: 10.1186/1742-4682-10-67]

51 **Martufi G**, Auer M, Roy J, Swedenborg J, Sakalihasan N, Panuccio G, Gasser TC. Multidimensional growth measurements of abdominal aortic aneurysms. *J Vasc Surg* 2013; **58**: 748-755 [PMID: 23611712 DOI: 10.1016/j.jvs.2012.11.070]

P- Reviewer: Salemi VMC, Vargas HA **S- Editor**: Gong ZM
L- Editor: A **E- Editor**: Liu SQ

World Journal of Radiology

Submit a Manuscript: http://www.wjgnet.com/esps/
Help Desk: http://www.wjgnet.com/esps/helpdesk.aspx
DOI: 10.4329/wjr.v8.i2.159

World J Radiol 2016 February 28; 8(2): 159-173
ISSN 1949-8470 (online)

MINIREVIEWS

Blunt pancreatic trauma: A persistent diagnostic conundrum?

Atin Kumar, Ananya Panda, Shivanand Gamanagatti

Atin Kumar, Ananya Panda, Shivanand Gamanagatti, Department of Radiology, All India Institute of Medical Sciences, New Delhi 110029, India

Author contributions: Kumar A was responsible for deciding the overall contents and flow of information in the paper and editing the images; Panda A was responsible for the actual writing and organisng references and tables; Gamanagatti S gave inputs on contents and provided images.

Conflict-of-interest statement: The authors declare no conflicts of interest regarding this manuscript.

Correspondence to: Dr. Atin Kumar, MD, DNB, Additional Professor, Department of Radiodiagnosis, All India Institute of Medical Sciences, Ansari Nagar, Room no 63, New Delhi 110029, India. dratinkumar@gmail.com
Telephone: +91-98-68398507
Fax: +91-11-26588663

Received: June 1, 2015
Peer-review started: June 4, 2015
First decision: July 31, 2015
Revised: August 24, 2015
Accepted: December 13, 2015
Article in press: December 15, 2015
Published online: February 28, 2016

Abstract

Blunt pancreatic trauma is an uncommon injury but has high morbidity and mortality. In modern era of trauma care, pancreatic trauma remains a persistent challenge to radiologists and surgeons alike. Early detection of pancreatic trauma is essential to prevent subsequent complications. However early pancreatic injury is often subtle on computed tomography (CT) and can be missed unless specifically looked for. Signs of pancreatic injury on CT include laceration, transection, bulky pancreas, heterogeneous enhancement, peripancreatic fluid and signs of pancreatitis. Pan-creatic ductal injury is a vital decision-making parameter as ductal injury is an indication for laparotomy. While lacerations involving more than half of pancreatic parenchyma are suggestive of ductal injury on CT, ductal injuries can be directly assessed on magnetic resonance imaging (MRI) or endoscopic retrograde cholangio-pancreatography. Pancreatic trauma also shows temporal evolution with increase in extent of injury with time. Hence early CT scans may underestimate the extent of injures and sequential imaging with CT or MRI is important in pancreatic trauma. Sequential imaging is also needed for successful non-operative management of pancreatic injury. Accurate early detection on initial CT and adopting a multimodality and sequential imaging strategy can improve outcome in pancreatic trauma.

Key words: Computed tomography; Magnetic resonance imaging; Pancreatic trauma; Complications; Magnetic resonance cholangiopancreatography; Management; Pancreatic injury; Review

Core tip: Pancreatic trauma is an uncommon injury in blunt trauma abdomen. Despite improved multidetector computed tomography (CT) technology, early diagnosis of pancreatic trauma remains difficult. Moreover, pancreatic injury shows evolution with time which affects CT performance in early stages after injury. Diagnosis of pancreatic ductal injury is vital to decide operative *vs* non-operative management.

Magnetic resonance imaging (MRI) with magnetic resonance cholangiopancreatography has superseded encoscopic retrograde cholangio-pancreatography (ERCP) in evaluation of duct in acute injury. This review discusses injury mechanisms, laboratory diagnosis, CT and MRI evaluation, role of ERCP and contrast-enhanced ultrasound, management and complications of pancreatic trauma. Evolution of pancreatic injury has been specifically discussed as it has important management implications.

Kumar A, Panda A, Gamanagatti S. Blunt pancreatic trauma: A persistent diagnostic conundrum? *World J Radiol* 2016; 8(2): 159-173 Available from: URL: http://www.wjgnet.com/1949-8470/full/v8/i2/159.htm DOI: http://dx.doi.org/10.4329/wjr.v8.i2.159

INTRODUCTION

Pancreatic trauma in blunt trauma abdomen is an uncommon injury with an incidence of 2%-5%[1]. Despite its relatively uncommon incidence, diagnosis and management of pancreatic trauma remains a persistent challenge and generates continuous debate and search for new paradigms in trauma literature. While the deep retroperitoneal location of pancreas protects it from less severe trauma, it also renders diagnosis of injury more difficult. In an acute setting, pancreatic injury produces severe physiologic dysfunction and traumatic pancreatitis; chiefly due to leakage of enzymes from pancreatic ductal injury while in the chronic setting, duct injury leads to pseudocyst and pancreatic fistula formation[2,3]. Computed tomography (CT) remains the mainstay for diagnosis of pancreatic trauma. Recently, with emphasis on early detection of ductal injury and an increasing trend towards non-operative management of low-grade pancreatic injuries, magnetic resonance imaging (MRI), encoscopic retrograde cholangio-pancreatography (ERCP) and endoscopic stenting have also been incorporated into pancreatic trauma management protocols[2,4-8].

This article provides a review of pancreatic injury and discusses the mechanisms of injury, clinical and laboratory diagnosis, classification, imaging techniques, management, outcome and complications of blunt pancreatic trauma.

MECHANISMS OF INJURY

The common mechanisms of blunt pancreatic trauma are motor vehicle accidents (steering wheel and seat-belt impact injuries) in adults and impact due to bicycle handlebar injuries in children[9-11]. Other mechanisms include fall of heavy objects over abdomen, fall from height and direct blunt assault to abdomen. Injury occurs due to the anteroposterior force compressing the pancreas against the spine with injury most commonly occurring just left to the mesenteric vessels at the junction of neck and body[10]. A slightly left-sided force of impact directed at left upper quadrant causes injury to distal pancreas along with spleen, left kidney and stomach. Similarly right sided forces injure the head or uncinate process of pancreas along with liver, gall bladder and duodenum[9,12]. Hence concomitant injuries of adjacent organs are not uncommon in blunt pancreatic trauma and should be actively sought for while analysing CT scans. Children are more susceptible to pancreatic injury because of the minimal protective retroperitoneal fat mantle unlike adults[11].

CLINICAL AND LABORATORY DIAGNOSIS

Pancreatic injury should be suspected in all polytrauma patients or in patients with history of any high-risk mechanism of injury. Due to the deep retroperitoneal location of pancreas, early diagnosis of pancreatic injury may be missed. Isolated pancreatic trauma may be clinically occult initially and can present later with complications while in polytrauma patients, pancreatic trauma may be masked by signs of more severe other organ injuries[13]. Clinically, patients may present with diffuse abdominal or epigastric pain, epigastric ecchymosis , abdominal guarding, tenderness and absent bowel sounds and along with metabolic acidosis and leucocytosis secondary to the inflammatory response induced by leakage of pancreatic enzymes[13,14].

Both serum amylase and lipase are unreliable markers for pancreatic trauma. While serum amylase is usually elevated after pancreatic trauma, it can also be normal in up to 40% of patients[15]. Thus initial serum amylase levels are neither sensitive nor specific for diagnosis of pancreatic trauma and can also be elevated in non-pancreatic abdominal and bowel injuries[16,17]. In a retrospective study of 1821 pediatric trauma patients by Adamson *et al*[16], 116 (23%) had elevated amylase or lipase levels while only eight patients had pancreatic injury. Seventy-four of 116 (64%) patients with elevated amylase/lipase levels underwent abdominal and pelvic CT scanning, yet 38 (51%) of these had completely normal scans. Many patients with elevated levels underwent screening CT scans based on amylase/lipase levels alone and had no evidence of pancreatic injury. Hence serum amylase determinations may support clinical suspicion in the diagnosis of pancreatic trauma but are not reliable or cost effective as screening tools. Moreover, serum amylase levels are also time-dependent and in two studies by Matsuno *et al*[18] and Takishima *et al*[19], statistically significant increased serum amylase levels were seen only two and three hours after trauma respectively.

Determination of pancreatic amylase isoenzyme also does not add to the diagnosis as demonstrated by Bouwman *et al*[20]. The major concern raised by an elevated amylase level is differentiation between

Table 1 The American Association of Surgery for Trauma-organ injury scale pancreatic injury scale[25]

Grade	Description
I	Hematoma: Minor contusion without duct injury Laceration: Superficial laceration without duct injury
II	Hematoma: Major contusion without duct injury or tissue loss Laceration: Major laceration without duct injury or tissue loss
III	Laceration: Distal transection or parenchymal injury with duct injury
IV	Laceration: Proximal transection[1] or parenchymal injury involving ampulla or bile duct
V	Laceration: Massive disruption of pancreatic head

[1]Proximal injury is defined as lying to the right of the superior mesenteric vein.

pancreatic trauma and small bowel injury, which cannot be differentiated by measurement of amylase isoenzyme also[9].

While absolute values of serum amylase do not correspond to the grade and severity of injury, hyperamylasemia in general, is an indicator of development of complications, pancreatic fistula and pseudocyst formation[21]. Also while initial amylase may be normal, repeat amylase measurements at later intervals, persistent or significant hyperamylasemia (more than three times baseline) are suggestive. Thus the trend of serum amylase/lipase levels (increase/decrease) rather than any absolute value are helpful indicators of pancreatic involvement and development of subsequent complications[18,19].

CLASSIFICATION OF PANCREATIC INJURY

The classification of pancreatic trauma has evolved over the years. The earlier used clinical (grade Ⅰ-Ⅳ) and CT based grading systems[22-24] have given way to an universally accepted American Association of Surgery for Trauma (AAST)-organ injury scale (OIS) grading of pancreatic trauma (Table 1). This is a surgical grading and has management implications. First proposed by Moore *et al*[25,26] in 1990, the grading system has stood the test of time and remains unchanged in the latest revision.

IMAGING IN PANCREATIC TRAUMA

The objectives of imaging are: (1) to detect pancreatic trauma as early as possible to mitigate the consequences of delayed diagnosis; (2) to identify ductal injury; *i.e.,* identify grade 3 and above injuries as ductal involvement has higher morbidity and mortality; (3) to evaluate evolution of pancreatic trauma; and (4) to diagnose complications and facilitate image-guided interventions. With these objectives in mind, CT is the workhorse of imaging in pancreatic trauma. MRI with magnetic resonance cholangiopancreatography (MRCP) and ERCP are useful in definitive diagnosis of ductal injury both in early and late cases while a newer modality like contrast-enhanced ultrasound (CEUS) has also been evaluated in pancreatic trauma.

CT

CT is the modality of choice for evaluating pancreatic injury in polytrauma patients. CT has a reportedly variable sensitivity (65%-80%) and specificity for detecting pancreatic trauma[9,27,28]. With older generation single slice and helical CT scanners, diagnosis of pancreatic trauma was unreliable and detection of subtle signs of early pancreatic injury was difficult[13,29]. Newer multidetector CT (MDCT) scanners allow volumetric data acquisition and isovoxel reconstruction, thereby improving the sensitivity and the standard of diagnosis[30-33]. Applications such as curved multiplanar reconstruction (MPR) reconstruction are helpful in evaluating an anatomically curved and obliquely located organ like the pancreas[33]. Improved ductal visualisation has also been noted by MPR and minimum intensity projections[34,35].

Teh *et al*[30] were the first ones to publish data regarding evaluation of blunt pancreatic injuries with modern-era high resolution CT scanners. In a cohort of 50 patients with pancreatic trauma, operative correlation was available in 33 patients. CT findings corresponded precisely to the operative findings in 18 patients (55%). In the subset of 11 patients with confirmed pancreatic ductal injury (PDI), CT scan was truly positive in 10 patients, falsely positive in 2 patients, and falsely negative in 1 patient. Thus while CT was 55% sensitive for pancreatic injury, it was 91% sensitive and 91% specific for pancreatic ductal injury[30].

A multicentre study by Phelan *et al*[32] involving 20 centres and both 16 detector and 64 detector scanners found that sensitivity of CT in detecting pancreatic injury varied between 47%-60% (depending on type of scanner used). For PDI, the sensitivity was 52%-54% and specificity was 90%-95%.

In a study published by us[33], operative correlation was available in 24 patients and MDCT correctly identified the surgical grade in 22 out of 24 patients (91.7%). In the subset of 19 patients with PDI, CT correctly identified ductal injury in 18/19 patients (true positives) and correctly ruled out ductal injury in all 5/5 patients (true negatives) giving a sensitivity, specificity and accuracy of 94.7%, 100.0% and 95.8% respectively for PDI. The one patient, in whom CT did not identify ductal injury, had imaging appearances of contusion (grade Ⅱ) on CT while MRI performed 15 h later showed laceration (grade Ⅲ injury). Discrepancy in CT and operative findings in this patient was more likely due to evolution of injury rather than failure of MDCT technology[33].

Thus, MDCT scanners have improved accuracy for detecting pancreatic injury as compared to older

Table 2 Computed tomography signs of pancreatic injury[9,10,12,27,38-41]

"Hard" signs/specific signs	"Soft" signs/suggestive signs
Fracture of the pancreas	Fluid separating the splenic vein from posterior aspect of pancreas
Pancreatic laceration	Fluid surrounding the superior mesenteric artery/(SMV cuff sign)
Focal or diffuse pancreatic enlargement/edema	Fluid in the anterior and posterior pararenal spaces
Pancreatic hematoma	Fluid in transverse mesocolon and lesser sac
Active bleeding/extravasation of intravenous contrast	Inflammatory changes in peripancreatic fat and mentery
	Thickening of the left anterior renal fascia
	Delayed signs
	Pancreatic ductal dilatation
	Pseudocyst formation/peripancreatic fluid collection

SMV: Superior mesenteric vein.

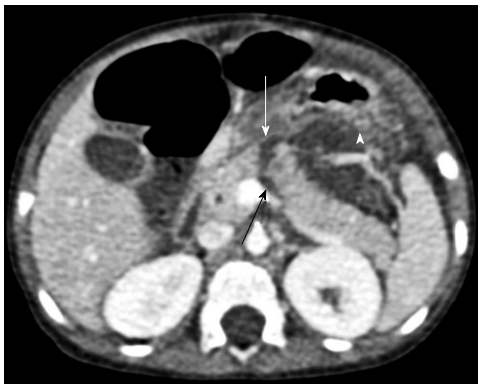

Figure 1 A 3-year-old girl with history of fall of heavy object over abdomen. CECT axial image shows full thickness laceration (grade Ⅲ injury) of neck of pancreas at level of splenoportal confluence (white arrow). Also note peripancreatic fluid (arrowhead) and fluid between splenic vein and body of pancreas (black arrow). Patient underwent a distal pancreatectomy. CECT: Contrast enhanced computed tomography.

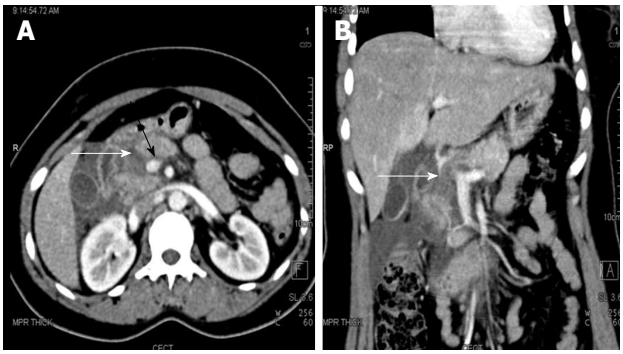

Figure 2 A 27-year-old woman with road traffic accident. CECT axial (A) and coronal (B) images show full thickness laceration in the head of pancreas (white arrows). The laceration is located to the right of splenoportal confluence suggestive of grade Ⅳ injury. There is also fluid around the superior mesenteric vein (black arrow) and adjacent superior mesentery artery; the so-called "SMV cuff" sign seen in proximal injuries of pancreas. CECT: Contrast enhanced computed tomography; SMV: Superior mesenteric vein.

generation scanners.

CT imaging technique

Wong *et al*[31] assessed overall accuracies of multiphasic CT in detecting main duct injuries and found that accuracies were 97.9% (pancreatic parenchymal phase), 100.0% (portal venous phase), and 96.8% (equilibrium phase) respectively. Thus the portal venous phase CT was the most accurate scan to detect pancreatic duct injurie.

In our level 1 apex trauma centre, we currently perform dual-phase protocol (arterial and venous phase) in all adult patients with focussed abdominal sonography for trauma (FAST) positive status and a portal venous phase scan in pediatric patients or patients with FAST negative status. Thus, pancreas is primarily assessed in portal venous phase. Both thin-section axial images and MPR images in sagittal, coronal and oblique planes are routinely viewed on 3D workstation. We also generate curved MPR images to estimate depth of laceration in equivocal cases to comment on ductal injury. As generally accepted in trauma CT protocols[36] oral contrast is not administered prior to initial CT scanning while oral contrast is given in patients come for routine follow-up CT scans.

CT signs of pancreatic trauma

Signs of pancreatic trauma can be divided into "hard" signs and "soft" signs (Table 2). "Hard" signs are specific and definitive CT evidence of pancreatic injury. "soft" signs are basically due to associated pancreatitis and, though non-specific, are supportive and should make one raise a possibility of pancreatic involvement in a patient with an appropriate mechanism of injury and associated injuries.

Hard signs (for grading pancreatic injuries)

Pancreatic laceration (AAST grade Ⅲ and above) is seen as a low-attenuating line oriented perpendicular to the long-axis of pancreas. The line ideally represents separation of fragments with fluid or blood within the fragments (Figures 1 and 2). However in early stage, a laceration may only be seen as a low-attenuation band without separation of fragments and may be underestimated as a contusion (Figure 3). Also a laceration may be seen on only one or two sections and can be missed if not carefully looked for. Pancreatic lacerations should also be differentiated from clefts. Usually the presence of fluid within the gap along with associated signs of inflammation favours laceration while a cleft is lined by fat with clear surrounding area[9,10,12,27,37-41].

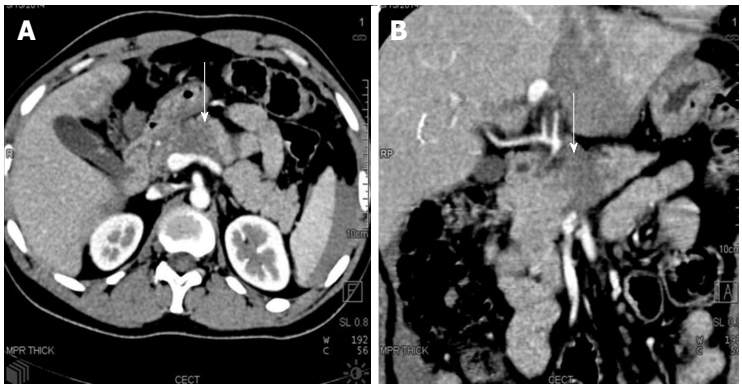

Figure 3 A 35-year-old truck driver with history of steering wheel impact injury. CECT axial (A) and coronal oblique (B) images show a full thickness hypoattenuating band involving neck and body of pancreas (white arrow). On imaging, it was considered as a major contusion/grade Ⅱ injury. Intraoperatively, full thickness laceration with duct injury was found suggestive of grade Ⅲ injury and distal pancreatectomy was done. CECT: Contrast enhanced computed tomography.

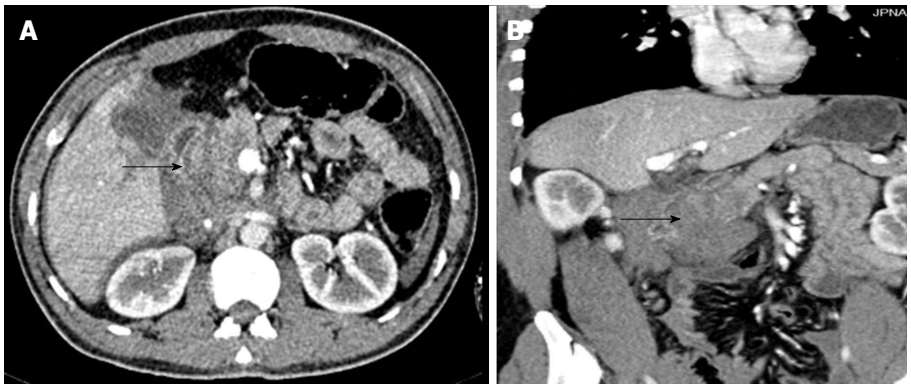

Figure 4 A 30-year-old man with road traffic accident. CECT axial (A) and coronal MPR (B) images show the hypoattenuating and bulky head of pancreas suggestive of major contusion with fluid in pancreaticoduodenal groove (arrow). Intra-operatively a hematoma was found in head and neck of pancreas (grade Ⅱ injury). No active surgical intervention was done for pancreatic injury. CECT: Contrast enhanced computed tomography; MPR: Multiplanar reconstruction.

Lacerations can be divided into superficial or deep. Superficial lacerations involve less than 50% of the gland thickness and imply non-involvement of the duct. Deep lacerations involve more than 50% of the gland and imply duct disruption. This 50% depth of laceration is used as a substitute marker for ductal involvement as the duct often cannot be made out or traced on CT. A full thickness laceration involves the whole thickness of gland and is termed as transection or fracture (Figure 1).

Pancreatic contusion (AAST grade Ⅰ and Ⅱ injury) is characterised by: (1) diffuse or focal enlargement; (2) heterogeneously attenuating pancreas; or (3) focal area of hypoattenuation against the background of normally enhancing pancreas (Figure 4). Usually less than involvement of one anatomical division of pancreas (head, neck, body or tail) is considered as minor contusion (AAST grade Ⅰ) or more than one anatomical division is considered a major contusion (AAST Grade Ⅱ).

An area of hyperattenuation within the substance of the gland is suggestive of pancreatic hematoma which is a very specific sign of pancreatic trauma (Figure 5). Similarly active extravasation within the gland, *i.e.,* contrast leak which increases on delayed scan, is specific for pancreatic injury[9] (Figure 6).

Soft signs (reflective of pancreatic injury-associated inflammatory changes)

Fluid between distal pancreas and splenic vein was first described by Lane *et al*[39] and was found in 90% of cases of pancreatic injury in their study. Normally the splenic vein is closely apposed to the posterior aspect of the pancreas or is separated from the pancreas by a thin layer of fat. In a patient with fluid insinuating between the splenic vein and the pancreas and a history of abdominal trauma, a pancreatic injury should be suspected. The fluid is believed to represent either a leak from transected duct or blood tracking into peripancreatic tissues and is more commonly seen in distal pancreatic injuries (Figures 1 and 5). Similarly, SMV cuff sign may be seen in more proximal injuries involving neck region (Figure 2).

Peripancreatic fat stranding and fluid collections around the pancreas in combination with one or more signs to be strongly predictive of pancreatic injury. Peripancreatic fluid collections in lesser sac, pararenal spaces and transverse mesocolon are seen in 70%-90% in patients with pancreatic injury[39,42]. Similarly inflammatory changes such as thickening of anterior renal facia was seen in 44% of patients with pancreatic trauma[42] (Figures 1 and 5).

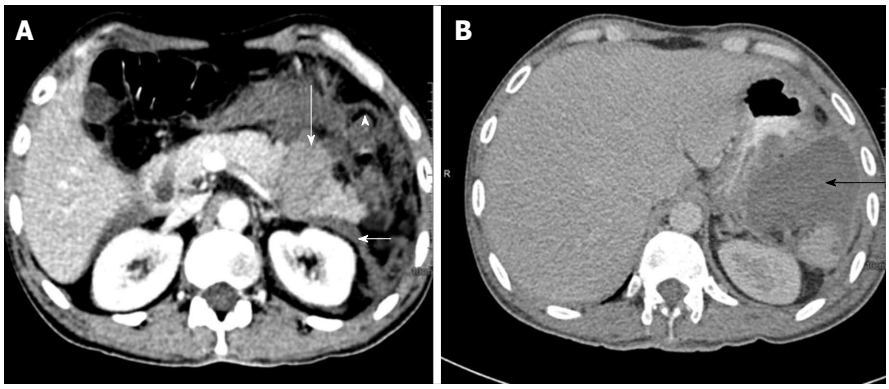

Figure 5 A 35-year-old man with road traffic accident. CECT axial image at time of trauma (A) shows distal transection with fragments that separated by hyperattenuating fluid suggestive of hematoma (long white arrow). The left anterior renal fascia is also thickened (arrowhead). Patient underwent distal pancreatectomy and 4 wk follow up CECT axial image (B) show a post-operative collection in lesser sac (black arrow). CECT: Contrast enhanced computed tomography.

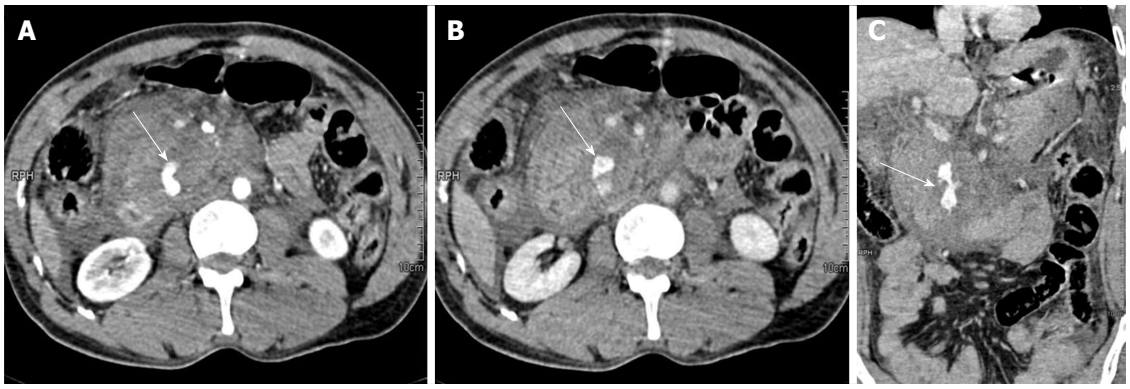

Figure 6 A 40-year-old man with history of fall of heavy object over abdomen. CECT axial images, initial scan (A) and delayed scan (B) show complete disruption of head of pancreas with a large retroperitoneal hematoma replacing the head region. There is active extravasation of contrast (arrows). On coronal oblique image (C), the disrupted head of pancreas (arrow) with active contrast extravasation can be seen. Surgically, a crush injury (grade Ⅴ) was confirmed and patient underwent Whipple's procedure. The patient eventually died due to sepsis and multiorgan failure. CECT: Contrast enhanced computed tomography.

While in isolation, soft signs may not be diagnostic of pancreatic injury, they are often found in combination with each other or with a hard sign such as pancreatic laceration/transection. Patients with only soft signs on CT should be closely monitored clinically, biochemically and radiologically with follow-up CT scan or MRI for confirmation of pancreatic injury.

MAGNETIC RESONANCE IMAGING

MRI with MRCP serves as a problem solving tool in pancreatic trauma. In acute pancreatic trauma wherein diagnosis of ductal injury is imperative, MRI is a non-invasive alternative to ERCP to evaluate pancreatic duct. The other advantages of MRI over ERCP include its ability to demonstrate the status of the duct upstream of the laceration, better definition of parenchymal injury and the extent and location of peripancreatic fluid collections.

MRI also has good correlation with CT and can well demonstrate features of pancreatic parenchymal injuries such as pancreatic contusion, lacerations and hematomas[33,38]. Pancreatic contusions are seen as focal T2 hyperintense areas (Figure 7) while lacerations are seen as linear T2 hyperintense areas within the gland (Figure 8). On MRI, the lacerations can be seen directly extending to the duct unlike CT. Pancreatic hematoma is seen as intrapancreatic T1 hyperintense area which has variablesignal intensity on T2 weighted images[43]. Apart from confirming ductal injury, MRI is useful in confirming ductal integrity so that surgeons can safely proceed with conservative management (Figure 9). MRI is also useful in evaluating evolution of pancreatic injury as described later. Thus in our institution, MRI is performed if CT findings are equivocal or if conservative management is planned to evaluate the MPD. The MRI protocol in our institution include axial T1 and T2 weighted images, axial and coronal fast spoiled gradient echo imaging with steady state precession (TRUFISP) and single shot fast spin-echo (SSFSE) T2-weighted MR imaging (T2 HASTE) sequences and heavily T2-weighted 3D sequences for MRCP.

MRI is useful in follow-up of conservatively managed cases or to diagnose sequelae of pancreatic trauma such as pseudocysts, pancreatic strictures and chronic pancreatitis[6,44-46]. MRI is also useful for follow-up evaluation in children as it provides a non-radiation alternative to CT.

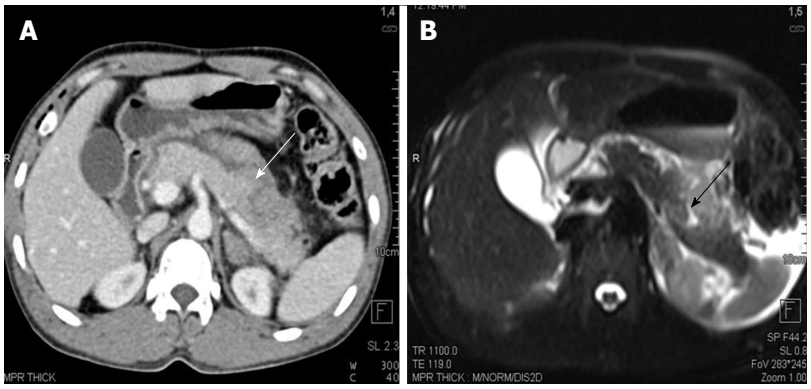

Figure 7 A 25-year-old man with history of blunt trauma abdomen. CECT axial image (A) shows injury of distal pancreas (white arrow). MRI T2 HASTE axial image show T2 weighted hyperintensity in pancreatic body suggestive of contusion/edema with a small laceration (black arrow). CECT: Contrast enhanced computed tomography; MRI: Magnetic resonance imaging.

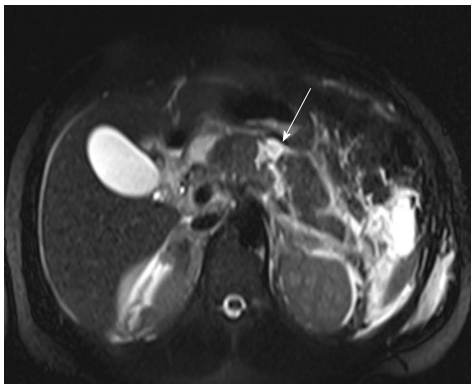

Figure 8 Magnetic resonance imaging T2 HASTE axial image of a 23-year-old man with road traffic accident show linear full thickness laceration in proximal body (arrow) suggestive of grade Ⅲ injury.

Secretin-enhanced MRCP, *i.e.,* MRCP obtained after intravenous injection of secretin may be helpful to further characterise pancreatic ductal injury. Secretin increases the output of pancreatic secretions and can be used to actively demonstrate leak from the disrupted pancreatic duct[47].

CEUS

CEUS using SonoVue® (sulphur hexafluoride, Bracco, Milan, Italy) has also been described for pancreatic trauma[48]. Unlike conventional US which performs poorly in detecting pancreatic injuries, CEUS provides better contrast between normal and contused pancreas due to differential blood supply. Pancreatic injuries appear as anechoic or hypoechoic irregular perfusion defects in both arterial and parenchymal phases. In a study by Lv *et al*[49], in comparison to CT, CEUS detected pancreatic injuries in 21/22 patients with a detection rate of 95.5%. Because of its portability, CEUS can be employed as a part of initial US protocol during resuscitation to detect solid organ injuries. CEUS may also serve as a non-radiation alternative to CT for follow-up in known cases of pancreatic trauma to assess pancreatic disruptions, peripancreatic collections and pseudocysts. The disadvantages include cost, learning curve, short window time to obtain useful information and limited information regarding extent of other injuries sustained by the patients compared to CT[48,49].

ERCP

ERCP is considered the traditional gold standard for pancreatic ductal injury but has been superseded by MRCP in acute pancreatic trauma. While ERCP can directly visualise ductal injury, disadvantages include its invasive nature, high rate of complications (5%-15%) such as pancreatitis, cholangitis and duodenal perforation and the lack of availability of the technique or trained personnel to do this procedure on emergent basis[50,51]. Because of its tendency to induce iatrogenic pancreatitis, most trauma surgeons are wary of subjecting critical polytrauma patients to ERCP in an acute setting. However, in subacute cases and in chronic follow-up cases, ERCP provides therapeutic options such as duct stenting and pancreatic sphincterotomies for pancreatic fistula, pseudocysts and strictures[52-54]. Also with recent emphasis on non-operative management, endoscopic trans papillary drainage and ERCP guided stenting can also be done for partial duct disruptions and in isolated grade 3 injuries respectively to avoid laparotomy[5].

EVOLUTION OF PANCREATIC INJURY

Another factor affecting diagnostic performance in pancreatic trauma is the evolution of pancreatic injury. Findings can be subtle in early cases leading to a low CT sensitivity. In the study by Arkovitz *et al*[11], CT had an 85% sensitivity within the initial 24 h after pancreatic injury while overall sensitivity was 90%. The pancreas can appear normal in 20%-40% of patients with acute blunt pancreatic injuries, especially when imaging is done within the first 12 h after injury. This is due to the obscuration of the fracture plane, hemorrhage, and close apposition of the pancreatic fragments. On repeat scanning at 12 to 24 h; an abnormality which was initially ambiguous or subtle becomes more evident.

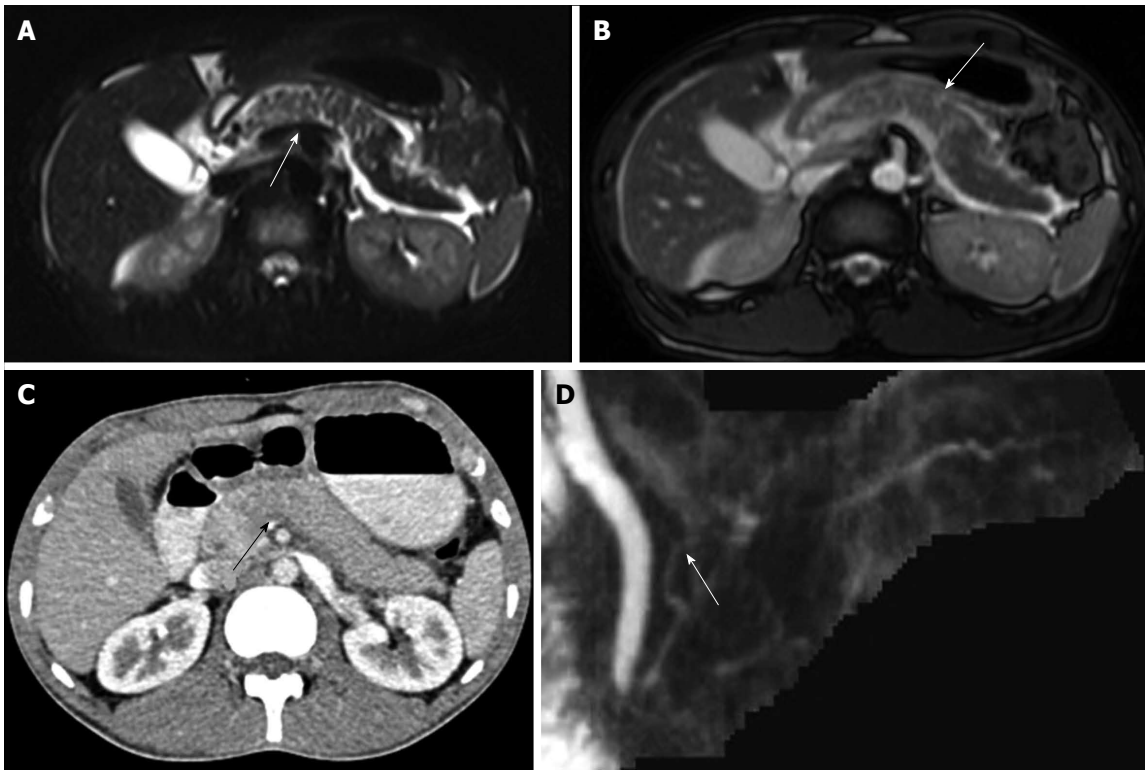

Figure 9 A 25-year-old man was involved in road traffic accident. CECT axial image (A) shows ill-defined hypoattenuating area in neck of pancreas suggestive of contusion (arrow). MRI done 10 h after CT shows extent of contusion better with wider area of involvement on both T2 HASTE (B) and TRUFISP (C) images. MRCP thick MPR (D) image shows ductal integrity. Patient was conservatively managed and follow-up imaging showed decrease in area of contusion. CECT: Contrast enhanced computed tomography; MPR: Multiplanar reconstruction; TRUFISP: True fast imaging with steady-state free precession; MRI: Magnetic resonance imaging; MRCP: Magnetic resonance pancreatography; CT: Computed tomography.

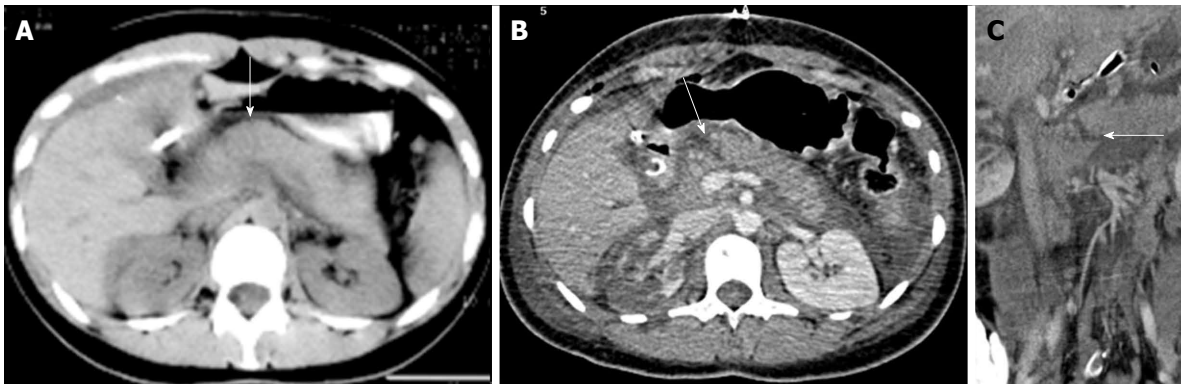

Figure 10 A 23-year-old woman with history of road traffic accident. Day 1 CECT axial image (A) shows ill-defined contusion in pancreatic neck (arrow). No obvious laceration was seen. Day 3 CECT axial (B) and coronal oblique (C) images show a full-thickness laceration in neck of pancreas s/o grade Ⅲ injury with ductal involvement. Patient was operated and distal pancreatectomy was done. Thus there was evolution of injury from contusion to laceration. CECT: Contrast enhanced computed tomography.

Findings become more radiologically apparent over time with the development of post-traumatic pancreatitis, edema, leakage of pancreatic enzymes, and subsequent auto-digestion of the surrounding parenchyma[9,29]. The delay in CT findings of pancreatic injury is especially pronounced in pediatric or thin patients who often lack the contrast provided by surrounding adipose tissue to appreciate pancreatic injuries[11,55]. CT can either miss or underestimate depth of laceration too in very early stage because accumulation of fluid within the gap and separation of fragments is a time-dependent phenomenon[32] (Figure 10). Thus, the inability to detect early pancreatic trauma even with advanced multi-detector CT technology is not a reflection of failure of technology but due to the natural history and evolution of trauma[32].

Delayed diagnosis or the missed early diagnosis is more likely in patients with isolated pancreatic injuries, absent or minimal other associated abdominal injuries or in those undergoing non-operative management without any follow-up imaging[56]. Thus it is recommended to do a sequential imaging along with correlation with

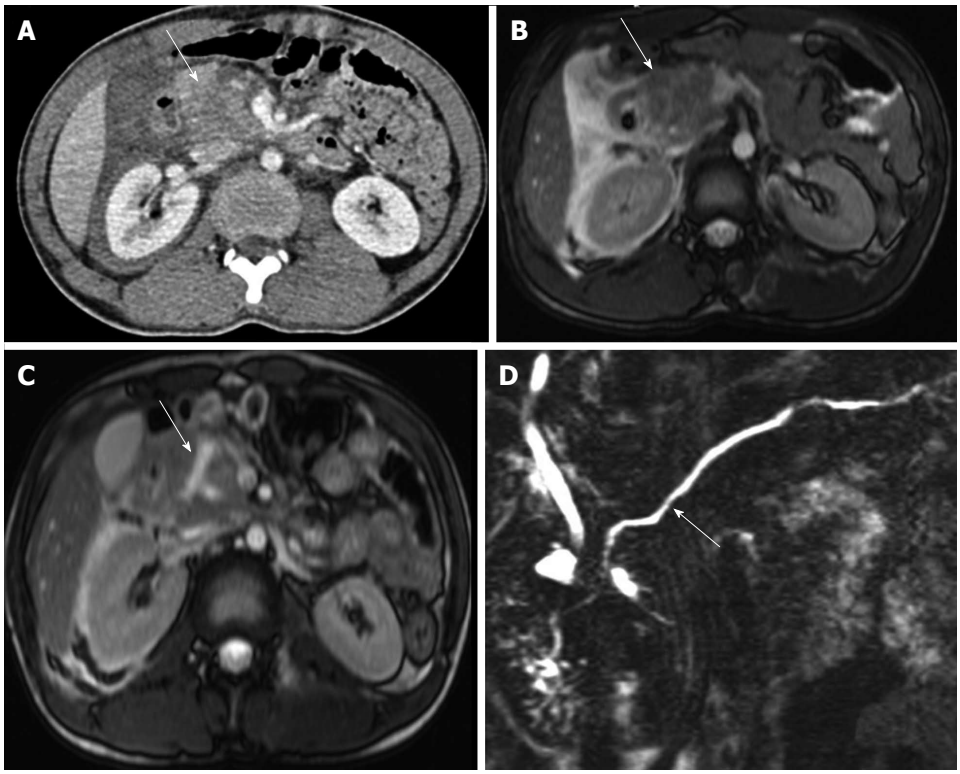

Figure 11 A 22-year-old man with history of fall of heavy object over abdomen. CECT axial image (A) shows bulky heterogeneously attenuating head of pancreas (arrow). MRI done 28 h after CT (B) shows similar findings with bulky head and altered signal intensity with adjacent fluid (arrow B). No definite laceration seen. Follow-up MRI on day 6 (C) shows a Y shaped laceration in inferior part of head and uncinate process. However the main pancreatic duct was normal (arrow D). Since the MPD was not involved, conservative management was continued. CECT: Contrast enhanced computed tomography; MRI: Magnetic resonance imaging; CT: Computed tomography.

clinical and laboratory parameters to avoid a missed diagnosis[57].

Another scenario where sequential imaging plays a role is in non-operative management of pancreatic injury. The key factor in non-operative management is identification of low grade pancreatic injury (grade 2 or less) like contusion and superficial laceration not involving duct as these injuries can be managed conservatively. An inability to correctly estimate the grade of injury on first day imaging and absence of follow-up imaging with either CT, MRI, MRCP or ERCP is associated with higher incidence of failure of non-operative management in pancreatic injury[8]. Thus, once a pancreatic trauma is identified and the patient is considered for non-operative management, follow-up imaging with either CT or MRI should be done again to look for evolution of findings and guide management[58]. Follow-up imaging with MRI is preferred because of its superior soft tissue resolution, lack of radiation exposure and its ability to directly evaluate the duct. If a follow-up MRI reveals ductal integrity, then conservative management can be continued while evidence of ductal involvement on follow-up would necessitate surgical intervention (Figures 11 and 12).

MANAGEMENT

Management of pancreatic trauma depends on: (1) grade/ severity of injury; (2) location of injury; (3) other associated abdominal injuries; and (4) time elapsed after injury[2,9,14]. If CT shows ductal involvement (more than 50% depth of laceration), the operative management is preferred. If CT is equivocal, MRI (or ERCP) should be done to look for ductal involvement followed by laparotomy in presence of ductal involvement.

Low grade pancreatic injuries are usually managed conservatively. If laparotomy is indicated in these patients for other associated abdominal injuries, then simple external drainage of pancreatic bed can be done concomitantly. The management options based on grade of pancreatic injury have been summarised in Table 3.

For grade Ⅰ and Ⅱ injuries, placement of suction drain suffices to promote external drainage of pancreatic secretions and promote natural healing of minor ductal injuries. Omental pancreatorrhaphy may be done after repair of superficial lacerations and placement of omental graft over site of injury to promote healing[2].

For grade Ⅲ injuries, distal pancreatectomy is the standard surgery of choice. Associated splenic injuries may necessitateconcomitant splenectomy. If the injury occurs at the neck, then pancreaticojejunostomy may be done as an alternative to distal pancreatectomy to preserve the intact entire distal pancreas[59].

For grade Ⅳ injuries, currently pancreatic drainage is recommended as part of damage control surgery.

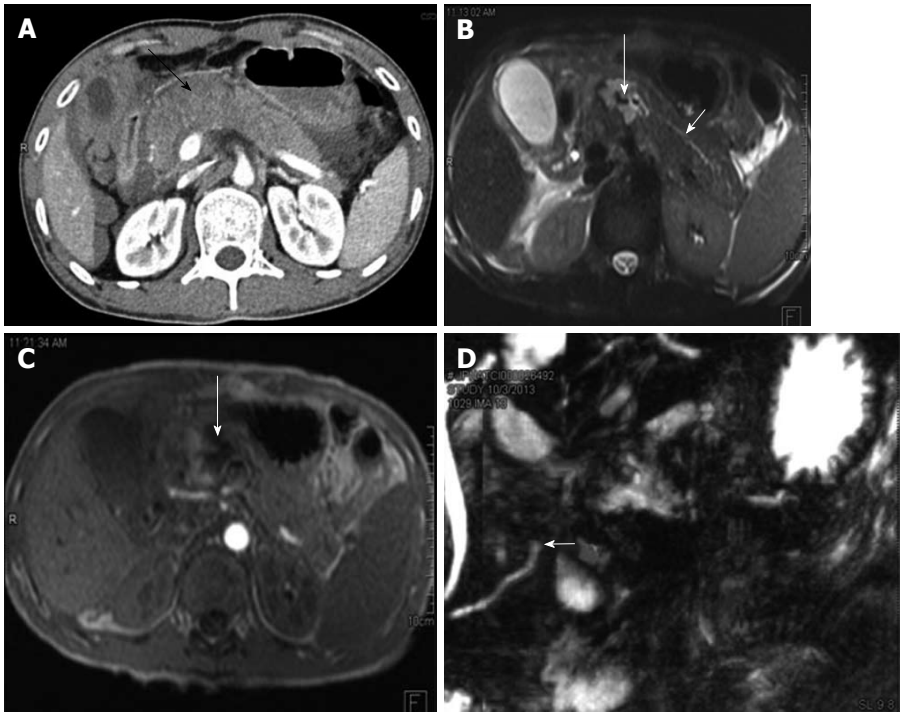

Figure 12 A 35-year-old man with history of road traffic accident. CECT axial image (A) shows bulky hypoattenuating pancreas (black arrow) with peripancreatic fluid. No definite laceration was seen on CT and patient was kept on conservative management. MRI done 4 d later show hematoma/collection in neck of pancreas (long white arrows B and C). The duct was seen to communicate with the hematoma and MRCP showed cut off of duct at site of injury (short white arrow D). The patient subsequently underwent distal pancreatectomy. CECT: Contrast enhanced computed tomography; MRI: Magnetic resonance imaging; MRCP: Magnetic resonance pancreatography; CT: Computed tomography.

Table 3 Treatment options for isolated pancreatic injuries based on the American Association of Surgery for Trauma pancreas organ injury scale[2,14,40]

AAST grade	Treatment options
I	Observation/conservative management
	Simple external drainage
	Omental pancreatorrhaphy and drainage
II	Observation/conservative management
	Simple external drainage
	Omental pancreatorrhaphy and drainage
III	Distal pancreatectomy +/- splenectomy
	Roux-en-Y distal pancreatojejunostomy
IV	Simple drainage in damage control situations
	Pancreatoduodenectomy (Whipple procedure)
	Distal Roux-en-Y pancreatojejunostomy
	Anterior Roux-en-Y pancreatojejunostomy
	Endoscopically placed stent
V	Pancreatoduodenectomy
	Drainage in damage control situations

AAST: American Association of Surgery for Trauma.

When clinical condition improves, then either resection or reconstruction with pancreatic enteric anastomosis may be done[60,61].

For grade Ⅴ injuries, Whipple's procedure (pancreaticoduodenectomy) may be done at first stage[62]. However since most patients with grade Ⅴ injuries are poor candidates to withstand extensive surgeries, initial damage control with drainage followed by resection-anastomosis may be done[63,64]. Grade Ⅳ and Ⅴ injuries are often associated with duodenal injuries which may be subjected to primary repair and diversion or duodenum is resected along with pancreas.

Non-operative management

Literature on non operative management of injuries (NOMI) mostly pertains to pediatric patients with reported outcomes similar to operative management[65,66]. However this approach can also be extended to adults[8]. Proper patient selection (patients with low-grade injuries, isolated pancreatic injuries and absence of ductal involvement on MRI or ERCP), continuous patient monitoring and radiological follow-up and availability of radiological or endoscopic interventions for management of local/pancreatic complications are keystones to successful NOMI[8,67]. In case of clinical and radiological progression of injury, subsequent surgical management is preferred over endoscopy as the laparotomy has better outcomes with lesser complications[2,3].

COMPLICATIONS, MORBIDITY AND MORTALITY

Despite the relatively low incidence of pancreatic trauma, morbidity and mortality are high. While isolated pancreatic trauma has an incidence of less than 30% and a lower mortality of 3%-10%[68], the overall morbidity is 30%-50% and mortality is 10%-30%. There is a proportionately direct increase in adverse outcome with: (1) increasing grade of injury; (2) associated organ

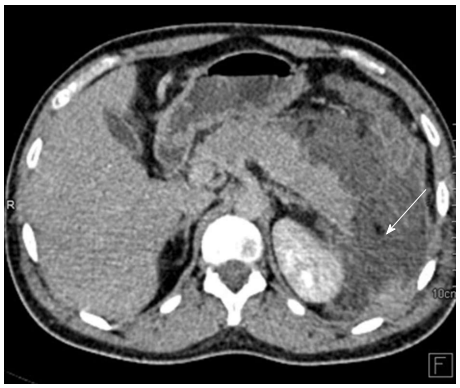

Figure 13 A 22-year-old man with history of road traffic accident, presenting on day 17 after trauma. CECT axial image shows injury to distal body and tail of pancreas with peripancreatic collection (arrow). No imaging was done at time of trauma. Features are suggestive of traumatic pancreatitis following initial missed injury. Patient was conservatively managed with percutaneous drainage. CECT: Contrast enhanced computed tomography.

injuries; and (3) delay in diagnosis with failure to identify ductal injuries[3,9,13,24,29,69,70].

Approximately, one-third of the patients survive the first 48 h develop complications due to pancreatic injury. Complications include traumatic pancreatitis, pancreatitis induced vascular complications such as pseudoaneurysms, pseudocysts, pancreatic fistulas, intraabdominal abscesses, pancreatic strictures and chronic obstructive pancreatitis, wound complications, septicaemia and multiorgan failure[14,69,71-73].

Post-traumatic pancreatitis occurs due to missed or delayed diagnosis of ductal injury. The incidence of pancreatitis is 17% after pancreatic injury[74]. Patients present with abdominal pain and hyperamylasemia. CT demonstrates typical imaging features of pancreatitis with bulky, heterogeneously enhancing pancreas, intra-pancreatic and peripancreatic collections and can lead to sepsis and multiorgan failure (Figure 13). Treatment is usually conservative while pancreatectomy, debridement and drainage may be done for failure of conservative treatment. Patients may also present with recurrent episodes of pancreatitis months after trauma due to persistent duct leak. This may require surgical intervention or endoscopic stenting[74].

Pancreatic fistula is one of the commonest complications after pancreatic trauma. Its incidence varies from 20% in isolated pancreatic trauma to 35% in combined pancreaticoduodenal injuries[61,75,76]. Fistula output more than 200 mL/d is a low output fistula while output more than 500 mL/d is a high output fistula. Conservative management with CT guided drainage of fistula over weeks is the treatment of choice[77]. In case of persistently high output drainage or internal communication with a hollow viscus or pleural cavity, ERCP may be done to delineate the fistulous anatomy followed by surgery or endoscopic stenting[5]. Proximal fistulas are better treated by stenting or Roux-en-Y procedures while distal fistulas are treated by pancreatectomy[3,14].

Pancreatic pseudocysts more commonly occur after missed injuries to distal pancreas or as a sequelae of NOMI[14,66]. These are commonly located anterior to body and tail of pancreas. MRCP or ERCP should be done to look for communication with pancreatic duct. If communication is present, endoscopic stenting along with CT guided percutaneous drainage is done[78,79]. If there is no communication with pancreatic duct, drainage alone is sufficient. If closely apposing stomach or bowel walls, surgical or endoscopic cystogastostomy or cystoenterosotmy are other therapeutic options[77].

Peripancreatic abscess/infected walled-off collections usually occur secondary to contamination from hollow viscus or from skin flora through the external drain. These increase morbidity and mortality due to ensuing sepsis[61,69,80]. On imaging, air foci within peripancreatic collections are suggestive of infection (Figure 14). However, if external drainage is maintained, presence of air foci may be normal. In such cases MRI can show debris within the collections while positive culture of fluid in the presence of fever, leucocytosis and acidosis are diagnostic.

Vascular complications such as pseudoaneurysms either occur due to complications of surgery or secondary to erosion of vessel wall by pancreatic enzymes[81,82]. Post-pancreatitis and post-traumatic pancreatic pseudoaneurysms commonly involve splenic, gastroduodenal and common hepatic arteries. Pseudoaneurysms are potentially life threatening events and if untreated can rupture leading to haemorrhagic death. Imminent rupture or bleeding pseudoaneuryms manifest as upper gastrointestinal bleed (hematemesis/melena) or hemobilia. If patient is hemodynamically stable, CT angiography is the modality of choice to diagnose site and size of pseudoaneurysms followed by angio-embolization with coils, glue or thrombin. If hemodynamically unstable, patients can directed be taken for embolization[83-85]. In cases of failure of embolization or in cases non-amenable to embolization, surgical management is done (Figure 15).

Pancreatic duct strictures and chronic obstructive pancreatitis can occur as sequelae of NOMI wherein fibrosis at injury site can lead to pancreatic duct strictures. Chronic obstruction and raised intraductal pressure leads to chronic obstructive pancreatitis, presenting months to years after trauma[72] (Figure 16). MRI is useful in diagnosis while ERCP and endoscopic stenting are therapeutic. Other options include surgical pancreaticojejunostomy and distal pancreatectomy for distal strictures[77].

SUMMARY

Pancreatic trauma remains a difficult diagnosis with high morbidity and mortality. While MDCT is the mainstay for diagnosing pancreatic injury, early scans may miss pancreatic trauma, especially if not carefully looked for. Thus radiologists should have a very high index of suspicion for pancreatic injury and should carefully

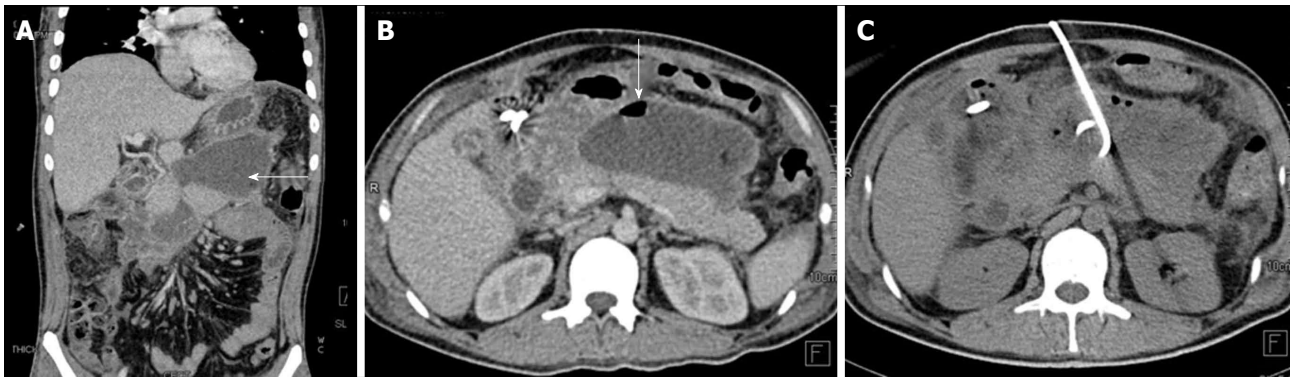

Figure 14 A 45-year-old man with missed pancreatic injury. CECT coronal (A) and axial (B) image done weeks after injury shows an ill-defined walled off necrosis (arrow A) with air foci within (arrow B). CT guided pigtail drainage of collection was done (C) with antibiotic coverage. CECT: Contrast enhanced computed tomography; CT: Computed tomography.

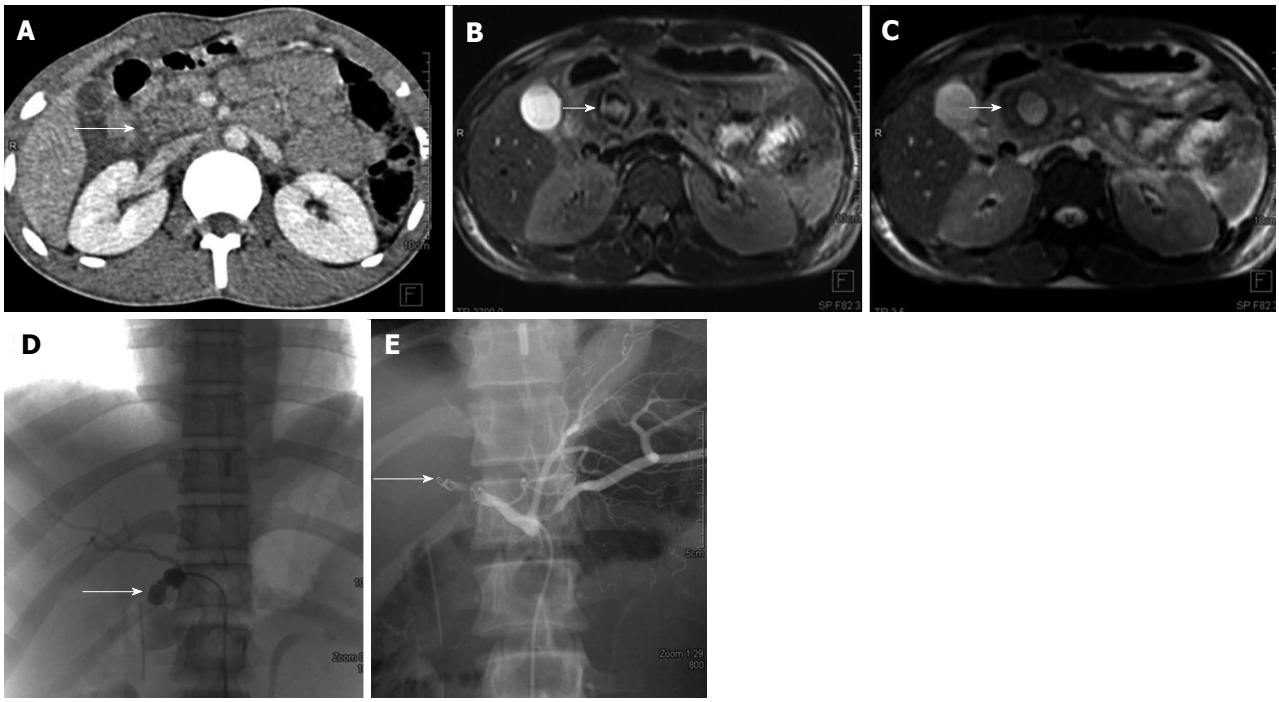

Figure 15 Post-traumatic common hepatic artery pseudoaneurysm 22 years old man with blunt trauma abdomen. CECT axial image shows injury to head of pancreas (arrow A). MRI done 3 d later showed well defined lesion in head of pancreas with heterogeneous signal intensity on T1 weighted image (arrow B) and hyperintense on TRUFISP image (arrow C). A possibility of pseudoaneurysm was given. Angiogram showed pseudoaneurysm arising from proximal common hepatic artery (arrow D) which was embolised with Nester coils (arrow E). CECT: Contrast enhanced computed tomography; MRI: Magnetic resonance imaging; TRUFISP: True fast imaging with steady-state free precession.

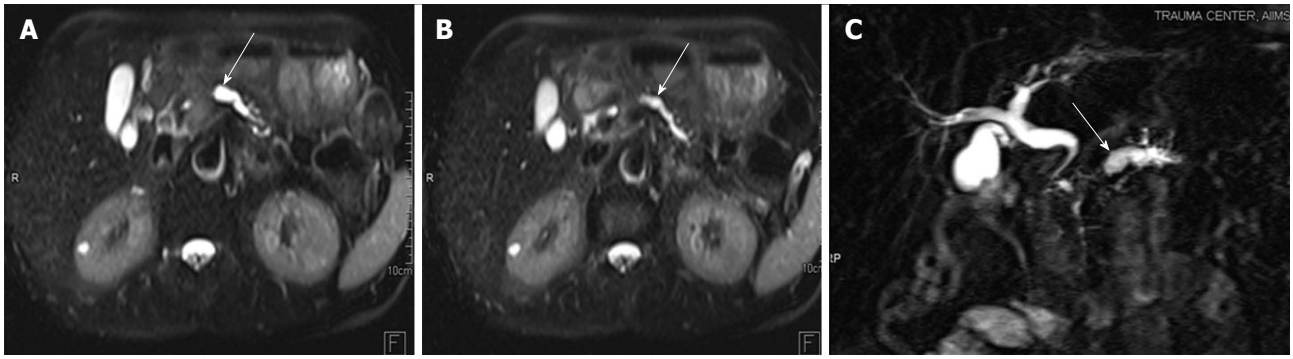

Figure 16 A 40-year-old male with previous history of pancreatic trauma. Injury was missed at time of presentation. Follow up MRI T2 HASTE images (A and B) and MRCP image (C) show dilated main pancreatic duct and side branches (arrows A and B) with cut off in proximal body region (arrow C) suggestive of post-traumatic pancreatic stricture. MRI: Magnetic resonance imaging; MRCP: Magnetic resonance pancreatography.

evaluate all CT scans for signs of pancreatic involvement. Early diagnosis of ductal injury is essential to improve outcomes. If ductal involvement is equivocal on CT, MRI should be done to comment on ductal injury *vs* integrity and guide management. ERCP has selective role in management of complications of pancreatic trauma and its complications. Since pancreatic injury is an evolving process, serial imaging with CT or MRI should be done to look for temporal evolution and for follow-up in non-operative management of pancreatic trauma. Radiology also plays a crucial role in follow-up and management of complications in pancreatic trauma.

REFERENCES

1 **Stawicki SP**, Schwab CW. Pancreatic trauma: demographics, diagnosis, and management. *Am Surg* 2008; **74**: 1133-1145 [PMID: 19097525]

2 **Biffl WL**, Moore EE, Croce M, Davis JW, Coimbra R, Karmy-Jones R, McIntyre RC, Moore FA, Sperry J, Malhotra A, Feliciano D. Western Trauma Association critical decisions in trauma: management of pancreatic injuries. *J Trauma Acute Care Surg* 2013; **75**: 941-946 [PMID: 24256664 DOI: 10.1097/TA.0b013e3182a96572]

3 **Lin BC**, Chen RJ, Fang JF, Hsu YP, Kao YC, Kao JL. Management of blunt major pancreatic injury. *J Trauma* 2004; **56**: 774-778 [PMID: 15187740 DOI: 10.1097/01.TA.0000087644.90727.DF]

4 **Fisher M**, Brasel K. Evolving management of pancreatic injury. *Curr Opin Crit Care* 2011; **17**: 613-617 [PMID: 21986464 DOI: 10.1097/MCC.0b013e32834cd374]

5 **Bhasin DK**, Rana SS, Rawal P. Endoscopic retrograde pancreatography in pancreatic trauma: need to break the mental barrier. *J Gastroenterol Hepatol* 2009; **24**: 720-728 [PMID: 19383077 DOI: 10.1111/j.1440-1746.2009.05809]

6 **Nirula R**, Velmahos GC, Demetriades D. Magnetic resonance cholangiopancreatography in pancreatic trauma: a new diagnostic modality? *J Trauma* 1999; **47**: 585-587 [PMID: 10498321 DOI: 10.1097/00005373-199909000-00031]

7 **Kong Y**, Zhang H, He X, Liu C, Piao L, Zhao G, Zhen Y. Endoscopic management for pancreatic injuries due to blunt abdominal trauma decreases failure of nonoperative management and incidence of pancreatic-related complications. *Injury* 2014; **45**: 134-140 [PMID: 23948236 DOI: 10.1016/j.injury.2013.07.017]

8 **Duchesne JC**, Schmieg R, Islam S, Olivier J, McSwain N. Selective nonoperative management of low-grade blunt pancreatic injury: are we there yet? *J Trauma* 2008; **65**: 49-53 [PMID: 18580509 DOI: 10.1097/TA.0b013e318176c00d]

9 **Cirillo RL**, Koniaris LG. Detecting blunt pancreatic injuries. *J Gastrointest Surg* 2002; **6**: 587-598 [PMID: 12127126 DOI: 10.1016/S1091-255X(01)00028-2]

10 **Daly KP**, Ho CP, Persson DL, Gay SB. Traumatic Retroperitoneal Injuries: Review of Multidetector CT Findings. *Radiographics* 2008; **28**: 1571-1590 [PMID: 18936022 DOI: 10.1148/rg.286075141]

11 **Arkovitz MS**, Johnson N, Garcia VF. Pancreatic trauma in children: mechanisms of injury. *J Trauma* 1997; **42**: 49-53 [PMID: 9003257 DOI: 10.1097/00005373-199701000-00009]

12 **Linsenmaier U**, Wirth S, Reiser M, Körner M. Diagnosis and classification of pancreatic and duodenal injuries in emergency radiology. *Radiographics* 2008; **28**: 1591-1602 [PMID: 18936023 DOI: 10.1148/rg.286085524]

13 **Bradley EL**, Young PR, Chang MC, Allen JE, Baker CC, Meredith W, Reed L, Thomason M. Diagnosis and initial management of blunt pancreatic trauma: guidelines from a multiinstitutional review. *Ann Surg* 1998; **227**: 861-869 [PMID: 9637549 DOI: 10.1097/00000658-199806000-00009]

14 **Chrysos E**, Athanasakis E, Xynos E. Pancreatic trauma in the adult: current knowledge in diagnosis and management. *Pancreatology* 2002; **2**: 365-378 [PMID: 12138225 DOI: 10.1159/000065084]

15 **Moretz JA**, Campbell DP, Parker DE, Williams GR. Significance of serum amylase level in evaluating pancreatic trauma. *Am J Surg* 1975; **130**: 739-741 [PMID: 1200292 DOI: 10.1016/0002-9610(75)90432-8]

16 **Adamson WT**, Hebra A, Thomas PB, Wagstaff P, Tagge EP, Othersen HB. Serum amylase and lipase alone are not cost-effective screening methods for pediatric pancreatic trauma. *J Pediatr Surg* 2003; **38**: 354-357; discussion 354-357 [PMID: 12632348]

17 **Olsen WR**. The serum amylase in blunt abdominal trauma. *J Trauma* 1973; **13**: 200-204 [PMID: 4695069 DOI: 10.1097/00005373-197303000-00003]

18 **Matsuno WC**, Huang CJ, Garcia NM, Roy LC, Davis J. Amylase and lipase measurements in paediatric patients with traumatic pancreatic injuries. *Injury* 2009; **40**: 66-71 [PMID: 19135195 DOI: 10.1016/j.injury.2008.10.003]

19 **Takishima T**, Sugimoto K, Hirata M, Asari Y, Ohwada T, Kakita A. Serum amylase level on admission in the diagnosis of blunt injury to the pancreas: its significance and limitations. *Ann Surg* 1997; **226**: 70-76 [PMID: 9242340 DOI: 10.1097/00000658-199707000-00010]

20 **Bouwman DL**, Weaver DW, Walt AJ. Serum amylase and its isoenzymes: a clarification of their implications in trauma. *J Trauma* 1984; **24**: 573-578 [PMID: 6205162 DOI: 10.1097/00005373-198407000-00004]

21 **Herman R**, Guire KE, Burd RS, Mooney DP, Ehlrich PF. Utility of amylase and lipase as predictors of grade of injury or outcomes in pediatric patients with pancreatic trauma. *J Pediatr Surg* 2011; **46**: 923-926 [PMID: 21616253 DOI: 10.1016/j.jpedsurg.2011.02.033]

22 **Wong YC**, Wang LJ, Lin BC, Chen CJ, Lim KE, Chen RJ. CT grading of blunt pancreatic injuries: prediction of ductal disruption and surgical correlation. *J Comput Assist Tomogr* 1997; **21**: 246-250 [PMID: 9071293 DOI: 10.1097/00004728-199703000-00014]

23 **Lucas CE**. Diagnosis and treatment of pancreatic and duodenal injury. *Surg Clin North Am* 1977; **57**: 49-65 [PMID: 854854]

24 **Smego DR**, Richardson JD, Flint LM. Determinants of outcome in pancreatic trauma. *J Trauma* 1985; **25**: 771-776 [PMID: 4020911 DOI: 10.1097/00005373-198508000-00007]

25 **Moore EE**, Cogbill TH, Malangoni MA, Jurkovich GJ, Champion HR, Gennarelli TA, McAninch JW, Pachter HL, Shackford SR, Trafton PG. Organ injury scaling, II: Pancreas, duodenum, small bowel, colon, and rectum. *J Trauma* 1990; **30**: 1427-1429 [PMID: 2231822 DOI: 10.1097/00005373-199011000-00035]

26 **Moore EE**, Moore FA. American Association for the Surgery of Trauma Organ Injury Scaling: 50th anniversary review article of the Journal of Trauma. *J Trauma* 2010; **69**: 1600-1601 [PMID: 21150537 DOI: 10.1097/TA.0b013e318201124e]

27 **Gupta A**, Stuhlfaut JW, Fleming KW, Lucey BC, Soto JA. Blunt trauma of the pancreas and biliary tract: a multimodality imaging approach to diagnosis. *Radiographics* 2004; **24**: 1381-1395 [PMID: 15371615 DOI: 10.1148/rg.245045002]

28 **Stuhlfaut JW**, Anderson SW, Soto JA. Blunt abdominal trauma: current imaging techniques and CT findings in patients with solid organ, bowel, and mesenteric injury. *Semin Ultrasound CT MR* 2007; **28**: 115-129 [PMID: 17432766 DOI: 10.1053/j.sult.2007.01.004]

29 **Akhrass R**, Kim K, Brandt C. Computed tomography: an unreliable indicator of pancreatic trauma. *Am Surg* 1996; **62**: 647-651 [PMID: 8712562]

30 **Teh SH**, Sheppard BC, Mullins RJ, Schreiber MA, Mayberry JC. Diagnosis and management of blunt pancreatic ductal injury in the era of high-resolution computed axial tomography. *Am J Surg* 2007; **193**: 641-643; discussion 643 [PMID: 17434373 DOI: 10.1016/j.amjsurg.2006.12.024]

31 **Wong YC**, Wang LJ, Fang JF, Lin BC, Ng CJ, Chen RJ. Multi-detector-row computed tomography (CT) of blunt pancreatic injuries: can contrast-enhanced multiphasic CT detect pancreatic duct injuries? *J Trauma* 2008; **64**: 666-672 [PMID: 18332806 DOI: 10.1097/TA.0b013e31802c5ba0]

32 **Phelan HA**, Velmahos GC, Jurkovich GJ, Friese RS, Minei JP, Menaker JA, Philp A, Evans HL, Gunn ML, Eastman AL, Rowell

SE, Allison CE, Barbosa RL, Norwood SH, Tabbara M, Dente CJ, Carrick MM, Wall MJ, Feeney J, O'Neill PJ, Srinivas G, Brown CV, Reifsnyder AC, Hassan MO, Albert S, Pascual JL, Strong M, Moore FO, Spain DA, Purtill MA, Edwards B, Strauss J, Durham RM, Duchesne JC, Greiffenstein P, Cothren CC. An evaluation of multidetector computed tomography in detecting pancreatic injury: results of a multicenter AAST study. *J Trauma* 2009; **66**: 641-646; discussion 646-647 [PMID: 19276732 DOI: 10.1097/TA.0b013e3181991a0e]

33 **Panda A**, Kumar A, Gamanagatti S, Bhalla AS, Sharma R, Kumar S, Mishra B. Evaluation of diagnostic utility of multidetector computed tomography and magnetic resonance imaging in blunt pancreatic trauma: a prospective study. *Acta Radiol* 2015; **56**: 387-396 [PMID: 24760286 DOI: 10.1177/0284185114529949]

34 **Wu B**, Song B. [Curved planar reformations in multi-slice spiral CT in pancreatic adenocarcinoma: prediction of invasion of pancreatic and peripancreatic ductal structures]. *Zhongguo Yixue Kexueyuan Xuebao* 2006; **28**: 71-75 [PMID: 16548194]

35 **Paspulati RM**. Multidetector CT of the pancreas. *Radiol Clin North Am* 2005; **43**: 999-1020, viii [PMID: 16253659 DOI: 10.1016/j.rcl.2005.07.001]

36 **Shanmuganathan K**. Multi-detector row CT imaging of blunt abdominal trauma. *Semin Ultrasound CT MR* 2004; **25**: 180-204 [PMID: 15160797 DOI: 10.1016/j.sult.2004.02.002]

37 **Venkatesh SK**, Wan JM. CT of blunt pancreatic trauma: a pictorial essay. *Eur J Radiol* 2008; **67**: 311-320 [PMID: 17709222 DOI: 10.1016/j.ejrad.2007.07.003]

38 **Rekhi S**, Anderson SW, Rhea JT, Soto JA. Imaging of blunt pancreatic trauma. *Emerg Radiol* 2010; **17**: 13-19 [PMID: 19396480 DOI: 10.1007/s10140-009-0811-0]

39 **Lane MJ**, Mindelzun RE, Sandhu JS, McCormick VD, Jeffrey RB. CT diagnosis of blunt pancreatic trauma: importance of detecting fluid between the pancreas and the splenic vein. *AJR Am J Roentgenol* 1994; **163**: 833-835 [PMID: 7503824 DOI: 10.2214/ajr.163.4.7503824]

40 **Sivit CJ**, Eichelberger MR, Taylor GA, Bulas DI, Gotschall CS, Kushner DC. Blunt pancreatic trauma in children: CT diagnosis. *AJR Am J Roentgenol* 1992; **158**: 1097-1100 [PMID: 1566674 DOI: 10.2214/ajr.158.5.1566674]

41 **Holalkere NS**, Soto J. Imaging of miscellaneous pancreatic pathology (trauma, transplant, infections, and deposition). *Radiol Clin North Am* 2012; **50**: 515-528 [PMID: 22560695 DOI: 10.1016/j.rcl.2012.03.011]

42 **Sivit CJ**, Eichelberger MR. CT diagnosis of pancreatic injury in children: significance of fluid separating the splenic vein and the pancreas. *AJR Am J Roentgenol* 1995; **165**: 921-924 [PMID: 7676993]

43 **Yang L**, Zhang XM, Xu XX, Tang W, Xiao B, Zeng NL. MR imaging for blunt pancreatic injury. *Eur J Radiol* 2010; **75**: e97-101 [PMID: 20056369 DOI: 10.1016/j.ejrad.2009.12.017]

44 **Soto JA**, Alvarez O, Múnera F, Yepes NL, Sepúlveda ME, Pérez JM. Traumatic disruption of the pancreatic duct: diagnosis with MR pancreatography. *AJR Am J Roentgenol* 2001; **176**: 175-178 [PMID: 11133562]

45 **Fulcher AS**, Turner MA, Yelon JA, McClain LC, Broderick T, Ivatury RR, Sugerman HJ. Magnetic resonance cholangiopancreatography (MRCP) in the assessment of pancreatic duct trauma and its sequelae: preliminary findings. *J Trauma* 2000; **48**: 1001-1007 [PMID: 10866243]

46 **Ragozzino A**, Manfredi R, Scaglione M, De Ritis R, Romano S, Rotondo A. The use of MRCP in the detection of pancreatic injuries after blunt trauma. *Emerg Radiol* 2003; **10**: 14-18 [PMID: 15290524]

47 **Gillams AR**, Kurzawinski T, Lees WR. Diagnosis of duct disruption and assessment of pancreatic leak with dynamic secretin-stimulated MR cholangiopancreatography. *AJR Am J Roentgenol* 2006; **186**: 499-506 [PMID: 16423959]

48 **Valentino M**, Ansaloni L, Catena F, Pavlica P, Pinna AD, Barozzi L. Contrast-enhanced ultrasonography in blunt abdominal trauma: considerations after 5 years of experience. *Radiol Med* 2009; **114**: 1080-1093 [PMID: 19774445 DOI: 10.1007/s11547-009-0444-0]

49 **Lv F**, Tang J, Luo Y, Nie Y, Liang T, Jiao Z, Zhu Z, Li T. Emergency contrast-enhanced ultrasonography for pancreatic injuries in blunt abdominal trauma. *Radiol Med* 2014; **119**: 920-927 [PMID: 24865939 DOI: 10.1007/s11547-014-0410-3]

50 **Pannu HK**, Fishman EK. Complications of endoscopic retrograde cholangiopancreatography: spectrum of abnormalities demonstrated with CT. *Radiographics* 2001; **21**: 1441-1453 [PMID: 11706215]

51 **Stone A**, Sugawa C, Lucas C, Hayward S, Nakamura R. The role of endoscopic retrograde pancreatography (ERP) in blunt abdominal trauma. *Am Surg* 1990; **56**: 715-720 [PMID: 2240868]

52 **Rogers SJ**, Cello JP, Schecter WP. Endoscopic retrograde cholangiopancreatography in patients with pancreatic trauma. *J Trauma* 2010; **68**: 538-544 [PMID: 20016385 DOI: 10.1097/TA.0b013e3181b5db7a]

53 **Kim HS**, Lee DK, Kim IW, Baik SK, Kwon SO, Park JW, Cho NC, Rhoe BS. The role of endoscopic retrograde pancreatography in the treatment of traumatic pancreatic duct injury. *Gastrointest Endosc* 2001; **54**: 49-55 [PMID: 11427841]

54 **Kozarek RA**. Endoscopic therapy of complete and partial pancreatic duct disruptions. *Gastrointest Endosc Clin N Am* 1998; **8**: 39-53 [PMID: 9405750]

55 **Bosboom D**, Braam AW, Blickman JG, Wijnen RM. The role of imaging studies in pancreatic injury due to blunt abdominal trauma in children. *Eur J Radiol* 2006; **59**: 3-7 [PMID: 16781837]

56 **Leppäniemi AK**, Haapiainen RK. Risk factors of delayed diagnosis of pancreatic trauma. *Eur J Surg* 1999; **165**: 1134-1137 [PMID: 10636545 DOI: 10.1080/110241599750007649]

57 **Brestas PS**, Karakyklas D, Gardelis J, Tsouroulas M, Drossos C. Sequential CT evaluation of isolated non-penetrating pancreatic trauma. *JOP* 2006; **7**: 51-55 [PMID: 16407619]

58 **Horst HM**, Bivins BA. Pancreatic transection. A concept of evolving injury. *Arch Surg* 1989; **124**: 1093-1095 [PMID: 2789030 DOI: 10.1001/archsurg.1989.01410090107024]

59 **Subramanian A**, Dente CJ, Feliciano DV. The management of pancreatic trauma in the modern era. *Surg Clin North Am* 2007; **87**: 1515-1532, x [PMID: 18053845 DOI: 10.1016/j.suc.2007.08.007]

60 **Patton JH**, Lyden SP, Croce MA, Pritchard FE, Minard G, Kudsk KA, Fabian TC. Pancreatic trauma: a simplified management guideline. *J Trauma* 1997; **43**: 234-239; discussion 239-241 [PMID: 9291366]

61 **Sharpe JP**, Magnotti LJ, Weinberg JA, Zarzaur BL, Stickley SM, Scott SE, Fabian TC, Croce MA. Impact of a defined management algorithm on outcome after traumatic pancreatic injury. *J Trauma Acute Care Surg* 2012; **72**: 100-105 [PMID: 22310122 DOI: 10.1097/TA.0b013e318241f09d]

62 **Asensio JA**, Petrone P, Roldán G, Kuncir E, Demetriades D. Pancreaticoduodenectomy: a rare procedure for the management of complex pancreaticoduodenal injuries. *J Am Coll Surg* 2003; **197**: 937-942 [PMID: 14644281]

63 **Seamon MJ**, Kim PK, Stawicki SP, Dabrowski GP, Goldberg AJ, Reilly PM, Schwab CW. Pancreatic injury in damage control laparotomies: Is pancreatic resection safe during the initial laparotomy? *Injury* 2009; **40**: 61-65 [PMID: 19054513 DOI: 10.1016/j.injury.2008.08.010]

64 **Wang GF**, Li YS, Li JS. Damage control surgery for severe pancreatic trauma. *Hepatobiliary Pancreat Dis Int* 2007; **6**: 569-571 [PMID: 18086619]

65 **Paul MD**, Mooney DP. The management of pancreatic injuries in children: operate or observe. *J Pediatr Surg* 2011; **46**: 1140-1143 [PMID: 21683212 DOI: 10.1016/j.jpedsurg.2011.03.041]

66 **Wood JH**, Partrick DA, Bruny JL, Sauaia A, Moulton SL. Operative vs nonoperative management of blunt pancreatic trauma in children. *J Pediatr Surg* 2010; **45**: 401-406 [PMID: 20152361 DOI: 10.1016/j.jpedsurg.2009.10.095]

67 **Velmahos GC**, Tabbara M, Gross R, Willette P, Hirsch E, Burke P, Emhoff T, Gupta R, Winchell RJ, Patterson LA, Manon-Matos Y, Alam HB, Rosenblatt M, Hurst J, Brotman S, Crookes B, Sartorelli K, Chang Y. Blunt pancreatoduodenal injury: a multicenter study

of the Research Consortium of New England Centers for Trauma (ReCONECT). *Arch Surg* 2009; **144**: 413-419; discussion 419-420 [PMID: 19451482 DOI: 10.1001/archsurg.2009.52]
68 **Wilson RH**, Moorehead RJ. Current management of trauma to the pancreas. *Br J Surg* 1991; **78**: 1196-1202 [PMID: 1958984]
69 **Oláh A**, Issekutz A, Haulik L, Makay R. Pancreatic transection from blunt abdominal trauma: early versus delayed diagnosis and surgical management. *Dig Surg* 2003; **20**: 408-414 [PMID: 12900531]
70 **Silveira HJ**, Mantovani M, Fraga GP. [Trauma of pancreas: predictor's factors of morbidity and mortality related to trauma index]. *Arq Gastroenterol* 2009; **46**: 270-278 [PMID: 20232005]
71 **Recinos G**, DuBose JJ, Teixeira PG, Inaba K, Demetriades D. Local complications following pancreatic trauma. *Injury* 2009; **40**: 516-520 [PMID: 19111300 DOI: 10.1016/j.injury.2008.06.026]
72 **Bradley EL**. Chronic obstructive pancreatitis as a delayed complication of pancreatic trauma. *HPB Surg* 1991; **5**: 49-59; discussion 59-60 [PMID: 1777410]
73 **Akhrass R**, Yaffe MB, Brandt CP, Reigle M, Fallon WF, Malangoni MA. Pancreatic trauma: a ten-year multi-institutional experience. *Am Surg* 1997; **63**: 598-604 [PMID: 9202533]
74 **Fleming WR**, Collier NA, Banting SW. Pancreatic trauma: Universities of Melbourne HPB Group. *Aust N Z J Surg* 1999; **69**: 357-362 [PMID: 10353551]
75 **Jones RC**. Management of pancreatic trauma. *Am J Surg* 1985; **150**: 698-704 [PMID: 4073362]
76 **Balasegaram M**. Surgical management of pancreatic trauma. *Curr Probl Surg* 1979; **16**: 1-59 [PMID: 391497]
77 **Ahmed N**, Vernick JJ. Pancreatic injury. *South Med J* 2009; **102**: 1253-1256 [PMID: 20016434 DOI: 10.1097/SMJ.0b013e3181c0dfca]
78 **Lin BC**, Fang JF, Wong YC, Liu NJ. Blunt pancreatic trauma and pseudocyst: management of major pancreatic duct injury. *Injury* 2007; **38**: 588-593 [PMID: 17306266]
79 **Coelho DE**, Ardengh JC, Carbalo MT, de Lima-Filho ER, Baron TH, Coelho JF. Clinicopathologic characteristics and endoscopic treatment of post-traumatic pancreatic pseudocysts. *Pancreas* 2011; **40**: 469-473 [PMID: 21343833 DOI: 10.1097/MPA.0b013e31820bf898]
80 **Patton JH**, Fabian TC. Complex pancreatic injuries. *Surg Clin North Am* 1996; **76**: 783-795 [PMID: 8782473]
81 **Pang TC**, Maher R, Gananadha S, Hugh TJ, Samra JS. Peripancreatic pseudoaneurysms: a management-based classification system. *Surg Endosc* 2014; **28**: 2027-2038 [PMID: 24519028 DOI: 10.1007/s00464-014-3434-9]
82 **Zhu YP**, Ni JJ, Chen RB, Matro E, Xu XW, Li B, Hu HJ, Mou YP. Successful interventional radiological management of postoperative complications of laparoscopic distal pancreatectomy. *World J Gastroenterol* 2013; **19**: 8453-8458 [PMID: 24363541 DOI: 10.3748/wjg.v19.i45.8453]
83 **Otah E**, Cushin BJ, Rozenblit GN, Neff R, Otah KE, Cooperman AM. Visceral artery pseudoaneurysms following pancreatoduodenectomy. *Arch Surg* 2002; **137**: 55-59 [PMID: 11772216]
84 **De Rosa A**, Gomez D, Pollock JG, Bungay P, De Nunzio M, Hall RI, Thurley P. The radiological management of pseudoaneurysms complicating pancreatitis. *JOP* 2012; **13**: 660-666 [PMID: 23183395 DOI: 10.6092/1590-8577/1193]
85 **Hur S**, Yoon CJ, Kang SG, Dixon R, Han HS, Yoon YS, Cho JY. Transcatheter arterial embolization of gastroduodenal artery stump pseudoaneurysms after pancreaticoduodenectomy: safety and efficacy of two embolization techniques. *J Vasc Interv Radiol* 2011; **22**: 294-301 [PMID: 21353982 DOI: 10.1016/j.jvir.2010.11.020]

P- Reviewer: Chow J, Li YZ, Nouh MR **S- Editor**: Qiu S
L- Editor: A **E- Editor**: Liu SQ

World Journal of Radiology

Submit a Manuscript: http://www.wjgnet.com/esps/
Help Desk: http://www.wjgnet.com/esps/helpdesk.aspx
DOI: 10.4329/wjr.v8.i2.174

World J Radiol 2016 February 28; 8(2): 174-182
ISSN 1949-8470 (online)

MINIREVIEWS

Benign neck masses showing restricted diffusion: Is there a histological basis for discordant behavior?

Abanti Das, Ashu S Bhalla, Raju Sharma, Atin Kumar, Meher Sharma, Shivanand Gamanagatti, Alok Thakar, Suresh Sharma

Abanti Das, Ashu S Bhalla, Raju Sharma, Atin Kumar, Shivanand Gamanagatti, Department of Radiodiagnosis, All India Institute of Medical Sciences, New Delhi 110029, India

Meher Sharma, Department of Pathology, All India Institute of Medical Sciences, New Delhi 110029, India

Alok Thakar, Suresh Sharma, Department of Otolaryngorhinology, All India Institute of Medical Sciences, New Delhi 110029, India

Author contributions: Das A, Bhalla AS, Sharma R and Kumar A contributed to study design and conception and writing the article; critically analyzing the scientific content and image preparation; Sharma M contributed to image preparation and reviewing the article; Gamanagatti S, Thakar A and Sharma S contributed to article preparation and approving the final version.

Conflict-of-interest statement: The authors declare no conflicts of interest regarding this manuscript.

Correspondence to: Ashu Seith Bhalla, Professor, Department of Radiodiagnosis, All India Institute of Medical Sciences, Ansari Nagar, New Delhi 110029, India. ashubhalla1@yahoo.com
Telephone: +91-011-26594925

Received: June 16, 2015
Peer-review started: June 17, 2015
First decision: August 22 2015
Revised: September 29, 2015
Accepted: December 18, 2015
Article in press: December 21, 2015
Published online: February 28, 2016

Abstract

Diffusion weighted imaging (DWI) evolved as a complementary tool to morphologic imaging by offering additional functional information about lesions. Although the technique utilizes movement of water molecules to characterize biological tissues in terms of their cellularity, there are other factors related to the histological constitution of lesions which can have a significant bearing on DWI. Benign lesions with atypical histology including presence of lymphoid stroma, inherently increased cellularity or abundant extracellular collagen can impede movement of water molecules similar to malignant tissues and thereby, show restricted diffusion. Knowledge of these atypical entities while interpreting DWI in clinical practice can avoid potential misdiagnosis. This review aims to present an imaging spectrum of such benign neck masses which, owing to their distinct histology, can show discordant behavior on DWI.

Key words: Diffusion weighted imaging; Benign neck masses; Restricted diffusion

Core tip: Diffusion weighted imaging improves lesion characterization by providing functional information. However, apart from tissue cellularity, histological background of the lesion can significantly influence the diffusion characteristics of the lesion. Consequently, even benign lesions with atypical histology can show restricted diffusion leading to potential errors in diagnosis.

Das A, Bhalla AS, Sharma R, Kumar A, Sharma M, Gamanagatti S, Thakar A, Sharma S. Benign neck masses showing restricted diffusion: Is there a histological basis for discordant behavior? *World J Radiol* 2016; 8(2): 174-182 Available from: URL: http://www.wjgnet.com/1949-8470/full/v8/i2/174.htm DOI: http://dx.doi.org/10.4329/wjr.v8.i2.174

INTRODUCTION

Diffusion weighted imaging (DWI) was introduced as an adjunct to conventional magnetic resonance imaging (MRI) to enable better characterization of biological tissues. This MR technique interrogates diffusivity of water molecules in tissues and the functional information obtained can be used to predict the biological nature of tissues. Clinical application of this technique began in early nineties with neuroimaging, mainly due to favourable MR characteristics and technical factors, but gradually its use has been extended to extracranial sites. Its application in head and neck lesions include characterization of cervical lymph nodes, salivary gland tumours, skull base lesions, differentiation of necrotic and viable parts of tumours with varying levels of success.

The basic principle of DWI is based on the fact that water molecules are always in random "Brownian" motion. This free movement is somewhat impeded in biological tissues due to interaction of water molecules with cell membranes and intracellular organelles. Benign tissues with relatively sparse cellularity and smaller nucleus to cytoplasmic ratio have sufficient space and allow relatively free mobility of water molecules[1]. This translates into facilitated diffusion on DWI. On the other hand, malignant tissues have densely packed cells which tend to have a larger nucleus occupying a relatively larger area of cytoplasm (higher nucleus to cytoplasmic ratio). As a result, malignant tissues offer more resistance to free movement of water molecules resulting in restricted diffusion.

However, while interpreting DWI in clinical practice; one needs to be aware of the fact that apart from tissue cellularity, tumours can have other histologic attributes including matrix composition which can have significant bearing on diffusion characteristics. Examples include fibrous tissues with extracellular collagen and lymphoid stroma which is known to show restricted diffusion[2]. In addition, some atypical entities despite being benign can have inherently increased cellularity and hence, can mimic malignant lesions on DWI. Prior knowledge of these lesions can reduce the possibility of potential misdiagnosis thereby, improving the diagnostic accuracy.

This article presents a spectrum of benign neck masses which show restricted pattern of diffusion and hence can lead to potential errors in diagnosis.

WARTHIN'S TUMOUR

Warthin's tumour (papillary cystadenoma lymphomatosum) is the second most common benign salivary gland neoplasm following pleomorphic adenoma. It constitutes about 4%-15% of all salivary gland neoplasms[3]. It commonly presents as slow-growing painless masses in middle-aged men, occurring almost exclusively in parotid gland mostly involving the lower portion over the angle of mandible[4]. Bilaterality and multicentricity are frequently observed in this group of tumors.

Histologically, it is an adenoma containing both solid and cystic areas. The cysts are lined by papillary projections containing oncocytic epithelial cells, while the supporting stroma contains abundant lymphoid tissue with lymphoid follicles and germinal centres[5] (Figure 1). These tumors have also been shown to have the highest microvessel count of all the parotid gland tumours[6].

The appearance of Warthin's tumour on DWI has been well documented in literature. Despite a wide range of reported mean apparent diffusion coefficient (ADC) values ranging from 0.72 to 0.96 × 10^{-3} mm^2/s, the presence of restricted diffusion has been reported uniformly in this entity[7-10] (Figure 1). Motoori *et al*[11] have in fact, reported an overlap of mean ADC values with those of malignant salivary gland tumors, especially salivary duct carcinoma. The proposed reason for such an appearance is the presence of predominant lymphoid stroma along with cysts containing thick proteinaceous content which inhibit free movement of water molecules[5]. Hence one needs to be aware of this entity and not to depend solely on DWI for characterization of parotid gland lesions.

NERVE SHEATH TUMOUR

Benign nerve sheath tumours are common in head and neck region accounting for about 25%-45% of all locations[12]. Histologically, they belong to two distinct groups namely schwannoma and neurofibroma, with the former being more common. Anatomically, parapharyngeal space is the most common location of nerve sheath tumours. Majority arise from the vagus nerve followed by cervical sympathetic chain and glossopharyngeal nerve. They mostly present as slow-growing, painless masses and hence, are late to come to clinical attention.

Schwannomas are known to have a heterogeneous appearance due to high propensity of cystic degeneration, xanthomatous changes and microhemorrhages[13] (Figure 2). Two distinct patterns of cellular arrangement are noted in schwannoma: Antoni A and Antoni B. Antoni A areas are highly cellular and composed of compact stacked arrangement of elongated cells. Alternating with these are relatively hypocellular Antoni B areas which contain loosely spaced cells with intervening microcystic spaces filled with mucin[14] (Figure 2).

Diffusion characteristics of schwannoms are not well documented in literature. Sener[15] reported facilitated diffusion in their series of six solid vestibular schwannoma while, isolated case reports have mentioned restricted diffusion in benign schwannomas. However, all the studies mention variable diffusion characteristics with a wide range of mean ADC values[16-20]. From a histological point of view, presence of areas of relative hypocellularity adjacent to either hypercellular or collagenous areas can probably explain the regional

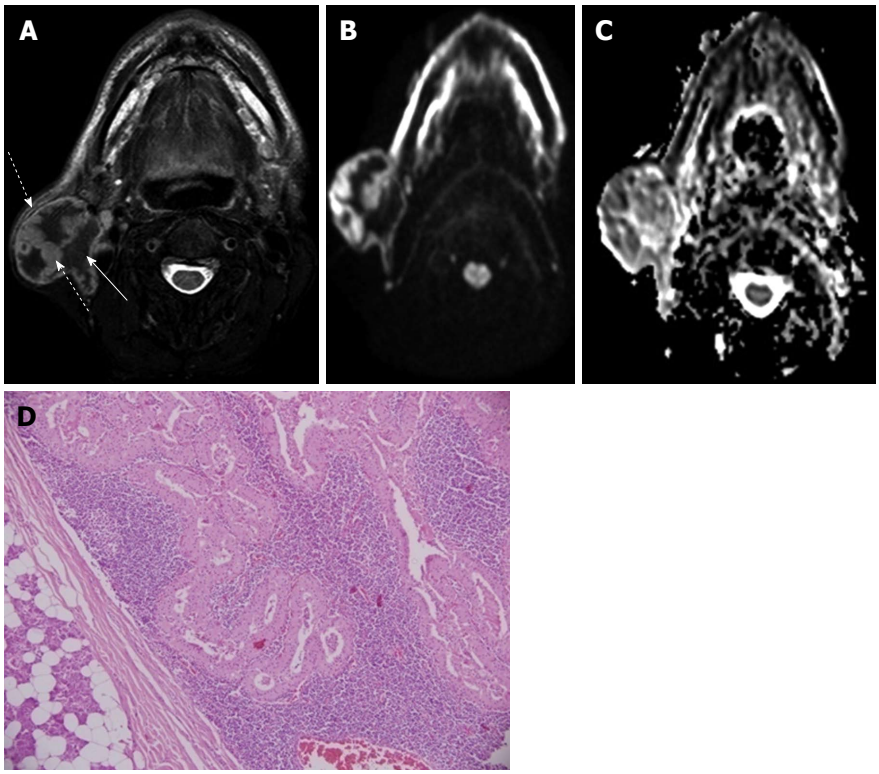

Figure 1 Warthin's tumour in right parotid gland in a 60-year-old man. A: Axial T2W FS image shows heterogeneous solid-cystic mass arising exophytically from right parotid gland with mildly hyperintense septae and mural nodules (dashed arrow) while cystic areas are hypointense (solid arrow); B and C: DWI at b1000 (B) s/mm² and ADC map (C) show restricted diffusion in septae and mural nodules of the mass; D: Photomicrograph shows a well encapsulated tumor comprising of acini with oncocytic change separated by sheets of lymphocytes (H-E; original magnification: × 100). DWI: Diffusion weighted imaging; ADC: Apparent diffusion coefficient.

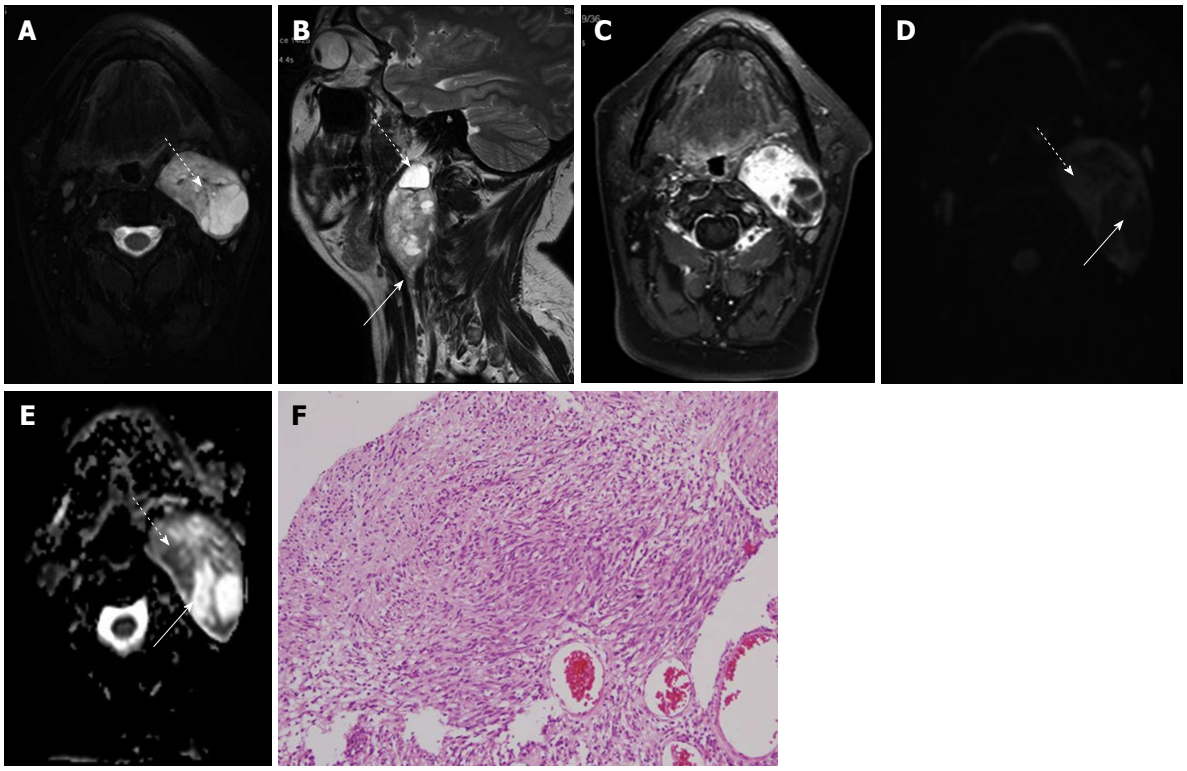

Figure 2 Left parapharyngeal space nerve sheath tumour in a 35-year-old lady. A: Axial T2W FS image shows multiple intensely T2 hyperintense areas within suggestive of cystic degeneration (dashed arrow); B: Sagittal T2W image shows blood fluid level within the cystic areas (dashed arrow) along with thickened distal exiting nerve (solid arrow); C: Axial T1W FS post contrast image shows intense enhancement in solid areas of the mass while cystic areas are hypointense; D and E: DWI at b1000 (D) s/mm² and ADC map (E) show restricted diffusion in solid areas of the mass (dashed arrow) while cystic areas show free diffusion (solid arrows); F: Photomicrograph shows alternating hypercellular (Antoni A) and hypocellular (Antoni B) areas (H-E; original magnification: × 100). DWI: Diffusion weighted imaging; ADC: Apparent diffusion coefficient.

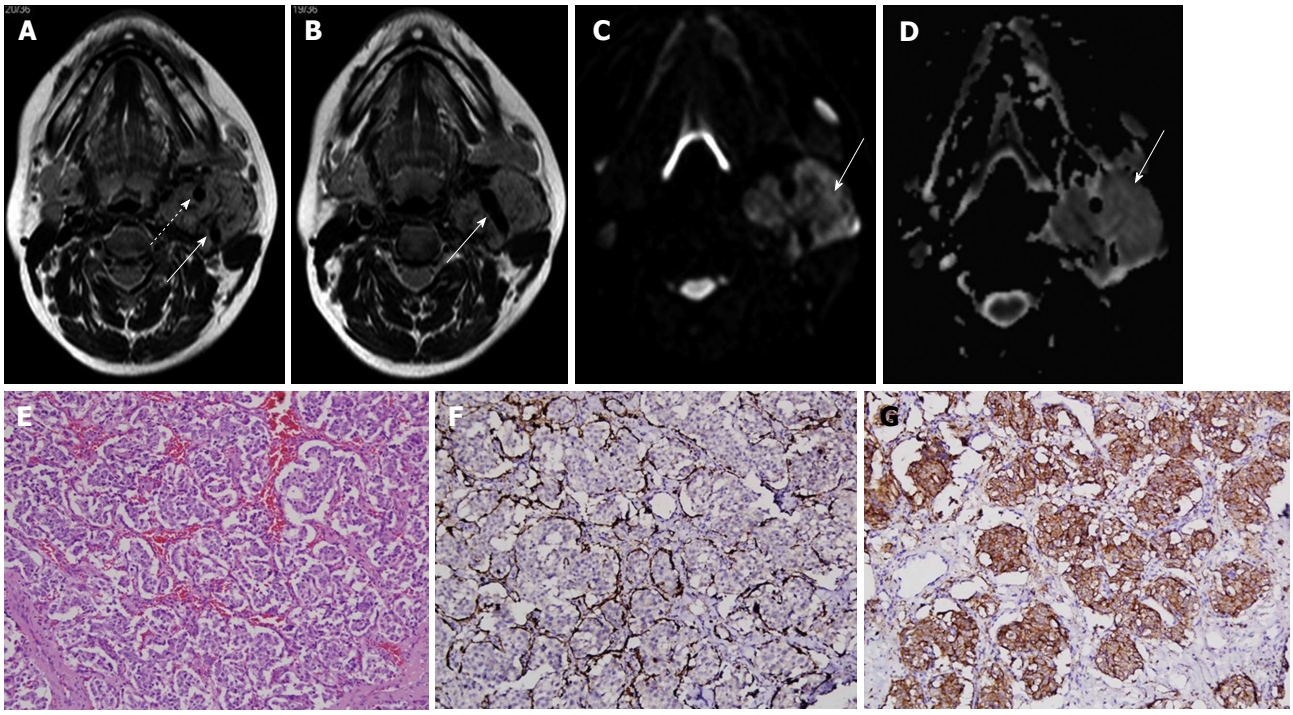

Figure 3 Carotid body tumour in a 30-year-old lady. A and B: Axial T2W images show heterogeneously hyperintense mass in left carotid space splaying the bifurcation of left common carotid artery (arrow in B) with encasement of both ECA and ICA (dashed arrow and solid arrow in A, respectively); C and D: DWI at b500 s/mm² (C) and ADC map (D) show restricted diffusion in the mass; E: Photomicrographs show tumor cells arranged in Zellballen pattern separated by thin fibrovascular septae (H-E; original magnification: × 200); F and G: S-100 immunostain demonstrating prominence of sustentacular cells at the periphery of the tumor cell nests (F, original magnification, × 200) and tumor cells are immunopositive for synaptophysin (G, original magnification: × 200). DWI: Diffusion weighted imaging; ADC: Apparent diffusion coefficient; ECA: External carotid artery; ICA: Internal carotid artery.

variation of diffusion characteristics in the same lesion. Peripheral areas of restriction likely correspond to hypercellular areas or areas with dense fibrous stroma while central areas of free diffusion correspond to hypocellular or cystic areas (Figure 2).

PARAGANGLIOMA

Paragangliomas are tumours of neural crest origin that occur along the distribution of these cells in specific locations of body. In head and neck, four common locations are observed: Carotid body at bifurcation of common carotid artery, jugular foramen, along the course of vagus nerve and middle ear cavity. Other less common locations include sella turcica[21], pineal gland, cavernous sinus and orbit. They comprise about 0.6% all tumours of head and neck[22]. Paraganglioma occurring in the neck produce characteristic displacement of adjacent vessels which help in their identification. Carotid body tumour splays the bifurcation of common carotid artery, encasing external carotid artery (ECA) and internal carotid artery (ICA) as it grows. However, the vessel lumen is usually not compromised[23] (Figure 3). Paraganglioma arising along the course of vagus nerve usually arise either from the superior ganglion (jugular ganglion) which is close to jugular foramen or from inferior ganglion (nodose ganglion). When arising from inferior ganglion, they produce anteromedial displacement of carotid vessels and posterolateral displacement of internal jugular vein, without any splaying of ECA and ICA.

Histologically, these tumours show a biphasic pattern composed of chief cells and supporting sustentacular cells with a fibrovascular stroma. The chief cells are more numerous and are compactly organized into cell rests known as zellballen pattern. The chief cells occupy central position in these clusters surrounded peripherally by sustentacular cells which characteristically have long cytoplasmic processes. This arrangement gives an overall whorled configuration to the cell clusters. The background stroma shows varying degree of hyalinization which tends to be higher in carotid body tumour. Immunohistochemical techniques can detect specific markers elicited by chief and sustentacular cells which includes chromagranin (present in neurosecretory granules of chief cells) and S-100 (sustentacular cell marker) and are widely used for diagnosis[23] (Figure 3).

The DWI appearance of paragangliomas has not been well documented in literature. Aschenbach *et al*[24] in their study of skull base lesions evaluated seven paragangliomas and found a mean ADC value of 1.304 ± 0.257 × 10^{-3} mm^2/s which was significantly different from other jugular fossa lesions. Others have reported hyperintense signal in urinary bladder paragangliomas on DWI, implying restricted diffusion[25]. DWI has also been used to differentiate between benign and malignant paragangliomas with the latter showing significantly lower mean ADC values than the former (0.918 ± 0.124) × 10^{-3} mm^2/s *vs* (1.175 ± 0.132) × 10^{-3} mm^2/s[26].

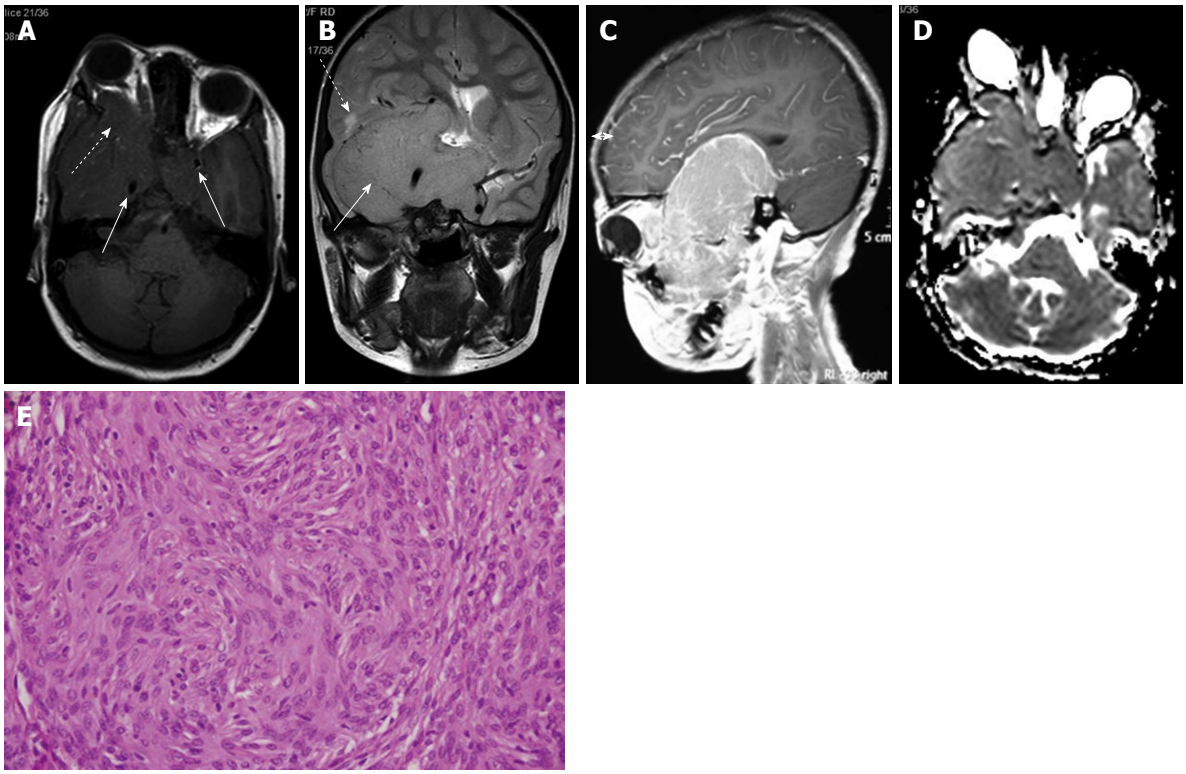

Figure 4 Craniofacial meningioma in a 7-year-old girl. A: Axial T1W image shows isointense homogenous mass involving bilateral cavernous sinuses (solid arrows) encasing bilateral ICAs and extending to right orbit causing proptosis (dashed arrow); B: Coronal T2W image shows intracranial extension in right middle cranial fossa (solid arrow) with mild perilesional edema in adjacent cerebral parenchyma (dashed arrow); C: Sagittal T1W FS post-gadolinium image reveals intense homogeneous enhancement in the mass; D: ADC map showing homogenous restricted diffusion in the mass; E: Photomicrograph show tumour composed of spindled to polygonal cells with moderate amount of cytoplasm, vesicular nuclei and whorl formation at places (H-E; original magnification: × 400). ADC: Apparent diffusion coefficient; ICA: Internal carotid artery.

Such atypical behavior of paragangliomas on DWI can be explained to some extent, by the compact histological arrangement of its constituent cells. These tumours show whorled arrangement of cells with presence of variable amount of collagen deposition in their stroma which leaves little extracellular space for free movement of water molecules (Figure 3). This hypothesis can be extrapolated to explain the lower ADC observed in malignant pheochromocytomas with increased cellularity and reduced extracellular space compared to their benign counterparts. However, a definite histological explanation warrants large scale studies to validate these findings.

MENINGIOMA

Primary extracranial meningiomas are rare tumours (< 2%) and their most common location includes head and neck especially sinonasal region, ear, temporal bone and scalp[27]. Their origin is hypothesized to be from arachnoidal cells which tend to migrate outside the neuraxis producing extracranial meningiomas. In about 20% cases, extracranial meningiomas have an intracranial extension. These tumors have a female preponderance which can be attributed to presence of progesterone-dependent growth[28].

Histologically, meningiomas are made up of whorls of neoplastic epitheloid cells with indistinct borders (Figure 4). They frequently show psammoma bodies and intranuclear pseudo-inclusions[27,29]. In addition, various histologic subtypes have been identified including meningothelial, fibrous, angiomatous, transitional, psammomatous or atypical. Increased collagen formation has been noted in meningiomas irrespective of tumour grade which has been attributed to presence of meningiothelial cells[28]. Such fibrous stroma coupled with heterogeneous histologic composition leads to variable diffusion characteristics.

There are limited studies documenting the role of DWI in meningiomas. While the major emphasis has been on differentiation of benign and atypical/malignant meningiomas using mean and normalized ADC values, the variable nature of diffusion characteristics in benign meningiomas has also been mentioned[30-32] (Figure 4).

Hakyemez *et al*[32] have reported different ranges of mean ADC values in different subtypes of benign meningiomas. Others have also mentioned variable signal intensity of benign meningiomas on DWI with malignant/atypical meningiomas showing relative restriction compared to their benign counterparts[31].

SOLITARY FIBROUS TUMOUR

Solitary fibrous tumour (SFT) is a rare neoplasm of mesenchymal origin[33]. Although, most frequently seen

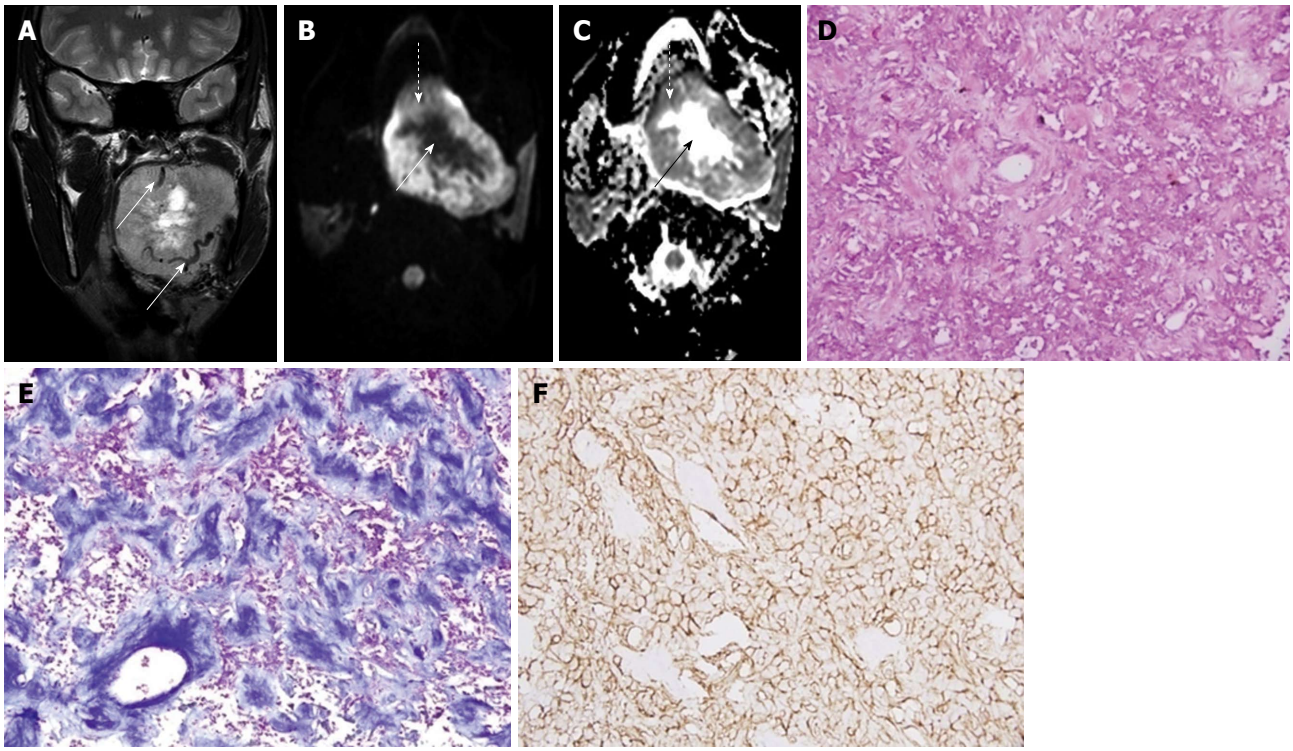

Figure 5 Solitary fibrous tumour in a 24-year-old man. A: Coronal T2W image shows well defined left parapharyngeal space mass with heterogeneously hyperintense signal. The core is more hyperintense than the periphery. Multiple tortuous flow voids seen in the mass (solid arrows); B and C: DWI at b1000 (B) s/mm² and corresponding ADC map (C) show restricted diffusion in the periphery of the mass (dashed arrows) while the centre shows free diffusion (solid arrow); D: Photomicrographs show alternating cellular and hypocellular areas with abundant collagen (H-E; original magnification: × 200); E and F: Masson trichrome stain highlighting abundant collagen (E; original magnification: × 200); tumor cells are diffusely immunopositive for CD34 (F; original magnification: × 400). DWI: Diffusion weighted imaging; ADC: Apparent diffusion coefficient.

to arise from pleura, occasional SFTs have been documented at various extra-pleural sites including lung, mediastinum, pericardium, liver and head and neck. Extracranial head and neck SFTs have been reported in oral cavity, paranasal sinuses, orbit, nasal cavity and parapharyngeal space. Most of these tumours are benign with complete surgical excision being the treatment of choice.

Histologically, they are well circumscribed masses predominantly populated by spindle cells with abundant extracellular collagen. Distinct immunohistochemical features characterize these tumours which include diffuse CD34 positivity and epithelial membrane antigen negativity[34] (Figure 5). Some tumours may show hypocellular areas with profuse extra-cellular collagen deposition alternating with hypercellular areas[35].

MRI reveals heterogeneous appearance of SFTs on T2 weighted images. They show focal areas of relative T2 hypointensity interspersed with hyperintense areas which corresponds to hypocellular collagenous areas and hypercellular areas respectively. These contrasting signal intensities on T2 weighted images produce the so called "yin-yang" appearance[36]. These tumours are usually hypervascular with frequent presence of vascular flow voids[37]. Diffusion weighted imaging shows areas of restricted diffusion in some parts of these lesions which has been attributed to the presence of focal areas of hypercellularity in them[36,38] (Figure 5).

HEMANGIOPERICYTOMA

Hemangiopericytoma (HPC) is a rare mesenchymal neoplasm originating from Zimmermann pericytes which are modified smooth muscle cells outlining capillaries and post-capillary venules[39]. Although any age group can be affected, they are most frequently seen in fifth and sixth decades[40]. About 15%-30% of them occur in head and neck which is the third most common site following lower extremities and retroperitoneum-pelvis, respectively[41]. Tumours in head and neck commonly arise in the neck, perioral soft tissue and sinonasal tract[41]. Sinonasal HPCs are believed to have less aggressive biological behaviour compared to their peripheral counterparts. Complete surgical excision with negative margins is the treatment of choice.

HPCs belong to the same histological spectrum as SFTs with common imaging and clinical features. They are hypercellular and vascular lesions with compact arrangement of cells containing scant cytoplasm (Figure 6). Dilated vessels are interspersed showing a branching pattern resembling "staghorn" appearance[42].

DWI has been used to differentiate intracranial HPCs from meningiomas based on significantly lower minADC values in meningiomas as compared to HPCs ($0.875 \pm 0.014 \times 10^{-3}$ mm²/s and $1.116 \pm 0.127 \times 10^{-3}$ mm²/s, respectively)[43]. The possible explanation being offered is a relatively lower cellularity and prominent vascularity

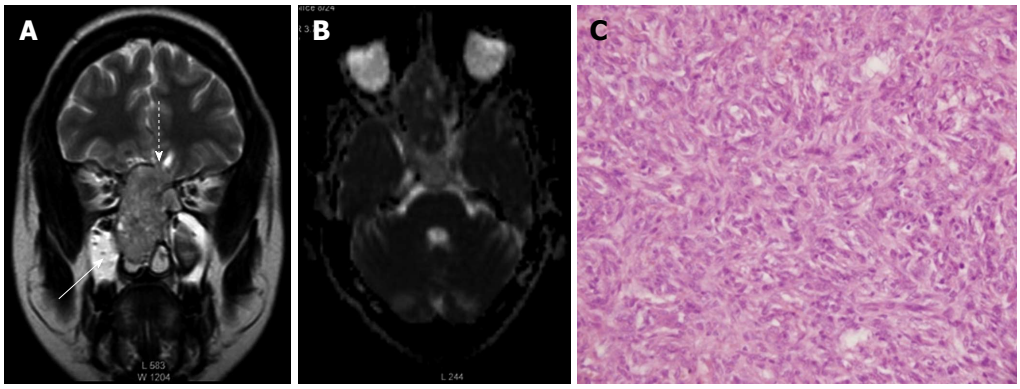

Figure 6 Sinonasal hemangiopericytoma in a 45-year-old lady. A: Coronal T2W image shows mildly expansile sinonasal mass involving, extending to bilateral ethmoid sinuses. Small intracranial extension noted in anterior cranial fossa (dashed arrow); Retained secretions in right maxillary sinus (solid arrow); B: ADC map shows restricted diffusion in the mass; C: Photomicrograph shows spindle cells with mild pleomorphism (H-E; original magnification: × 100). ADC: Apparent diffusion coefficient.

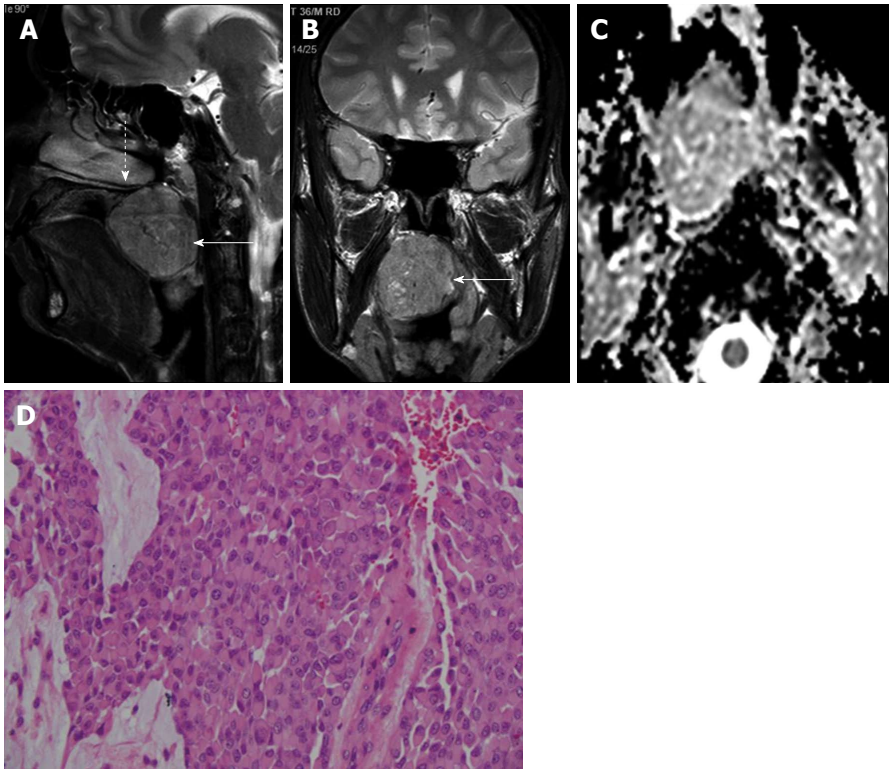

Figure 7 Myoepithelial tumour in a 36-year-old man. A and B: Sagittal T2W image shows well defined T2 hyperintense mass arising from posterior part of soft palate (dashed arrow in A and B) and into the oropharynx (solid arrow in A and B); C: ADC map shows restricted diffusion in the mass; D: Photomicrograph shows cells with abundant cytoplasm and minimal pleomorphism (H-E; original magnification: × 100).

in HPCs as compared to meningiomas. However, owing to the inherently hypercellular tumour matrix of HPCs, free movement of water molecules is hindered producing a qualitative pattern of restricted diffusion (Figure 6).

MYOEPITHELIAL TUMOUR

Myoepithelial tumours are rare benign neoplasms constituting about 1%-1.5% of salivary tumours. About 40% of them occur in parotid glands followed by submandibular glands and minor salivary glands; most common location being the palate[44,45] (Figure 7). They belong to the same histological spectrum as pleomorphic adenoma but are more aggressive. However, World Health Organization has recognized it as a separate entity showing less than 5% or no ductal and acinar differentiation, which are present in pleomorphic adenoma[45].

Histologically, myoepithelial tumours can be composed of spindle-shaped, plasmacytoid, epitheloid or clear cells in varying proportions. The growth pattern can appear as solid (non-myxoid), reticular or mixed type[46]. Histological subtype is related to the location of these tumours. Plasmacytoid type occurs more commonly in

Table 1 Space-wise distribution of benign entities showing restricted diffusion in head and neck

Neck space	Benign entities with restricted diffusion
Parapharyngeal space	Nerve sheath tumour
Carotid space	Paraganglioma
	Nerve sheath tumour
Parotid space	Warthin's tumour
	Myoepithelial tumour
Oral cavity	Myoepithelial tumour
Sinonasal cavity	Meningioma
	Hemangiopericytoma
	Solitary fibrous tumour
Ear/temporal bone	Paraganglioma (glomus tympanicum)
	Meningioma
	Nerve sheath tumour
Miscellaneous	Nerve sheath tumour
	Hemangiopericytoma
	Solitary fibrous tumour

minor salivary glands of oral cavity, while spindle-cell and clear cell type are more often seen in parotid glands[47]. The background stroma is composed of variable amount of fibro-collagenous or myxoid stroma.

The MR imaging appearance of myoepithelial tumours has sporadically been reported in literature. They are isointense on T1 weighted image and intensely hyperintense on T2 weighted images with homogenous contrast enhancement. However, their behavior on DWI has not been documented earlier. We have observed hyperintense signal on DWI in myoepithelial tumour which can possibly be attributed to its plasmacytoid histology characterized by closely packed arrangement of neoplastic cells (Figure 7). However, keeping in view the variable histological make-up of these tumours, they can have variable appearance on DWI. Further studies are therefore, needed to validate these findings.

DWI has long been used successfully for diagnosis and characterization of lesions as benign and malignant; there are few atypical entities which do not conform to the expected behavior according to their biological nature. While some of these entities occur in specific neck spaces, others are more non-specific in their distribution (Table 1). A knowledge of these exceptions and their preferred distribution in various neck spaces helps to narrow the possible list of differential diagnoses and avoid possible errors in diagnosis.

REFERENCES

1 **Wang J**, Takashima S, Takayama F, Kawakami S, Saito A, Matsushita T, Momose M, Ishiyama T. Head and neck lesions: characterization with diffusion-weighted echo-planar MR imaging. *Radiology* 2001; **220**: 621-630 [PMID: 11526259 DOI: 10.1148/radiol.2202010063]

2 **Qayyum A**. Diffusion-weighted imaging in the abdomen and pelvis: concepts and applications. *Radiographics* 2009; **29**: 1797-1810 [PMID: 19959522 DOI: 10.1148/rg.296095521]

3 **Som PM**, Brandwein MS. Salivary glands: anatomy and pathology. In: Som PM, Curtin HD, editors. Head and neck imaging. 4th ed. St. Louis, Mo: Mosby, 2003: 2005-2133

4 **Eveson JW**, Cawson RA. Salivary gland tumours. A review of 2410 cases with particular reference to histological types, site, age and sex distribution. *J Pathol* 1985; **146**: 51-58 [PMID: 4009321 DOI: 10.1002/path.1711460106]

5 **Ikeda M**, Motoori K, Hanazawa T, Nagai Y, Yamamoto S, Ueda T, Funatsu H, Ito H. Warthin tumor of the parotid gland: diagnostic value of MR imaging with histopathologic correlation. *AJNR Am J Neuroradiol* 2004; **25**: 1256-1262 [PMID: 15313720]

6 **Yabuuchi H**, Fukuya T, Tajima T, Hachitanda Y, Tomita K, Koga M. Salivary gland tumors: diagnostic value of gadolinium-enhanced dynamic MR imaging with histopathologic correlation. *Radiology* 2003; **226**: 345-354 [PMID: 12563124 DOI: 10.1148/radiol.2262011486]

7 **Habermann CR**, Gossrau P, Graessner J, Arndt C, Cramer MC, Reitmeier F, Jaehne M, Adam G. Diffusion-weighted echo-planar MRI: a valuable tool for differentiating primary parotid gland tumors? *Rofo* 2005; **177**: 940-945 [PMID: 15973595 DOI: 10.1055/s-2005-858297]

8 **Yoshino N**, Yamada I, Ohbayashi N, Honda E, Ida M, Kurabayashi T, Maruyama K, Sasaki T. Salivary glands and lesions: evaluation of apparent diffusion coefficients with split-echo diffusion-weighted MR imaging--initial results. *Radiology* 2001; **221**: 837-842 [PMID: 11719687 DOI: 10.1148/radiol.2213010131]

9 **Habermann CR**, Arndt C, Graessner J, Diestel L, Petersen KU, Reitmeier F, Ussmueller JO, Adam G, Jaehne M. Diffusion-weighted echo-planar MR imaging of primary parotid gland tumors: is a prediction of different histologic subtypes possible? *AJNR Am J Neuroradiol* 2009; **30**: 591-596 [PMID: 19131405 DOI: 10.3174/ajnr.A1412]

10 **Şerifoğlu İ**, Oz İİ, Damar M, Tokgöz Ö, Yazgan Ö, Erdem Z. Diffusion-weighted imaging in the head and neck region: usefulness of apparent diffusion coefficient values for characterization of lesions. *Diagn Interv Radiol* 2015; **21**: 208-214 [PMID: 25910284 DOI: 10.5152/dir.2014.14279]

11 **Motoori K**, Iida Y, Nagai Y, Yamamoto S, Ueda T, Funatsu H, Ito H, Yoshitaka O. MR imaging of salivary duct carcinoma. *AJNR Am J Neuroradiol* 2005; **26**: 1201-1206 [PMID: 15891184]

12 **Colreavy MP**, Lacy PD, Hughes J, Bouchier-Hayes D, Brennan P, O'Dwyer AJ, Donnelly MJ, Gaffney R, Maguire A, O'Dwyer TP, Timon CV, Walsh MA. Head and neck schwannomas--a 10 year review. *J Laryngol Otol* 2000; **114**: 119-124 [PMID: 10748827 DOI: 10.1258/0022215001905058]

13 **Cohen LM**, Schwartz AM, Rockoff SD. Benign schwannomas: pathologic basis for CT inhomogeneities. *AJR Am J Roentgenol* 1986; **147**: 141-143 [PMID: 3487205 DOI: 10.2214/ajr.147.1.141]

14 **McLendon RE**, Bigner DD, Bigner SH. Intracranial and intraspinal schwannomas (WHO grade I). In: Pathology of Tumors of the Central Nervous System: A Guide to Histologic Diagnosis. London: Arnold; 2000: 71-81

15 **Sener RN**. Diffusion magnetic resonance imaging of solid vestibular schwannomas. *J Comput Assist Tomogr* 2003; **27**: 249-252 [PMID: 12703020 DOI: 10.1097/00004728-200301000-00007]

16 **Srinivasan A**, Dvorak R, Perni K, Rohrer S, Mukherji SK. Differentiation of benign and malignant pathology in the head and neck using 3T apparent diffusion coefficient values: early experience. *AJNR Am J Neuroradiol* 2008; **29**: 40-44 [PMID: 17921228 DOI: 10.3174/ajnr.A0743]

17 **Khedr SA**, Hassan MA, Abdelrazek NM, Sakr Ay. Diagnostic impact of echo planar diffusion-weighted magnetic resonance imaging (DWI) in musculoskeletal neoplastic masses using apparent diffusion coefficient (ADC) mapping as a quantitative assessment tool. *Egyptian J Radiol Nuc Med* 2012; **43**: 249-256 [DOI: 10.1016/j.ejrnm.2012.01.003]

18 **Fayad LM**, Blakeley J, Plotkin S, Widemann B, Jacobs MA. Whole Body MRI at 3T with Quantitative Diffusion Weighted Imaging and Contrast-Enhanced Sequences for the Characterization of Peripheral Lesions in Patients with Neurofibromatosis Type 2 and Schwannomatosis. *ISRN Radiol* 2013; **2013**: 9 [DOI: 10.5402/2013/627932]

19 **Chhabra A**, Thakkar RS, Andreisek G, Chalian M, Belzberg AJ,

Blakeley J, Hoke A, Thawait GK, Eng J, Carrino JA. Anatomic MR imaging and functional diffusion tensor imaging of peripheral nerve tumors and tumorlike conditions. *AJNR Am J Neuroradiol* 2013; **34**: 802-807 [PMID: 23124644 DOI: 10.3174/ajnr.A3316]

20 **Sumi M**, Nakamura T. Head and neck tumours: combined MRI assessment based on IVIM and TIC analyses for the differentiation of tumors of different histological types. *Eur Radiol* 2014; **24**: 223-231 [PMID: 24013848 DOI: 10.1007/s00330-013-3002-z]

21 **Noble ER**, Smoker WR, Ghatak NR. Atypical skull base paragangliomas. *AJNR Am J Neuroradiol* 1997; **18**: 986-990 [PMID: 9159383]

22 **Borba LA**, Al-Mefty O. Intravagal paragangliomas: report of four cases. *Neurosurgery* 1996; **38**: 569-575; discussion 575 [PMID: 8837811 DOI: 10.1227/00006123-199603000-00030]

23 **Rao AB**, Koeller KK, Adair CF. From the archives of the AFIP. Paragangliomas of the head and neck: radiologic-pathologic correlation. Armed Forces Institute of Pathology. *Radiographics* 1999; **19**: 1605-1632 [PMID: 10555678]

24 **Aschenbach R**, Basche S, Vogl TJ, Klisch J. Diffusion-weighted imaging and ADC mapping of head-and-neck paragangliomas: initial experience. *Klin Neuroradiol* 2009; **19**: 215-219 [PMID: 19705076 DOI: 10.1007/s00062-009-9004-1]

25 **Wang H**, Ye H, Guo A, Wei Z, Zhang X, Zhong Y, Fan Z, Wang Y, Wang D. Bladder paraganglioma in adults: MR appearance in four patients. *Eur J Radiol* 2011; **80**: e217-e220 [PMID: 20950973 DOI: 10.1016/j.ejrad.2010.09.020]

26 **Dong Y**, Liu Q. Differentiation of malignant from benign pheochromocytomas with diffusion-weighted and dynamic contrast-enhanced magnetic resonance at 3.0 T. *J Comput Assist Tomogr* 2012; **36**: 361-366 [PMID: 22805661 DOI: 10.1097/RCT.0b013e31825975f8]

27 **Rushing EJ**, Bouffard JP, McCall S, Olsen C, Mena H, Sandberg GD, Thompson LD. Primary extracranial meningiomas: an analysis of 146 cases. *Head Neck Pathol* 2009; **3**: 116-130 [PMID: 19644540 DOI: 10.1007/s12105-009-0118-1]

28 **Backer-Grøndahl T**, Moen BH, Torp SH. The histopathological spectrum of human meningiomas. *Int J Clin Exp Pathol* 2012; **5**: 231-242 [PMID: 22558478]

29 **Thompson LD**, Gyure KA. Extracranial sinonasal tract meningiomas: a clinicopathologic study of 30 cases with a review of the literature. *Am J Surg Pathol* 2000; **24**: 640-650 [PMID: 10800982 DOI: 10.1097/00000478-200005000-00002]

30 **Nagar VA**, Ye JR, Ng WH, Chan YH, Hui F, Lee CK, Lim CC. Diffusion-weighted MR imaging: diagnosing atypical or malignant meningiomas and detecting tumor dedifferentiation. *AJNR Am J Neuroradiol* 2008; **29**: 1147-1152 [PMID: 18356472 DOI: 10.3174/ajnr.A0996]

31 **Filippi CG**, Edgar MA, Uluğ AM, Prowda JC, Heier LA, Zimmerman RD. Appearance of meningiomas on diffusion-weighted images: correlating diffusion constants with histopathologic findings. *AJNR Am J Neuroradiol* 2001; **22**: 65-72 [PMID: 11158890]

32 **Hakyemez B**, Yildirim N, Erdoğan C, Kocaeli H, Korfali E, Parlak M. Meningiomas with conventional MRI findings resembling intraaxial tumors: can perfusion-weighted MRI be helpful in differentiation? *Neuroradiology* 2006; **48**: 695-702 [PMID: 16896907 DOI: 10.1007/s00234-006-0115-y]

33 **Goodlad JR**, Fletcher CD. Solitary fibrous tumour arising at unusual sites: analysis of a series. *Histopathology* 1991; **19**: 515-522 [PMID: 1786936 DOI: 10.1111/j.1365-2559.1991.tb01499.x]

34 **Mekni A**, Kourda J, Hammouda KB, Tangour M, Kchir N, Zitouna M, Haouet S. Solitary fibrous tumour of the central nervous system: pathological study of eight cases and review of the literature. *Pathology* 2009; **41**: 649-654 [PMID: 19672786 DOI: 10.3109/00313020903071439]

35 **Smith AB**, Horkanyne-Szakaly I, Schroeder JW, Rushing EJ. From the radiologic pathology archives: mass lesions of the dura: beyond meningioma-radiologic-pathologic correlation. *Radiographics* 2014; **34**: 295-312 [PMID: 24617680 DOI: 10.1148/rg.342130075]

36 **Kim HJ**, Lee HK, Seo JJ, Kim HJ, Shin JH, Jeong AK, Lee JH, Cho KJ. MR imaging of solitary fibrous tumors in the head and neck. *Korean J Radiol* 2005; **6**: 136-142 [PMID: 16145288 DOI: 10.3348/kjr.2005.6.3.136]

37 **Tateishi U**, Nishihara H, Morikawa T, Miyasaka K. Solitary fibrous tumor of the pleura: MR appearance and enhancement pattern. *J Comput Assist Tomogr* 2002; **26**: 174-179 [PMID: 11884769 DOI: 10.1097/00004728-200203000-00002]

38 **Clarençon F**, Bonneville F, Rousseau A, Galanaud D, Kujas M, Naggara O, Cornu P, Chiras J. Intracranial solitary fibrous tumor: imaging findings. *Eur J Radiol* 2011; **80**: 387-394 [PMID: 20303226 DOI: 10.1016/j.ejrad.2010.02.016]

39 **Stout AP**, Murray MR. Hemangiopericytoma: a vascular tumor featuring zimmermann's pericytes. *Ann Surg* 1942; **116**: 26-33 [PMID: 17858068 DOI: 10.1097/00000658-194207000-00004]

40 **McMaster MJ**, Soule EH, Ivins JC. Hemangiopericytoma. A clinicopathologic study and long-term followup of 60 patients. *Cancer* 1975; **36**: 2232-2244 [PMID: 1203874 DOI: 10.1002/cncr.2820360942]

41 **Enzinger FM**, Smith BH. Hemangiopericytoma. An analysis of 106 cases. *Hum Pathol* 1976; **7**: 61-82 [PMID: 1244311 DOI: 10.1016/S0046-8177(76)80006-8]

42 **Giannini C**, Rushing EJ, Hainfellner JA. Haemangiopericytoma. In: Louis DN, Ohagaki H, Wiestler OD, Cavanees WK, editors. WHO classifiation of tumours of the central nervous system. Lyon, France: IARC, 2007: 178-180

43 **Liu G**, Chen ZY, Ma L, Lou X, Li SJ, Wang YL. Intracranial hemangiopericytoma: MR imaging findings and diagnostic usefulness of minimum ADC values. *J Magn Reson Imaging* 2013; **38**: 1146-1151 [PMID: 23463687 DOI: 10.1002/jmri.24075]

44 **Ferri E**, Pavon I, Armato E, Cavaleri S, Capuzzo P, Ianniello F. Myoepithelioma of a minor salivary gland of the cheek: case report. *Acta Otorhinolaryngol Ital* 2006; **26**: 43-46 [PMID: 18383757]

45 **Cuadra Zelaya F**, Quezada Rivera D, Tapia Vazquez JL, Paez Valencia C, Gaitán Cepeda LA. Plasmacytoid myoepithelioma of the palate. Report of one case and review of the literature. *Med Oral Patol Oral Cir Bucal* 2007; **12**: E552-E555 [PMID: 18059237]

46 **Dardick I**. Myoepithelioma: definitions and diagnostic criteria. *Ultrastruct Pathol* 1995; **19**: 335-345 [PMID: 7483010 DOI: 10.3109/01913129509021906]

47 **Bakshi J**, Parida PK, Mahesha V, Radotra BD. Plasmacytoid myoepithelioma of palate: three rare cases and literature review. *J Laryngol Otol* 2007; **121**: e13 [PMID: 17640425 DOI: 10.1017/S002221510700000X]

P- Reviewer: Chow J **S- Editor**: Qiu S
L- Editor: A **E- Editor**: Liu SQ

World Journal of Radiology

Submit a Manuscript: http://www.wjgnet.com/esps/
Help Desk: http://www.wjgnet.com/esps/helpdesk.aspx
DOI: 10.4329/wjr.v8.i2.183

World J Radiol 2016 February 28; 8(2): 183-191
ISSN 1949-8470 (online)

MINIREVIEWS

Xanthogranulomatous cholecystitis: What every radiologist should know

Vaibhav P Singh, S Rajesh, Chhagan Bihari, Saloni N Desai, Sudheer S Pargewar, Ankur Arora

Vaibhav P Singh, S Rajesh, Saloni N Desai, Sudheer S Pargewar, Ankur Arora, Division of Diagnostic and Interventional Radiology, Department of Radiology, Institute of Liver and Biliary Sciences, New Delhi, Delhi 110070, India

Chhagan Bihari, Department of Pathology, Institute of Liver and Biliary Sciences, New Delhi, Delhi110070, India

Author contributions: Singh VP, Desai SN and Pargewar SS contributed to this paper with conception and design of the study, literature review and analysis as well as drafting; Rajesh S, Bihari C and Arora A contributed to this paper with critical revision, editing and final approval of the final revision; Bihari C also provided with valuabe pathological inputs.

Conflict-of-interest statement: No potential conflicts of interest.

Correspondence to: S Rajesh, MD, PDCC, Assistant Professor, Division of Diagnostic and Interventional Radiology, Department of Radiology, Institute of Liver and Biliary Sciences, D1, Vasant Kunj, New Delhi, Delhi 110070, India. rajesh387@gmail.com
Telephone: +91-78-38233499

Received: August 28, 2015
Peer-review started: September 18, 2015
First decision: October 30, 2015
Revised: November 8, 2015
Accepted: December 17, 2015
Article in press: December 18, 2015
Published online: February 28, 2016

Abstract

Xanthogranulomatous cholecystitis (XGC) is an uncommon variant of chronic cholecystitis characterized by xanthogranulomatous inflammation of the gallbladder. Intramural accumulation of lipid-laden macrophages and acute and chronic inflammatory cells is the hallmark of the disease. The xanthogranulomatous inflammation of the gallbladder can be very severe and can spill over to the neighbouring structures like liver, bowel and stomach resulting in dense adhesions, perforation, abscess formation, fistulous communication with adjacent bowel. Striking gallbladder wall thickening and dense local adhesions can be easily mistaken for carcinoma of the gallbladder, both intraoperatively as well as on preoperative imaging. Besides, cases of concomitant gallbladder carcinoma complicating XGC have also been reported in literature. So, we have done a review of the imaging features of XGC in order to better understand the entity as well as to increase the diagnostic yield of the disease summarizing the characteristic imaging findings and associations of XGC. Among other findings, presence of intramural hypodense nodules is considered diagnostic of this entity. However, in some cases, an imaging diagnosis of XGC is virtually impossible. Fine needle aspiration cytology might be handy in such patients. A preoperative counselling should include possibility of differential diagnosis of gallbladder cancer in not so characteristic cases.

Key words: Hypodense nodules; Carcinoma gallbladder; Xanthogranulomatous; Cholecystitis; Adenomyomatosis

Core tip: A pre-operative diagnosis of xanthogranulomatous cholecystitis always comes handy for the surgeons. Diagnosing atypical cases can be challenging and acknowledge of pathological changes occurring in the disease along with the spectrum of imaging findings can be a useful armoury in hands of the radiologist. So we have tried to give a concise review of this entity emphasizing on radiological and pathological aspects. Few points in differential diagnosing with other entities

especially carcinoma gallbladder have also been entailed.

Singh VP, Rajesh S, Bihari C, Desai SN, Pargewar SS, Arora A. Xanthogranulomatous cholecystitis: What every radiologist should know. *World J Radiol* 2016; 8(2): 183-191 Available from: URL: http://www.wjgnet.com/1949-8470/full/v8/i2/183.htm DOI: http://dx.doi.org/10.4329/wjr.v8.i2.183

INTRODUCTION

Xanthogranulomatous cholecystitis (XGC) is a chronic inflammatory disease of the gallbladder characterized by focal or diffuse destructive inflammatory process followed by marked proliferative fibrosis along with infiltration of macrophages and foamy cells[1].

The nomenclature was done by McCoy *et al*[2] in 1976 though it was first described in 1970 by Christensen *et al*[3]. Christensen *et al*[3] and Amazon *et al*[4] had noted a pseudotumoral form of chronic cholecystitis that was characterized by the presence of xanthoma-like foam cells and scarring and that contained ceroid (wax-like) nodules in an inflammed gallbladder wall. They used the terms fibroxanthogranulomatous inflammation and ceroid granulomas of the gallbladder, respectively, which are now known as synonyms of XGC[3,4].

DEMOGRAPHICS

Albeit a common gallbladder pathology with an incidence rate of 0.7% to 10 %, it has been sparsely described in literature and is poorly understood[1]. It occurs in a wide range of age groups but the incidence is higher in the sixth and seventh decades of life. It's occurrence in a two month old infant has also been described in literature[5]. Male preponderance has been reported with a male to female ratio of 2:1[6]. However one of the Indian studies found a marked female preponderance with a male to female ratio of 1:9[7]. The most important association of XGC is with gall stones which are seen in as many as 80% of cases[8].

CLINICAL FEATURES AND LABORATORY MARKERS

Patients can present with features of acute cholecystitis (22%), chronic cholecystitis (88%), pain (95%), obstructive jaundice (22%), cholangitis (2%) and palpable mass (5%)[6]. On examination, a palpable mass or positive Murphy's sign can be localised. However, these clinical features are not specific for XGC and often no clinical difference between patients with XGC and carcinoma gallbladder can be found[9].

Leukocytosis has been observed though there is no specific biochemical test or liver function discordance pointing towards the diagnosis of XGC. Complications are present in 32% of cases and include perforation, abscess formation, fistulous tracts to the duodenum or skin, and extension of the inflammatory process to the liver, colon, or surrounding soft tissues[10].

Yu *et al*[11] found that elevation of tumor biomarkers is frequent in XGC which further creates confusion in differentiating the disease with carcinoma of gallbladder.

PATHOLOGY

XGC is characterized pathologically by the presence of greyish-yellow nodules or streaks in the gallbladder wall which are mainly caused by lipid laden macrophages. The exact etiopathogenesis is unclear. One proposed theory behind the xanthogranulomatous etiology is mucosal ulceration or rupture of Rokitansky-Aschoff sinuses due to increased intraluminal pressure secondary to gallbladder or cystic duct obstruction which leads to entry of bile in gallbladder wall. This intramural bile is incompletely engulfed by the macrophages leading to chronic granulomatous inflammatory response (Figure 1A).

The histological diagnosis is based on diffuse or focal mural changes in the form of xanthoma cells (foamy histiocytes containing lipids and bile pigment), giant multinucleate histiocytes and acute or chronic inflammatory cells. These histiocytes are positive for CD68 on immunohistochemistry (Figures 1B, C and 2). Microabscesses also tend to form in the gallbladder wall and finally a fibrous reaction and scarring results from healing of the inflammatory reaction[12]. Rupture of gallbladder serosal lining and spread of the inflammatory response leads to adhesions with adjacent liver, duodenum and transverse colon (Figure 3).

XGC is associated with gallbladder carcinoma in 8.5% to 30.5% cases[13]. Gallbladder carcinoma may provide route for bile entry into the stroma owing to its greater degree of tissue destruction[14]. Obstruction of the cystic duct by a neoplasm may initiate the histiocytic inflammatory process of XGC[15]. The association is important because when both lesions are present in the same specimen, there is a possibility of overlooking the carcinoma altogether[16].

Possibility of coexisting infection has also been proposed. Howard *et al*[17] have reported that intraoperative cultures of the bile and gallbladder have been positive usually for *Escherichia coli*, Klebsiella, *Enterococcus* and, less frequently, for *Pseudomonas*, *Serratia* and *Staphylococcus* aureus.

RADIOLOGICAL FINDINGS

Ultrasonography

The sonographic findings include the presence of gallstones or sludge and moderate to marked focal or diffuse thickening of the gallbladder wall. Parra *et al*[18] observed that the wall thickening was hyperechoic in comparison to the liver in 100% of patients (Figure 4). Presence of hypoechoic nodules or bands in the thickened wall can occasionally be seen, the presence of which is considered a characteristic finding. Hypoechoic

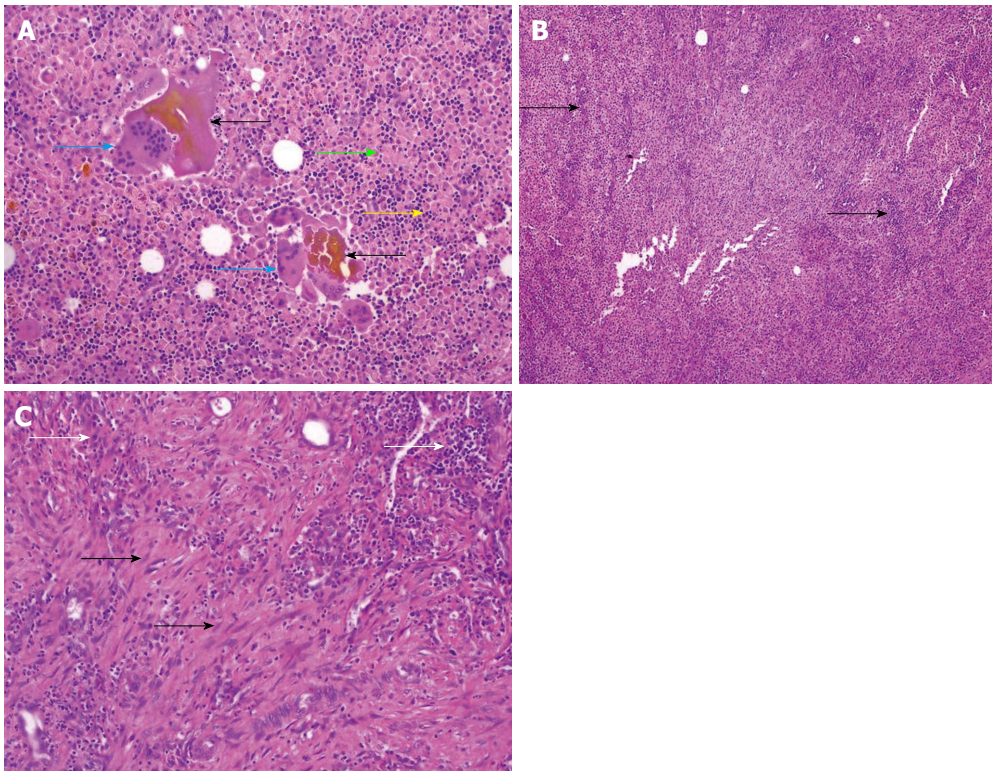

Figure 1 High power and low power view. A: High power (HE, 200 ×) view showing inspissated bile (black arrows) with giant cells (blue arrows) in the vicinity. Green arrows denote histiocytes while the yellow arrows denote lymphoid cells; B: Low power (HE, 40 ×) view showing sheets of lympho-histiocytes in the gallbladder wall; C: High power (HE, 200 ×) view showing myofibroblasts (black arrows) with inflammatory cells (white arrows).

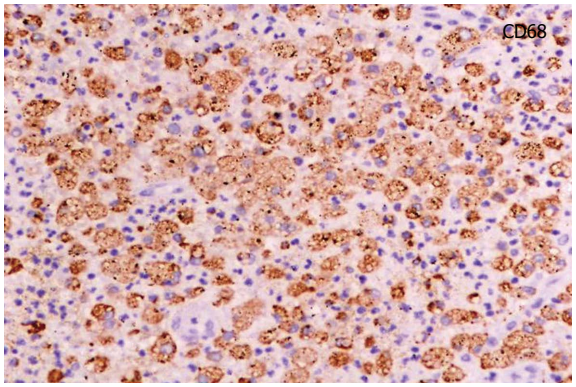

Figure 2 Immunohistochemistry revealing positivity for CD68 signifying sheets of histiocytes.

nodules on sonography have been observed in 15% and 73% cases by Parra *et al*[18] and Kim *et al*[19] respectively. Hypoechoic band has been observed in around 19% cases of XGC[18,20]. Xanthogranulomatous nodules behave as well-defined hypoechoic areas on sonography (Figure 5). Hypoechoic bands might be caused by a more generalized involvement of the mucosa[18]. Complications like perforation, abscess and hepatic infiltration can also be seen on sonography[18,19].

Computed tomography

Computed tomography (CT) findings of patients presenting with acute symptoms and patients presenting with chronic symptoms are usually not much different[21]. CT findings include - diffuse or focal wall thickening, intramural hypoattenuating nodules in thickened walls, luminal surface enhancement (LSE) with continuous mucosal lines or mucosal lines with focal breach. Cholelithiasis and choledocholithiasis are often seen associated with XGC.

Gallbladder wall thickening can range from 4.0 mm to 18.5 mm and is usually diffuse in nature[21]. Diffuse gallbladder (GB) wall thickening has been observed in 88.9% and 87.8% of patients by two independent researchers Goshima *et al*[22] and Zhao *et al*[21] respectively. Focal thickening is less commonly seen in XGC, and is more likely to be associated with carcinoma of gallbladder. Diffuse thickening associated with XGC is usually symmetrical but diffuse asymmetrical thickening has also been described with XGC in 22.2% cases[21,22]. To the best of our knowledge, XGC presenting as mass replacing gallbladder, intra-luminal mass or polypoidal mass-like thickening has not yet been described in literature.

The intramural nodules detected on imaging studies (85.7% and 61.1% by Zhao *et al*[21] and Goshima *et al*[22] respectively) are either xanthogranulomas or abscesses. Occupation of a large area of the thickened gallbladder wall by intramural nodules is highly suggestive of XGC[23] (Figure 6). Xanthogranulomas are more often revealed on imaging than abscesses though the later cause more clinical complications[15]. In acute inflammatory phase intramural nodules were abscesses in contrast to xanthogranulomas in the latter phase[15].

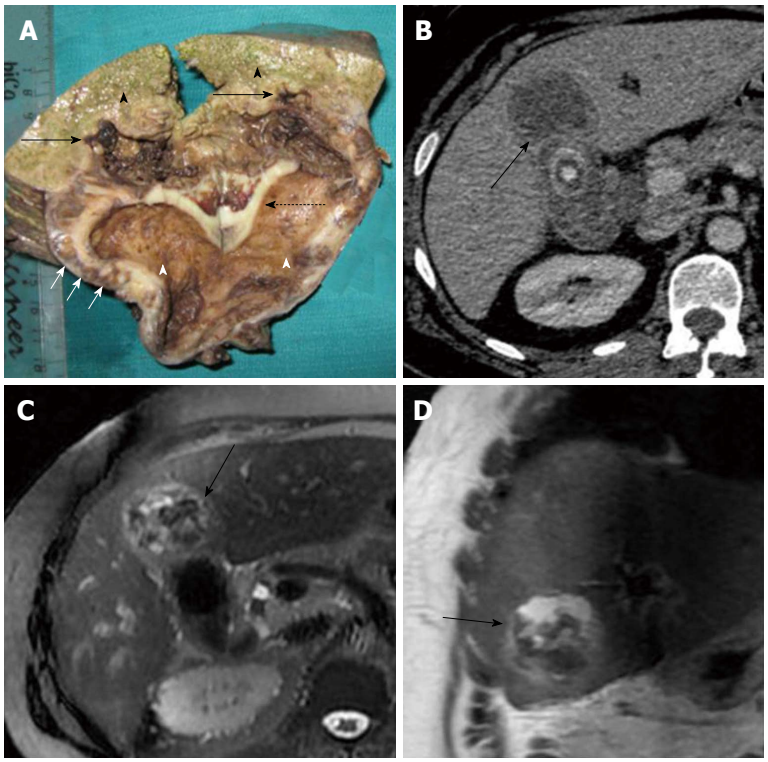

Figure 3 Rupture of gallbladder serosal lining and spread of the inflammatory response leads to adhesions with adjacent liver, duodenum and transverse colon. Gross pathology specimen (A) demonstrating a thickened gallbladder wall (dotted arrow) showing multiple yellowish nodules (xanthoma nodules) within (short arrows). Infiltration into the adjoining liver parenchyma is seen (black arrows). Black arrowheads denote the normal liver parechyma while the white arrowheads denote gallbladder lumen. Corresponding computed tomography images (B) of the same patient showing focal mural thickening involving the gallbladder fundal region with poor fat planes and infiltration into the adjacent hepatic parenchyma (black arrows). Magnetic resonance axial and coronal images (C and D) of the same patient showing heterogeneous mass like thickening involving the gallbladder fundal region with poor fat planes to adjacent hepatic parenchyma (black arrows).

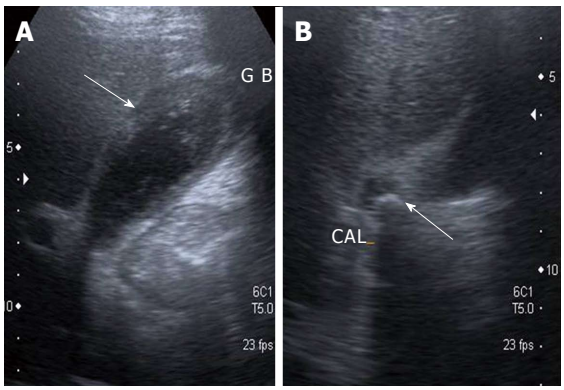

Figure 4 Ultrasound image showing a well distended gallbladder. The diffuse hyperechoic wall thickening (arrow, A) and obstructive calculus in gallbladder neck region (arrow, B). GB: Gallbladder.

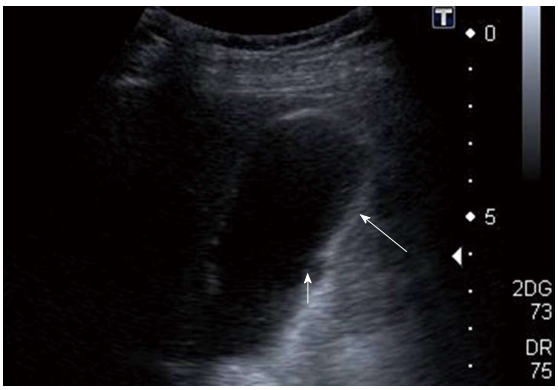

Figure 5 A well distended gallbladder showing diffuse hyperechoic wall thickening (long arrow). Note is made of a small mucosal defect (short arrow) with a small hypoechoic collection in thickened gallbladder wall.

A continuous mucosal lining is more often observed with XGC (66.7% of cases) compared to a disrupted mucosal lining (33.3%)[22]. XGC is pathology of gallbladder wall and hence mucosal surface is intact or only focally denuded. On the contrary, carcinoma of gallbladder arises from the gallbladder epithelium and causes mucosal disruption in majority of the cases. Mucosal line disruption has been observed in 82.2% cases of carcinoma of gallbladder. Mucosal disruption in XGC is only seen with diffuse thickening of the gallbladder wall and patients with disrupted mucosal lining are more likely to have complications[21].

LSE is defined as enhancement of the gallbladder wall predominantly at the luminal surface. This finding was noted in 85.7% of cases by Zhao *et al*[21] and 70% cases by Shuto *et al*[24]. LSE noted in XGC is more apparent in the portal venous phase and represents preservation of the epithelial layer[21,24]. This further points towards the intramural location of the disease process with an intact overlying mucosa as opposed to the disrupted mucosa in gallbladder carcinoma.

Cholelithiasis, choledocholithiasis (Figure 7), hepa-

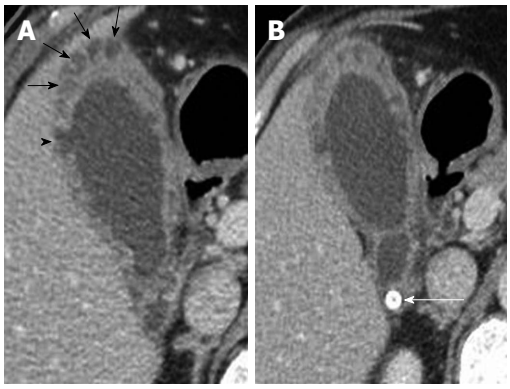

Figure 6 Axial computed tomography section showing multiple hypodense nodules (black arrows) in a diffusely thickened gallbladder wall (A) and the same patient showing gallbladder neck calculus (white arrow) (B). Also seen is an area of mucosal defect with associated small intramural collection (black arrowhead).

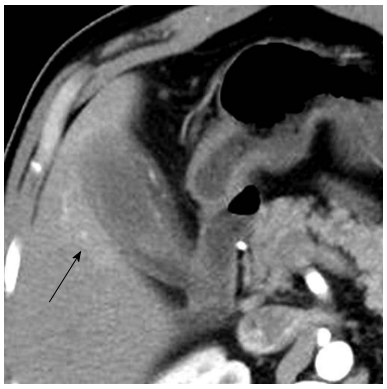

Figure 8 Axial arterial phase computed tomography image showing an area of hyper perfusion in the segment V of liver adjoining a gallbladder showing diffusely thickened walls. Also noted is the blurring of interfaces between gallbladder wall and adjoining liver parenchyma. Liver infiltration can demonstrate an early enhancement of the parenchyma which pathologically corresponds with accumulation of inflammatory cells and abundant fibrosis.

ticolithiasis have all been described frequently with XGC. Resultant gallbladder distention and biliary dilatation can be observed (Figure 7).

The infiltration of adjacent structurescan manifest as pericholecystic fat strandings, blurring of interface between gallbladder and liver, early enhancement of liver (or transient hepatic attenuation difference) (Figure 8), infiltration of bowel (duodenum/colon) (Figure 9), infiltration of stomach and invasion of abdominal wall (Figure 10). While pericholecystic fat stranding and blurring of interface between gallbladder and liver are quite frequent, the other findings are sparsely observed. Liver infiltration can result in an early enhancement of parenchyma in 40% of cases[21] (Figure 8). Other complications include gallbladder perforation, abscess formation (Figure 11) or fistulous communications. Involvement of the biliary tree by the inflammatory process (xanthogranulomatous choledochitis) can also be seen[25]. However, the absence of intrahepatic biliary dilatation is more frequently observed in XGC and is an important finding in differentiating it from carcinoma of

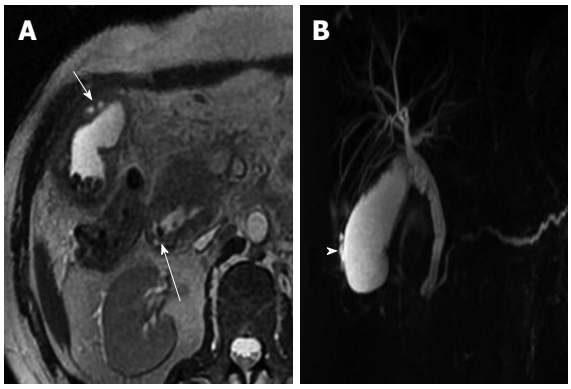

Figure 7 Axial T2W image (A) and corresponding magnetic resonance cholangiopancreatography image (B). Axial T2W image (A) showing multiple gallbladder calculi with a diffusely thickened wall showing multiple intramural nodules (short arrow). Note is also made of a small filling defect involving the ampullary common duct (long arrow). Corresponding MRCP image (B) showing multiple intramural nodules (white arrowhead) along with a dilated pancreaticobiliary system secondary to calculus in ampullary region. MRCP: Magnetic resonance cholangiopancreatography.

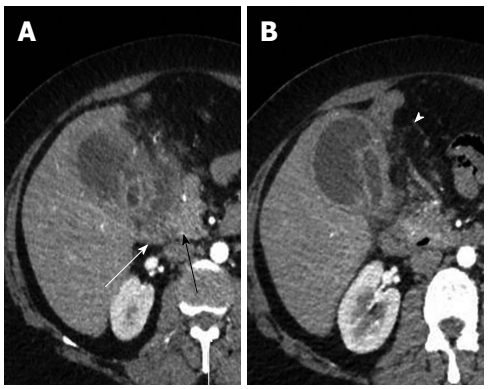

Figure 9 Axial computed tomography sections (A and B) showing thickened and irregular walls with small intramural and pericholecystic collections. Note the extension of the inflammatory process to involve the duodenum (white arrow) and pancreatic head (black arrow). Also pericholecystic fat strandings are seen (white arrowhead).

gallbladder.

Occurrence of lymphadenopathy (> 10 mm in short axis diameter) has been variably described by different researchers. While Zhao *et al*[21] have described an incidence of 10.2%, Goshima *et al*[22] found an incidence of 90%. But both the researchers were of the opinion that loco-regional lymphadenopathy can be useful in differentiation from carcinoma of gallbladder. Only 41% patients with gallbladder carcinoma showed homogeneous enhancement of enlarged nodes compared to 100% patients with XGC[22].

Associated gallbladder or biliary malignancies can also be visualized on CT[13]. Notably, Indian researchers, Krishnani *et al*[13] have described a high coexistence of carcinoma gallbladder with XGC (19.6% of cases). Although the causative mechanism behind the association between the two entities is unclear, both are complications of cholelithiasis and cholecystitis of a particular duration. XGC may obscure the adenocarcino-

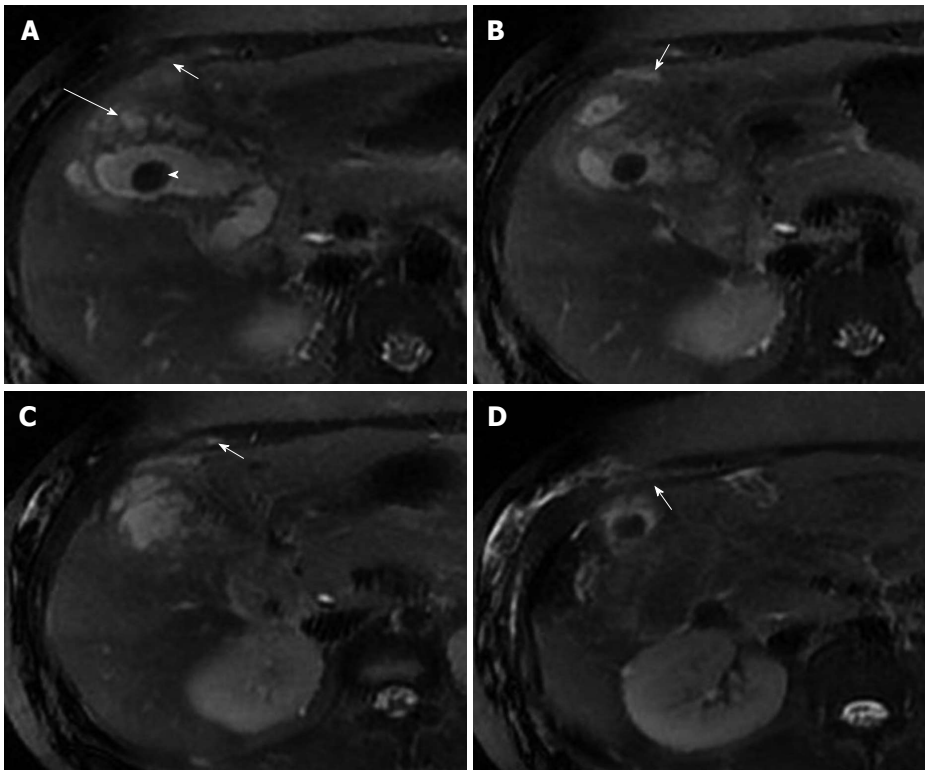

Figure 10 Axial sequential T2W magnetic resonance images (A-D) showing multiple hyper-intense intramural collections in gallbladder (long arrow) with extension of inflammatory process into the pericholecystic region, poor fat planes and involvement of the anterior abdominal wall (multiple short arrows). Note presence of intraluminal calculus (white arrowhead).

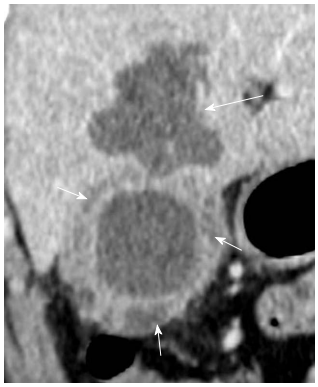

Figure 11 Coronal computed tomography section image showing multiple hypodense nodules (short arrows) in thickened gallbladder wall with an associated abscess in the adjoining liver (long arrow).

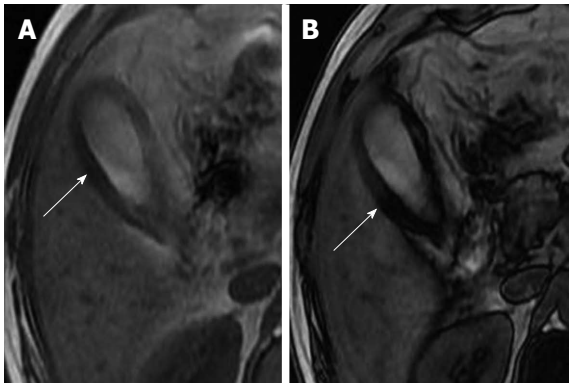

Figure 12 3.0 T magnetic resonance axial chemical shift imaging using in-phase (A) and out-phase sequences (B). Presence of intramural fat is markedly evident in the form of loss of signal from gallbladder wall on out of phase imaging (arrow) compared to in-phase image (arrow).

ma[13]. Also, the extent of carcinoma may be considerably overestimated or underestimated, especially since XGC is also known to form adhesions to other organs; features conventionally attributed to malignancies[9].

Magnetic resonance imaging

In-phase and opposed-phase chemical shift imaging is helpful in demonstrating fat within the thickened gallbladder wall in patients with XGC[26] (Figure 12). Zhao *et al*[21] subjected intramural nodules to chemical shift imaging. Seventy-seven point seven percent of XGC nodules showed reduced signal intensity on out-of-phase images. This variable nature of the intramural nodule on magnetic resonance imaging (MRI) can be attributed to the presence of diverse contents like foamy histiocytes, lymphocytes, plasma cells, polymorphonuclear leucocytes, fibrosis, giant cells, micro-abscess and necrosis within these nodules[22]. The researchers also observed that few nodules (2 out of 11) were detected only on CT and not seen on MRI and attributed this to a lower spatial resolution of MRI. Areas of iso- to slightly high signal intensity on T2-weighted images, showing slight enhancement at early phase and strong enhancement during delayed phase of dynamic study, corresponded with areas of abundant

Table 1 Summary of imaging findings of xanthogranulomatous cholecystitis

Findings
Diffuse or focal mural thickening
Luminal surface enhancement
Intramural fat
Hypodense/hypoechoic nodules or bands
Associations
Cholelithiasis
Choledocholithiasis
Gallbladder carcinoma
Complications
Gallbladder perforation
Abscesses
Adhesions and fistulas to liver, duodenum, gatric outlet, colon (hepatic flexure/transverse colon) and anterior abdominal wall

xanthogranulomas[24]. Areas with very high signal intensity on T2-weighted images without enhancement corresponded with necrosis and/or abscesses[24].

LSE of gallbladder wall represented preservation of the epithelial layer[24]. The early-enhanced areas of the liver bed on dynamic CT and MR images can be seen sometimes associated with XGC which correspond with accumulation of inflammatory cells and abundant fibrosis[24].

Kang *et al*[27] have revealed the benefit of diffusion-weighted magnetic resonance imaging (DWI) in differentiating XGC from the wall-thickening type of gallbladder cancer. Diffusion restriction was more frequently seen in gallbladder cancer (68%) than in XGC (7%). They also found out that the mean ADC value of XGC was higher than that of the wall-thickening type of gallbladder cancer with statistical significance (1.637×10^{-3} mm^2/s *vs* 1.076×10^{-3} mm^2/s respectively, $P = 0.005$)[27]. The authors concluded that the addition of DWI to conventional MRI improves discrimination between XGC and the wall-thickening type of gallbladder cancer.

Positron emission tomography

Sawada *et al*[28] have described positive uptake of XGC on ^{18}F-FDG positron emission tomography (PET) scan which again adds to the confusion. They have described the expression of GLUT1 and GLUT3 receptors in XGC to be the causative factor behind the false positive PET scan[28]. Radiological feature of XGC have been summarized in Table 1.

DIFFERENTIAL DIAGNOSIS

Adenomyomatosis

Gallbladder adenomyomatosis is a process of diffuse epithelial and smooth muscle proliferation likely in response to chronic gallbladder obstruction. Dilated Rokitansky-Aschoff sinuses contribute to formation of intramural diverticula that may contain bile, cholesterol, sludge or stones. Cholesterol crystals show characteristic reverberation or V-shaped comet tail artefacts on sonography. On T2-weighted MRI a characteristic "pearl necklace sign" is noted (Figure 13). Intramural foci of adenomyomatosis are often small and aligned in a linear fashion[29]. Presence of intramural nodules covering a large area of thickened gallbladder wall is specific for XGC[30]. Rate of complications is higher in XGC compared to adenomyomatosis. Inflammatory changes outside the gallbladder should raise suspicion of XGC over adenomyomatosis[31].

Carcinoma of gallbladder

Although accurate pre-operative differentiation of XGC from carcinoma purely on the basis of radiological and clinical features may be difficult, there are some pointers on imaging that have been found to be helpful. In a study done by Goshima *et al*[22], five CT findings showed significant difference between XGC and carcinoma of gallbladder. These findings were diffuse gallbladder wall thickening, continuous mucosal lining, intramural hypo-attenuating nodules in the thickened walls, absence of macroscopic hepatic invasion and absence of intrahepatic bile duct dilatation[22]. They reported that the diagnostic accuracy of XGC increases with the presence of three or more of the above mentioned findings. Besides, presence of regional lymphadenopathy is more prevalent in carcinoma compared to XGC. While 58.9% cases with gallbladder carcinoma had retroperitoneal lymph nodes enlargement, only 10.2% cases of XGC had mild lymph node enlargement (1-1.5 cm in diameter)[21].

Actinomycosis of the gallbladder

Actinomycosis of the gallbladder presenting as a mass with extensive infiltration into surrounding structures by sonography and CT is very difficult to differentiate from gallbladder carcinoma and XGC, as radiologic features overlap considerably[32]. In cases where a correct diagnosis is impossible, either close clinical and radiological follow up or imaging-guided aspiration or biopsy may be useful.

MANAGEMENT

Fine needle aspiration cytology (FNAC) plays an important role in making pre-operative differentiation between carcinoma and XGC or in co-existent lesions. Percutaneous as well as endoscopic needle biopsy can be done in patients suspicious of malignancy. In personal experience of the authors, approaching the lesion with a transhepatic route can minimise the risk of potential complications. The sensitivity of detecting malignancy is around 80% when adenocarcinoma is associated with XGC and overall sensitivity and specificity of detecting carcinoma is approximately 90% and 94% respectively[14].

Most gallbladder carcinomas associated with XGC occur in the GB neck region which is due to increased pressure within the gallbladder. Thus, careful observation of the GB neck and cystic duct region by endoscopic ultrasound (EUS) and adequate sampling from this region can greatly reduce the incidence of false negative

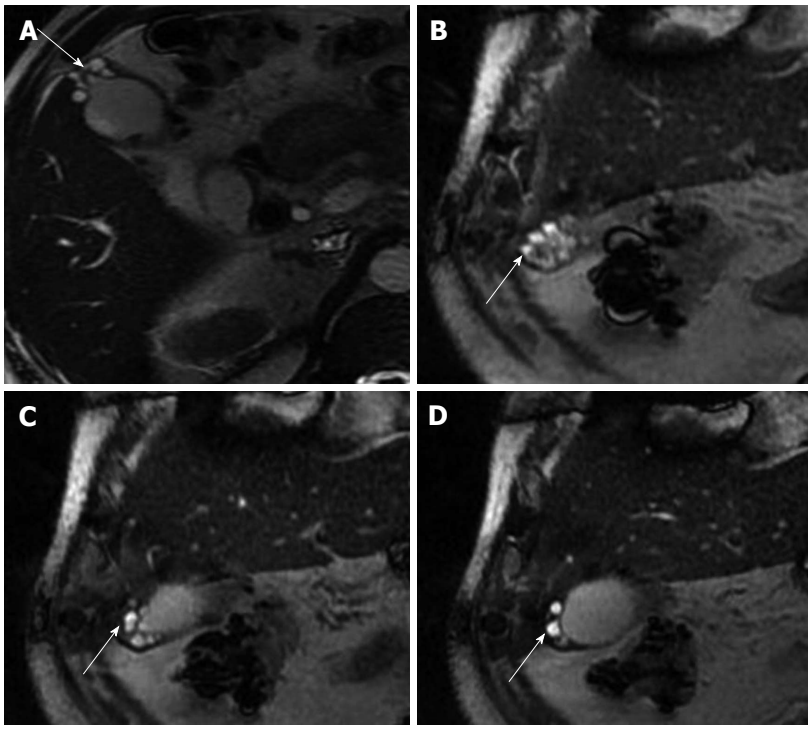

Figure 13 Axial (A) and coronal (B-D) T2W magnetic resonance images showing multiple curvilinearly arranged hyperintense intramural cavities (arrows) in gallbladder fundal region ("pearl necklace" appearance) - a characteristic feature of gallbladder adenomyomatosis.

diagnosis of co-existing gallbladder carcinomas. Hijioka *et al*[33] have reported an accuracy of 93.3% using EUS guided FNAC.

At operation,XGC may give appearance of an advanced gallbladder carcinoma due to wall thickening and local destructive spread of inflammation[12]. A carcinoma may be masked by the severe inflammation[12]. Intraoperative frozen section investigation or FNAC has been suggested to confirm the diagnosis. In cases with no invasion of adjacent organs these tools are indicated because they can change the surgical strategy (*e.g.*, simple cholecystectomy *vs* associated liver resection).

Complete resection of the gallbladder is not always possible especially due to poor visualization of the Calot's triangle. Prolonged operating time and technical difficulties are noted along with a high conversion rate (laparoscopic to open cholecystectomy) of upto 80%[34]. The complication rates may be as high as 20% and length of hospital stay is also generally longer[12].

CONCLUSION

XGC can be a diagnostic dilemma and a correct pre-operative diagnosis can be aided by awareness of characteristic findings on CT and MRI. In some cases diagnosing this entity only on imaging can be extremely challenging and FNAC may be helpful in pre-operative diagnosis.

REFERENCES

1 **Rammohan A**, Cherukuri SD, Sathyanesan J, Palaniappan R, Govindan M. Xanthogranulomatous cholecystitis masquerading as gallbladder cancer: can it be diagnosed preoperatively? *Gastroenterol Res Pract* 2014; **2014**: 253645 [PMID: 25404941 DOI: 10.1155/2014/253645]

2 **McCoy JJ**, Vila R, Petrossian G, McCall RA, Reddy KS. Xanthogranulomatous cholecystitis. Report of two cases. *J S C Med Assoc* 1976; **72**: 78-79 [PMID: 1063276]

3 **Christensen AH**, Ishak KG. Benign tumors and pseudotumors of the gallbladder. Report of 180 cases. *Arch Pathol* 1970; **90**: 423-432 [PMID: 4319984]

4 **Amazon K**, Rywlin AM. Ceroid granulomas of the gallbladder.*Am J ClinPathol* 1980; **73**: 123-127 [PMID: 7352416]

5 **Kim SH**, Kim HY, Jung SE, Park KW, Choi YH, Kim WS, Park SH. Xanthogranulomatous cholecystits in 2-month-old infant. *J Korean Surg Soc* 2013; **85**: 191-194 [PMID: 24106687 DOI: 10.4174/jkss.2013.85.4.191]

6 **Guzmán-Valdivia G**. Xanthogranulomatous cholecystitis in laparoscopic surgery. *J Gastrointest Surg* 2005; **9**: 494-497 [PMID: 15797229]

7 **Balagué C**, Targarona EM, Sugrañes G, Rey MJ, Arce Y, Viella P, Trias M. [Xanthogranulomatous cholecystitis simulating gallbladder neoplasm: therapeutic implications]. *Gastroenterol Hepatol* 1996; **19**: 503-506 [PMID: 9044748]

8 **Ros PR**, Goodman ZD. Xanthogranulomatous cholecystitis versus gallbladder carcinoma. *Radiology* 1997; **203**: 10-12 [PMID: 9122374]

9 **Roberts KM**, Parsons MA. Xanthogranulomatous cholecystitis: clinicopathological study of 13 cases. *J Clin Pathol* 1987; **40**: 412-417 [PMID: 3584484]

10 **Houston JP**, Collins MC, Cameron I, Reed MW, Parsons MA, Roberts KM. Xanthogranulomatous cholecystitis. *Br J Surg* 1994; **81**: 1030-1032 [PMID: 7922056]

11 **Yu H**, Yu TN, Cai XJ. Tumor biomarkers: help or mislead in the diagnosis of xanthogranulomatous cholecystitis?-analysis of serum CA 19-9, carcinoembryonic antigen, and CA 12-5. *Chin Med J* (Engl) 2013; **126**: 3044-3047 [PMID: 23981609]

12 **Srinivas GN**, Sinha S, Ryley N, Houghton PW. Perfidious gallbladders - a diagnostic dilemma with xanthogranulomatous cholecystitis. *Ann R Coll Surg Engl* 2007; **89**: 168-172 [PMID: 17346415]

13 **Krishnani N**, Shukla S, Jain M, Pandey R, Gupta RK. Fine needle aspiration cytology in xanthogranulomatous cholecystitis, gallbladder adenocarcinoma and coexistent lesions. *Acta Cytol* 2000; **44**: 508-514 [PMID: 10934941]

14 **Benbow EW**. Xanthogranulomatous cholecystitis associated with carcinoma of the gallbladder. *Postgrad Med J* 1989; **65**: 528-531 [PMID: 2690047]

15 **Kim PN**, Lee SH, Gong GY, Kim JG, Ha HK, Lee YJ, Lee MG, Auh YH. Xanthogranulomatous cholecystitis: radiologic findings with histologic correlation that focuses on intramural nodules. *AJR Am J Roentgenol* 1999; **172**: 949-953 [PMID: 10587127]

16 **Benbow EW**, Taylor PM. Simultaneous xanthogranulomatous cholecystitis and primary adenocarcinoma of gallbladder. *Histopathology* 1988; **12**: 672-675 [PMID: 3417248]

17 **Howard TJ**, Bennion RS, Thompson JE. Xanthogranulomatous cholecystitis: a chronic inflammatory pseudotumor of the gallbladder. *Am Surg* 1991; **57**: 821-824 [PMID: 1746802]

18 **Parra JA**, Acinas O, Bueno J, Güezmes A, Fernández MA, Fariñas MC. Xanthogranulomatous cholecystitis: clinical, sonographic, and CT findings in 26 patients. *AJR Am J Roentgenol* 2000; **174**: 979-983 [PMID: 10749233]

19 **Kim PN**, Ha HK, Kim YH, Lee MG, Kim MH, Auh YH. US findings of xanthogranulomatous cholecystitis. *Clin Radiol* 1998; **53**: 290-292 [PMID: 9585046]

20 **Casas D**, Pérez-Andrés R, Jiménez JA, Mariscal A, Cuadras P, Salas M, Gómez-Plaza MC. Xanthogranulomatous cholecystitis: a radiological study of 12 cases and a review of the literature. *Abdom Imaging* 1996; **21**: 456-460 [PMID: 8832871]

21 **Zhao F**, Lu PX, Yan SX, Wang GF, Yuan J, Zhang SZ, Wang YX. CT and MR features of xanthogranulomatous cholecystitis: an analysis of consecutive 49 cases. *Eur J Radiol* 2013; **82**: 1391-1397 [PMID: 23726123 DOI: 10.1016/j.ejrad.2013.04.026]

22 **Goshima S**, Chang S, Wang JH, Kanematsu M, Bae KT, Federle MP. Xanthogranulomatous cholecystitis: diagnostic performance of CT to differentiate from gallbladder cancer. *Eur J Radiol* 2010; **74**: e79-e83 [PMID: 19446416 DOI: 10.1016/j.ejrad.2009.04.017]

23 **Chun KA**, Ha HK, Yu ES, Shinn KS, Kim KW, Lee DH, Kang SW, Auh YH. Xanthogranulomatous cholecystitis: CT features with emphasis on differentiation from gallbladder carcinoma. *Radiology* 1997; **203**: 93-97 [PMID: 9122422]

24 **Shuto R**, Kiyosue H, Komatsu E, Matsumoto S, Kawano K, Kondo Y, Yokoyama S, Mori H. CT and MR imaging findings of xanthogranulomatous cholecystitis: correlation with pathologic findings. *Eur Radiol* 2004; **14**: 440-446 [PMID: 12904879]

25 **Goldar-Najafi A**, Khettry U. Xanthogranulomatous choledochitis: a previously undescribed mass lesion of the hepatobiliary and ampullary region. *Semin Liver Dis* 2003; **23**: 101-106 [PMID: 12616455]

26 **Hatakenaka M**, Adachi T, Matsuyama A, Mori M, Yoshikawa Y. Xanthogranulomatous cholecystitis: importance of chemical-shift gradient-echo MR imaging. *Eur Radiol* 2003; **13**: 2233-2235 [PMID: 12928971]

27 **Kang TW**, Kim SH, Park HJ, Lim S, Jang KM, Choi D, Lee SJ. Differentiating xanthogranulomatous cholecystitis from wall-thickening type of gallbladder cancer: added value of diffusion-weighted MRI. *Clin Radiol* 2013; **68**: 992-1001 [PMID: 23622795 DOI: 10.1016/j.crad.2013.03.022]

28 **Sawada S**, Shimada Y, Sekine S, Shibuya K, Yoshioka I, Matsui K, Okumura T, Yoshida T, Nagata T, Uotani H, Tsukada K. Expression of GLUT-1 and GLUT-3 in xanthogranulomatous cholecystitis induced a positive result on 18F-FDG PET: report of a case. *Int Surg* 2013; **98**: 372-378 [PMID: 24229026 DOI: 10.9738/INTSURG-D-13-00092.1]

29 **Yoshimitsu K**, Irie H, Aibe H, Tajima T, Nishie A, Asayama Y, Matake K, Yamaguchi K, Matsuura S, Honda H. Well-differentiated adenocarcinoma of the gallbladder with intratumoral cystic components due to abundant mucin production: a mimicker of adenomyomatosis. *Eur Radiol* 2005; **15**: 229-233 [PMID: 15662477]

30 **Shetty GS**, Abbey P, Prabhu SM, Narula MK, Anand R. Xanthogranulomatous cholecystitis: sonographic and CT features and differentiation from gallbladder carcinoma: a pictorial essay. *Jpn J Radiol* 2012; **30**: 480-485 [PMID: 22488612 DOI: 10.1007/s11604-012-0080-9]

31 **Cecava ND**, Andrews R. Case report of xanthogranulomatous cholecystitis, review of its sonographic and magnetic resonance findings, and distinction from other gallbladder pathology. *J Radiol Case Rep* 2011; **5**: 19-24 [PMID: 22470787 DOI: 10.3941/jrcr.v5i4.696]

32 **Lee YH**, Kim SH, Cho MY, Rhoe BS, Kim MS. Actinomycosis of the gallbladder mimicking carcinoma: a case report with US and CT findings. *Korean J Radiol* 2007; **8**: 169-172 [PMID: 17420635]

33 **Hijioka S**, Mekky MA, Bhatia V, Sawaki A, Mizuno N, Hara K, Hosoda W, Shimizu Y, Tamada K, Niwa Y, Yamao K. Can EUS-guided FNA distinguish between gallbladder cancer and xanthogranulomatous cholecystitis? *Gastrointest Endosc* 2010; **72**: 622-627 [PMID: 20630515 DOI: 10.1016/j.gie.2010.05.022]

34 **Guzmán-Valdivia G**. Xanthogranulomatous cholecystitis: 15 years' experience. *World J Surg* 2004; **28**: 254-257 [PMID: 14961199]

P- Reviewer: Cha SH, Lipar M **S- Editor**: Ji FF
L- Editor: A **E- Editor**: Liu SQ

World Journal of Radiology

Submit a Manuscript: http://www.wjgnet.com/esps/
Help Desk: http://www.wjgnet.com/esps/helpdesk.aspx
DOI: 10.4329/wjr.v8.i2.192

World J Radiol 2016 February 28; 8(2): 192-199
ISSN 1949-8470 (online)

ORIGINAL ARTICLE

Retrospective Cohort Study

Impaired swallowing mechanics of post radiation therapy head and neck cancer patients: A retrospective videofluoroscopic study

William G Pearson Jr, Alisa A Davidoff, Zachary M Smith, Dorothy E Adams, Susan E Langmore

William G Pearson Jr, Department of Cellular Biology and Anatomy, Medical College of Georgia at Georgia Regents University, Augusta, GA 30912, United States

William G Pearson Jr, Department of Otolaryngology, Medical College of Georgia at Georgia Regents University, Augusta, GA 30912, United States

Alisa A Davidoff, Zachary M Smith, Dorothy E Adams, Sargent College, Boston University, Boston, MA 02118, United States

Susan E Langmore, Department of Otolaryngology Head and Neck Surgery, Boston University School of Medicine, Boston, MA 02118, United States

Author contributions: All authors contributed to this study in accordance with the standard proposed by International Committee of Medical Journal Editors; Pearson WG Jr and Langmore SE designed the research study; Pearson WG Jr, Davidoff AA, Smith ZM and Adams DE performed the research; Pearson WG Jr analyzed the data and wrote the paper with input from all other authors.

Institutional review board statement: The study was reviewed and approved by the Boston University School of Medicine Institutional Review Board.

Informed consent statement: The Boston University School of Medicine Institutional Review Board approved a waiver of informed consent due to the use of existing clinical data collected in a manner that subjects cannot be identified, and the added risk of the invasion of privacy and possible compromise of confidentiality introduced by obtaining consent.

Conflict-of-interest statement: All the authors have no conflict of interest related to the manuscript.

Data sharing statement: Data were collected and analyzed under a research protocol approved by the Boston University School of Medicine Institutional Review Board that waived consent due to the added risk of the invasion of privacy and possible compromise of confidentiality introduced by obtaining consent. These data were first reported in the doctoral dissertation of William G Pearson, Jr., with the copyright belonging to the author.

Correspondence to: William G Pearson Jr, PhD, Assistant Professor of Cellular Biology and Anatomy, Medical College of Georgia at Georgia Regents University, 1120 15th Street, CB-1101, Augusta, GA 30912, United States. wpearson@gru.edu
Telephone: +1-706-7213811
Fax: +1-706-7216120

Received: July 31, 2015
Peer-review started: August 1, 2015
First decision: September 28, 2015
Revised: October 24, 2015
Accepted: December 18, 2015
Article in press: December 18, 2015
Published online: February 28, 2016

Abstract

AIM: To determine swallowing outcomes and hyolaryngeal mechanics associated with post radiation therapy head and neck cancer (rtHNC) patients using videofluoroscopic swallow studies.

METHODS: In this retrospective cohort study, video-

fluoroscopic images of rtHNC patients (n = 21) were compared with age and gender matched controls (n = 21). Penetration-aspiration of the bolus and bolus residue were measured as swallowing outcome variables. Timing and displacement measurements of the anterior and posterior muscular slings elevating the hyolaryngeal complex were acquired. Coordinate data of anatomical landmarks mapping the action of the anterior muscles (suprahyoid muscles) and posterior muscles (long pharyngeal muscles) were used to calculate the distance measurements, and slice numbers were used to calculate time intervals. Canonical variate analysis with post-hoc discriminant function analysis was performed on coordinate data to determine multivariate mechanics of swallowing associated with treatment. Pharyngeal constriction ratio (PCR) was also measured to determine if weak pharyngeal constriction is associated with post radiation therapy.

RESULTS: The rtHNC group was characterized by poor swallowing outcomes compared to the control group in regards to: Penetration-aspiration scale (P < 0.0001), normalized residue ratio scale (NRRS) for the valleculae (P = 0.002) and NRRS for the piriform sinuses (P = 0.003). Timing and distance measurements of the anterior muscular sling were not significantly different in the two groups, whereas for the PMS time of displacement was abbreviated (P = 0.002) and distance of excursion was reduced (P = 0.02) in the rtHNC group. A canonical variate analysis shows a significant reduction in pharyngeal mechanics in the rtHNC group (P < 0.0001). The PCR was significantly higher in the test group than the control group (P = 0.0001) indicating reduced efficiency in pharyngeal clearance.

CONCLUSION: Using videofluoroscopy, this study shows rtHNC patients have worse swallowing outcomes associated with reduced hyolaryngeal mechanics and pharyngeal constriction compared with controls.

Key words: Swallow mechanics; Post radiation; Head and neck cancer; Fluoroscopy; Anatomy

Core tip: Quality videofluoroscopic imaging of barium swallows is useful to determine swallowing outcomes for safe and efficient swallowing, conventional kinematics, and underlying functional anatomy associated with outcomes. This retrospective study of radiation therapy head and neck cancer (rtHNC) patients compared with age and gender matched controls and found that swallowing outcomes were significantly worse in rtHNC patients. Conventional kinematics indicated a reduction in laryngeal elevation. Computational analysis of swallowing mechanics using coordinate data of anatomical landmarks is here used to visualize impaired functional anatomy associated with poor outcomes in order to suggest particular targets for rehabilitation.

Pearson WG Jr, Davidoff AA, Smith ZM, Adams DE, Langmore SE. Impaired swallowing mechanics of post radiation therapy head and neck cancer patients: A retrospective videofluoroscopic study. *World J Radiol* 2016; 8(2): 192-199 Available from: URL: http://www.wjgnet.com/1949-8470/full/v8/i2/192.htm DOI: http://dx.doi.org/10.4329/wjr.v8.i2.192

INTRODUCTION

The oropharyngeal phase of swallowing is a complex physiological process involving the conversion of a respiratory conduit into an alimentary canal in less than one second. Videofluoroscopic swallowing studies, also known as modified barium swallows (MBS), are the standard instrumental tool for assessing oropharyngeal swallowing safety and efficiency. Swallowing safety is threatened when a bolus penetrates or is aspirated into the airway. The retention of a bolus in the valleculae or piriform sinuses is an indication of swallowing inefficiency. Reduced hyolaryngeal elevation is thought to underlie incomplete clearance of the bolus from the pharynx[1]. Residual bolus retained in pharyngeal spaces such as the piriform sinuses (residue) is predictive of aspiration[2]. Both outcomes are observed among post radiation therapy head and neck cancer (rtHNC) patients[3]. However, the underlying mechanics associated with these outcomes is poorly understood.

Recent anatomical and magnetic resonance imaging (MRI) studies have shown that two muscular slings elevate the hyolaryngeal complex to stretch open the upper esophageal sphincter in young healthy adults[4-6]. It is not known if altered function of one or both of these slings is associated with poor swallowing outcomes (penetration, aspiration, or residue). To determine if poor swallowing outcomes are associated with altered function of the two-sling mechanism, we compared kinematic and morphological data collected from MBS imaging of rtHNC patients with age and gender matched controls.

The hyolaryngeal complex is comprised of the hyoid bone, laryngeal cartilages, and associated structures including the cricopharyngeus muscle, which forms the upper esophageal sphincter. Two muscular slings elevate the hyolaryngeal complex in swallowing[5] (Figure 1). The suprahyoid muscles (mylohyoid, geniohyoid, stylohyoid, and digastric) form an anterior sling with proximal attachments to the mandible and cranial base and distal attachments to the body of the hyoid, which translates force to the larynx *via* the thyrohyoid membrane and likely assisted by the thyrohyoid muscle[4]. A posterior sling comprised of the long pharyngeal muscles (stylopharyngeus, palatopharyngeus and salpingopharyngeus) has superior attachments to the styloid process, auditory tube, and structures associated with the palate, and inferior attachments inserting primarily on the lateral pharyngeal wall and thyroid cartilage[7,8]. These muscular slings function to elevate the hyolaryngeal complex and

Table 1 Inter-rater reliability of each swallowing outcome and kinematic measurement as determined by intraclass correlation coefficients

	Intraclass correlation coefficient	Lower 95%CI limit	Upper 95%CI limit
Penetration-aspiration scale	0.87	0.75	0.93
Normalized residue ratio scale (valleculae)	0.93	0.85	0.97
Normalized residue ratio scale (piriform recess)	0.91	0.82	0.96
Anterior sling distance measurement	0.87	0.75	0.93
Posterior sling distance measurement	0.88	0.77	0.94
Anterior sling time measurement	0.88	0.74	0.95
Posterior sling time measurement	0.90	0.77	0.96
Pharyngeal constriction ratio	0.81	0.66	0.90

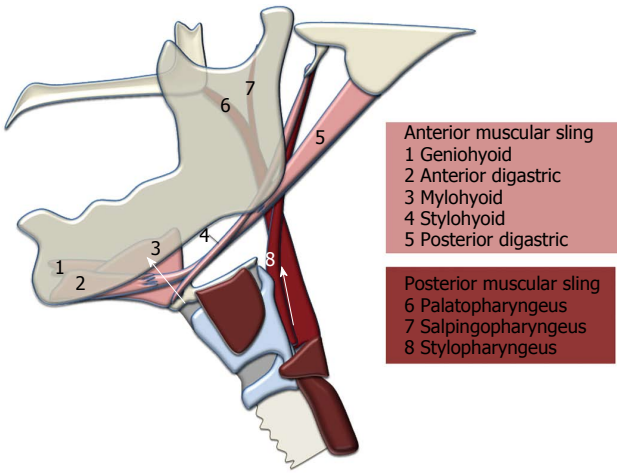

Figure 1 Two-sling mechanism for hyolaryngeal elevation in swallowing.

stretch open the upper esophageal sphincter, but it is unknown whether pathology changes the function of the two-sling mechanism.

High quality MBS imaging that is well collimated provides data useful for analyzing outcomes as well as the underlying mechanisms of swallowing[9]. In this study, outcome variables measuring penetration-aspiration and residue were used to verify differences between test and control groups[10], whereas kinematic measurements[11,12] and multivariate morphometric analysis[6] were used to determine which of the two slings described above is impaired. Additionally, the pharyngeal constriction ratio (PCR), a reliable surrogate for strength of pharyngeal constriction, was measured for each group to document the effect of treatment on the pharyngeal constrictor muscles and the long pharyngeal muscles[13]. We hypothesized that swallowing outcome variables, kinematic measurements, multivariate morphometric analysis, and PCR of the rtHNC group will indicate impairment when compared to the control group.

MATERIALS AND METHODS

Under a research protocol approved by the Boston University Medical Campus Institutional Review Board, a review of patient records was used to establish a test and control group. MBS imaging studies were recorded under routine radiographic protocols. An attempt was made to attach a radiopaque marker to each subject as an external scalar. Images were produced by a GE Precision Fluoroscopic unit and recorded digitally by a computer workstation at 30 frames/s. QuickTime™ software was used to trim each imaging study to include one episode of cued lateral view 5 mL swallows of thin liquid barium solution [Varibar Thin Liquid (40% wt/vol)].

Ninety-three patients with MBS studies were identified. Dysphagic patients related to rtHNC were placed in the test group (n = 28), while patients complaining of swallowing difficulty who showed no instrumental evidence of dysphagia were placed in the control group (n = 45). Of the 28 subjects in the rtHNC group, two lacked scalars and five could not be age or gender matched with the "normal" group. This left a final cohort of 21 subjects in each group composed of 14 males and 7 females with a mean age of 64 ± 13 years (test group) and 63 ± 11 years (control group).

Swallowing outcomes were collected along with spatial and temporal data from video files using ImageJ image analysis software equipped with QuickTime™ plug-ins (http://rsbweb.nih.gov/ij). Raters blinded to group assignment analyzed video files. Reliability was tested for all measurements by using a second judge to re-measure variables in 50% of MBS studies. Inter-rater reliability is reported in Table 1. In swallowing episodes requiring more than one swallow to clear the bolus, measurements were taken from the first swallow.

To measure penetration and aspiration we used a 1-8 ordinal scale called the penetration-aspiration scale (PAS)[14]. In the PAS scoring system 1-2 is considered functionally normal, 3-5 indicates bolus penetration into the laryngeal vestibule, and 6-8 indicates aspiration of the bolus into the airway. To quantify residue we used the normalized residue ratio scale (NRRS) for the valleculae and piriform sinuses[15]. The NRRS is a continuous measurement that incorporates the ratio of residue relative to pharyngeal space (valleculae and piriform sinuses) and the amount of residue scaled by an internal anatomical scalar (C2-C4 measurement described above). Differences in PAS in the two groups were evaluated using Mann-Whitney U tests, and differences in NRRS for the valleculae and piriform sinuses were compared using two-tailed t-tests with Bonferroni correction ($\alpha = 0.05$, $P < 0.025$).

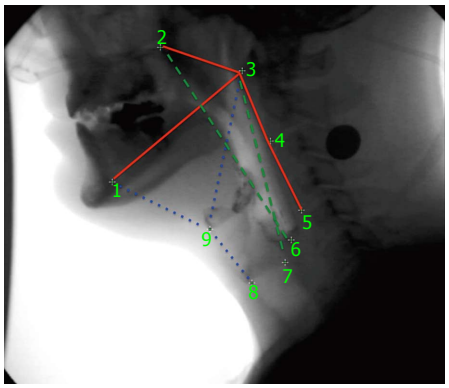

Figure 2 Pictured here are the nine coordinates mapping three skeletal levers (in red) and muscular slings displacing the hyolaryngeal complex with coordinates 1, 3, 8, 9 mapping the anterior muscular sling (in blue) and coordinates 2, 3, 6, 7 mapping the posterior muscular sling (in green).

Figure 3 Procrustes fit of coordinates adjusts for differences in rotation and scale.

Kinematic data collected from video files included duration and displacement measurements representing the anterior and posterior slings. The movement of the hyoid towards the mandible represented the action of the anterior muscular sling (AMS). The movement of the larynx towards the cranial base represented the action of the posterior muscular sling (PMS). Each AMS and PMS time and distance measurement was measured at minimum and maximum elevation. For the AMS, the minimum position was defined as one frame prior to the first rostral movement of the hyoid related to pharyngeal swallowing and maximum position was defined as the most rostral movement of the hyoid during swallowing. For the PMS, the minimum position was defined as one frame prior to the first rostral movement of the larynx during pharyngeal swallowing and maximum position was defined as the frame where the larynx reaches its superior position during swallowing.

Duration of AMS and PMS movement was determined by dividing the difference in minimum and maximum frame numbers by 30 (fps). Displacement of the hyoid (representing the action of the AMS) and elevation of the posteroinferior edge of the cricoid toward the cranial base (representing the action of the PMS) were calculated using a coordinate mapping technique designed to track the components of the two-sling mechanism of hyolaryngeal elevation[16] (Figure 2). Displacement measurements of the hyoid and larynx were mathematically calculated from coordinate data. Timing and spatial measurements were compared using two-tailed *t*-tests with Bonferroni correction ($\alpha = 0.05$, $P < 0.025$).

The nine coordinates mapping the elements of the anterior and PMSs in order to calculate kinematic variables were also used in a computational analysis of swallowing mechanics. The coordinate data set included nine coordinates for each subject at minimum and maximum excursion for the test group and control group. MorphoJ, software for geometric morphometric analysis, was used to perform a procrustes fit of all coordinates[17] (Figure 3). The procrustes fit resolved differences in scale and rotation between all subjects at both excursion points. Following the procrustes superimposition of coordinates, a canonical variate analysis was executed with classification variables assigned to each set of coordinates named by condition (test and control group) and excursion (minimum and maximum position of the hyolaryngeal complex).

To evaluate differences in pharyngeal constriction between test and control groups, the PCR was measured using the lateral view MBS studies[13]. PCR is a ratio of the area of the hypopharynx at maximum constriction to the area of the hypopharynx at rest. Significance of differences in PCR was determined using a two-tailed *t*-test.

RESULTS

All swallowing outcome variables indicated significantly worse swallowing in the rtHNC group than in the control group. PAS scores were highly significantly ($P < 0.0001$) greater in rtHNC (4.43 ± 2.42) than in the control (1.29 ± 0.56), NRRS scores for the valleculae were significantly ($P = 0.002$) greater in rtHNC (0.22 ± 0.20) than in the control (0.05 ± 0.11), and NRRS scores for the piriform sinuses were significantly ($P = 0.003$) greater in HNC (0.31 ± 0.36) than in the control (0.05 ± 0.14).

The duration of PMS elevating the larynx was significantly ($P = 0.002$) briefer in rtHNC (0.29 ± 0.11 s) than in the control (0.48 ± 0.23 s), and the displacement of the larynx by the posterior sling muscles is significantly ($P = 0.02$) reduced in rtHNC (0.89 ± 0.63 cm) than in the control (1.41 ± 0.73 cm). While these PMS measurements showed significant differences, the AMS measurements did not (Figure 4).

PCR was highly significantly ($P = 0.0001$) worse in rtHNC (0.16 ± 0.11) than in the control (0.05 ± 0.04).

The scatter plot of canonical variate scores with classification variable highlighted indicated that CV1 is associated with the excursion of the hyolaryngeal complex and CV2 is associated the test and control groups (Figure 5). Swallowing mechanics indicated by differences in shape change was highly significantly (*P*

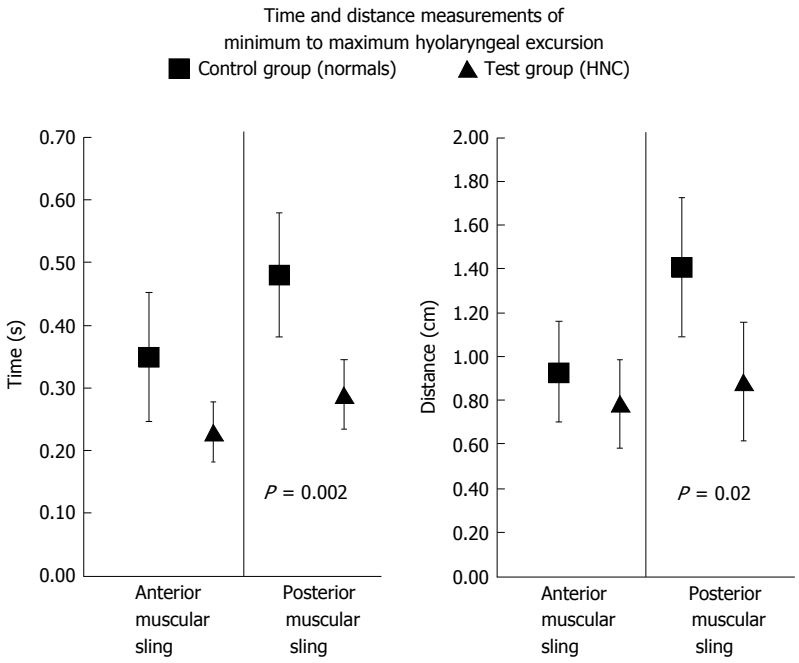

Figure 4 Significant differences between control and test groups. HNC: Head and neck cancer.

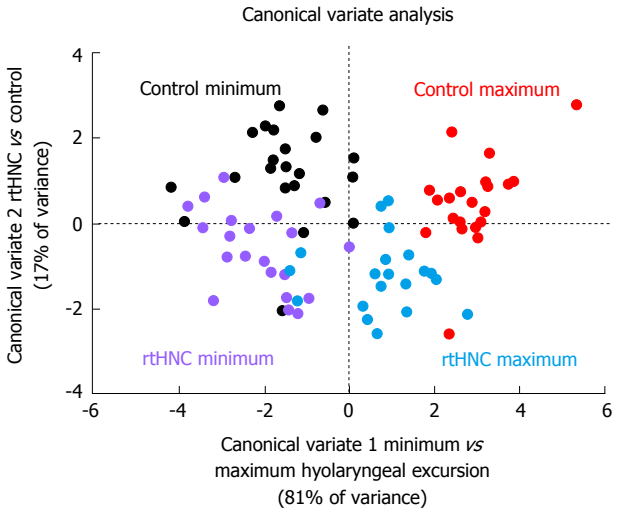

Figure 5 Canonical variate analysis showing differences in coordinate configuration plotted by canonical variate scores with classification variables highlighted. rtHNC: Radiation therapy head and neck cancer.

< 0.0001) reduced in the rtHNC (D = 2.98) than in the control (D = 4.54). Eigenvectors for each coordinate demonstrate the direction and degree of covariant shape change of the control (Figure 6) and test (Figure 7) groups for visual comparison.

DISCUSSION

This study shows significant differences in swallowing safety and efficiency as measured by PAS and NRRS, respectively. Kinematic measurements showed that reduced function of the PMS which elevates the hyolaryngeal complex is associated with rtHNC. In contrast, the anterior sling was not significantly reduced in the test group. Finally, a computational analysis of swallowing mechanics confirms that the long pharyngeal muscles are implicated in this cohort of dysphagic patients, and that extending the head and neck while swallowing is presumably attempted to compensate for loss of pharyngeal function.

Swallowing outcomes

Poor swallowing outcomes among rtHNC patients, including increased penetration-aspiration and residue, are consistent with other findings in the literature[18,19]. However, this is the first time that the NRRS has been used to quantify residue in head and neck cancer patients. These findings confirm that the test and control groups used here are appropriate for a retrospective pseudo-experimental design for investigating underlying mechanisms of dysphagia, specifically focusing on the role of the two-sling mechanism of hyolaryngeal elevation.

Kinematic measurements

Reduced hyolaryngeal elevation and hyoid movement has been noted among rtHNC patients[20,21], and reduced hyoid and laryngeal motility have also been associated with penetration-aspiration[10,22]. Association of the structures that underlie laryngeal elevation with poor swallowing outcomes has not been reported. Our data indicate a significantly diminished function of the PMS among rtHNC patients in both time and distance measurements with a large effect size changes for both timing and distance measurements (Cohen's D = 1.46 for timing and 0.77 for distance). This is consistent with findings in the radiation oncology literature that the longitudinal PMS presumed to lie within the pharyngeal constrictor region of interest in computed tomography

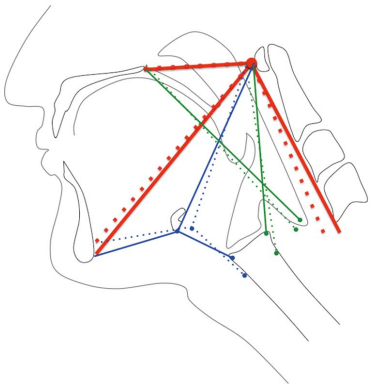

Figure 6 Eigenvectors indicating mechanics of hyolaryngeal elevation of the control group from minimum (dotted lines) to maximum (solid lines) excursion.

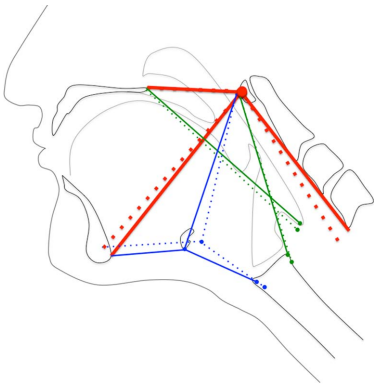

Figure 7 Eigenvectors indicating mechanics of hyolaryngeal elevation of the radiation therapy head and neck cancer group from minimum (dotted lines) to maximum (solid lines) excursion.

scans are more important than the anterior sling of muscles to swallowing function[18,23]. However, other published studies of rtHNC patients showed decreased hyoid displacement[20]. While our results do not reach statistical significance, timing and distance measurements of the hyoid was reduced when compared to the test group. The cohort did show a significant though small effect size change with Cohen's D = 0.30 for distance and a medium effect size change for timing with Cohen's D = 0.48. With these additional statistics, what can be said is that impairment of the posterior sling is much greater than the anterior sling in this cohort. The consensus in the literature is that the suprahyoid muscles (AMS) along with the thyrohyoid elevate the hyolaryngeal complex[24-26]. However, the results of this study indicate that the PMS appears to have a more significant role in swallowing dysfunction in rtHNC patients. Previous studies have not consistently taken into account the two-sling mechanism of hyolaryngeal elevation.

It is important to note that we did not include hyolaryngeal approximation, the movement of the anterior aspect of the larynx towards the hyoid bone, in this study. This movement is thought to be the unique function of the thyrohyoid muscle[27]. However, in a cohort of young healthy subjects the thyrohyoid was not found to be consistently active[4]. It has also been shown that the stylopharyngeus attaches to the larynx and elevates the thyroid cartilage toward the hyoid bone[5,28]. Conversely, it could be argued that the thyrohyoid (if active) assists the approximation of the posterior larynx towards the cranial base, which would in turn confound our PMS measurement. However, data show that the long pharyngeal muscles have a significantly greater mechanical advantage than the thyrohyoid in elevating the larynx[5].

Computational analysis of multivariate swallowing mechanics

Deglutition is a dynamic process of interrelated structures that covary in function, a fact that complicates univariate kinematic studies of swallowing. For example, the thyrohyoid membrane connects the hyoid and larynx and translates force to the larynx. A simple distance measurement cannot determine if the anterior sling muscles or the posterior sling muscles underlie elevation of the larynx. We propose a more informative approach using vectors to characterize how various elements interact as an integrated apparatus. In this present study we introduce a computational analysis of swallowing mechanics using a multivariate morphometric analysis of coordinates that map the two muscular slings elevating the hyoid, and the movement of the cranial base, mandible, and vertebrae as three skeletal levers from which the swallowing apparatus is suspended. Here we use a multivariate morphometric analysis of these coordinates to visualize vectors representing underlying muscle groups displacing the hyolaryngeal complex.

Canonical variate analysis of landmark coordinates showed overall shape changes judged on the basis of the Mahalanobis distance statistic (D-score). The Mahalanobis distance, also referred to as a generalized distance, is a dimensionless quantity that indicates how the covariance of one set of variables (in this study, a set of 9 coordinates) differs from the mean. A smaller D-score is interpreted as less overall shape change to the swallowing apparatus as mapped by 9 coordinates. As predicted, mean D-scores of the control group at maximum excursion were greater than the test group.

More interesting than the overall shape change scores are the eigenvector plots for each group (Figures 6 and 7). By comparing vectors of control and test groups it can be observed that there are small differences in the covariant distance of hyoid movement or pharyngeal shortening. The large differences are associated with laryngeal elevation and extension of the head and neck in the test group. This observation suggests that subjects with reduced hyolaryngeal elevation may attempt to compensate by hyperextending the neck. More importantly, the vectors show that the long pharyngeal muscles, not the suprahyoid muscles, underlie this impairment. This visual analysis indicates that the long pharyngeal muscles are primary targets for rehabilitation[29]. These kinds of multivariate observations of an interrelated dynamic system are not

possible using kinematic variables alone.

Relative importance of pharyngeal constriction

While this study demonstrates that the two-sling mechanism is important to hyolaryngeal elevation, we cannot say that reduced function of the two-sling mechanism is solely responsible for the poor swallowing outcomes. It is also possible that the functional difference between the groups could be explained by the significantly different degrees of pharyngeal constriction as measured by the PCR between the test and control groups (P = 0.0001). A higher PCR indicates weaker pharyngeal constriction[13]. A Spearman rank-order correlation of PCR with the PAS for the entire sample was r = 0.74, whereas distance measurements of the PMS correlated with PAS was r = -0.42, suggesting that poor swallowing outcomes in rtHNC patients are more strongly correlated with PCR than with PMS function. A recent study shows the correlation between PCR and residue as measured by NRRS[30]. However, it is likely that a reduced function of the posterior sling contributes to higher PCR. Leonard *et al*[31] have suggested that reduced hyolaryngeal approximation, a function that can be related to the PMS, is associated with weaker pharyngeal constriction.

It remains unclear how to best characterize differences in the two-sling mechanism associated with disordered swallowing. While diminished PMS function is indicated by kinematic measurements, eigenvectors of coordinates also demonstrate differences in the skeletal elements of the two-sling mechanism (Figures 6 and 7). Computational analysis of swallowing is currently being developed to include tongue base retraction and pharyngeal wall movement to provide a comprehensive approach to determining swallowing mechanics underlying effective and disordered swallowing. Registration of soft tissue landmarks is a confounding factor in this development.

In conclusion, this study demonstrates significant differences in swallowing outcomes between rtHNC patients and "normal" controls. We demonstrate reduced laryngeal elevation kinematics attributable to deficits in the PMS in the rtHNC group compared to the control group. Furthermore, multivariate computational analysis of swallowing reveals functional differences in the two-sling mechanism associated with pathology including different positioning of skeletal levers in addition to reduced laryngeal elevation. Whether the shape changes in the test group represent compensatory or maladaptive behaviors remains unclear. While videofluoroscopic imaging has been in use for some time, the investigative and diagnostic power of this modality is likely underutilized.

COMMENTS

Background

Dysphagia is a comorbidity head and neck cancer radiation treatment and presents a serious quality of life issue. The most important consideration for patients receiving radiation treatment second to cancer remission is swallowing function. Radiation damage to tissues can reduce salivary flow, and fibrosis impacts swallowing mechanics. Swallowing exercises have been shown to help mitigate the impact of fibrosis, and targeted treatment is thought to improve swallowing safety and facilitate patient compliance. A thorough understanding of swallowing mechanics associated with impairment enables clinicians to provide effective dysphagia management. In this paper multiple methods were used to document the impact of head and neck cancer treatment on swallowing safety, efficiency, and mechanics.

Research frontiers

Modified barium swallows (MBS) studies are the diagnostic standard for dysphagia. These imaging studies are often underutilized to merely establish penetration-aspiration status. However, this singular assessment does not provide useful information to clinicians managing swallowing rehabilitation. Many methods have been developed to address this problem. Analytical tools applied to high quality imaging are essential to achieve better outcomes for patients.

Innovations and breakthroughs

Kinematic methods that document timing and movement of swallowing structures have been in use in research for some time and are now clinically accessible. In recent years the MBS impairment profile was developed allowing for a standardized, reliable and valid approach for the clinical assessment of swallowing physiology. In this paper coordinate mapping of muscle functional groups underlying oropharyngeal swallowing, coordinates are reliably collected using digital analysis tools such as ImageJ. These coordinates are used to calculate displacement measurements and for multivariate morphometric analysis using computational tools such as MorphoJ.

Applications

Computational analysis of swallowing mechanics allows for visualization of impaired functional anatomy of swallowing and can guide rehabilitation efforts along with other useful measurements. Future directions include patient specific analysis to guide dysphagia management.

Terminology

Computational analysis of swallowing mechanics is a multivariate morphometric analysis of coordinates mapping the functional anatomy of swallowing and swallowing impairment using MBS imaging.

Peer-review

This is a very good manuscript studying the effects of radiotherapy in the swallowing mechanism of patients. The method used, the evaluation of data and the presentation is excellent (very instructive figures, extensive statistics, *etc.*).

REFERENCES

1 **Kahrilas PJ**, Logemann JA, Lin S, Ergun GA. Pharyngeal clearance during swallowing: a combined manometric and videofluoroscopic study. *Gastroenterology* 1992; **103**: 128-136 [PMID: 1612322]

2 **Eisenhuber E**, Schima W, Schober E, Pokieser P, Stadler A, Scharitzer M, Oschatz E. Videofluoroscopic assessment of patients with dysphagia: pharyngeal retention is a predictive factor for aspiration. *AJR Am J Roentgenol* 2002; **178**: 393-398 [PMID: 11804901 DOI: 10.2214/ajr.178.2.1780393]

3 **Langmore SE**, Krisciunas GP. Dysphagia After Radiotherapy for Head and Neck Cancer: Etiology, Clinical Presentation, and Efficacy of Current Treatments. *Perspectives on Swallowing and Swallowing Disorders* (Dysphagia) 2010; **19**: 32-38

4 **Pearson WG**, Hindson DF, Langmore SE, Zumwalt AC. Evaluating swallowing muscles essential for hyolaryngeal elevation by using muscle functional magnetic resonance imaging. *Int J Radiat Oncol Biol Phys* 2013; **85**: 735-740 [PMID: 22995662 DOI: 10.1016/j.ijrobp.2012.07.2370]

5 **Pearson WG**, Langmore SE, Yu LB, Zumwalt AC. Structural analysis of muscles elevating the hyolaryngeal complex. *Dysphagia* 2012; **27**: 445-451 [PMID: 22278076 DOI: 10.1007/s00455-011-9392-7]

6 **Pearson WG Jr**, Zumwalt AC. Visualizing Hyolaryngeal Mechanics in Swallowing Using Dynamic MRI. *Comput Methods Biomech Biomed Eng Imaging Vis* 2013 [PMID: 25090608 DOI: 10.1080/21681163.2013.846231]

7 **Okuda S**, Abe S, Kim HJ, Agematsu H, Mitarashi S, Tamatsu Y, Ide Y. Morphologic characteristics of palatopharyngeal muscle. *Dysphagia* 2008; **23**: 258-266 [PMID: 18568287 DOI: 10.1007/s00455-007-9133-0]

8 **Choi DY**, Bae JH, Youn KH, Kim HJ, Hu KS. Anatomical considerations of the longitudinal pharyngeal muscles in relation to their function on the internal surface of pharynx. *Dysphagia* 2014; **29**: 722-730 [PMID: 25142243 DOI: 10.1007/s00455-014-9568-z]

9 **Jaffer NM**, Ng E, Au FW, Steele CM. Fluoroscopic evaluation of oropharyngeal dysphagia: anatomic, technical, and common etiologic factors. *AJR Am J Roentgenol* 2015; **204**: 49-58 [PMID: 25539237 DOI: 10.2214/AJR.13.12374]

10 **Steele CM**, Bailey GL, Chau T, Molfenter SM, Oshalla M, Waito AA, Zoratto DC. The relationship between hyoid and laryngeal displacement and swallowing impairment. *Clin Otolaryngol* 2011; **36**: 30-36 [PMID: 21414151 DOI: 10.1111/j.1749-4486.2010.02219.x]

11 **Kendall KA**, McKenzie S, Leonard RJ, Gonçalves MI, Walker A. Timing of events in normal swallowing: a videofluoroscopic study. *Dysphagia* 2000; **15**: 74-83 [PMID: 10758189 DOI: 10.1007/s004550010004]

12 **Leonard RJ**, Kendall KA, McKenzie S, Gonçalves MI, Walker A. Structural displacements in normal swallowing: a videofluoroscopic study. *Dysphagia* 2000; **15**: 146-152 [PMID: 10839828 DOI: 10.1007/s004550010017]

13 **Leonard R**, Rees CJ, Belafsky P, Allen J. Fluoroscopic surrogate for pharyngeal strength: the pharyngeal constriction ratio (PCR). *Dysphagia* 2011; **26**: 13-17 [PMID: 19856026 DOI: 10.1007/s00455-009-9258-4]

14 **Rosenbek JC**, Robbins JA, Roecker EB, Coyle JL, Wood JL. A penetration-aspiration scale. *Dysphagia* 1996; **11**: 93-98 [PMID: 8721066 DOI: 10.1007/BF00417897]

15 **Pearson WG**, Molfenter SM, Smith ZM, Steele CM. Image-based measurement of post-swallow residue: the normalized residue ratio scale. *Dysphagia* 2013; **28**: 167-177 [PMID: 23089830 DOI: 10.1007/s00455-012-9426-9]

16 **Thompson TZ**, Obeidin F, Davidoff AA, Hightower CL, Johnson CZ, Rice SL, Sokolove RL, Taylor BK, Tuck JM, Pearson WG. Coordinate mapping of hyolaryngeal mechanics in swallowing. *J Vis Exp* 2014; (**87**) [PMID: 24836901]

17 **Klingenberg CP**. MorphoJ: an integrated software package for geometric morphometrics. *Mol Ecol Resour* 2011; **11**: 353-357 [PMID: 21429143 DOI: 10.1111/j.1755-0998.2010.02924.x]

18 **Feng FY**, Kim HM, Lyden TH, Haxer MJ, Feng M, Worden FP, Chepeha DB, Eisbruch A. Intensity-modulated radiotherapy of head and neck cancer aiming to reduce dysphagia: early dose-effect relationships for the swallowing structures. *Int J Radiat Oncol Biol Phys* 2007; **68**: 1289-1298 [PMID: 17560051 DOI: 10.1016/j.ijrobp.2007.02.049]

19 **Gillespie MB**, Brodsky MB, Day TA, Lee FS, Martin-Harris B. Swallowing-related quality of life after head and neck cancer treatment. *Laryngoscope* 2004; **114**: 1362-1367 [PMID: 15280708 DOI: 10.1097/00005537-200408000-00008]

20 **Kendall KA**, McKenzie SW, Leonard RJ, Jones C. Structural mobility in deglutition after single modality treatment of head and neck carcinomas with radiotherapy. *Head Neck* 1998; **20**: 720-725 [PMID: 9790294]

21 **Pauloski BR**, Rademaker AW, Logemann JA, Newman L, MacCracken E, Gaziano J, Stachowiak L. Relationship between swallow motility disorders on videofluorography and oral intake in patients treated for head and neck cancer with radiotherapy with or without chemotherapy. *Head Neck* 2006; **28**: 1069-1076 [PMID: 16823874 DOI: 10.1002/hed.20459]

22 **Bingjie L**, Tong Z, Xinting S, Jianmin X, Guijun J. Quantitative videofluoroscopic analysis of penetration-aspiration in post-stroke patients. *Neurol India* 2010; **58**: 42-47 [PMID: 20228462 DOI: 10.4103/0028-3886.60395]

23 **Eisbruch A**, Schwartz M, Rasch C, Vineberg K, Damen E, Van As CJ, Marsh R, Pameijer FA, Balm AJ. Dysphagia and aspiration after chemoradiotherapy for head-and-neck cancer: which anatomic structures are affected and can they be spared by IMRT? *Int J Radiat Oncol Biol Phys* 2004; **60**: 1425-1439 [PMID: 15590174 DOI: 10.1016/j.ijrobp.2004.05.050]

24 **Cook IJ**, Dodds WJ, Dantas RO, Massey B, Kern MK, Lang IM, Brasseur JG, Hogan WJ. Opening mechanisms of the human upper esophageal sphincter. *Am J Physiol* 1989; **257**: G748-G759 [PMID: 2596608]

25 **Matsuo K**, Palmer JB. Anatomy and physiology of feeding and swallowing: normal and abnormal. *Phys Med Rehabil Clin N Am* 2008; **19**: 691-707, vii [PMID: 18940636 DOI: 10.1016/j.pmr.2008.06.001]

26 **Shaw SM**, Martino R. The normal swallow: muscular and neurophysiological control. *Otolaryngol Clin North Am* 2013; **46**: 937-956 [PMID: 24262952 DOI: 10.1016/j.otc.2013.09.006]

27 **Mepani R**, Antonik S, Massey B, Kern M, Logemann J, Pauloski B, Rademaker A, Easterling C, Shaker R. Augmentation of deglutitive thyrohyoid muscle shortening by the Shaker Exercise. *Dysphagia* 2009; **24**: 26-31 [PMID: 18685891 DOI: 10.1007/s00455-008-9167-y]

28 **Meng H**, Murakami G, Suzuki D, Miyamoto S. Anatomical variations in stylopharyngeus muscle insertions suggest inter-individual and left/right differences in pharyngeal clearance function of elderly patients: a cadaveric study. *Dysphagia* 2008; **23**: 251-257 [PMID: 18427898 DOI: 10.1007/s00455-007-9131-2]

29 **Miloro KV**, Pearson WG, Langmore SE. Effortful pitch glide: a potential new exercise evaluated by dynamic MRI. *J Speech Lang Hear Res* 2014; **57**: 1243-1250 [PMID: 24686494 DOI: 10.1044/2014_JSLHR-S-13-0168]

30 **Stokely SL**, Peladeau-Pigeon M, Leigh C, Molfenter SM, Steele CM. The Relationship Between Pharyngeal Constriction and Post-swallow Residue. *Dysphagia* 2015; **30**: 349-356 [PMID: 25920993 DOI: 10.1007/s00455-015-9606-5]

31 **Leonard R**, Kendall KA, McKenzie S. Structural displacements affecting pharyngeal constriction in nondysphagic elderly and nonelderly adults. *Dysphagia* 2004; **19**: 133-141 [PMID: 15382802 DOI: 10.1007/s00455-003-0508-6]

P- Reviewer: Gao BL, Tsalafoutas IA **S- Editor**: Song XX
L- Editor: A **E- Editor**: Liu SQ

World Journal of Radiology

Submit a Manuscript: http://www.wjgnet.com/esps/
Help Desk: http://www.wjgnet.com/esps/helpdesk.aspx
DOI: 10.4329/wjr.v8.i2.200

World J Radiol 2016 February 28; 8(2): 200-209
ISSN 1949-8470 (online)

ORIGINAL ARTICLE

Observational Study

Comparisons between glucose analogue 2-deoxy-2-(^{18}F)fluoro-D-glucose and ^{18}F-sodium fluoride positron emission tomography/computed tomography in breast cancer patients with bone lesions

Selene Capitanio, Francesca Bongioanni, Arnoldo Piccardo, Claudio Campus, Roberta Gonella, Lucia Tixi, Mehrdad Naseri, Michele Pennone, Vania Altrinetti, Ambra Buschiazzo, Irene Bossert, Francesco Fiz, Andrea Bruno, Andrea DeCensi, Gianmario Sambuceti, Silvia Morbelli

Selene Capitanio, Andrea Bruno, Department of Nuclear Medicine, A.O. Papa Giovanni XXIII, 24127 Bergamo, Italy

Francesca Bongioanni, Michele Pennone, Ambra Buschiazzo, Irene Bossert, Francesco Fiz, Gianmario Sambuceti, Silvia Morbelli, Nuclear Medicine, IRCCS AOU San Martino-IST, Department of Health Sciences, University of Genoa, 16132 Genoa, Italy

Arnoldo Piccardo, Mehrdad Naseri, Vania Altrinetti, Department of Nuclear Medicine, E.O. Ospedali Galliera, 16128 Genoa, Italy

Andrea DeCensi, Department of Medical Oncology, E.O. Ospedali Galliera, 16128 Genoa, Italy

Claudio Campus, Istituto Italiano di Tecnologia, 16163 Genoa, Italy

Roberta Gonella, Lucia Tixi, Dipartimento di Terapie Oncologiche Integrate, Clinica di Medicina Interna a indirizzo oncologico, 16132 Genoa, Italy

Author contributions: Capitanio S performed the literature search and drafted the manuscript; Bongioanni F, Naseri M, Pennone M, Altrinetti V, Buschiazzo A, Bossert I and Fiz F collected the data and took care of patients during diagnostic exams; Campus C performed the statistical analysis; Gonella R, Tixi L and DeCensi A took care of patients during follow-up; Piccardo A, Bruno A, DeCensi A, Sambuceti G, and Morbelli S made critical revisions to the manuscript relating to important intellectual content; Morbelli S designed the study and gave final approval for the version of the article to be published; all authors read and approved the final manuscript.

Institutional review board statement: The Internal Review Board (Comitato Etico Regionale della Liguria) evaluated and approved this retrospective study.

Informed consent statement: All study participants, or their legal guardians, provided informed written consent prior to study enrollment. We did not report any details that might disclose the identity of the subjects under study.

Conflict-of-interest statement: The authors have no conflicts of interest to declare.

Data sharing statement: No additional data are available.

Correspondence to: Silvia Morbelli, Full Staff Nuclear Medicine Physician, Nuclear Medicine, IRCCS AOU San Martino-IST, Department of Health Sciences, University of Genoa, L.go R. Benzi 10, 16132 Genova, Italy. silviadaniela.morbelli@hsanmartino.it
Telephone: +39-010-5552025
Fax: +39-010-5556911

Received: May 28, 2015
Peer-review started: May 31, 2015
First decision: September 18, 2015
Revised: October 23, 2015
Accepted: December 9, 2015

Article in press: December 11, 2015
Published online: February 28, 2016

Abstract

AIM: To compare 2-deoxy-2-(^{18}F)fluoro-D-glucose(^{18}F-FDG) and ^{18}F-sodium (^{18}F-NaF) positron emission tomography/computed tomography (PET/CT) accuracy in breast cancer patients with clinically/radiologically suspected or known bone metastases.

METHODS: A total of 45 consecutive patients with breast cancer and the presence or clinical/biochemical or radiological suspicion of bone metastatic disease underwent ^{18}F-FDG and ^{18}F-fluoride PET/CT. Imaging results were compared with histopathology when available, or clinical and radiological follow-up of at least 1 year. For each technique we calculated: Sensitivity (Se), specificity (Sp), overall accuracy, positive and negative predictive values, error rate, and Youden's index. McNemar's χ^2 test was used to test the difference in sensitivity and specificity between the two diagnostic methods. All analyses were computed on a patient basis, and then on a lesion basis, with consideration ofthe density of independent lesions on the co-registered CT (sclerotic, lytic, mixed, no-lesions) and the divergent site of disease (skull, spine, ribs, extremities, pelvis). The impact of adding ^{18}F-NaF PET/CT to the work-up of patients was also measured in terms of change in their management due to ^{18}F-NaF PET/CT findings.

RESULTS: The two imaging methods of ^{18}F-FDG and ^{18}F-fluoride PET/CT were significantly different at the patient-based analysis: Accuracy was 86.7% and 84.4%, respectively (McNemar's χ^2 = 6.23, df = 1, P = 0.01). Overall, 244 bone lesions were detected in our analysis. The overall accuracy of the two methods was significantly different at lesion-based analysis (McNemar's χ^2 = 93.4, df = 1, P < 0.0001). In the lesion density-based and site-based analysis, ^{18}F-FDG PET/CT provided more accurate results in the detection of CT-negative metastasis (P < 0.002) and vertebral localizations (P < 0.002); ^{18}F-NaF PET/CT was more accurate in detecting sclerotic (P < 0.005) and rib lesions (P < 0.04). ^{18}F-NaF PET/CT led to a change of management in 3 of the 45 patients (6.6%) by revealing findings that were not detected at ^{18}F-FDG PET/CT.

CONCLUSION: ^{18}F-FDG PET/CT is a reliable imaging tool in the detection of bone metastasis in most cases, with a diagnostic accuracy that is slightly, but significantly, superior to that of ^{18}F-NaF PET/CT in the general population of breast cancer patients. However, the extremely high sensitivity of ^{18}F-fluoride PET/CT can exploit its diagnostic potential in specific clinical settings (*i.e.*, small CT-evident sclerotic lesions, high clinical suspicious of relapse, and negative ^{18}F-FDG PET and conventional imaging).

Key words: ^{18}F-sodium positron emission tomography/computed tomography; Breast cancer; Bone lesion; 2-deoxy-2-(^{18}F)fluoro-D-glucose

Core tip: ^{18}F-fluorodeoxyglucose (^{18}F-FDG) and ^{18}F-sodium positron (^{18}F-NaF) positron emission tomography/computed tomography (PET/CT) is undoubtedly an accurate and validated imaging tool in the general population of breast cancer patients for the detection of bone metastasis in most cases. However, thanks to its extremely high sensitivity, ^{18}F-NaF PET/CT could have an adjunctive value in selected patients, significantly impacting their management (*i.e.*, small CT-evident sclerotic lesions, high clinical suspicious of relapse, and negative ^{18}F-FDG PET and conventional imaging). This sensitivity might be particularly relevant for patients who are candidates for surgery or radiotherapy.

Capitanio S, Bongioanni F, Piccardo A, Campus C, Gonella R, Tixi L, Naseri M, Pennone M, Altrinetti V, Buschiazzo A, Bossert I, Fiz F, Bruno A, DeCensi A, Sambuceti G, Morbelli S. Comparisons between glucose analogue 2-deoxy-2-(^{18}F)fluoro-D-glucose and ^{18}F-sodium fluoride positron emission tomography/computed tomography in breast cancer patients with bone lesions. *World J Radiol* 2016; 8(2): 200-209 Available from: URL: http://www.wjgnet.com/1949-8470/full/v8/i2/200.htm DOI: http://dx.doi.org/10.4329/wjr.v8.i2.200

INTRODUCTION

Breast cancer is the most prevalent form of cancer in women of Western countries[1-3], with the skeleton being the most common site of distant metastases. Presence, distribution, and type of bone localizations have relevant prognostic implications[4,5]. In particular, with the growing availability of new therapeutic strategies which could potentially improve survival, the early detection of bone metastases has gained pivotal importance[6,7].

Conventional bone scintigraphy (BS) remains the most suitable technique for whole-body screening of bone metastasis due to its low cost and high availability. However, BS has several important limitations, and so additional imaging procedures are often necessary to determine the real significance of scintigraphic abnormalities[8].

During the last decade, positron emission tomography (PET) has evolved from a research tool to an established imaging modality for the staging of different types of malignant tumors, owing to its better spatial resolution and superior image quality with respect to conventional single-photon imaging. Among PET tracers, glucose analogue 2-deoxy-2-(^{18}F)fluoro-D-glucose (^{18}F-FDG) has become the most widely used in clinical routine, resulting in a major impact on the practice of oncology[9]. In breast cancer patients, ^{18}F-FDG-PET enables the detection

of neoplastic lesions on the basis of their increased glucose metabolism, potentially allowing for an accurate assessment of local disease, lymph nodes, and visceral metastases in a single imaging study. Furthermore, by directly reflecting tumor cell viability in bone metastases, this technique can potentially be used for therapy response assessments. In fact, changes in ^{18}F-FDG activity after therapy may reflect an early response to therapy that could be potentially prognostic[10].

Characterization of bone metastases is also possible with ^{18}F-sodium fluoride (^{18}F-NaF), which reflects the increased regional blood flow and osteoblastic bone reaction[8]. Specifically, greater activity of remodeling and bone turnover determines greater blood flow and exchange surface for ^{18}F-fluoride ion absorption and subsequent irreversible incorporation into the bone matrix as fluorapatite[11-13].

Both PET tracers have shown a better diagnostic value compared to BS in detecting bone metastases in patients with breast cancer and several other malignancies[14-20]. Conversely, very limited and controversial information exists in comparing the diagnostic accuracy of ^{18}F-FDG and ^{18}F-NaF PET[19,21,22]. The different uptake mechanisms of these two tracers might be complementary in the context of evaluating lytic and sclerotic lesions, which can both coexist in bone localizations of breast cancer patients[23].

Furthermore, it has been suggested[24] that anatomical localization of the lesions could also influence the accuracy of each technique; this finding is likely to be related to the morphology of bone metastasis. In fact, the involvement of different skeletal segments could determine different degrees of osteoblastic reaction[25,26]. At the time of writing, controversial results have been reported about the accuracy of these two tracers in breast cancer patients[19,21,22], with some authors even proposing their combined use[27,28]. In particular, ^{18}F-FDG PET/computed tomography (CT) can provide information about the presence/absence of disease in the skeleton, as well as in non-skeletal districts. In this context, it not been clearly investigated whether ^{18}F-NaF PET/CT can provide incremental information for the management of breast cancer patients that have already been evaluated by means of ^{18}F-FDG PET/CT.

The current study aims to evaluate the role of the two imaging modalities in the restaging of breast cancer patients with clinically/radiologically suspected or known metastatic bone lesions. In particular, we planned to verify whether the accuracy of the two imaging methods could be influenced by lesion density and location.

MATERIALS AND METHODS

Patient population

Between January 2010 and June 2012, 45 breast cancer patients were referred to our institutions for the execution of both ^{18}F-NaF and ^{18}F-FDG PET/CT for the restaging of clinically/radiologicallysuspected or proven metastatic bone lesions. All study participants, or their legal guardians, provided informed written consent prior to study enrollment, and practices were performed in accordance with the ethical standards laid down in the Declaration of Helsinki. We included only patients who performed the two PET scans within 1 mo and did not received chemotherapy or radiotherapy between the two examinations. By contrast, chemotherapy administration in the month before the two PET/CT exams was not an exclusion criterion. Patient characteristics are listed in Table 1.

PET/CT protocols

Image acquisition was performed according to standard procedures and international guidelines[29,30].

Patients were submitted to ^{18}F-NaF PET/CT using two 16 slices PET/CT hybrid systems: (1) Biograph 16 (Siemens Medical Solutions, Knoxville TN, United States); and (2) Discovery LS (GE Medical Systems, Milwaukee, WI, United States) according to the standard procedure as previously detailed[31].

Image interpretation

Each ^{18}F-FDG-PET/CT and ^{18}F-NaF-PET/CT scan were independently evaluated by two nuclear medicine physicians aware of the patient's clinical history but blinded to the results of the other PET/CT scan and that of other cross-sectional morphological imaging modalities [magnetic resonance imaging (MRI)/CT]. In cases of disagreement,a consensus obtained among readers was used for the final decision. For both ^{18}F-NaF and ^{18}F-FDG PET/CT, scans were interpreted as negative for bone lesions when no pathologic tracer uptake was present within the skeleton. In cases of increased uptake within the joints, the exam was also considered negative. Similarly, for both ^{18}F-NaF and ^{18}F-FDG, avid lesions were diagnosed as benign when degenerative changes or fractures were detected on non-diagnostic CT. Conversely, the presence of focal tracer uptake associated with suspicious or indeterminate morphological changes on non-diagnostic CT were considered as positive. Similarly, for both ^{18}F-NaF and ^{18}F-FDG, high and focal uptake in the absence of lesions on the non-diagnostic CT was considered likely to be "micro-scleroses", and thus classified as positive/malignant.

For each lesion, density on the co-registered CT was recorded and lesions were divided into four groups: Sclerotic, lytic, mixed, and no-lesions. Similarly, lesion localizations were also recorded to assess the impact of the divergent disease sites (skull, spine, ribs, extremities, and pelvis).

Standard references

Since a bone biopsy of all lesions for histology was not considered appropriate for obvious ethical reasons, the radiological and clinical follow-up at 12 mo served as the standard of reference for the final evaluation of the results as true-positive, true-negative, false-positive, and false-negative. Follow-up information included physical examination, laboratory tests, tumor markers,

Table 1 Patient characteristics (n = 45)

Demography	
Age (yr)	61 ± 10
Stage at diagnosis	
I	5
II	21
III	14
IV	5
Histology	
Ductal	35
Lobular	8
Other	2
Tumor receptor (+/-/unknown)	
Estrogen receptor	39/2/4
PgR	29/11/5
c-erb B2	14/24/7
Site of metastatic disease other than bone	
Lung	27%
Liver	20%
Lymph nodes	30%
Systemic therapy	
First-line	81%
Second-line	62%
Third-line	36%
Bisphosphonates	22%
Follow-up (mean 28 mo range 22-39)	
Patients with disease progression	58%
Patients dead from disease	30%

and other independent imaging studies (CT, MRI, ^{18}F-FDG PET/CT, X-ray studies, and bone scans).

Statistical analysis

For statistical analysis we used the "R" software program[32] and DiagnosisMed software package[33]. We compared ^{18}F-NaF PET/CT and ^{18}F-FDG PET/CT results through patient-, lesion density-, and site-based analyses.

Cochran Q test followed by multiple comparisons using McNemar's test with continuity correction and Bonferroni adjustment were used in order to assess differences among imaging modalities. P values less than 0.05 were considered statistically significant. The impact of adding ^{18}F-NaF PET/CT to the work-up of patients was also measured in terms of changes to their management due to findings related to this functional imaging.

The statistical methods of this study were reviewed by a biomedical statistician.

RESULTS

Overall diagnostic accuracy and patient-based analysis

Sixteen patients were negative and 16 patients were positive at both imaging modalities. Eleven and two patients were positive only ata single tracer (^{18}F-FDG and ^{18}F-NaF, respectively). Histology was used as standard references in two patients (specifically in one patient who was true positive for bone marrow involvement at ^{18}F-FDG PET and in one patient who was true positive for the presence of an osteosclerotic lesion in the ribs detected by ^{18}F-NaF only).

Table 2 Patient-based analysis: Performance comparisons between 2-deoxy-2-(^{18}F)fluoro-D-glucose and ^{18}F-sodium positron emission tomography/computed tomography

	^{18}F-FDG	^{18}F-NaF
Sensitivity (%)	75.00 (55.10-88.00)	91.67 (74.15-97.68)
Specificity (%)	99.00 (84.54-100)	76.19 (54.91-89.37)
Positive predictive value (%)	99.00 (82.41-100)	81.48 (63.3 91.82)
Negative predictive value (%)	77.78 (59.24-89.39)	88.89 (67.2-96.90)
Error rate (%)	13.33 (6.26-26.18)	15.56 (7.75-28.78)
Accuracy (%)	86.67 (73.82-93.74)	84.44 (71.22-92.25)
Youden's index	0.75 (0.75-0.74)	0.6786 (0.68-0.6718)

Estimated parameters corresponding to each technique are presented with 95%CI between square brackets. ^{18}F-FDG: 2-deoxy-2-(^{18}F)fluoro-D-glucose; ^{18}F-NaF: ^{18}F-sodium.

The two imaging methods were significantly different in the patient-based analysis, with anaccuracy of 86.7% and 84.4%, respectively (McNemar's χ^2 = 6.23, df = 1, P = 0.01.). See Table 2 for details on sensitivity, specificity, and predictive values of the two PET/CT modalities.

Overall lesion-based analysis

Overall, 244 bone lesions were detected in our analysis. The overall accuracy of the two methods was significantly different in the lesion-based analysis (McNemar's χ^2 = 93.4, df = 1, P < 0.0001). ^{18}F-NaF showed high sensitivity (90.5%), but a very low specificity (17.5%). By contrast, although ^{18}F-FDG PET/CT showed a lower sensitivity (66%), it was characterized by a significantly higher specificity (96.2%).

Lesion density- and site-based analysis

Significant differences were highlighted in the lesion density- and site- based analysis, as ^{18}F-FDG PET/CT was more accurate in the detection of CT-negative metastasis (P < 0.002),vertebral localizations (P < 0.002), and sclerotic (P < 0.005) and rib lesions (P < 0.04). No significant differences were highlighted with respect to accuracy in evaluating lytic and mixed lesions, or in lesions localized in the skull, distal extremities or pelvis. See Table 3 for details on sensitivity, specificity, and accuracy. Figures 1-3 show representative examples of the different performance of the two imaging modalities.

Impact on patient management

Findings that were found only in ^{18}F-NaF PET/CT imaging led to a change of management for 3 of the 45 patients (6.6%). In particular, two patients underwent chemotherapy rather than targeted radiotherapy due to the detection of further skeletal lesions. One patient was excluded from surgical treatment of lung metastasis due to the presence of bone involvement.

DISCUSSION

In this study, we aimed to elucidate the role of ^{18}F-FDG and ^{18}F-NaF PET/CT in restaging breast cancer patients

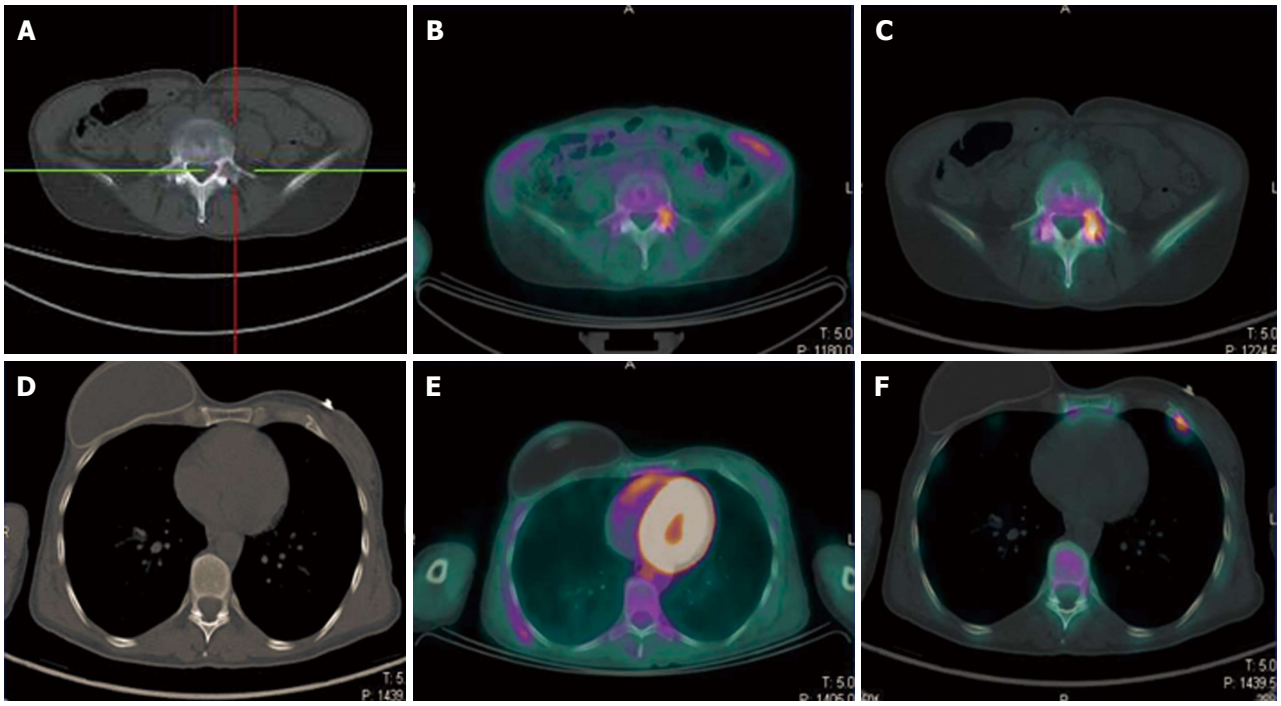

Figure 1 A 49-year-old breast cancer patient with bone relapse. A lytic lesion on the fifth lumbar vertebra was detected with computed tomography in absence of local pain (A). The lesion showed high uptake both at ^{18}F-FDG PET/CT (B) and ^{18}F-NaF PET/CT (C), thus confirming its malignant nature. No further ^{18}F-FDG avid metastasis was highlighted (E). By contrast a focal area of high ^{18}F-NaF uptake was evident in the anterior branch of the seventh rib on the left side (F). This area was indeed corresponding to a small sclerotic indeterminate lesion on the CT and was considered as a further site of disease (D). The patient started systemic therapy rather than a targeted radiotherapy on the fifth lumbar vertebra. ^{18}F-FDG: 2-deoxy-2-(^{18}F)fluoro-D-glucose; ^{18}F-NaF: ^{18}F-sodium; PET/CT: Positron emission tomography/computed tomography.

Table 3 Sites and density characteristics showing different performance between 2-deoxy-2-(^{18}F)fluoro-D-glucose and ^{18}F-sodium positron emission tomography/computed tomography

	n	^{18}F-FDG	^{18}F-NaF	*P*
Density				
Osteosclerotic	89			0.005
Sensitivity (%):		42.86 (15.82-74.95)	99.00 (64.57-99.00)	
Specificity (%):		97.00 (60.97-97.00)	48.15 (35.39-61.15)	
No lesion/bone marrow	29			0.002
Sensitivity(%):		100.00 (60.97-100.00)	48.15 (30.74-66.01)	
Specificity(%):		100.00 (34.24-100.00)	100.00 (34.24-100.00)	
Site				
Spine	81			0.002
Sensitivity (%):		65.38 (51.80-76.85)	100.00 (93.12-100.00)	
Specificity (%):		98.00 (88.30-98.00)	13.45 (0.61-27.18)	
Ribs	118			0.04
Sensitivity (%):		83.96 (75.81-89.74)	96.23 (90.70-98.52)	
Specificity (%):		78.37 (52.33-92.50)	78.57 (52.41-92.43)	

^{18}F-FDG: 2-deoxy-2-(^{18}F)fluoro-D-glucose; ^{18}F-NaF: ^{18}F-sodium.

with bone lesions by means of patient-, density-, and site-based analyses.

Slight, but significant, differences were highlighted between ^{18}F-FDG and ^{18}F-NaF in the patient-based analysis, with the former showing higher specificity and the latter being characterized by higher sensitivity. These differences were more markedly evident at the lesion-based analysis, where ^{18}F-FDG showed higher accuracy for detecting CT-negative (likely bone marrow confined) metastasis and lesions located in the spine, while ^{18}F-NaF PET/CT performed better with respect to osteosclerotic and rib lesions. Our results support the view that, when a functional method is needed, information derived by ^{18}F-FDG can correctly classify most breast cancer patients with suspected or known bone metastasis. However, the lesion-based analysis highlighted significant differences between the two imaging methods, which emphasize the different complementary information provided by

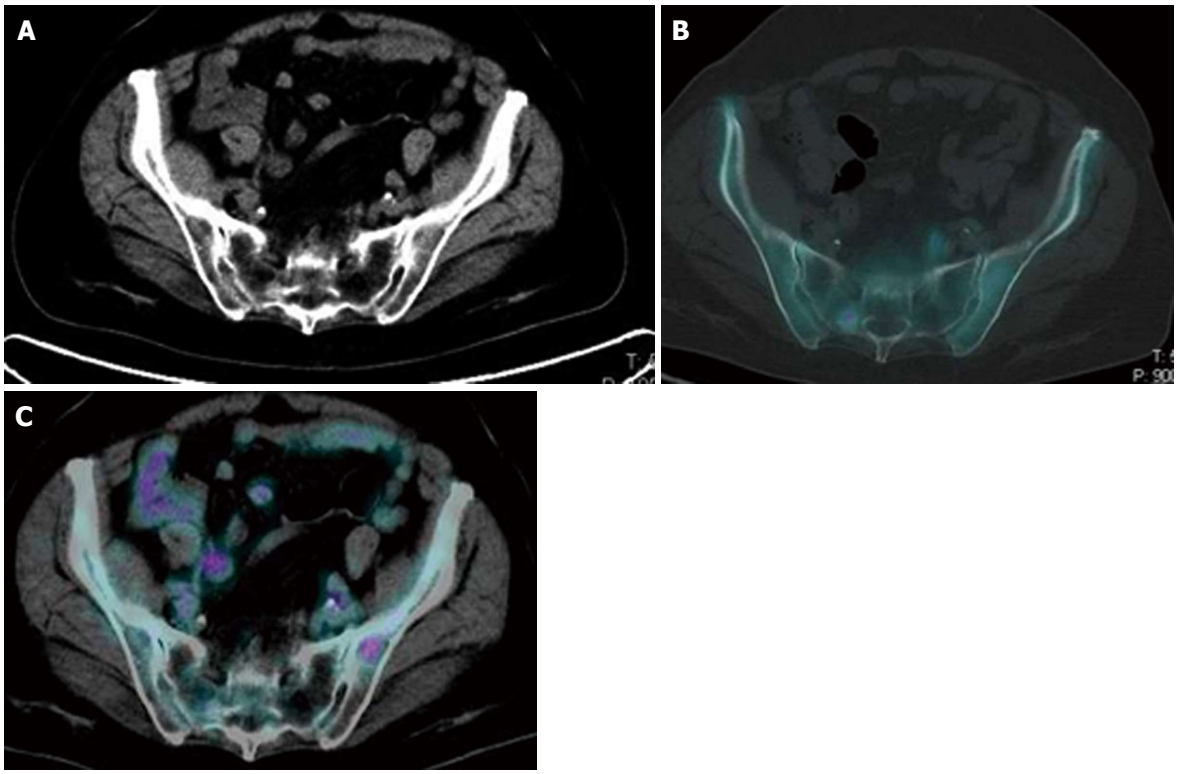

Figure 2 Evidence of the complementary features of 2-deoxy-2-(^{18}F)fluoro-D-glucose and ^{18}F-sodium positron emission tomography/computed tomography in the pelvis of the same breast cancer patient. An ^{18}F-NaF avid sclerotic lesion was detected in the right sacrum in absence of significant ^{18}F-FDG uptake. By contrast high uptake of ^{18}F-FDG was present in a small lytic lesion in the left iliac bone. Due to the absence of a significant local bone reaction, this small lesion did not show any uptake of ^{18}F-NaF. Both lesions corresponded to metastatic sites of disease and disappeared after chemotherapy. ^{18}F-FDG: 2-deoxy-2-(^{18}F)fluoro-D-glucose; ^{18}F-NaF: ^{18}F-sodium; PET/CT: Positron emission tomography/computed tomography.

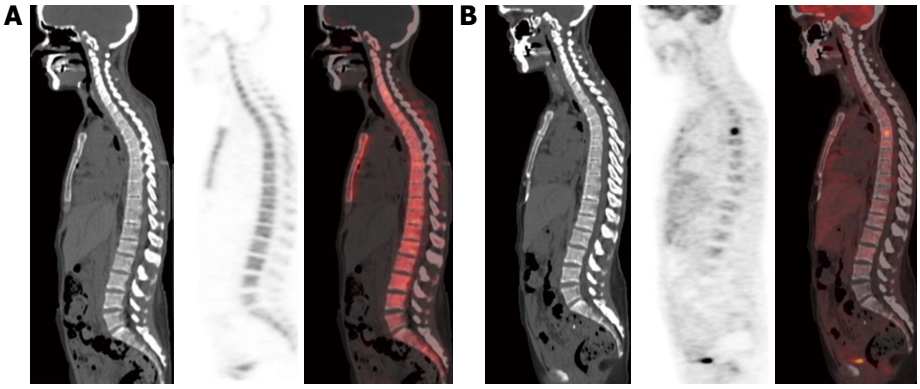

Figure 3 This area is likely to correspond to a bone marrow-confined metastasis not yet characterized by bone remodeling and thus falsely negative in both multidetector computed tomography and ^{18}F-sodium positron emission tomography/computed tomography. No structural lesions or area of ^{18}F-NaF uptake are evident in the vertebral column of this breast cancer patient (A); by contrast an area of high focal ^{18}F-FDG uptake was present in the sixth dorsal vertebra (B). ^{18}F-NaF: ^{18}F-sodium; ^{18}F-FDG: 2-deoxy-2-(^{18}F)fluoro-D-glucose.

the two tracers. In fact, these data fit with the different distribution mechanisms of the two tracers into bone metastases. More specifically, ^{18}F-FDG accumulates into viable, metabolically-active tumor cells[34,35], while ^{18}F-NaF is incorporated into bone crystals within the forming fluorapatite matrix, and thus tends to preferentially accumulate at sites of actively mineralizing bone[36,37]. Osseous metastases seed into the red bone marrow rather than the cortical bone, and this might explain the extremely high accuracy of ^{18}F-FDG PET in detecting metastases confined in the bone marrow, especially at an earlier stage before the occurrence of bone reaction[38,39]. Accordingly, it has been suggested that ^{18}F-FDG PET/CT can be assensitive as magnetic resonance imaging in this setting[40,41]. The relatively poor cellularity that may characterize sclerotic metastases, with relatively smaller volumes of tumor tissue in individual lesions, may influence the degree of ^{18}F-FDG uptake given the small number of elements able to trap it[42].

These findings are thus coherent with the fact

that ^{18}F-FDG uptake is more specific for malignant lesions than bone metabolism tracers, while ^{18}F-NaF is characterized by an extremely high sensitivity, rather than specificity, for both sclerotic and lytic lesions[43]. Surprisingly, both radiotracers showed high accuracy in the detection of lytic localizations, and no differences were highlighted between the accuracy of ^{18}F-FDG or ^{18}F-NaF in the evaluation of this type of lesion. Previous studies compared the accuracy of ^{18}F-FDG PET/CT and BS with respect to lytic lesions and found that ^{18}F-FDG PET/CT is superior to BS in this setting[42,44]. Accordingly, the present findings support the concept that, although ^{18}F-NaF and BS highlight the same pathophysiological mechanisms (increased osteoblastic activity), the greater spatial resolution of PET accounts for the better diagnostic accuracy of ^{18}F-NaF with respect to BS[24,43,45]. In fact, thanks to its better spatial resolution, this tracer is even capable of capturing the increased mineral metabolism related to the thin reactive border that may surround a lytic lesion. By contrast, this subtle reaction is generally too small to be detected by the limited spatial resolution of BS. However, it must be underlined that the extremely high sensitivity of ^{18}F-NaF PET/CT in the detection of both lytic and sclerotic metastases is paralleled by a relatively low specificity[30].

This behavior might represent an important limitation in the use of ^{18}F-NaF PET and strongly advise in favor of the use of hybrid PET/CT imaging, thus increasing the specificity of ^{18}F-NaF PET thanks to the CT-based characterization of bone remodeling (*i.e.*, exclusion of clearly degenerative lesions)[31].

Significant differences between the two tracers were also found in the site-based analysis. In particular, the ^{18}F-FDG results were more accurate in detecting lesions located in the spine, while ^{18}F-NaF provided a more accurate characterization of rib lesions. This could be related to the different structural modification induced by metastases as a function of their anatomical localization. Small lesions in the ribs can show an intense osteoblastic response, even in the presence of poor cellularity, and can therefore be easily identified by means of ^{18}F-NaF[25]. By contrast, the highlighted superiority of ^{18}F-FDG PET in the evaluation of spine lesions can be explained by the fact that many lesions located in the spine were, in this study, characterized by an absence of structural correlates in the co-registered CT. On the other hand, the age of our patient population (mean 60 years) may have also influenced the low accuracy of ^{18}F-NaF for spine lesions. In fact, the presence of areas of non-specific ^{18}F-NaF uptake due to age-related degenerative changes may partially explain the relatively lower accuracy of ^{18}F-NaF in this site. This finding is in line with the notion that ^{18}F-NaF is more accurate than BS, especially for evaluating vertebral localizations[46]. In fact, thanks to the greater resolution and fusion with CT, ^{18}F-NaF can reduce the number off alse positive/indeterminate findings due to degenerative lesions. Although ^{18}F-FDG can also be influenced by degenerative changes, the intensity and focality of these uptakes are lower with respect to bone metastasis; the glucose analogue is thus superior to both bone metabolism tracers in this setting.

Finally, when the specific influence of ^{18}F-NaF was evaluated with respect to patient management, we found that adding ^{18}F-NaF PET to patient work-up led to a change in management in 3 out of 45 patients, due to it revealing metastases undetected by ^{18}F-FDG scan. These findings may underline that the extremely high sensitivity of ^{18}F-NaF uptake can be useful in evaluating patients who are candidates for regional therapy (*i.e.*, surgery or radiotherapy) with the aim of excluding patients with further occult metastases.

The present study has some limitations. It is a two center, retrospective study whose results may have been influenced by its patient population's high pre-test probability of bone metastasis. Although the number of included patients was relatively small, it was comparable, or even higher, with respect to similar studies on the impact of different functional imaging techniques in breast cancer patients with bone metastasis[47,48]. Histological confirmation of metastases was not obtained in the majority of patients, for both practical and ethical reasons. A clinical, biochemical, and radiological follow-up of 12 mo was used as the standard of reference. Obviously, 12-mo follow-up findings might not be sufficient to exhaustively depict disease status. However, sclerotic and/or lytic bone lesions on CT are mostly accepted as metastases[49,50]. Additionally, in many other studies, clinical biopsy was performed only in a minority of patients and comparative imaging modalities were used as standard in order to assess metastatic bone involvement[51].

In conclusion, ^{18}F-FDG PET/CT is a reliable imaging tool in the detection of bone metastasis in most cases, with a high diagnostic accuracy and superior specificity with respect to ^{18}F-NaF PET/CT in the general population of breast cancer patients. However, the extremely high sensitivity of ^{18}F-NaF PET/CT can exploit its diagnostic potential in specific clinical settings, such as small CT-evident sclerotic lesions, possibly changing patient staging or management. Similarly, given the hereby proven complementary role of the two tracers, breast cancer patients could be candidates for ^{18}F-NaF when, despite negative results in ^{18}F-FDG and other imaging methods, they have suggestive clinical and biochemical sign of disease. Therefore ^{18}F-NaF PET/CT emerges as a powerful "second-line" functional imaging tool, which may be of use in selected patients on the basis of their specific clinical history, in order to identify a priori in those patients in which ^{18}F-NaF PET/CT may significantly impact their management.

COMMENTS

Background

Early detection of bone metastases is of pivotal importance in breast cancer patients. To this purpose, besides conventional bone scintigraphy, positron emission tomography has become an established imaging modality, with better spatial resolution and superior image quality. Among positron emission tomography (PET) tracers, 2-deoxy-2-(^{18}F)fluoro-D-glucose (^{18}F-FDG)

represents the most widely used tracer in clinical routine, and can provide information about the presence or absence of disease in the skeleton, as well as in non-skeletal districts. However, characterization of bone metastases is also possible with ^{18}F-sodium fluoride (^{18}F-NaF). In this context, it has not yet been clearly investigated whether ^{18}F-NaF PET/computed tomography (CT) can provide incremental information concerning breast cancer patients that have already been evaluated by means of FDG PET/CT.

Research frontiers

To date, controversial results have been reported about the accuracy of the two PET tracers in breast cancer patients,with some authors even proposing their combined use. This work aims to clarify whether, at least in specific conditions, these two tracers could be complementary in order to improve diagnostic accuracy in bone lesion characterization.

Innovations and breakthroughs

This work aims to compare the role of ^{18}F-FDG and ^{18}F-NaF PET/CT in re-staging breast cancer patients with bone lesions through patient-, lesion density-, and site-based analyses. A more prompt and accurate characterization of bone alterations could lead to more accurate patient management.

Applications

Besides ^{18}F-FDG, ^{18}F-NaF PET/CT emerges as a powerful "second-line" functional imaging tool, which may be useful in selected patients on the basis of their specific clinical history.

Terminology

Glucose analogue ^{18}F-FDG PET enables the detection of neoplastic lesions on the basis of their increased glucose metabolism directly reflecting tumor cell viability, thereby allowing forthe characterization of skeletal and extra-skeletal lesions. On the other hand, ^{18}F-NaF reflects the increased regional blood flow and osteoblastic bone reaction being irreversibly incorporated into the bone matrix as fluorapatite.

Peer-review

An agreement on which is the best PET tracer in the characterization of bone lesions has not been yet been reached. In this study, the authors compared ^{18}F-FDG and ^{18}F-NaF PET/CT accuracy in the restaging of breast cancer patients. They observed that, despite ^{18}F-FDG PET/CT possibly being considered the most reliable tool in the general population of breast cancer patients, it can exploit its diagnostic potential in specific clinical settings. These results were interesting and provided important information concerning the most appropriate management of breast cancer patients with suspected bone metastases.

REFERENCES

1 **Viadana E**, Cotter R, Pickren JW, Bross ID. An autopsy study of metastatic sites of breast cancer. *Cancer Res* 1973; **33**: 179-181 [PMID: 4682319]

2 **Scheid V**, Buzdar AU, Smith TL, Hortobagyi GN. Clinical course of breast cancer patients with osseous metastasis treated with combination chemotherapy. *Cancer* 1986; **58**: 2589-2593 [PMID: 3779609]

3 **Coleman RE**, Rubens RD. The clinical course of bone metastases from breast cancer. *Br J Cancer* 1987; **55**: 61-66 [PMID: 3814476 DOI: 10.1038/bjc.1987.13]

4 **Yamashita K**, Koyama H, Inaji H. Prognostic significance of bone metastasis from breast cancer. *Clin Orthop Relat Res* 1995; (**312**): 89-94 [PMID: 7634621]

5 **Yamashita K**, Ueda T, Komatsubara Y, Koyama H, Inaji H, Yonenobu K, Ono K. Breast cancer with bone-only metastases. Visceral metastases-free rate in relation to anatomic distribution of bone metastases. *Cancer* 1991; **68**: 634-637 [PMID: 2065284]

6 **Bergh J**, Jönsson PE, Glimelius B, Nygren P. A systematic overview of chemotherapy effects in breast cancer. *Acta Oncol* 2001; **40**: 253-281 [PMID: 11441936 DOI: 10.1080/02841860151116349]

7 **Hortobagyi GN**. Overview of treatment results with trastuzumab (Herceptin) in metastatic breast cancer. *Semin Oncol* 2001; **28**: 43-47 [PMID: 11774205 DOI: 10.1016/S0093-7754(01)90108-3]

8 **Schirrmeister H**. Detection of bone metastases in breast cancer by positron emission tomography. *Radiol Clin North Am* 2007; **45**: 669-676, vi [PMID: 17706531 DOI: 10.1016/j.rcl.2007.05.007]

9 **Hillner BE**, Siegel BA, Liu D, Shields AF, Gareen IF, Hanna L, Stine SH, Coleman RE. Impact of positron emission tomography/computed tomography and positron emission tomography (PET) alone on expected management of patients with cancer: initial results from the National Oncologic PET Registry. *J Clin Oncol* 2008; **26**: 2155-2161 [PMID: 18362365 DOI: 10.1200/JCO.2007.14.5631]

10 **Specht JM**, Tam SL, Kurland BF, Gralow JR, Livingston RB, Linden HM, Ellis GK, Schubert EK, Dunnwald LK, Mankoff DA. Serial 2-[18F] fluoro-2-deoxy-D-glucose positron emission tomography (FDG-PET) to monitor treatment of bone-dominant metastatic breast cancer predicts time to progression (TTP). *Breast Cancer Res Treat* 2007; **105**: 87-94 [PMID: 17268819 DOI: 10.1007/s10549-006-9435-1]

11 **Hsu WK**, Virk MS, Feeley BT, Stout DB, Chatziioannou AF, Lieberman JR. Characterization of osteolytic, osteoblastic, and mixed lesions in a prostate cancer mouse model using 18F-FDG and 18F-fluoride PET/CT. *J Nucl Med* 2008; **49**: 414-421 [PMID: 18287261 DOI: 10.2967/jnumed.107.045666]

12 **Blau M**, Nagler W, Bender MA. Fluorine-18: a new isotope for bone scanning. *J Nucl Med* 1962; **3**: 332-334 [PMID: 13869926]

13 **Narita N**, Kato K, Nakagaki H, Ohno N, Kameyama Y, Weatherell JA. Distribution of fluoride concentration in the rat's bone. *Calcif Tissue Int* 1990; **46**: 200-204 [PMID: 2106380 DOI: 10.1007/BF02555045]

14 **Liu T**, Xu JY, Xu W, Bai YR, Yan WL, Yang HL. Fluorine-18 deoxyglucose positron emission tomography, magnetic resonance imaging and bone scintigraphy for the diagnosis of bone metastases in patients with lung cancer: which one is the best?--a meta-analysis. *Clin Oncol* (R Coll Radiol) 2011; **23**: 350-358 [PMID: 21094027 DOI: 10.1016/j.clon.2010.10.002]

15 **Chang MC**, Chen JH, Liang JA, Lin CC, Yang KT, Cheng KY, Yeh JJ, Kao CH. Meta-analysis: comparison of F-18 fluoro-deoxyglucose-positron emission tomography and bone scintigraphy in the detection of bone metastasis in patients with lung cancer. *Acad Radiol* 2012; **19**: 349-357 [PMID: 22173321 DOI: 10.1016/j.acra.2011.10.018]

16 **Liu T**, Cheng T, Xu W, Yan WL, Liu J, Yang HL. A meta-analysis of 18FDG-PET, MRI and bone scintigraphy for diagnosis of bone metastases in patients with breast cancer. *Skeletal Radiol* 2011; **40**: 523-531 [PMID: 20495798 DOI: 10.1007/s00256-010-0963-8]

17 **Even-Sapir E**, Metser U, Mishani E, Lievshitz G, Lerman H, Leibovitch I. The detection of bone metastases in patients with high-risk prostate cancer: 99mTc-MDP Planar bone scintigraphy, single- and multi-field-of-view SPECT, 18F-fluoride PET, and 18F-fluoride PET/CT. *J Nucl Med* 2006; **47**: 287-297 [PMID: 16455635]

18 **Ben-Haim S**, Israel O. Breast cancer: role of SPECT and PET in imaging bone metastases. *Semin Nucl Med* 2009; **39**: 408-415 [PMID: 19801220 DOI: 10.1053/j.semnuclmed.2009.05.002]

19 **Iagaru A**, Mittra E, Dick DW, Gambhir SS. Prospective evaluation of (99m)Tc MDP scintigraphy, (18)F NaF PET/CT, and (18)F FDG PET/CT for detection of skeletal metastases. *Mol Imaging Biol* 2012; **14**: 252-259 [PMID: 21479710 DOI: 10.1007/s11307-011-0486-2]

20 **Withofs N**, Grayet B, Tancredi T, Rorive A, Mella C, Giacomelli F, Mievis F, Aerts J, Waltregny D, Jerusalem G, Hustinx R. 18F-fluoride PET/CT for assessing bone involvement in prostate and breast cancers. *Nucl Med Commun* 2011; **32**: 168-176 [PMID: 21076343 DOI: 10.1097/MNM.0b013e3283412ef5]

21 **Krüger S**, Buck AK, Mottaghy FM, Hasenkamp E, Pauls S, Schumann C, Wibmer T, Merk T, Hombach V, Reske SN. Detection of bone metastases in patients with lung cancer: 99mTc-MDP planar bone scintigraphy, 18F-fluoride PET or 18F-FDG

PET/CT. *Eur J Nucl Med Mol Imaging* 2009; **36**: 1807-1812 [PMID: 19504092 DOI: 10.1007/s00259-009-1181-2]
22 **Chan SC**, Wang HM, Ng SH, Hsu CL, Lin YJ, Lin CY, Liao CT, Yen TC. Utility of 18F-fluoride PET/CT and 18F-FDG PET/CT in the detection of bony metastases in heightened-risk head and neck cancer patients. *J Nucl Med* 2012; **53**: 1730-1735 [PMID: 22961077 DOI: 10.2967/jnumed.112.104893]
23 **Hortobagyi GN**. Bone metastases in breast cancer patients. *Semin Oncol* 1991; **18**: 11-15 [PMID: 1925624]
24 **Schirrmeister H**, Guhlmann A, Elsner K, Kotzerke J, Glatting G, Rentschler M, Neumaier B, Träger H, Nüssle K, Reske SN. Sensitivity in detecting osseous lesions depends on anatomic localization: planar bone scintigraphy versus 18F PET. *J Nucl Med* 1999; **40**: 1623-1629 [PMID: 10520701]
25 **Langsteger W**, Heinisch M, Fogelman I. The role of fluoro-deoxyglucose, 18F-dihydroxyphenylalanine, 18F-choline, and 18F-fluoride in bone imaging with emphasis on prostate and breast. *Semin Nucl Med* 2006; **36**: 73-92 [PMID: 16356797 DOI: 10.1053/j.semnuclmed.2005.09.002]
26 **Käkönen SM**, Mundy GR. Mechanisms of osteolytic bone metastases in breast carcinoma. *Cancer* 2003; **97**: 834-839 [PMID: 12548583 DOI: 10.1002/cncr.11132]
27 **Iagaru A**, Mittra E, Yaghoubi SS, Dick DW, Quon A, Goris ML, Gambhir SS. Novel strategy for a cocktail 18F-fluoride and 18F-FDG PET/CT scan for evaluation of malignancy: results of the pilot-phase study. *J Nucl Med* 2009; **50**: 501-505 [PMID: 19289439 DOI: 10.2967/jnumed.108.058339]
28 **Iagaru A**, Mittra E, Mosci C, Dick DW, Sathekge M, Prakash V, Iyer V, Lapa P, Isidoro J, de Lima JM, Gambhir SS. Combined 18F-fluoride and 18F-FDG PET/CT scanning for evaluation of malignancy: results of an international multicenter trial. *J Nucl Med* 2013; **54**: 176-183 [PMID: 23243299 DOI: 10.2967/jnumed.112.108803]
29 **Boellaard R**, Delgado-Bolton R, Oyen WJ, Giammarile F, Tatsch K, Eschner W, Verzijlbergen FJ, Barrington SF, Pike LC, Weber WA, Stroobants S, Delbeke D, Donohoe KJ, Holbrook S, Graham MM, Testanera G, Hoekstra OS, Zijlstra J, Visser E, Hoekstra CJ, Pruim J, Willemsen A, Arends B, Kotzerke J, Bockisch A, Beyer T, Chiti A, Krause BJ. FDG PET/CT: EANM procedure guidelines for tumour imaging: version 2.0. *Eur J Nucl Med Mol Imaging* 2015; **42**: 328-354 [PMID: 25452219 DOI: 10.1007/s00259-014-2961-x]
30 **Segall G**, Delbeke D, Stabin MG, Even-Sapir E, Fair J, Sajdak R, Smith GT. SNM practice guideline for sodium 18F-fluoride PET/CT bone scans 1.0. *J Nucl Med* 2010; **51**: 1813-1820 [PMID: 21051652 DOI: 10.2967/jnumed.110.082263]
31 **Piccardo A**, Altrinetti V, Bacigalupo L, Puntoni M, Biscaldi E, Gozza A, Cabria M, Iacozzi M, Pasa A, Morbelli S, Villavecchia G, DeCensi A. Detection of metastatic bone lesions in breast cancer patients: fused (18)F-Fluoride-PET/MDCT has higher accuracy than MDCT. Preliminary experience. *Eur J Radiol* 2012; **81**: 2632-2638 [PMID: 22227259 DOI: 10.1016/j.ejrad.2011.12.020]
32 **R Development Core Team**. The R project for statistical computing. [Accessed: 2013 Jan 21]. Available from: URL: http//www.R-project.org
33 **Brasil P**. Diagnosis Med: Diagnostic test accuracy evaluation for medical professionals. [Accessed: 2013 Jan 21]. Available from: URL: http//cran.r-project.org/src/contrib/Archive/DiagnosisMed
34 **Beheshti M**, Vali R, Waldenberger P, Fitz F, Nader M, Hammer J, Loidl W, Pirich C, Fogelman I, Langsteger W. The use of F-18 choline PET in the assessment of bone metastases in prostate cancer: correlation with morphological changes on CT. *Mol Imaging Biol* 2010; **12**: 98-107 [PMID: 19588206 DOI: 10.1007/s11307-009-0239-7]
35 **Cook GJ**. PET and PET/CT imaging of skeletal metastases. *Cancer Imaging* 2010; **10**: 1-8 [PMID: 20663736 DOI: 10.1102/1470-7330.2010.0022]
36 **Schiepers C**, Nuyts J, Bormans G, Dequeker J, Bouillon R, Mortelmans L, Verbruggen A, De Roo M. Fluoride kinetics of the axial skeleton measured in vivo with fluorine-18-fluoride PET. *J Nucl Med* 1997; **38**: 1970-1976 [PMID: 9430479]
37 **Cook GJ**, Fogelman I. The role of positron emission tomography in the management of bone metastases. *Cancer* 2000; **88**: 2927-2933 [PMID: 10898336 DOI: 10.1002/1097-0142(20000615)88:12]
38 **Basu S**, Alavi A. Bone marrow and not bone is the primary site for skeletal metastasis: critical role of [18F]fluorodeoxyglucose positron emission tomography in this setting. *J Clin Oncol* 2007; **25**: 1297; author reply 1297-1299 [PMID: 17401027 DOI: 10.1200/JCO.2006.10.0123]
39 **Basu S**, Tiwari BP. Complimentary role of FDG-PET imaging and skeletal scintigraphy in the evaluation of patients of prostate carcinoma. *Indian J Cancer* 2011; **48**: 513-514 [PMID: 22293270 DOI: 10.4103/0019-509X.92247]
40 **Yang HL**, Liu T, Wang XM, Xu Y, Deng SM. Diagnosis of bone metastases: a meta-analysis comparing 18FDG PET, CT, MRI and bone scintigraphy. *Eur Radiol* 2011; **21**: 2604-2617 [PMID: 21887484 DOI: 10.1007/s00330-011-2221-4]
41 **Basu S**, Torigian D, Alavi A. Evolving concept of imaging bone marrow metastasis in the twenty-first century: critical role of FDG-PET. *Eur J Nucl Med Mol Imaging* 2008; **35**: 465-471 [PMID: 17955239 DOI: 10.1007/s00259-007-0593-0]
42 **Abe K**, Sasaki M, Kuwabara Y, Koga H, Baba S, Hayashi K, Takahashi N, Honda H. Comparison of 18FDG-PET with 99mTc-HMDP scintigraphy for the detection of bone metastases in patients with breast cancer. *Ann Nucl Med* 2005; **19**: 573-579 [PMID: 16363622 DOI: 10.1007/BF02985050]
43 **Schirrmeister H**, Guhlmann A, Kotzerke J, Santjohanser C, Kühn T, Kreienberg R, Messer P, Nüssle K, Elsner K, Glatting G, Träger H, Neumaier B, Diederichs C, Reske SN. Early detection and accurate description of extent of metastatic bone disease in breast cancer with fluoride ion and positron emission tomography. *J Clin Oncol* 1999; **17**: 2381-2389 [PMID: 10561300]
44 **Cook GJ**, Houston S, Rubens R, Maisey MN, Fogelman I. Detection of bone metastases in breast cancer by 18FDG PET: differing metabolic activity in osteoblastic and osteolytic lesions. *J Clin Oncol* 1998; **16**: 3375-3379 [PMID: 9779715]
45 **Hoegerle S**, Juengling F, Otte A, Altehoefer C, Moser EA, Nitzsche EU. Combined FDG and [F-18]fluoride whole-body PET: a feasible two-in-one approach to cancer imaging? *Radiology* 1998; **209**: 253-258 [PMID: 9769840 DOI: 10.1148/radiology.209.1.9769840]
46 **Fogelman I**, Cook G, Israel O, Van der Wall H. Positron emission tomography and bone metastases. *Semin Nucl Med* 2005; **35**: 135-142 [PMID: 15765376 DOI: 10.1053/j.semnuclmed.2004.11.005]
47 **Uematsu T**, Yuen S, Yukisawa S, Aramaki T, Morimoto N, Endo M, Furukawa H, Uchida Y, Watanabe J. Comparison of FDG PET and SPECT for detection of bone metastases in breast cancer. *AJR Am J Roentgenol* 2005; **184**: 1266-1273 [PMID: 15788608 DOI: 10.2214/ajr.184.4.01841266]
48 **Damle NA**, Bal C, Bandopadhyaya GP, Kumar L, Kumar P, Malhotra A, Lata S. The role of 18F-fluoride PET-CT in the detection of bone metastases in patients with breast, lung and prostate carcinoma: a comparison with FDG PET/CT and 99mTc-MDP bone scan. *Jpn J Radiol* 2013; **31**: 262-269 [PMID: 23377765 DOI: 10.1007/s11604-013-0179-7]
49 **Haubold-Reuter BG**, Duewell S, Schilcher BR, Marincek B, von Schulthess GK. The value of bone scintigraphy, bone marrow scintigraphy and fast spin-echo magnetic resonance imaging in staging of patients with malignant solid tumours: a prospective study. *Eur J Nucl Med* 1993; **20**: 1063-1069 [PMID: 8287874 DOI: 10.1007/BF00173484]
50 **Goldhirsch A**, Ingle JN, Gelber RD, Coates AS, Thürlimann B, Senn HJ. Thresholds for therapies: highlights of the St Gallen International Expert Consensus on the primary therapy of early breast cancer 2009. *Ann Oncol* 2009; **20**: 1319-1329 [PMID: 19535820 DOI: 10.1093/annonc/mdp322]
51 **Braun S**, Vogl FD, Naume B, Janni W, Osborne MP, Coombes

RC, Schlimok G, Diel IJ, Gerber B, Gebauer G, Pierga JY, Marth C, Oruzio D, Wiedswang G, Solomayer EF, Kundt G, Strobl B, Fehm T, Wong GY, Bliss J, Vincent-Salomon A, Pantel K. A pooled analysis of bone marrow micrometastasis in breast cancer. *N Engl J Med* 2005; **353**: 793-802 [PMID: 16120859 DOI: 10.1056/NEJMoa050434]

P- Reviewer: Vinh-Hung V **S- Editor**: Qiu S
L- Editor: Rutherford A **E- Editor**: Liu SQ

World Journal of Radiology

Submit a Manuscript: http://www.wjgnet.com/esps/
Help Desk: http://www.wjgnet.com/esps/helpdesk.aspx
DOI: 10.4329/wjr.v8.i2.210

World J Radiol 2016 February 28; 8(2): 210-225
ISSN 1949-8470 (online)

SYSTEMATIC REVIEWS

Functional magnetic resonance imaging of internet addiction in young adults

Gianna Sepede, Margherita Tavino, Rita Santacroce, Federica Fiori, Rosa Maria Salerno, Massimo Di Giannantonio

Gianna Sepede, Department of Basic Medical Sciences, Neurosciences and Sense Organs, University "A. Moro", 70121 Bari, Italy

Gianna Sepede, Margherita Tavino, Rita Santacroce, Federica Fiori, Rosa Maria Salerno, Massimo Di Giannantonio, Department of Neuroscience, Imaging, and Clinical Sciences, University "G.d'Annunzio", 66100 Chieti, Italy

Author contributions: Sepede G, Salerno RM and Di Giannantonio M designed the research; Sepede G, Tavino M, Santacroce R and Fiori F performed the PubMed research, selected the papers included in the qualitative review and summarized the results; Sepede G, Salerno RM and Di Giannantonio M wrote the paper; Santacroce R performed the language editing.

Supported by Department of Neuroscience, Imaging, and Clinical Sciences, University "G.d'Annunzio", Chieti, Italy; Dr. Sepede's post hoc grant has been funded by the European Union's Seventh Framework Programme for research, technological development and demonstration under grant agreement, No. 602450.

Conflict-of-interest statement: All authors do not report any conflict of interest. This paper reflects only the authors' views and the European Union is not liable for any use that may be made of the information contained therein.

Data sharing statement: No additional data are available.

Correspondence to: Gianna Sepede, MD, PhD, Department of Basic Medical Sciences, Neurosciences and Sense Organs, University "A. Moro", Piazza G. Cesare, 11, 70121 Bari, Italy. gsepede@libero.it
Telephone: +39-0871-3556901
Fax: +39-0871-3556930

Received: July 27, 2015
Peer-review started: July 30, 2015
First decision: October 30, 2015
Revised: December 4, 2015
Accepted: December 18, 2015
Article in press: December 21, 2015
Published online: February 28, 2016

Abstract

AIM: To report the results of functional magnetic resonance imaging (fMRI) studies pertaining internet addiction disorder (IAD) in young adults.

METHODS: We conducted a systematic review on PubMed, focusing our attention on fMRI studies involving adult IAD patients, free from any comorbid psychiatric condition. The following search words were used, both alone and in combination: fMRI, internet addiction, internet dependence, functional neuroimaging. The search was conducted on April 20th, 2015 and yielded 58 records. Inclusion criteria were the following: Articles written in English, patients' age $\geqslant$ 18 years, patients affected by IAD, studies providing fMRI results during resting state or cognitive/emotional paradigms. Structural MRI studies, functional imaging techniques other than fMRI, studies involving adolescents, patients with comorbid psychiatric, neurological or medical conditions were excluded. By reading titles and abstracts, we excluded 30 records. By reading the full texts of the 28 remaining articles, we identified 18 papers meeting our inclusion criteria and therefore included in the qualitative synthesis.

RESULTS: We found 18 studies fulfilling our inclusion criteria, 17 of them conducted in Asia, and including a total number of 666 tested subjects. The included studies reported data acquired during resting state or different paradigms, such as cue-reactivity, guessing or cognitive control tasks. The enrolled patients were usually males

(95.4%) and very young (21-25 years). The most represented IAD subtype, reported in more than 85% of patients, was the internet gaming disorder, or videogame addiction. In the resting state studies, the more relevant abnormalities were localized in the superior temporal gyrus, limbic, medial frontal and parietal regions. When analyzing the task related fmri studies, we found that less than half of the papers reported behavioral differences between patients and normal controls, but all of them found significant differences in cortical and subcortical brain regions involved in cognitive control and reward processing: Orbitofrontal cortex, insula, anterior and posterior cingulate cortex, temporal and parietal regions, brain stem and caudate nucleus.

CONCLUSION: IAD may seriously affect young adults' brain functions. It needs to be studied more in depth to provide a clear diagnosis and an adequate treatment.

Key words: Internet addiction; Pathologic internet use; Functional magnetic resonance imaging; Internet gaming disorder; Functional neuroimaging

Core tip: We systematically reviewed the functional magnetic resonance imaging studies on adults affected by internet addiction disorder (IAD), without any other psychiatric condition. We found 18 studies, mostly conducted in East Asia and enrolling young males with internet gaming disorder. Internet addicts showed functional alterations in regions involved in cognitive control and reward/punishment sensitivity (orbitofrontal cortex, anterior and posterior cingulate, insula, dorsolateral prefrontal cortex, temporoparietal regions, brain stem and caudate nucleus) that are similar to those observed in substance use disorder. IAD is a disabling condition needing careful consideration due to its severe impact on young people's brain functioning.

Sepede G, Tavino M, Santacroce R, Fiori F, Salerno RM, Di Giannantonio M. Functional magnetic resonance imaging of internet addiction in young adults. *World J Radiol* 2016; 8(2): 210-225 Available from: URL: http://www.wjgnet.com/1949-8470/full/v8/i2/210.htm DOI: http://dx.doi.org/10.4329/wjr.v8.i2.210

INTRODUCTION

Internet addiction disorder (IAD), also called pathologic/problematic internet use (PIU), may be defined as an impulse control disorder characterized by an uncontrolled Internet use, associated with a significant functional impairment or clinical distress[1]. IAD is not classified as a mental disorder in the Diagnostic and Statistical Manual of Mental Disorders-fifth edition, but a subtype of IAD, the internet gaming disorder (IGD) (also called videogame addiction), is included in the section 3 as a topic deserving future studies[2]. A recent meta-analysis on IAD[3] involving more than 89000 participants from 31 nations reported a global prevalence estimate of 6%, with the higher prevalence in the Middle East (10.9%) and the lowest prevalence in Northern and Western Europe (2.6%). A higher prevalence of IAD was significantly associated with lower subjective and environmental conditions. A recent study conducted on Indian college students[4] reported 8% of moderate IAD and identified the following variables as risk factors: Male gender, continuous availability online, using the internet more for making new friendships/relationships and less for coursework/assignment. Due to their high computer skill and easy Internet access, young adults are at augmented risk for IAD[5].

Some of the clinical characteristics of IAD are similar to those observed in behavioral or substance misuse disorders (loss of control, craving, withdrawal symptoms), Obsessive Compulsive Disorder, or Bipolar Disorder so the nature of IAD (primary psychiatric disorder or "online variant" of other psychiatric conditions) is still debated[6-9].

Functional imaging techniques increase the possibility to investigate the neural basis of IAD, enhancing the sensitivity and the statistical power of clinical data. Functional magnetic resonance imaging (fMRI), in particular, is a worldwide used non-invasive technique to study the neural underpinnings of psychiatric disorders[10-12]. By means of fMRI, brain signal changes may be analyzed in terms of functional fluctuations with respect to a given "baseline" (activations/deactivations analysis) or in terms of functional connectivity among different brain regions (network analysis). Metabolic activity changes in the brain can be monitored during the execution of paradigms (task related fMRI) or during the spontaneous cerebral activity (resting state fMRI)[13-16].

Aim of the present study was to systematically review the resting state and task related fMRI studies conducted on adult subjects with IAD, looking for reliable biomarkers of this challenging mental condition.

MATERIALS AND METHODS

We searched PubMed to identify fMRI studies investigating IAD in adult subjects. The following search words were used, both alone and in combination: fMRI, Internet addiction, Internet dependence, functional neuroimaging. The search was conducted on April 20th, 2015 and yielded 58 records.

Inclusion criteria were the following: Articles written in English, patients' age $\geqslant$ 18 years, patients affected by IAD, studies providing fMRI results during resting state or cognitive/emotional paradigms. Structural MRI studies, functional imaging techniques other than fMRI, studies involving adolescents, patients with comorbid psychiatric, neurological or medical conditions were

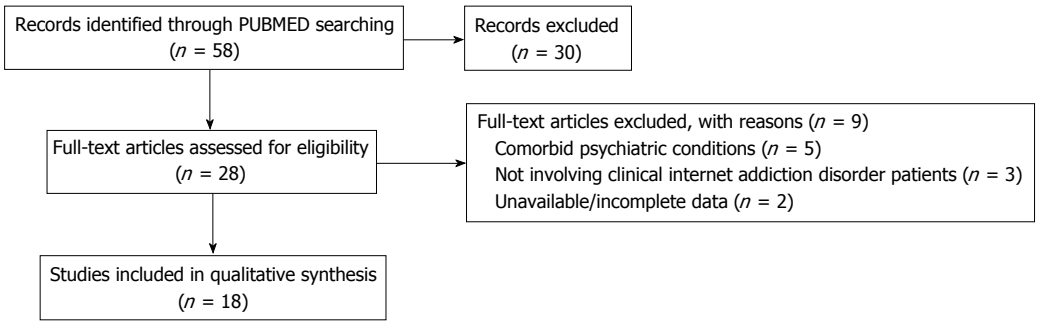

Figure 1 Flow diagram of the systematic review.

excluded.

By reading titles and abstracts, we excluded 30 records. By reading the full texts of the 28 remaining articles, we identified 18 papers meeting our inclusion criteria and therefore included in the qualitative synthesis (Figure 1).

Biostatistics

Statistics were performed by Dr. Gianna Sepede, who has a certificated experience in Biomedical Statistics, Systematic Reviews and Meta-analysis. In the present paper, PRISMA 2009 checklist (http://www.prisma-statement.org/) was used to describe eligibility criteria, conduct the search, select the studies and report the qualitative synthesis results. Statistical methods were therefore adequately described, correct and conducted on homogeneous data. Number of subjects and dropouts were given. When appropriate, confidence limits and significant *P* values were calculated and reported.

RESULTS

We found 18 papers fulfilling our inclusion criteria, all published from 2009 to 2015[17-35]. The studies were all conducted in the Asian Continent (China, South Korea, Taiwan), with the only exception of the paper published by Lorenz *et al*[23], which was conducted in Germany.

In total, 666 subjects were tested by the 18 studies included in the qualitative synthesis: 347 patients with IAD (IADp), 304 normal comparisons (NC) and 15 subjects with Alcohol Use Disorder (AUDp) The large majority of IADp were male (*n* = 331, 95.4%) and very young (mean age ranged from 21 to 25 year). The number of patients involved in each study ranged from 8 to 74. For what regards the subtypes of IAD, 15 out of 18 studies focused on IGD[19-24,26-34], so more than 85% of all the IADp (*n* = 297) were IGD patients (IGDp). Different diagnostic criteria were used to assess IAD, such as Beard's Diagnostic criteria for Internet addiction[35], Ko's diagnostic criteria of Internet addiction for college students[36], Chinese Internet addiction test (C-IAT)[37] and Grüsser and Thalemann's computer game addiction criteria[38].

The most used questionnaire to assess the severity of IAD was the Young's IAT[1], with different cut-off (usually > 80, in a few studies > 50). To diagnose IGD, online gaming was also required to be the principal Internet activity (more than 80% of the time spent online or more than 30 h/wk).

In order to exclude subjects with comorbid psychiatric conditions or substance use disorders, structured interviews and psychometric scales to address depression, anxiety, impulsivity, substance addiction were usually provided.

MRI data were acquired with a 3 T scanner in 17 studies, and with a 1.5 T scanner in one study[19]. In 4 articles, only resting state fMRI was recorded, whereas 13 articles reported task related fMRI data, and one paper acquired both resting state and task related functional activations[31]. Seventeen studies were transversal observational reports, whereas the paper by Han *et al*[19] was a 6-wk longitudinal study.

The participants in the 18 selected studies were all free of any psychopharmacological treatment at the moment of the scanning (and at study enter for the above mentioned longitudinal study).

Resting state fMRI studies on IAD

A total number of five studies were selected[18,21,31,32,34]. The characteristic of the groups and the results of the studies are reported in Table 1. Right-handedness was an inclusion criterion in 4 studies[18,21,31,34], as well as male gender[21,31,32,34]. A total number of 298 subjects (Males *n* = 280, 94%), all medication free, were involved: 159 IADp (140 IGDp), 124 NC and 15 AUDp. Patients were usually very young (mean age ranging from 21 to 24 years).

In all the five selected studies, fMRI images were acquired using a 3 T scanner and scan duration ranged from 7 to 9 min. Resting state functional connectivity (RsFc) and/or Regional Homogeneity (ReHo) were calculated to assess between group differences. As a result, all the selected studies identified significant differences between patients and controls.

Liu *et al*[18], in their research on 19 IAD patients, reported an increased synchronization among frontal areas, cingulate gyrus, temporal and occipital regions, cerebellum and brain stem, with respect to matched normal comparisons. So the authors suggested an altered functional connectivity in regions belonging

Table 1 Resting state functional magnetic resonance imaging studies in internet addiction disorder

Ref.	Design and aims	Participants	Diagnostic criteria and evaluation scales	fMRI methods	fMRI results
Liu *et al*[18]	Resting state fMRI study Aim: To analyze encephalic functional characteristic of IAD under resting state	*n* = 38, age range 18-25 yr Medication free 100% Right-handed 100% Normal neurological examination 100% No comorbid psychiatric disorders Groups: IGA *n* = 19 Mean age: 21.0 ± 1.3 yr Males *n* = 11 (57.9%) NC *n* = 19 (50%) Mean age: 20.0 ± 1.8 yr Males *n* = 11 (57.9%)	IAD: Beard's DQIA "5 + 1 criteria" plus any one of: ⩾ 6 h/d for 3 mo Decline in academic performance Unable to maintain normal school learning	Scanner: 3 T FMRI Scan duration: 9 min Software used: SPM2 ReHo measured by means of KCC Signal analyzed: BOLD Both whole brain and ROI based analysis	Between group significant effects: ReHo IAD > NC in: Cerebellum, brainstem, R CG, bilateral PH, R FL, L SFG, L precuneus, R PoCG, R MOG, R ITG, L STG, MTG
Dong *et al*[21]	Resting state fMRI study Aim: To investigate the effects of long-time online game playing on visual and auditory brain regions	*n* = 29, age 24.2 ± 3.8 yr Males 100% Medication free 100% Right-handed 100% No nicotine, cocaine or marijuana use Groups: IGD *n* = 15; Age 24.2 ± 3.5 yr NC *n* = 14; Age 24.6 ± 3.8 yr	IGD: YIAT ⩾ 80 > 80% of the online time was spent playing videogames BDI < 5; MINI: No Axis Ⅰ psychiatric disorders	Scanner: 3 T FMRI Scan duration: 9 min Software used: DPARSF; ReHo measured by means of KCC; Signal analyzed: BOLD; Both whole brain and ROI based analysis Seed based connectivity analysis	Between group significant effects: ReHo IGA > NC in: Bilateral brainstem, bilateral IPL, L posterior cerebellum, L MiFG; IGA < NC in: L STG, L ITG, L OL, L PL
[1]Dong *et al*[31]	Resting-state and task related fMRI Aim: To examine the Fc of ECN during both resting state and Stroop task performing	*n* = 71 Age 22.35 Males 100% Medication free 100% Right-handed 100% No DSM 5 psychiatric disorders Groups: IGD *n* = 35 Age 22.2 ± 3.8 yr NC *n* = 36 Age 22.8 ± 2.4 yr	IGD: Young's IAT ⩾ 50 > 80% of the online time was spent playing videogames BDI < 5 MINI: No Axis Ⅰ psychiatric disorders	Scanner: 3 T Rs fMRI Scan duration: 7 min Software used: REST, DPARSF, SPM8, FSL Signal analyzed: BOLD Whole brain analysis	Between group significant effects: RsFc IGD < NC in: Total ECN and L ECN
Kim *et al*[32]	Resting state fMRI study Aim: To compare the brain functioning of IGD, AUD, and NC during resting state	*n* = 45 Males 100% Medication free 100% Groups: IGD *n* = 16 Age 21.6 ± 5.9 yr AUD *n* = 14 Age 28.6 ± 5.9 yr NC *n* = 15 Age 25.4 ± 5.9 yr IGD were significantly younger than AUD (P < 0.01)	For all participants: WAIS Ⅲ ⩾ 80 For IGD: YIAT ⩾ 70 > 4.5 h/d were spent playing online For AUD: SCID criteria AUDIT-K < 2 h/d were spent online Other scales administered to all subjects: BDI: IGD and AUD > NC (P < 0.01) BAI: AUD > NC (P < 0.01) BIS-11: IGD and AUD > NC (P < 0.01)	Scanner: 3 T Rs fMRI Scan duration: 8 min Software used: DPARSF, SPM8, REST ReHo measured by means of KCC Signal analyzed: BOLD Whole brain analysis	Between group significant effects: ReHo (1) IGD *vs* NC IGD > NC in L PCC IGD < NC in R STG (2) IGD *vs* AUD IGD < NC in R STG (3) AUD *vs* NC AUD > NC in R PCC, R insula, L MTG AUD < NC in R ACC
Zhang *et al*[34]	Resting state fMRI study fMRI in young adults with Internet gaming disorder using rsFC Aim: To study resting-state functional connectivity of the insula in IGD	*n* = 115 Males 100%; Medication free 100% Right-handed 100%; Groups: IGD *n* = 74 age 22.3 ± 2 yr; *n* = 57 alcohol drinkers *n* = 8 cigarette smokers NC *n* = 41; age 23.0 ± 2.1 yr *n* = 29 alcohol drinkers	IGD: CIAS ⩾ 67 Internet gaming > 14 h/wk for 1 yr Playing as the principal online activity NC: CIAS < 60 internet gaming < 2 h/wk Other scales: FTND BDI: IGD > NC	Scanner: 3 T Rs fMRI Scan duration: 7 min Software used: DPABI, REST, SPM8 Signal analyzed: BOLD Seed based connectivity analysis	Between group significant effects: RsFC; L anterior insula IGD > NC in R putamen, R angular gyrus, IFG R anterior insula; IGD > NC in ACC, middle CG, L angular gyrus, L precuneus, Bilateral SFG and STG L posterior insula IGD > NC in bilateral PoCG, L

	Cigarette use and frequency of alcohol use were higher in IGD with respect to NC ($P < 0.05$ and $P < 0.01$) No comorbid psychiatric disorders	($P < 0.001$); BAI: IGD > NC ($P < 0.01$)	precentral gyrus, R SMA, STG; R posterior insula; IGD > NC in bilateral STG

[1]Only resting state results are showed. AUD: Alcohol use disorder; IAD: Internet addiction disorder; IGD: Internet gaming disorder; NC: Normal controls; AUDIT-K: Korean version of alcohol use disorder identification test; BAI: Beck anxiety inventory; BDI: Beck depression inventory; BIS-11: Barratt impulsiveness scale-version 11; CIAS: Chen internet addiction scale; DQIA: Beard's diagnostic questionnaire for internet addiction; FTND: Fagerstrom test for nicotine dependence; MINI: Mini international neuropsychiatric interview; SCID: Structured clinical interview for DSM-IV; YIAT: Young's internet addiction test; WAIS: Wechsler adult intelligence scale; DPARSF: Data processing assistant for resting-state fMRI; KCC: Kendall's coefficient of concordance; ReHo: Regional homogeneity; RsFC: Resting state functional connectivity; SPM: Statistical parametric mapping; R: Right; L: Left; ACC: Anterior cingulate cortex; CG: Cingulate gyrus; ECN: Executive control network; FL: Frontal lobe; IFG: Inferior frontal gyrus; IPL: Inferior parietal lobule; ITG: Inferior temporal gyrus; MiFG: Middle frontal gyrus; MOG: Middle occipital gyrus; MTG: Middle temporal gyrus; OL: Occipital lobe; PCC: Posterior cingulate cortex; PH: Parahippocampus; PL: Parietal lobe; PoCG: Postcentral gyrus; SFG: Superior frontal gyrus; SMA: Supplementary motor area; STG: Superior temporal gyrus.

to the reward system of the brain. All the four papers focused on IGD patients[21,31,32,34] reported significant between group effects. Dong *et al*[21] observed that, when compared to controls, IGD patients showed an enhanced ReHo in sensorimotor coordination areas (brainstem, cerebellum, bilateral inferior parietal lobule, and left middle frontal gyrus), and a reduced ReHO in left-sided visual and auditory cortex. In a larger sample of IGD patients, Dong and colleagues[31] observed a reduced functional connectivity in areas belonging to the Executive Control Network, especially in the left hemisphere: Ventromedial prefrontal cortex, dorsolateral prefrontal cortex and parietal cortex.

In a recent study, Kim *et al*[32] compared the resting state brain functioning of IGD patients not only with healthy subjects, but also with a group of AUD patients, looking for similarities and differences between these two "addictive conditions". As a result, they found that both IGD and AUD shared an augmented ReHo in posterior cingulate cortex with respect to healthy controls, whereas a reduced ReHo in the right superior temporal gyrus was observed in the IGD patients only. The authors also reported a negative correlation between the left inferior temporal cortex and the level of impulsivity.

To assess the role of the insular cortex in IGD, Zhang *et al*[34] conducted a seed-based resting state connectivity study in 74 patients with IGD and compared them with 41 normal controls. IGD patients exhibited enhanced rsFC between the anterior insula and anterior cingulate cortex, precuneus, angular gyrus and basal ganglia (all areas involved in cognitive control, salience, attention and craving). When analyzing the posterior part of the insula, they found an augmented rsFC in areas playing a key role in sensory-motor integration, such as post central and precentral gyrus, supplementary motor area and superior temporal gyrus. Moreover, they observed a positive correlation between the insula-superior temporal gyrus connectivity and the level of IGD severity.

Summarizing the rsfMRI studies, the more relevant abnormalities observed in IGD were localized in the superior temporal gyrus. Other important alterations were detected in limbic areas, medial frontal regions (anterior cingulate cortex, supplementary motor area) and parietal regions. Results in not gaming IAD were limited due to the small number of patients involved ($n = 19$) and reported altered functioning in reward-related brain regions (frontal, parietal, temporal regions, cingulated gyrus, brain stem and cerebellum).

Task-related fMRI studies on IAD

We found 14 studies reporting task-related neural correlates of IAD[17,19,20,22-31,33]. The characteristic of the groups and the results of the studies are reported in Table 2. Right-handedness was an inclusion criterion in all but two studies[19,23]. Only male participants were included in 13 studies, whereas a mixed gender sample was enrolled by Liu *et al*[33] (2015).

A total number of 368 subjects (males $n = 352$, 95.6%: Mean age ranging from 21 to 25 years) were involved: 188 IADs (IGDs $n = 157$) and 180 NC. Participants were all medication free at the moment of the scanning and at study enter for the longitudinal study by Han *et al*[19]. FMRI images were acquired using a 3 T scanner and scan duration ranged from 5 to 30 min.

The paradigms administered to the participants were: cue-reactivity tasks (three studies)[17,19,33], guessing tasks (three studies)[20,25,26] or cognitive control tasks of different kinds (eight studies)[22-24,27-31]. In more than half of the studies[20,22,24,27,28,30,31,33] no behavioral differences were found between cases and controls, but all of them reported significant group effects in functional activation of several brain regions, especially orbitofrontal gyrus, anterior cingulate cortex, insula, dorsolateral prefrontal cortex, precuneus, posterior cingulate cortex and superior temporal gyrus.

In cue-reactivity paradigms, addicted subjects are exposed to stimuli designed to elicit a craving for substance or behavior: In case of IAD, *i.e.*, viewing images or videos related to videogames or Internet scenarios[17,39,40].

In probabilistic guessing tasks, participants are required to bet on different outcomes (*i.e.*, on cards, dices, colors) and their brain response to win or loss

Table 2 Task related functional magnetic resonance imaging studies on internet addiction disorder

Ref.	Design and aims	Participants	Diagnostic criteria and evaluation scales	Task and behavioral results	fMRI methods	fMRI results
Ko *et al*[17]	Task related fMRI study Aim: To identify the neural substrates of IGD by means of a cue-reactivity paradigm	*n* = 20; Males 100% Medication free 100% Right-handed 100% Normal neurological examination 100% No comorbid psychiatric disorders or substance use Groups: IGD *n* = 10 Mean age: 22 ± 1.5 yr NC *n* = 10 Mean age: 22.7 ± 1.3 yr	DCIA-C MINI CIAS AUDIT FTND Gaming craving scale For IGD: Addiction to World of Warcraft Playing > 30 h/wk	Task used: Cue-reactivity paradigm. Task design: Videogame viewing Behavioral results: Gaming craving: IGD > NC	Scanner: 3 T fMRI scan duration: 4.8 min Acquisition method: Block design Software used: SPM2 Signal analyzed: BOLD Whole brain and ROI based analysis	Between group significant effects: IGD > NC in: R OFC, R basal ganglia (caudatum and accumbens), bilateral ACC, bilateral MFG, R DLPFC
Han *et al*[19]	Six-week open label pharmacological study with task related fMRI acquisition Aim: To evaluate the efficacy of bupropion SR in reducing game craving and influencing brain activity in IGD	*n* = 19; Males 100% Medication free (at study enter) 100% Normal neurological examination 100% No comorbid psychiatric disorders or substance use disorders Groups: IGD *n* = 11 Mean age: 21.5 ± 5.6 yr Study treatment: Bupropion SR for 6 wk NC *n* = 8 Mean age: 20.3 ± 4.1 yr	SCID BDI < 17 7 point Gaming Craving VAS For IGD: YIAT > 50 Playing > 4 h/d and 30 h/wk Addiction to star craft	Task used: Cue-reactivity paradigm. Task design: Videogame viewing Behavioral results: Gaming craving: IGD > NC Bupropion effects in the IGD group: Significant decreases of: Craving (23.6%, *P* = 0.04) Playing game time (35.4%, *P* = 0.01) YIAT scores (15.4%, *P* = 0.01)	Scanner: 1.5 T fMRI scan duration: 7.5 min Acquisition method: Block design Software used: Brain voyager Signal analyzed: BOLD Acquisition time: (1) At study enter (baseline); (2) After 6 wk of Bupropion treatment Whole brain analysis	Between group significant effects: At baseline: (1) IGD > NC in: L occipital lobe, cuneus, L DLPFC, L PH After 6 wk of Bupropion treatment on IGD: (2) Significant decreased activation in L DLPFC
Dong *et al*[20]	Task related fMRI study Aim: To investigate reward and punishment processing in IGD during a guessing task	*n* = 27; Males 100% Medication free 100% Right-handed 100% Normal neurological examination 100% No comorbid psychiatric disorders or substance use disorders	MINI For IGD: YIAT > 80 C-IAT criteria Spending most of their time playing online Internet games For NC: YIAT < 20	Task used: Guessing task Task design: Two-choices gain or loss guessing task Behavioral results: No between group significant differences in accuracy and reaction times	Scanner: 3 T fMRI scan duration: 16.3 min Acquisition method: Block design Software used: SPM5 Signal analyzed: BOLD	Between group significant effects: In WIN condition: IGD > NC in L OFC (BA 11) In LOSS condition: NC > IGD in ACC

		Groups: IGD n = 14 Mean age: 23.4 ± 3.3 yr NC n = 13 Mean age: 24.1 ± 3.2 yr			Whole brain analysis	
Dong *et al*[22]	Task related fMRI study Aim: To identify the neural correlates of response inhibition in individuals with and without IGD	n = 24; Males 100% Medication free 100% Right-handed 100% No comorbid psychiatric disorders or substance use disorders Non smokers 100% Groups: IGD n = 12 Mean age: 23.6 ± 3.5 yr NC n = 12 Mean age: 24.2 ± 3.1 yr	For all participants: BDI < 13 For IGD: YIAT > 80 C-IAT criteria Spending most of their time playing online Internet games YIAT < 20	Task used: Cognitive control task Task design: Three-choices color-word Stroop task Behavioral results: No between group significant differences	Scanner: 3 T fMRI scan duration: 12 min Acquisition method: Event-related design Software used: SPM5 Signal analyzed: BOLD Whole brain analysis	Between group significant effects: During Stroop effect: IGD > HC in: ACC, PCC, L insula, MiFG, MFG, L thalamus, R IFG, R SFG
Lorenz *et al*[23]	Task related fMRI study Aim: To assess neural correlates of attentional bias and cue reactivity in IGD	n = 17; Males 100% Groups: IGD n = 8 Mean age: 25 ± 7.4 yr NC n = 9 Mean age: 24.8 ± 6.9 yr	World of warcraft addiction inventory CSVK Vocabulary test (WST-IQ) Test of attention Social interaction anxiety scale STAI BDI BIS 11 Iowa Gambling test For IGD: ≥ 3 Grüsser and Thalemann's criteria for computer game addiction	Task used: Attentional bias/cue reactivity task Task design: Two-choice dot probe paradigm during SP and LP trials Stimulus class: (1) IAPS based emotional images (neutral and positive valences) (2) Computer generated stimuli (neutral images and World of Warcraft based images) Behavioral results: In SP trials: IGD: RT congruent < RT incongruent	Scanner: 3 T fMRI scan duration: 30 min Acquisition method: Block design Software used: SPM8b Signal analyzed: BOLD Whole brain analysis Connectivity analysis: Post hoc PPI, using R IFG as seed region	Between group significant effects During SP trials IGD > NC in bilateral ACC, R MPFC, L OFC, L PH, MTG, precuneus, cerebellum, R amygdala During LP trials IGD > NC in: R IFG, R Hippocampus, bilateral lingual gyrus and R calcarine gyrus PPI results: IGD > NC in connectivity between R IFG and: IFG, orbital gyrus, MFG, MTG, MOG, STG, ITG, Angular gyrus, precuneus, basal ganglia
Dong *et al*[24]	Task related fMRI study Aim: To investigate error-monitoring ability in IGD	n = 30; Males 100% Medication free 100% Right-handed 100% Non smokers 100%	MINI For IGD YIAT > 80 Spending > 80% of their time online playing games	Task used: Cognitive control task Task design: Three-choices color-word Stroop task Focus: Error monitoring Behavioral results: No significant between	Scanner: 3 T fMRI scan duration: 12 min Acquisition method: Event-related design Software used: SPM8	Between group significant effects During correct responses: IGD < NC in OFC and ACC During incorrect responses: IGD > NC in ACC

		No comorbid psychiatric disorders or substance use disorders Groups: IGD n = 15 Mean age: 23.8 ± 3.7 yr NC n = 15 Mean age: 24.1 ± 3.3 yr	For NC: YIAT < 30	group effects	Signal analyzed: BOLD Whole brain analysis	
Dong *et al*[25]	Task related fMRI study Aim: To investigate brain correlates of decision-making in IAD	n = 31; Males 100% Medication free 100% Right-handed 100% No comorbid psychiatric disorders or substance use disorders Groups: IAD n = 16 Mean age 21.4 ± 3.1 yr NC n = 15 Mean age: 22.1 ± 3.6 yr	MINI BDI < 5 For IAD: YIAT > 80 For NC: YIAT < 30	Task used: Guessing task Task design: Two-choices gain or loss guessing task Behavioral results: In LOSS condition: RT IAD > NC	Scanner: 3 T fMRI scan duration: 21 min Acquisition method: Block design Software used: SPM5 Signal analyzed: BOLD Whole brain analysis	Between group significant effects In WIN condition: IAD > NC in: ACC, insula and IFG IAD < NC in: PCC and caudatum In LOSS condition: IAD > NC in: Inferior CG IAD < NC in: PCC
Dong *et al*[26]	Task related fMRI study Aim: To investigate reward/punishment sensitivities in IGD during a guessing task	n = 31; Males 100% Medication free 100% Right-handed 100% No comorbid psychiatric disorders or substance use disorders Groups: IGD n = 16 Mean age 21.4 ± 3.1 yr NC n = 15 Mean age: 22.1 ± 3.6 yr	MINI BDI < 5 For IGD: YIAT > 80 Spending > 80% of their time online playing games For NC: YIAT < 30	Task used: Guessing task Task design: Two-choices gain or loss guessing task No behavioral response was required Post scanning self-report questionnaire (1) On subjective experiences During LOSS condition: IGD < NC in reporting negative emotions (2) On craving for win: IGD > NC in both WIN and LOSS conditions	Scanner: 3 T fMRI scan duration: 21 min Acquisition method: Block design Software used: SPM5 Signal analyzed: BOLD Whole brain analysis	Between group significant effects In WIN condition: IGD > NC in L SFG In LOSS condition: IGD > NC in L SFG IGD < NC in bilateral PCC In WIN-LOSS contrast condition IGD > NC in L SFG
Dong *et al*[27]	Task related fMRI study Aim: To explore cognitive flexibility in IGD during a color-word Stroop task	n = 30; Males 100% Medication free 100% Right-handed 100%	MINI BDI < 5 For IGD: YIAT > 80	Task used: Cognitive control task Task design: Three-choices color-word Stroop task Focus: Cognitive flexibility during task switching (from easy to difficult condition and viceversa)	Scanner: 3 T fMRI scan duration: 16 min Acquisition method: Event-related design	Between group significant effects Task switching (1) From difficult to easy condition

		No comorbid psychiatric disorders or substance use disorders	Spending > 80% of their time online playing games	Behavioral results: No significant between group differences	Software used: SPM5	IGD > NC in: Bilateral insula, R STG
		Groups: IGD *n* = 15 Mean age 21.2 ± 3.2 yr NC *n* = 15 Mean age: 22.1 ± 3.6 yr	For NC: YIAT < 30		Signal analyzed: BOLD Whole brain analysis	(2) From easy to difficult condition: IGD > NC in: Bilateral precuneus, L STG, L angular gyrus
Ko *et al*[28]	Task related fMRI study	*n* = 49; Males 100%	MINI	Task used: Cognitive control task	Scanner: 3 T	Between group significant effects
	Aim: To evaluate impulsivity and brain correlates of response inhibition and error processing in IGD	Medication free 100%	CIAS	Task design: Go/No-go Task	fMRI scan duration: 15.5 min	During response inhibition
		Right-handed 100%	BIS-11	Behavioral results: No significant between group differences	Acquisition method: event-related design	IGD > NC in bilateral caudate and L OFG (BA 47)
		No comorbid psychiatric disorders or substance use disorders	Dickman's impulsivity scale		Software used: SPM5	During error processing
		Groups: IGD *n* = 26 Mean age 24.6 ± 3.2 NC *n* = 23 Mean age: 24.4 ± 2.1 yr	For IGD: Fulfilling DCIA criteria Addiction to online gaming		Signal analyzed: BOLD Whole brain and ROI based analysis	IGD < NC in R insula
Liu *et al*[29]	Task related fMRI study	*n* = 22; Males 100%	DCIA-C	Task used: Cognitive control task	Scanner: 3 T	Between group significant effects
	Aim: To investigate brain correlates of response inhibition under gaming cue distraction in IGD	Medication free 100%	MINI	Task design: Modified Go/no-go Task with gaming cue distracters	fMRI scan duration: 8.5 min	During no gaming distracting condition
		Right-handed 100%	CIAS	Behavioral results: During gaming distracting condition	Acquisition method: Block design	IGD > NC in R SPL
		No comorbid psychiatric disorders or substance use disorders	FTND < 5	Commission errors IGD > NC	Software used: SPM5	During gaming distracting condition
		Groups: IGD *n* = 11 Mean age 23.4 ± 2.3 yr NC *n* = 11 Mean age: 22.4 ± 1.7 yr			Signal analyzed: BOLD Whole brain and ROI based analysis	NC > IGD in R DLPFC, R SPL and cerebellum ROI based analysis results In IGD R DLPFC and R SPL activations were positively associated to commission errors during gaming distracting condition
Chen *et al*[30]	Task related fMRI study	*n* = 30; Males 100%	MINI	Task used: Cognitive control task	Scanner: 3 T	Between group significant effects
	Aim: To evaluate neural correlates of response inhibition among subjects with IGD	Medication free 100%	CIAS	Task design: Go/no-go Task	fMRI scan duration: 6 min	During response inhibition
		Right-handed 100%		Behavioral results: No significant between group differences	Acquisition method: Block design	NC > IGD in R SMA/pre-SMA
		No comorbid psychiatric disorders or substance use disorders	BIS-11		Software used: SPM5	

		Groups: IGD *n* = 15 Mean age 24.7 ± 3.1 yr NC *n* = 15 Mean age: 24.5 ± 2.8 yr	For IGD: Fulfilling DCIA criteria Addiction to World of Warcraft		Signal analyzed: BOLD ROI based analysis	
[1]Dong *et al*[31]	Resting-state and task related fMRI Aim: To examine the Fc of ECN during both resting state and Stroop task performing	All participants: *n* = 71 age 22.35 Participants who performed the fMRI Stroop task: *n* = 35 Males 100% Medication free 100% Right-handed 100% No DSM 5 psychiatric disorders Groups performing fMRI Stroop task: IGD n = 16 NC n = 15	IGD: YIAT ⩾ 50 > 80% of the online time was spent playing videogames BDI < 5 MINI: No Axis Ⅰ psychiatric disorders IAD	Task used: Cognitive control task Task design: Three-choices color-word Stroop task Behavioral results: No significant between group differences	Scanner: 3 T fMRI scan duration: 15 min Acquisition method: Event-related design Software used: SPM8 Signal analyzed: BOLD Whole brain and ROI based analysis	Between group significant effects During incongruent trials: IGD > NC in bilateral SFG IGD < NC in L DLPFC, ACC and left OFC
Liu *et al*[33]	Task related fMRI study Aim: To investigate brain function in IGD individuals during a cue-reactivity paradigm	*n* = 38; Males 58% Medication free 100% Right-handed 100% No comorbid psychiatric disorders or substance use disorders Groups: IGD *n* = 19 Males *n* = 11 (58%) Mean age 21.4 ± 1.0 yr NC *n* = 19 Mean age: 20.1 ± 1.1 yr Males *n* = 11 (58%)	HAM-A BDI For IGD: Beard's DQIA "5 + 1 criteria" plus any one of: ⩾ 6 h/d for 3 mo; Decline in academic performance; Unable to maintain normal school learning	Task used: Cue-reactivity paradigm. Task design: Videogame viewing No behavioral response was required	Scanner: 3 T fMRI scan duration: 7.5 min Acquisition method: Block design Software used: Brain Voyager Signal analyzed: BOLD Whole brain analysis	Between group significant effects IGD > NC in: R SPL, R precuneus, R insula, R CG, R STG, L brain stem

[1]Only task related fMRI results are showed. IAD: Internet addiction disorder; IGD: Internet gaming disorder; NC: Normal controls; AUDIT: Alcohol use disorder identification test; BDI: Beck depression inventory; BIS-11: Barratt impulsiveness scale-version 11; CIAS: Chen internet addiction scale; C-IAT: Chinese internet addiction test; CSVK: Pathological computer gaming scale; DCIA-C: Diagnostic criteria of Internet addiction for college students; FTND: Fagerstrom test for nicotine dependence; HAM-A: Hamilton anxiety scale; IAPS: International affective picture system; MINI: Mini international neuropsychiatric interview; RT: reaction times; SCID: Structured clinical interview for DSM-IV; VAS: Visual analogue scale; YIAT: Young's internet addiction test; R: Right; L: Left; ACC: Anterior cingulate cortex; CG: Cingulate gyrus; DLPFC: Dorsolateral prefrontal cortex; IFG: Inferior frontal gyrus; IPL: Inferior parietal lobule; ITG: Inferior temporal gyrus; MFG: Medial frontal gyrus; MPFC: Medial prefrontal cortex; MiFG: Middle frontal gyrus; MOG: Middle occipital gyrus; MTG: Middle temporal gyrus; OFC: Orbitofrontal cortex; PCC: Posterior cingulate cortex; PH: Parahippocampus; SMA: Supplementary motor area; SFG: Superior frontal gyrus; SPM: Statistical parametric mapping; SPL: Superior parietal lobe; STG: Superior temporal gyrus; SP: Short presentation; LP: Long presentation.

conditions can be analyzed, to evaluate reward and punishment neural systems[41].

In cognitive control tasks, participants have to choice between different conflicting responses. Stimuli can be manipulated to increase difficulty and to measure particular cognitive abilities, such as sustained attention, response inhibition, impulsivity, task switching ability and error processing. Frequently used cognitive control tasks are the Stroop tasks: Participants are required to detect only a salient characteristic of the stimuli, ignoring the others (*i.e.*, color words printed in different colored ink and participants have to ignore the word and name its color)[42]. When the different features of the stimuli are incongruent, the task difficulty increases and affects

the performance (Stroop effect)[43]. Another important category of control tasks is the "go no-go paradigm": Stimuli (*i.e.*, digits, letters, shapes) are presented in a continuous stream and participants perform a binary decision on each stimulus. One of the outcomes requires participants to make a motor response (go), whereas the other requires participants to withhold a response (no-go)[44].

When the study is focused on the influence of emotion or salience on selective attention, dot prob paradigms are frequently used: Participants view neutral or salient stimuli appearing randomly on either side of the screen, then a dot is presented in the location of one former stimulus and participants have to indicate the correct location of the dot, so an attentional bias toward salient stimuli can be detected[45,46].

Cue-reactivity task fMRI studies in IAD

In their study on 10 IGDp addicted to the videogame World of Warcraft (WOW) Ko *et al*[17] found that IGDp reported a higher gaming urge when passive viewing WOW images with respect to NC. Moreover, a significant higher activation was observed in right orbitofrontal cortex, right basal ganglia (caudatum and accumbens), bilateral anterior cingulate cortex, bilateral medial prefrontal cortex, right dorsolateral prefrontal cortex.

Han *et al*[19] conducted a six-week open label pharmacological study aiming to evaluate bupropion efficacy in reducing game craving and modulate brain activation in 11 IGDp addicted to the videogame Starcraft. At baseline, all participants were medication free and the authors observed an higher game urging and an augmented activation of left dorsolateral prefrontal cortex, L parahippocampus, left occipital lobe and cuneus in IGDp, with respect to NC during Starcraft cue presentation. After bupropion treatment, a significant decreased activation of left dorsolateral prefrontal cortex was observed in IGDp. Bupropion, being an antidepressant agent modulating dopamine and norepinephrine reuptake, was reported to be efficacious in patients with substance use disorder, with or without comorbid mood disorders[47,48] and in pathological gambling[49]. So the authors hypothesized that bupropion reduced craving in IGD by modulating dorsolateral prefrontal cortex functional activity.

In a recent study using videogame stimuli, Liu *et al*[33] (2015) enrolled a mixed-gender sample of 19 IGDp (males 58%) and reported a significant dysfunction of the frontal cortex, with increased activation in right-sided temporo-parietal and limbic regions: Superior parietal lobe, insula, cingulate gyrus and superior temporal gyrus.

Guessing task fMRI studies in IAD

To evaluate reward and punishment sensitivity in IGDp, Dong *et al*[20] simulated a gain/loss situation: Participants had to choice between two covered playing cards and at the end of the fMRI scan session they received a money sum based on their wins and losses. fMRI data analysis revealed that during win condition IGDs showed an higher activation of left orbitofrontal cortex (BA11) with respect to NC, whereas in loss condition the opposite was true for anterior cingulate cortex activation. So the authors concluded that a reduced sensitivity to negative experiences (monetary loss) and an augmented sensitivity to positive events (monetary gain) throughout an altered functioning of orbitofrontal cortex and anterior cingulate cortex could explain why IADp persisted in their habit despite the negative consequences on their everyday life.

Using a similar guessing task, Dong *et al*[25] found that IGDp were significantly slower than NC when exposed to continuous losses, whereas no behavioral group effects were observed after continuous wins. In terms of brain activations, IGDs showed a reduced activation of posterior cingulate cortex and an increased activation of inferior frontal gyrus during both win and loss conditions, whereas an augmented activation of anterior cingulate cortex and insula was observed during win condition only. These results suggested that decision-making ability was impaired in IGDp, due to a functional inefficiency in the inferior frontal gyrus (higher activation but lower behavioral performance) and a reduced involvement of posterior cingulate cortex and caudate. In the same study sample, with a modified guessing paradigm (a different control condition was added to wins and losses) Dong *et al*[26] asked the participants to describe their subjective experience after the scan section: IGDp reported higher craving for win in both continuous win and loss conditions and reduced negative emotions during loss conditions. In terms of functional activations, the results were similar, but not identical to those previously reported[25] (probably due to the different control condition): IGDp hyperactivated the left superior frontal gyrus in both wins and losses (but the level of activation was higher during wins) and hypoactivated the posterior cingulate cortex during losses. The authors concluded that superior frontal gyrus in IGDp was insensitive to negative situations and posterior cingulate cortex failed to exert its cognitive control on environmental changes.

Cognitive control task fMRI studies in IAD

In the eight cognitive controls fMRI studies we selected, Stroop tasks were used in four studies[22,24,27,31], go/no-go paradigms in three studies[28-30] and a dot/prob paradigm in one study[23].

Dong *et al*[22] enrolled 12 male, drug free and no-smokers IGDp and compared them with healthy peers during a three-choices color-word Stroop task. The groups did not differ in terms of behavioral performance, but during Stroop effect (incongruent - congruent stimuli contrast) IGDp showed a significant hyperactivation in anterior cingulate cortex, posterior cingulate cortex, left insula, middle frontal gyrus, medial frontal gyrus, left thalamus, right inferior frontal gyrus, right superior frontal gyrus.

The authors speculated that a greater activation of

posterior cingulate cortex in IGD group could indicate a failure to optimize task related attentional resources due to an incomplete disengagement of Default Mode Network. Furthermore, the hyperactivation of the anterior cingulate cortex, insula and prefrontal regions might reflect a cognitive inefficiency of fronto-limbic regions playing a key role in conflict monitoring and "top down" inhibitory control.

In a larger sample, Dong *et al*[24] administered the same Stroop paradigm with an event-related design and separately analyzed the functional correlates of correct and error responses to stimuli. IGDp and NC performed similarly, but differences emerged in activation patterns: during correct responses IGDp failed to activate anterior cingulate cortex and orbitofrontal cortex, whereas an abnormal activation of anterior cingulate cortex was observed during errors, thus suggesting an impaired error monitoring ability.

More recently, Dong *et al*[27] analyzed the cognitive flexibility of a group of IGD during a modified version of the Stroop task, adding a monetary reward for correct responses and creating easy and difficult task conditions. The two group did not significantly differ behaviorally. On the other hand, when the task switched from difficult to easy condition IGDp activated the bilateral insula and right superior temporal gyrus more than NC; when the task switched from easy to difficult condition, they hyperactivated the bilateral precuneus, left superior temporal gyrus and left angular gyrus. The authors hypothesized that an higher (and therefore less efficient) activation of limbic and temporoparietal regions playing a key role in inhibitory control and cognitive flexibility was a biomarker of IGD.

The same inhibitory control impairment was found in another study by Dong *et al*[31]. As a part of a larger resting state connectivity study, a subsample of IGDs performed a Stroop task during an event related fMRI scanning. The authors observed that during incongruent trials, IGDs showed an augmented activation of bilateral superior frontal gyrus and a reduced activation of left dorsolateral prefrontal cortex, left orbitofrontal cortex and anterior cingulate cortex, all regions implicated in executive control.

Ko *et al*[28] used a go/no-go paradigm with digit stimuli to assess response inhibition and error processing in 26 male IGDp. The authors did not found significant behavioral deficits in IGDp, with respect to NC. On the contrary, when analyzing fMRI data, they reported significant group effects: During successful response inhibition, IGDp activated the bilateral caudate and left orbitofrontal gyrus more than NC; during error committion they failed to activate the right insula. Orbitofrontal gyrus and insula are key regions in modulating inhibitory control and error processing, so the authors suggested that IGDp needed to hyperactivate the orbitofrontal gyrus to successfully perform the task and compensate for the insular hypofunction.

In a recent article, Chen *et al*[30] used a block design to analyze the functional correlates of cognitive control in IGDp by means of a short go/no-go task. Even though behaviorally intact, IGDp showed a reduced activation of supplementary motor area/pre supplementary motor area, a key region in selecting the appropriate behavior, withholding wrong responses.

Liu *et al*[29] enrolled a mixed gender sample of IGDp and used a modified go/no-go paradigm, entering gaming picture as background distracters. They observed similar group performance in the original paradigm, but more commission errors during the cue distraction condition in the IGD group. Moreover, during the original task, IGDp hyperactivated the right superior parietal lobe, whereas during the gaming distracting condition they hypoactivated right dorsolateral prefrontal cortex, right superior parietal lobe and cerebellum. A Region of Interest based analysis revealed that in IGDp the rate of commission errors was positively associated with the right dorsolateral prefrontal cortex and right superior parietal lobe activation. The authors therefore suggested that gaming cues significantly affected inhibitory control in IGDp, throughout a failure of dorsolateral prefrontal cortex and superior parietal lobe function.

A cognitive task with emotional and cue distracters was also used by Lorenz *et al*[23] in a small group of IGDp: They administered a two-choice dot probe paradigm during short (SP) and long presentation (LP) trials in order to elicit attentional bias and cue reactivity, respectively. Stimuli were International Affective Picture System based emotional images (with neutral or positive valence) and computer generated images (neutral pictures or images based on World of Warcraft videogame). IGDp showed a significant attentional bias *vs* both game related and affective pictures with positive valence. Compared to NC, IGDp showed an abnormal activation of medial prefrontal cortex, anterior cingulate cortex, left orbitofrontal cortex and amygdala during SP trials and of occipital regions, right inferior frontal gyrus and right hippocampus during LP trials. In authors' opinion, IGDp patients showed a behavioral and neural response similar to that observed in patients with substance use disorder, giving more attention to positive stimuli.

DISCUSSION

In this paper we systematically reviewed the resting state and task related fMRI studies on adult patients with IAD. All but one of the papers included in our qualitative synthesis were conducted in the Asian continent, confirming the great attention given to this potential harmful condition by Eastern governments[50].

The majority of the studies were conducted on young male IGDp (mean age $\leqslant$ 25 years), with only a few females and subjects with non-gaming Internet addiction. To avoid any confounding effects of other conditions, we included only studies conducted in subjects free of any comorbid psychiatric or substance use disorder.

Summarizing the literature findings, we highlighted

that IGDp differed from healthy comparisons in the functioning of several brain regions involved in reward and executive control/attention processing, even when they were behaviorally intact.

In particular, the most reported cortical dysfunctions were located in orbitofrontal gyrus, anterior cingulate cortex, insula, dorsolateral prefrontal cortex, superior temporal gyrus, inferior frontal gyrus, precuneus and posterior cingulate cortex, whereas for subcortical regions, functional alterations were often found in brainstem and caudate.

Orbitofrontal cortex is involved in decision-making, value-guided behaviors and reward/punishment sensitivity[51,52]: Through its multiple connections with prefrontal, limbic and sensorial regions, it estimates the potential reward of a given stimulus and the appropriate behavior in order to achieve a positive outcome. In patients with substance addiction, an altered functioning of orbitofrontal cortex has been linked to craving and impaired decision-making[53]. Anterior cingulate cortex and insular cortex are both relevant in sustained attention, conflict monitoring, error signaling[54] and processing of unpleasant stimuli[55]. They provide a hub between different cerebral systems, binding emotion to cognition[56,57]. Altered functioning of anterior cingulate cortex and insula have been found in alcohol and drug addiction[58,59].

Dorsolateral prefrontal cortex is a region involved in different cognitive tasks, such as working memory[60] and motor skill learning[61]. An abnormal activation of dorsolateral prefrontal cortex was found in heavy alcohol drinkers with respect to light drinkers during a go/no go task[62] and in pathological gamblers during a cue-reactivity task[63].

Superior temporal gyrus was found activated in the processing of audiovisual stimuli with an emotional content[64] and during task shifting[65]. A reduced activation of superior temporal gyrus was reported in cocaine addicts during a Stroop task[66].

Inferior frontal gyrus has a role in cognitive inhibition[67], target detection[68], decision making[69] and emotional processing[70]. In response to decision-making involving uncertainty and during aversive interoceptive processing, young adults with problematic use of cocaine and amphetamine exhibited a reduced inferior frontal gyrus activation with respect to both former stimulant users and healthy controls[71]. The precuneus has a pivotal role in self-consciousness, visuo-spatial imagery, episodic memory retrieval[72] and target detection during high difficulty tasks[73]. In their work on internet addicts with comorbid nicotine dependence, Ko *et al*[74] reported an increased activation of precuneus during game cue exposure in acutely ill IGDp, but not in remitted IGD.

Posterior cingulate cortex is considered part of the default mode of the brain[75] and its deactivation during high demanding cognitive tasks is seen as an expression of a reallocation of processing resources[76]. An altered function of posterior cingulate cortex and other components of Default Mode Network was reported in cocaine addicts, especially in those with chronic use[77].

The importance of brainstem in providing ascending and descending pathways between brain and body is well documented[78]. In particular, prefrontal regions and anterior cingulate cortex are deeply connected to the brainstem, so a dysfunction of this subcortical structure leads to attentional and executive impairment[79].

Caudate nucleus is involved in posture, motor control and modulation of approach/attachment behavior[80]. In response to alcohol cues, heavy alcohol users showed higher caudate activation with respect to moderate users[81].

Radiological imaging is a useful research strategy in psychiatric and neurological fields, and may be considered as a form of "molecular pathological epidemiology"[82,83], an interdisciplinary research area aiming to investigate the complex relationships among genes, environment, molecular alterations and long term outcome of clinical disorders[84].

Taken together, the results of our systematic review suggest that young adult with IGD, without any other psychiatric disorder, showed a pattern of functional brain alterations similar to those observed in substance addiction.

Altered functioning of anterior and posterior cingulate cortex, prefrontal and parietal regions, limbic areas and subcortical structures results in impaired response inhibition and abnormal sensitivity to reward and punishment. As observed in substance use disorders, patients with IAD show a reduced cognitive flexibility, more stereotyped responses and inappropriate behavior, with negative consequences on social and working life[85-87].

Limits of the study

The majority of patients enrolled in the reviewed studies were males IGDp, so the conclusions can't be extended to other subtypes of IAD or to female patients. Focusing our review on adult subjects, we excluded fMRI studies conducted on pediatric and adolescent populations.

COMMENTS

Background

Internet addiction disorder (IAD) is an impulse control disorder characterized by an uncontrolled Internet use, associated with a significant functional impairment or clinical distress. Even if it is not classified as a mental disorder in the current edition of the Diagnostic and Statistical Manual of Mental Disorders (DSM-5), it is a highly debated condition, due to its relevant prevalence among adolescents and young adults.

Research frontiers

Some of the clinical characteristics of IAD, such as loss of control, craving and withdrawal symptoms when patients are not allowed to use the Internet are similar to those observed in behavioral or substance use disorders. Therefore, in the last years several neuroimaging studies have been conducted aiming to investigate the relation between the clinical presentation of IAD and the functioning of cortical and subcortical regions involved in reward processing and cognitive control.

Innovations and breakthroughs

Neuroimaging research is nowadays a promising approach to fill the gap between the molecular basis of psychiatric disorders and their clinical manifestations. The scientific literature on debated diagnosis such as IAD is rapidly growing, so providing an updated review of the last published data may be of interest for the readers. Focusing the authors' systematic review on homogeneous study samples (only adult patients, no psychiatric comorbid conditions allowed) results of different researches can be easily compared to find similarities and discordances.

Applications

In clinical settings, patients with the same psychiatric condition often differ from one another in terms of clinical symptoms, response to pharmacological treatments and long-term outcome. Studying their brains and behaviors in details could help to provide more accurate diagnosis and treatments.

Terminology

IAD: An impulse control disorder characterized by an uncontrolled Internet use, associated with a significant functional impairment or clinical distress; IGD: A subtype of IAD, also called videogame addiction, characterized by excessive online gaming as the principal Internet activity.

Peer-review

This is a very interesting article.

REFERENCES

1 **Young KS**. Internet addiction: the emergence of a new clinical disorder. *Cyberpsychol Behav* 1998; **1**: 237-244 [DOI: 10.1089/cpb.1998.1.237]

2 American Psychiatric Association (APA) Diagnostic and statistical manual of mental disorders (5th ed). Washington, DC, 2013. Available from: URL: http://www.psychiatry.org/

3 **Cheng C**, Li AY. Internet addiction prevalence and quality of (real) life: a meta-analysis of 31 nations across seven world regions. *Cyberpsychol Behav Soc Netw* 2014; **17**: 755-760 [PMID: 25489876 DOI: 10.1089/cyber.2014.0317]

4 **Krishnamurthy S**, Chetlapalli SK. Internet addiction: Prevalence and risk factors: A cross-sectional study among college students in Bengaluru, the Silicon Valley of India. *Indian J Public Health* 2015; **59**: 115-121 [PMID: 26021648 DOI: 10.4103/0019-557X.157531]

5 **Rumpf HJ**, Vermulst AA, Bischof A, Kastirke N, Gürtler D, Bischof G, Meerkerk GJ, John U, Meyer C. Occurence of internet addiction in a general population sample: a latent class analysis. *Eur Addict Res* 2014; **20**: 159-166 [PMID: 24401314 DOI: 10.1159/000354321]

6 **Choi SW**, Kim HS, Kim GY, Jeon Y, Park SM, Lee JY, Jung HY, Sohn BK, Choi JS, Kim DJ. Similarities and differences among Internet gaming disorder, gambling disorder and alcohol use disorder: a focus on impulsivity and compulsivity. *J Behav Addict* 2014; **3**: 246-253 [PMID: 25592310 DOI: 10.1556/JBA.3.2014.4.6]

7 **Bipeta R**, Yerramilli SS, Karredla AR, Gopinath S. Diagnostic Stability of Internet Addiction in Obsessive-compulsive Disorder: Data from a Naturalistic One-year Treatment Study. *Innov Clin Neurosci* 2015; **12**: 14-23 [PMID: 26000201]

8 **Wölfling K**, Beutel ME, Dreier M, Müller KW. Bipolar spectrum disorders in a clinical sample of patients with Internet addiction: hidden comorbidity or differential diagnosis? *J Behav Addict* 2015; **4**: 101-105 [PMID: 26132914 DOI: 10.1556/2006.4.2015.011]

9 **Tonioni F**, Mazza M, Autullo G, Cappelluti R, Catalano V, Marano G, Fiumana V, Moschetti C, Alimonti F, Luciani M, Lai C. Is Internet addiction a psychopathological condition distinct from pathological gambling? *Addict Behav* 2014; **39**: 1052-1056 [PMID: 24630825 DOI: 10.1016/j.addbeh.2014.02.016]

10 **Walton E**, Turner JA, Ehrlich S. Neuroimaging as a potential biomarker to optimize psychiatric research and treatment. *Int Rev Psychiatry* 2013; **25**: 619-631 [PMID: 24151806 DOI: 10.3109/09540261.2013.816659]

11 **Bullmore E**. The future of functional MRI in clinical medicine. *Neuroimage* 2012; **62**: 1267-1271 [PMID: 22261374 DOI: 10.1016/j.neuroimage.2012.01.026]

12 **Mitterschiffthaler MT**, Ettinger U, Mehta MA, Mataix-Cols D, Williams SC. Applications of functional magnetic resonance imaging in psychiatry. *J Magn Reson Imaging* 2006; **23**: 851-861 [PMID: 16652410]

13 **van den Heuvel MP**, Hulshoff Pol HE. Exploring the brain network: a review on resting-state fMRI functional connectivity. *Eur Neuropsychopharmacol* 2010; **20**: 519-534 [PMID: 20471808 DOI: 10.1016/j.euroneuro.2010.03.008]

14 **Sava S**, Yurgelun-Todd DA. Functional magnetic resonance in psychiatry. *Top Magn Reson Imaging* 2008; **19**: 71-79 [PMID: 19363430 DOI: 10.1097/RMR.0b013e318184187c]

15 **Greicius M**. Resting-state functional connectivity in neuropsychiatric disorders. *Curr Opin Neurol* 2008; **21**: 424-430 [PMID: 18607202 DOI: 10.1097/WCO.0b013e328306f2c5]

16 **Honey GD**, Fletcher PC, Bullmore ET. Functional brain mapping of psychopathology. *J Neurol Neurosurg Psychiatry* 2002; **72**: 432-439 [PMID: 11909899]

17 **Ko CH**, Liu GC, Hsiao S, Yen JY, Yang MJ, Lin WC, Yen CF, Chen CS. Brain activities associated with gaming urge of online gaming addiction. *J Psychiatr Res* 2009; **43**: 739-747 [PMID: 18996542 DOI: 10.1016/j.jpsychires.2008.09.012]

18 **Liu J**, Gao XP, Osunde I, Li X, Zhou SK, Zheng HR, Li LJ. Increased regional homogeneity in internet addiction disorder: a resting state functional magnetic resonance imaging study. *Chin Med J* (Engl) 2010; **123**: 1904-1908 [PMID: 20819576]

19 **Han DH**, Hwang JW, Renshaw PF. Bupropion sustained release treatment decreases craving for video games and cue-induced brain activity in patients with Internet video game addiction. *Exp Clin Psychopharmacol* 2010; **18**: 297-304 [PMID: 20695685 DOI: 10.1037/a0020023]

20 **Dong G**, Huang J, Du X. Enhanced reward sensitivity and decreased loss sensitivity in Internet addicts: an fMRI study during a guessing task. *J Psychiatr Res* 2011; **45**: 1525-1529 [PMID: 21764067 DOI: 10.1016/j.jpsychires.2011.06.017]

21 **Dong G**, Huang J, Du X. Alterations in regional homogeneity of resting-state brain activity in internet gaming addicts. *Behav Brain Funct* 2012; **8**: 41 [PMID: 22901705 DOI: 10.1186/1744-9081-8-41]

22 **Dong G**, Devito EE, Du X, Cui Z. Impaired inhibitory control in 'internet addiction disorder': a functional magnetic resonance imaging study. *Psychiatry Res* 2012; **203**: 153-158 [PMID: 22892351 DOI: 10.1016/j.pscychresns.2012.02.001]

23 **Lorenz RC**, Krüger JK, Neumann B, Schott BH, Kaufmann C, Heinz A, Wüstenberg T. Cue reactivity and its inhibition in pathological computer game players. *Addict Biol* 2013; **18**: 134-146 [PMID: 22970898 DOI: 10.1111/j.1369-1600.2012.00491.x]

24 **Dong G**, Shen Y, Huang J, Du X. Impaired error-monitoring function in people with Internet addiction disorder: an event-related fMRI study. *Eur Addict Res* 2013; **19**: 269-275 [PMID: 23548798 DOI: 10.1159/000346783]

25 **Dong G**, Hu Y, Lin X, Lu Q. What makes Internet addicts continue playing online even when faced by severe negative consequences? Possible explanations from an fMRI study. *Biol Psychol* 2013; **94**: 282-289 [PMID: 23933447 DOI: 10.1016/j.biopsycho.2013.07.009]

26 **Dong G**, Hu Y, Lin X. Reward/punishment sensitivities among internet addicts: Implications for their addictive behaviors. *Prog Neuropsychopharmacol Biol Psychiatry* 2013; **46**: 139-145 [PMID: 23876789 DOI: 10.1016/j.pnpbp.2013.07.007]

27 **Dong G**, Lin X, Zhou H, Lu Q. Cognitive flexibility in internet addicts: fMRI evidence from difficult-to-easy and easy-to-difficult switching situations. *Addict Behav* 2014; **39**: 677-683 [PMID: 24368005 DOI: 10.1016/j.addbeh.2013.11.028]

28 **Ko CH**, Hsieh TJ, Chen CY, Yen CF, Chen CS, Yen JY, Wang PW, Liu GC. Altered brain activation during response inhibition and error processing in subjects with Internet gaming disorder: a functional magnetic imaging study. *Eur Arch Psychiatry Clin Neurosci* 2014; **264**: 661-672 [PMID: 24469099 DOI: 10.1007/

s00406-013-0483-3]
29 **Liu GC**, Yen JY, Chen CY, Yen CF, Chen CS, Lin WC, Ko CH. Brain activation for response inhibition under gaming cue distraction in internet gaming disorder. *Kaohsiung J Med Sci* 2014; **30**: 43-51 [PMID: 24388058 DOI: 10.1016/j.kjms.2013.08.005]
30 **Chen CY**, Huang MF, Yen JY, Chen CS, Liu GC, Yen CF, Ko CH. Brain correlates of response inhibition in Internet gaming disorder. *Psychiatry Clin Neurosci* 2015; **69**: 201-209 [PMID: 25047685 DOI: 10.1111/pcn.12224]
31 **Dong G**, Lin X, Potenza MN. Decreased functional connectivity in an executive control network is related to impaired executive function in Internet gaming disorder. *Prog Neuropsychopharmacol Biol Psychiatry* 2015; **57**: 76-85 [PMID: 25445475 DOI: 10.1016/j.pnpbp.2014.10.012]
32 **Kim H**, Kim YK, Gwak AR, Lim JA, Lee JY, Jung HY, Sohn BK, Choi SW, Kim DJ, Choi JS. Resting-state regional homogeneity as a biological marker for patients with Internet gaming disorder: A comparison with patients with alcohol use disorder and healthy controls. *Prog Neuropsychopharmacol Biol Psychiatry* 2015; **60**: 104-111 [PMID: 25689820 DOI: 10.1016/j.pnpbp.2015.02.004]
33 **Liu J**, Li W, Zhou S, Zhang L, Wang Z, Zhang Y, Jiang Y, Li L. Functional characteristics of the brain in college students with internet gaming disorder. *Brain Imaging Behav* 2015; Epub ahead of print [PMID: 25763841]
34 **Zhang JT**, Yao YW, Li CS, Zang YF, Shen ZJ, Liu L, Wang LJ, Liu B, Fang XY. Altered resting-state functional connectivity of the insula in young adults with Internet gaming disorder. *Addict Biol* 2015; Epub ahead of print [PMID: 25899520 DOI: 10.1111/adb.12247]
35 **Beard KW**, Wolf EM. Modification in the proposed diagnostic criteria for Internet addiction. *Cyberpsychol Behav* 2001; **4**: 377-383 [PMID: 11710263]
36 **Ko CH**, Yen JY, Chen SH, Yang MJ, Lin HC, Yen CF. Proposed diagnostic criteria and the screening and diagnosing tool of Internet addiction in college students. *Compr Psychiatry* 2009; **50**: 378-384 [PMID: 19486737]
37 **Wang WZ**, Tao R, Niu YJ, Chen Q, Jia J, Wang XL, Kong QM, Tian CH. Preliminarily proposed diagnostic criteria of pathological Internet use. *Chinese Ment Health J* 2009; **23**: 890e4
38 **Grüsser SM**, Thalemann CN. Verhaltenssucht: Diagnostik, Therapie, Forschung. Bern: Huber, 2006
39 **Franken IH**. Drug craving and addiction: integrating psychological and neuropsychopharmacological approaches. *Prog Neuropsychopharmacol Biol Psychiatry* 2003; **27**: 563-579 [PMID: 12787841]
40 **Wilson SJ**, Sayette MA, Fiez JA. Prefrontal responses to drug cues: a neurocognitive analysis. *Nat Neurosci* 2004; **7**: 211-214 [PMID: 15001989]
41 **Reuter J**, Raedler T, Rose M, Hand I, Gläscher J, Büchel C. Pathological gambling is linked to reduced activation of the mesolimbic reward system. *Nat Neurosci* 2005; **8**: 147-148 [PMID: 15643429]
42 **MacLeod CM**. Half a century of research on the Stroop effect: an integrative review. *Psychol Bull* 1991; **109**: 163-203 [PMID: 2034749]
43 **Stroop JR**. Studies of interference in serial verbal reactions. *J Exp Psychol* 1935; **18**: 643-662 [DOI: 10.1037/h0054651]
44 **Hester R**, Fassbender C, Garavan H. Individual differences in error processing: a review and reanalysis of three event-related fMRI studies using the GO/NOGO task. *Cereb Cortex* 2004; **14**: 986-994 [PMID: 15115734]
45 **Bradley B**, Field M, Mogg K, De Houwer J. Attentional and evaluative biases for smoking cues in nicotine dependence: component processes of biases in visual orienting. *Behav Pharmacol* 2004; **15**: 29-36 [PMID: 15075624]
46 **MacLeod C**, Mathews A, Tata P. Attentional bias in emotional disorders. *J Abnorm Psychol* 1986; **95**: 15-20 [PMID: 3700842]
47 **Castells X**, Casas M, Pérez-Mañá C, Roncero C, Vidal X, Capellà D. Efficacy of psychostimulant drugs for cocaine dependence. *Cochrane Database Syst Rev* 2010; (**2**): CD007380 [PMID: 20166094]
48 **Sepede G**, Di lorio G, Lupi M, Sarchione F, Acciavatti T, Fiori F, Santacroce R, Martinotti G, Gambi F, Di Giannantonio M. Bupropion as an add-on therapy in depressed bipolar disorder type I patients with comorbid cocaine dependence. *Clin Neuropharmacol* 2014; **37**: 17-21 [PMID: 24434527 DOI: 10.1097/WNF.0000000000000011]
49 **Dannon PN**, Lowengrub K, Musin E, Gonopolski Y, Kotler M. Sustained-release bupropion versus naltrexone in the treatment of pathological gambling: a preliminary blind-rater study. *J Clin Psychopharmacol* 2005; **25**: 593-596 [PMID: 16282845]
50 **Ahn DH**. Korean policy on treatment and rehabilitation for adolescents' Internet addiction in 2007 International Symposium on the Counseling and Treatment of Youth Internet Addiction. Seoul, Korea, National Youth Commission, 2007: 49
51 **Rangel A**, Camerer C, Montague PR. A framework for studying the neurobiology of value-based decision making. *Nat Rev Neurosci* 2008; **9**: 545-556 [PMID: 18545266]
52 **Rolls ET**, Grabenhorst F. The orbitofrontal cortex and beyond: from affect to decision-making. *Prog Neurobiol* 2008; **86**: 216-244 [PMID: 18824074 DOI: 10.1016/j.pneurobio.2008.09.00]
53 **London ED**, Ernst M, Grant S, Bonson K, Weinstein A. Orbitofrontal cortex and human drug abuse: functional imaging. *Cereb Cortex* 2000; **10**: 334-342 [PMID: 10731228]
54 **Bush G**, Luu P, Posner MI. Cognitive and emotional influences in anterior cingulate cortex. *Trends Cogn Sci* 2000; **4**: 215-222 [PMID: 10827444]
55 **Petrovic P**, Pleger B, Seymour B, Klöppel S, De Martino B, Critchley H, Dolan RJ. Blocking central opiate function modulates hedonic impact and anterior cingulate response to rewards and losses. *J Neurosci* 2008; **28**: 10509-10516 [PMID: 18923027]
56 **Kühn S**, Gallinat J. Common biology of craving across legal and illegal drugs - a quantitative meta-analysis of cue-reactivity brain response. *Eur J Neurosci* 2011; **33**: 1318-1326 [PMID: 21261758]
57 **Kurth F**, Zilles K, Fox PT, Laird AR, Eickhoff SB. A link between the systems: functional differentiation and integration within the human insula revealed by meta-analysis. *Brain Struct Funct* 2010; **214**: 519-534 [PMID: 20512376 DOI: 10.1007/s00429-010-0255-z]
58 **Goldstein RZ**, Volkow ND. Drug addiction and its underlying neurobiological basis: neuroimaging evidence for the involvement of the frontal cortex. *Am J Psychiatry* 2002; **159**: 1642-1652 [PMID: 12359667]
59 **Schacht JP**, Anton RF, Myrick H. Functional neuroimaging studies of alcohol cue reactivity: a quantitative meta-analysis and systematic review. *Addict Biol* 2013; **18**: 121-133 [PMID: 22574861 DOI: 10.1111/j.1369-1600.2012.00464.x]
60 **Petrides M**. The role of the mid-dorsolateral prefrontal cortex in working memory. *Exp Brain Res* 2000; **133**: 44-54 [PMID: 10933209]
61 **Seidler RD**, Bo J, Anguera JA. Neurocognitive contributions to motor skill learning: the role of working memory. *J Mot Behav* 2012; **44**: 445-453 [PMID: 23237467 DOI: 10.1080/00222895.2012.672348]
62 **Ames SL**, Wong SW, Bechara A, Cappelli C, Dust M, Grenard JL, Stacy AW. Neural correlates of a Go/NoGo task with alcohol stimuli in light and heavy young drinkers. *Behav Brain Res* 2014; **274**: 382-389 [PMID: 25172182 DOI: 10.1016/j.bbr.2014.08.039]
63 **Crockford DN**, Goodyear B, Edwards J, Quickfall J, el-Guebaly N. Cue-induced brain activity in pathological gamblers. *Biol Psychiatry* 2005; **58**: 787-795 [PMID: 15993856]
64 **Robins DL**, Hunyadi E, Schultz RT. Superior temporal activation in response to dynamic audio-visual emotional cues. *Brain Cogn* 2009; **69**: 269-278 [PMID: 18809234]
65 **Buchsbaum BR**, Greer S, Chang WL, Berman KF. Meta-analysis of neuroimaging studies of the Wisconsin card-sorting task and component processes. *Hum Brain Mapp* 2005; **25**: 35-45 [PMID: 15846821]
66 **Barrós-Loscertales A**, Bustamante JC, Ventura-Campos N, Llopis JJ, Parcet MA, Avila C. Lower activation in the right frontoparietal

network during a counting Stroop task in a cocaine-dependent group. *Psychiatry Res* 2011; **194**: 111-118 [PMID: 21958514 DOI: 10.1016/j.pscychresns.2011.05.001]
67 **Aron AR**, Robbins TW, Poldrack RA. Inhibition and the right inferior frontal cortex. *Trends Cogn Sci* 2004; **8**: 170-177 [PMID: 15050513]
68 **Mantini D**, Corbetta M, Perrucci MG, Romani GL, Del Gratta C. Large-scale brain networks account for sustained and transient activity during target detection. *Neuroimage* 2009; **44**: 265-274 [PMID: 18793734]
69 **Reckless GE**, Ousdal OT, Server A, Walter H, Andreassen OA, Jensen J. The left inferior frontal gyrus is involved in adjusting response bias during a perceptual decision-making task. *Brain Behav* 2014; **4**: 398-407 [PMID: 24944869 DOI: 10.1002/brb3.223]
70 **Frühholz S**, Grandjean D. Processing of emotional vocalizations in bilateral inferior frontal cortex. *Neurosci Biobehav Rev* 2013; **37**: 2847-2855 [PMID: 24161466 DOI: 10.1016/j.neubiorev.2013.10.007]
71 **Stewart JL**, Parnass JM, May AC, Davenport PW, Paulus MP. Altered frontocingulate activation during aversive interoceptive processing in young adults transitioning to problem stimulant use. *Front Syst Neurosci* 2013; **7**: 89 [PMID: 24298242 DOI: 10.3389/fnsys.2013.00089]
72 **Cavanna AE**, Trimble MR. The precuneus: a review of its functional anatomy and behavioural correlates. *Brain* 2006; **129**: 564-583 [PMID: 16399806]
73 **Astafiev SV**, Shulman GL, Stanley CM, Snyder AZ, Van Essen DC, Corbetta M. Functional organization of human intraparietal and frontal cortex for attending, looking, and pointing. *J Neurosci* 2003; **23**: 4689-4699 [PMID: 12805308]
74 **Ko CH**, Liu GC, Yen JY, Chen CY, Yen CF, Chen CS. Brain correlates of craving for online gaming under cue exposure in subjects with Internet gaming addiction and in remitted subjects. *Addict Biol* 2013; **18**: 559-569 [PMID: 22026537 DOI: 10.1111/j.1369-1600.2011.00405.x]
75 **Fransson P**, Marrelec G. The precuneus/posterior cingulate cortex plays a pivotal role in the default mode network: Evidence from a partial correlation network analysis. *Neuroimage* 2008; **42**: 1178-1184 [PMID: 18598773]
76 **McKiernan KA**, Kaufman JN, Kucera-Thompson J, Binder JR. A parametric manipulation of factors affecting task-induced deactivation in functional neuroimaging. *J Cogn Neurosci* 2003; **15**: 394-408 [PMID: 12729491]
77 **Konova AB**, Moeller SJ, Tomasi D, Goldstein RZ. Effects of chronic and acute stimulants on brain functional connectivity hubs. *Brain Res* 2015; **1628**: 147-156 [PMID: 25721787 DOI: 10.1016/j.brainres.2015.02.002]
78 **Angeles Fernández-Gil M**, Palacios-Bote R, Leo-Barahona M, Mora-Encinas JP. Anatomy of the brainstem: a gaze into the stem of life. *Semin Ultrasound CT MR* 2010; **31**: 196-219 [PMID: 20483389]
79 **Hurley RA**, Flashman LA, Chow TW, Taber KH. The brainstem: anatomy, assessment, and clinical syndromes. *J Neuropsychiatry Clin Neurosci* 2010; **22**: iv, 1-7 [PMID: 20160204]
80 **Villablanca JR**. Why do we have a caudate nucleus? *Acta Neurobiol Exp* (Wars) 2010; **70**: 95-105 [PMID: 20407491]
81 **Dager AD**, Anderson BM, Rosen R, Khadka S, Sawyer B, Jiantonio-Kelly RE, Austad CS, Raskin SA, Tennen H, Wood RM, Fallahi CR, Pearlson GD. Functional magnetic resonance imaging (fMRI) response to alcohol pictures predicts subsequent transition to heavy drinking in college students. *Addiction* 2014; **109**: 585-595 [PMID: 24304235 DOI: 10.1111/add.12437]
82 **Ogino S**, Chan AT, Fuchs CS, Giovannucci E. Molecular pathological epidemiology of colorectal neoplasia: an emerging transdisciplinary and interdisciplinary field. *Gut* 2011; **60**: 397-411 [PMID: 21036793 DOI: 10.1136/gut.2010.217182]
83 **Nishi A**, Kawachi I, Koenen KC, Wu K, Nishihara R, Ogino S. Lifecourse epidemiology and molecular pathological epidemiology. *Am J Prev Med* 2015; **48**: 116-119 [PMID: 25528613 DOI: 10.1016/j.amepre.2014.09.031]
84 **Ogino S**, Lochhead P, Chan AT, Nishihara R, Cho E, Wolpin BM, Meyerhardt JA, Meissner A, Schernhammer ES, Fuchs CS, Giovannucci E. Molecular pathological epidemiology of epigenetics: emerging integrative science to analyze environment, host, and disease. *Mod Pathol* 2013; **26**: 465-484 [PMID: 23307060 DOI: 10.1038/modpathol.2012.214]
85 **Lundqvist T**. Imaging cognitive deficits in drug abuse. *Curr Top Behav Neurosci* 2010; **3**: 247-275 [PMID: 21161756 DOI: 10.1007/7854_2009_26]
86 **Luijten M**, Machielsen MW, Veltman DJ, Hester R, de Haan L, Franken IH. Systematic review of ERP and fMRI studies investigating inhibitory control and error processing in people with substance dependence and behavioural addictions. *J Psychiatry Neurosci* 2014; **39**: 149-169 [PMID: 24359877]
87 **Zhu Y**, Zhang H, Tian M. Molecular and functional imaging of internet addiction. *Biomed Res Int* 2015; **2015**: 378675 [PMID: 25879023 DOI: 10.1155/2015/378675]

P- Reviewer: Gumustas OG, Matsumoto S **S- Editor**: Ji FF
L- Editor: A **E- Editor**: Liu SQ

Published by **Baishideng Publishing Group Inc**
8226 Regency Drive, Pleasanton, CA 94588, USA
Telephone: +1-925-223-8242
Fax: +1-925-223-8243
E-mail: bpgoffice@wjgnet.com
Help Desk: http://www.wjgnet.com/esps/helpdesk.aspx
http://www.wjgnet.com